SPECTRAL CHARACTERISTICS OF STIMULATED RAMAN SCATTERED RADIATION IN A WAVEGUIDE

by

Johann A. du Plessis

Thesis presented in the partial fulfillment of the requirements for the degree of Master of Science at the University of Stellenbosch.

Supervisor : Dr E. G. Rohwer

January 1992

Declaration

I the undersigned hereby declare that the work contained in this thesis is my original work and has not previously in its entirety or in part been submitted at any university for a degree.

Aan my Ouers en Madelein

Acknowledgements

I wish to express my gratitude to the people and organizations who contributed towards the development of this thesis.

First I want to thank my promotor, Dr Rohwer, for his assistance and the time he shared with me these past two years. Although engaged in his own research, he always found time to discuss physics with me.

I would also like to thank Trevor Gordon and Ulrich Deutschländer for their eager assistance and advice concerning various pratical aspects of my project.

I would like to thank the personnel of the mechanical workshop who assisted in the solving of numerous pratical problems which had occured during this project.

I want to thank my wife, Madelein for her encouragement and support the past two years. At times when I lacked motivation, she was the one to encourage and support me. To Madelein, my parents and all my friends who have given help and encouragement I express my gratitude.

I would also like to thank the FRD for providing financial assistance for this project.

Finally I want to thank God for given me the understanding and insight to be able to study physics.

Abstract

The spectral characteristics of stimulated Raman scattered radiation in a waveguide was investigated using a laser as source of pump radiation.

The pump laser is focussed into the waveguide to obtain a high intensity region necessary to enhance the Raman effect. The propagation of laser radiation through a medium was investigated as well as the coupling of the laser to the waveguide. A model which describes the transmission of laser radiation through the waveguide was derived and the parameters which influences the transmission were identified.

The theory of the Raman scattering process was studied and and the parameters which influence the gain factor for the process, were investigated. The influence of these parameters on the gain were experimentally determined and comparison was made with theoretical predictions.

Various Stokes and Anti-Stokes orders with hydrogen as the Raman medium were measured and identified. Further studies were proposed involving the use of an interferometer to measure the spectral line profiles.

Opsomming

Die spektraal eienskappe van gestimuleerde Ramanverstrooide straling in a golfgeleier is ondersoek deur 'n laser as bron van straling aan te wend.

Die laser word gefokusser in die golfgeleier om 'n gebied van hoë intensiteit te voorsien wat noodsaaklik is om die Ramaneffek te versterk. Die voortplanting van laserstraling deur 'n medium is ondersoek sowel as die koppeling van die laser met die golfgeleier. 'n Model wat die transmissie van die laser deur die golfgeleier beskryf is afgelei, en die parameters wat 'n invloed op die transmissie het, is geïdentifiseer.

Die teorie van die Ramanproses is bestudeer en die faktore wat die Ramanwinsfaktor beïnvloed, is vasgestel. Hierdie invloed is eksperimenteel ondersoek en vergelykings is getref met teoretiese voorspellings.

Verskeie Stokes en Anti-Stokes ordes in waterstof is gemeet en geïdentifiseer. Verdere studies wat die gebruik van 'n interferometer behels om die spektraallynprofiele te meet, is voorgestel.

Table of contents

1

LASER MODES AND RESONATORS

1.1 Introduction

The laser has always been one of the more exciting and spectacular scientific instruments. The intense and narrow beam of light produced by a laser inevitably leads one to the conclusion that the laser is indeed very different from other light sources like for example, a light bulb.

A laser beam is usually very narrow with a small divergence. The linewidth is also extremely narrow, in fact very much narrower than a spontaneous linewidth transition. All these extremely important features of a laser can only be understood if one considers the construction of a laser, specifically the resonator which is responsible for these features.

Laser beams propagate in modes which may be understood as a distribution of energy in a certain specified manner. The intensity distribution of laser beams is not uniform and one finds that the radiation is mostly concentrated near the propagation axis of the beam and that the phase fronts are curved.

One now seeks a mathematical form of the spatial distribution of laser radiation which will describe the intensity distributions in and outside a specific resonator by assuming a certain distribution for the laser radiation. Using this function one may determine the assumed laser intensity distribution in the resonator and compare it with practical results. Comparison will be good if the assumed function is an accurate description of the laser radiation. This method is described in section 1.2 where a certain form of the laser beam is assumed. This in fact means that one is able to calculate the distribution of the laser radiation without considering the resonator. As one will see later in section 1.4.2, the function of the resonator is to select a certain form of propagation of the laser beam.

The aim of this chapter is to explain the different modes in which laser radiation propagates and how the form of these modes may be derived without explicitly considering the resonator from which these modes originate. The subject of laser beams and resonators has been looked

at in various articles [Ko 66].

In section 1.4.2 it will be shown how the laser resonator may be used to select certain modes of propagation and how these modes are influenced when focussed by a lens, especially to show how to create new beam diameters. Focussing with a lens is required when one wants to match the laser with another optical element such as a waveguide or a Raman cell. This is called mode matching.

1.1.1 The Wave Equation

The wave equation which describes the propagation of radiation through free space is derived from the Maxwell's equations. The parameter u is related to the electric field.

$$\nabla^2 u + k^2 u = 0 \tag{1.1}$$

where $k = 2\pi/\lambda$ is the propagation constant in the medium.

1.1.2 Plane wave propagation

A simple solution that corresponds to differential equation 1.1 , is a plane wave solution given by

$$u = e^{-jkz} \tag{1.2}$$

where z is the distance travelled in the propagation direction.

A monochromatic plane wave propagating in the resonator would cause interference patterns due to diffraction at the edges of the resonator. These interference patterns are not generally found in the intensity distributions of a resonator so that the plane wave solution must be modified. This modification is attempted in the next section.

1.1.3 Modified wave propagation

For a beam travelling in the z-direction one assumes

$$u = \psi(x, y, z)e^{-jkz} \tag{1.3}$$

Because the propagation of laser radiation is considered, a complex function ψ is introduced which describes the differences between a plane wave and a laser wave. The basic differences described by this function are the non uniform intensity distribution normal to the axis of propagation, the fact that the beam expands as it propagates and the curvature of the phase front.

If the above form of u is substituted into the differential equation 1.1, the following is obtained [Ko 66].

$$\frac{\partial^2\psi}{\partial x^2} + \frac{\partial^2\psi}{\partial y^2} - 2jk\frac{\partial\psi}{\partial z} = 0 \tag{1.4}$$

In obtaining the above equation it is assumed that ψ varies so slowly with respect to z that its second derivative $\partial^2\psi/\partial z^2$ may be neglected.

A differential equation has thus been derived for which an infinite number of solutions exist. Each of these solutions corresponds to a certain transverse mode of propagation. The fundamental beam will first be discussed in detail and later the higher order modes will also be discussed.

1.2 The Fundamental Transverse Mode

The following equation

$$\psi = \exp\left[-j(P + \frac{k}{2q}r^2)\right] \tag{1.5}$$

is a test solution of the wave equation 1.4 where $r^2 = x^2 + y^2$.

The parameter P is a function of z and represents a complex phase shift which relates to the propagation of the beam. In effect it relates to the phase difference between a Gaussian beam and an ideal plane wave. It will later be shown that the form of ψ described by equation 1.5 leads to the description of a Gaussian beam.

The parameter $q(z)$ is also complex and describes the intensity variation with increasing distance r away from the optical axis. It also describes the curvature of the phase front. Because the

intensity profile is of a Gaussian form, this mode of propagation is often called the Gaussian mode or the fundamental mode. This is a very important mode of propagation as many lasers propagate in the Gaussian mode.

If the above form of ψ given by equation 1.5 is substituted into equation 1.4 the following is obtained.

$$q' = 1 \tag{1.6}$$

and

$$P' = -\frac{j}{q} \tag{1.7}$$

In both cases the prime indicates differentiation with respect to z.

Equation 1.6 may be written as

$$\frac{\partial q}{\partial z} = 1 \tag{1.8}$$

Intergration leads to

$$\int_{q_o}^{q} dq = \int_{z_o}^{z} dz \tag{1.9}$$

If equation 1.9 is integrated from arbitrary values q_1 to q_2 and $z_o = 0$ are chosen, one obtains the next equation. One has that $q = q_1 = q_o$ when $z = z_o = 0$.

$$q_2 = q_1 + z \tag{1.10}$$

This is an important result because it relates two beam parameters to each other. More explicitly it relates q_2 in one plane (output plane) to the parameter q_1 in a second plane (input plane). The two planes are separated a distance z from each other.

Two real parameters R and w are now introduced which relates to the complex parameter q in the following manner.

$$\frac{1}{q} = \frac{1}{R} - j\frac{\lambda}{\pi w^2} \tag{1.11}$$

The physical meaning of these parameters will be considered later and at this moment the mathematical form is of interest.

Since q is a function of R and w, one may define q_o as the value of q for which $R \to \infty$. The matching w value which corresponds to the above choice is called w_o.

From equation 1.11 the above definition of q_o leads to

$$q_o = j\frac{\pi w_o^2}{\lambda} \tag{1.12}$$

From this follows that q_o is purely imaginary. Using equation 1.10 the parameter q at a distance z away from w_o may be calculated. It is given by

$$q = q_o + z = j\frac{\pi w_o^2}{\lambda} + z \tag{1.13}$$

If equation 1.11 and equation 1.13 is combined and the real and imaginary parts are equated, one obtains

$$w^2(z) = w_o^2[1 + (\frac{\lambda z}{\pi w_o^2})^2] \tag{1.14}$$

$$R(z) = z[1 + (\frac{\pi w_o^2}{\lambda z})^2] \tag{1.15}$$

The derivation of above two equations is shown in Appendix A. These two equations form the basis on which one deals with the propagation of a Gaussian beam through space. By inserting equation 1.11 into equation 1.5 the physical meaning of these two new parameters becomes clear.

1.2.1 The beam parameter w

If one substitutes equation 1.11 into equation 1.5, the following is obtained.

$$\begin{aligned}\psi &= \exp[-j(P + \frac{k}{2q}r^2)] \\ &= \exp[-j(P + \frac{k}{2}(\frac{1}{R} - j\frac{\lambda}{\pi w^2})r^2)] \\ &= \exp[-j(P + \frac{kr^2}{2R} - j\frac{\lambda kr^2}{2\pi w^2})] \\ &= \exp[-j(P + \frac{kr^2}{2R}) - \frac{r^2}{w^2}] \end{aligned} \tag{1.16}$$

If the intensity I which is proportional to $\psi.\psi^*$ is calculated, one finds that [Mi 88]

$$I \sim \psi.\psi^* = e^{-\frac{2r^2}{w^2}} \tag{1.17}$$

Clearly the intensity distribution in the direction perpendicular to the propagation axis (or the z-axis) is of a Gaussian form which leads to the description of a Gaussian mode. From the form of the Gaussian equation it is easy to see that the parameter w is a measure of the decrease in the intensity with increasing distance perpendicular to the z-axis. This leads one to define the beam radius w as the distance at which the amplitude of the electric field is $\frac{1}{e}$ that of the maximum value it has on the z-axis. The value $2w$ is thus called the beam diameter. Since w increases as z increases, it means that the intensity for certain x, y coordinates decreases from a maximum at the smallest value of w. In figure 1.1 the intensity profile of a Gaussian beam is shown.

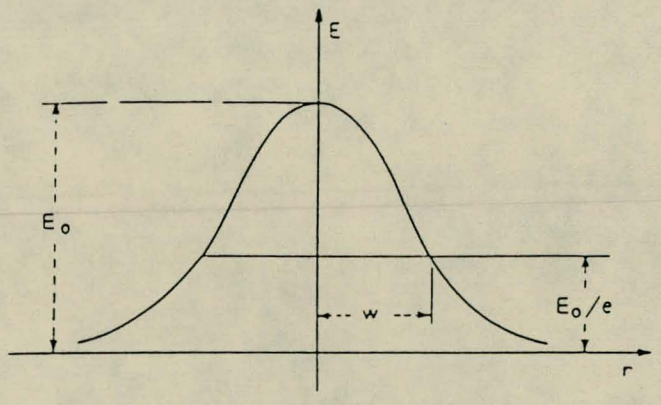

Figure 1.1 Gaussian Mode Profile

If one carefully considers equation 1.14, one notes that $w = w_o$ when $z = 0$ which is of course true per definition. For increasing z, w increases from a minimum value of w_o. The choice for q_o has thus been a good one because it defines a minimum beam diameter, called the beam waist, at $z = 0$. This is a good choice for the 'origin' of the beam.

In figure 1.2 it is shown how w changes with respect with z for a w_o value of 0.5 mm and $\lambda = 632.8$ nm.

1.2.2 The phase front parameter R

$R(z)$ is the radius of the phase front due to the phase difference between rays parallel to the axis of propagation and rays propagating at an angle to the z-axis. The radius intersects the z-axis at z.

The total wave function u which incorporates the plane wave characteristics and the non-plane wave part of the Gaussian beam may now be written down.

$$u = \psi(x, y, z)e^{-jkz} = \psi \exp[-j(P + \frac{k}{2q}r^2)]e^{-jkz} \tag{1.18}$$

This may be written as

$$u = \exp[-jP - j\frac{kr^2}{2q} - jkz] \tag{1.19}$$

The form for q given by equation 1.11 may now be substituted. This gives

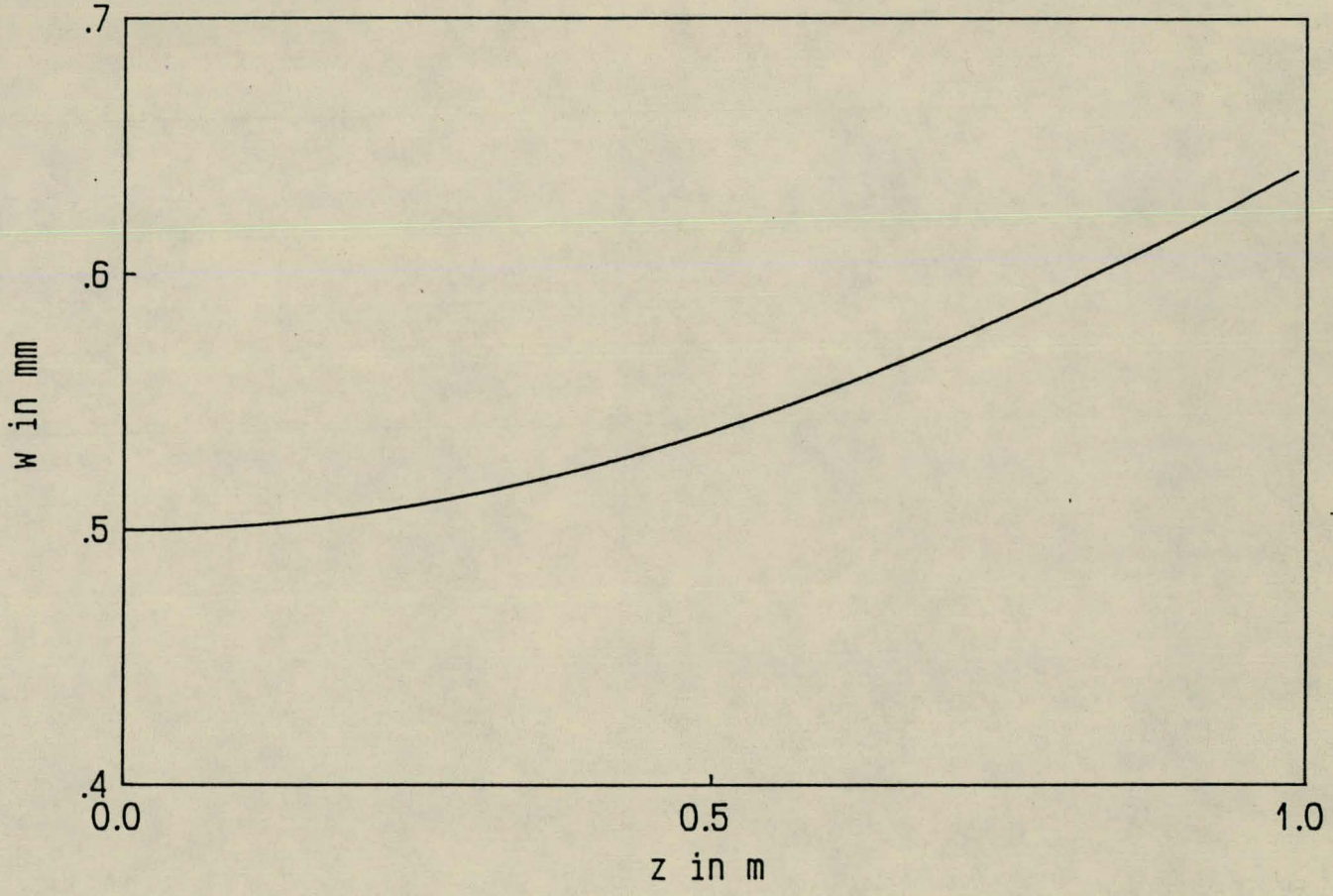

Figure 1.2 The beam parameter w as a function of z

$w_o = 0.5$ mm, $\lambda = 632.8$ nm

$$\begin{aligned} u &= \exp\left[-jP - j\left(\frac{kr^2}{2R}\right) - \frac{k\lambda r^2}{2\pi w^2} - jkz\right] \\ &= \exp\left[-jP - j\left(\frac{kr^2}{2R}\right) - \frac{r^2}{w^2} - jkz\right] \\ &= \exp\left[-jP - jkz - jk\left(\frac{r^2}{2R}\right) - \frac{r^2}{w^2}\right] \end{aligned} \tag{1.20}$$

Consider now a spherical wave of the following form.

$$\psi = e^{-jka} \tag{1.21}$$

where $a^2 = z^2 + x^2 + y^2 = z^2 + r^2$

In figure 1.3 the phase front of the above wave is shown.

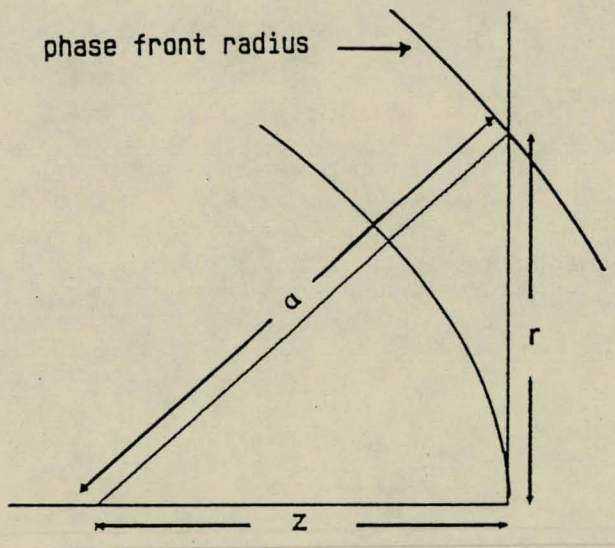

Figure 1.3 Phase front radius

Equation 1.21 may now be written as follows

$$\begin{aligned} e^{-jka} &= e^{-jk(z^2+r^2)^{1/2}} \\ &= e^{-jkz(1+r^2/z^2)^{1/2}} \\ &\simeq e^{-jkz-jk(r^2/2z)} \end{aligned} \tag{1.22}$$

by making use of a Taylor expansion [Mi 88]. The first term $-jkz$ is associated with a plane wave and the other term gives us the spherical character of the wave. This may now be compared with equation 1.21.

It has the same form as equation 1.21 and if one would replace z with R in the previous equation, the forms for both wave types would be the same. Since for a spherical wave, the radius is also equal to the z coordinate, (if one considers propagation in the z direction), one thus defines R as the radius of the phase front of the Gaussian wave at a particular z coordinate.

One must remember that the above equation derived for a spherical phase front is not exact for a spherical phase front, because the higher order terms in the Taylor expansion have been ignored.

Considering R in the Gaussian wave form, one notes that R is a function of z , and only approximately linear with respect to z. For large z, this relation becomes linear, that is $R = z$. Only a part of the Gaussian wave is thus associated with a spherical wave in the sense to define R as the radius of the phase front. The Gaussian beam thus has plane wave and spherical wave characteristics. For large z values, the above reasoning means that the Gaussian wave may be considered as a spherical wave to a good approximation.

From equation 1.15 for the phase front radius R, one sees that R reaches an infinite value for $z = 0$ and $z = \infty$. This means that if the beam starts at the w_o position, or $z = 0$, then $R = \infty$. Thus initially R starts to get smaller as z increases, but when $z \to \infty$, R reaches an infinite value again. This means that R decreases to a certain value and then increases again.

This is illustrated in the following figure 1.4 where the phase front radius R is plotted as a function of z. There is very sharp decrease in R in the beginning and this is where the second term in equation 1.15 is the dominant term because of the factor $\frac{1}{z}$ which is very large for small values of z. After this decrease, R is approximately linear with respect to z and thus the second

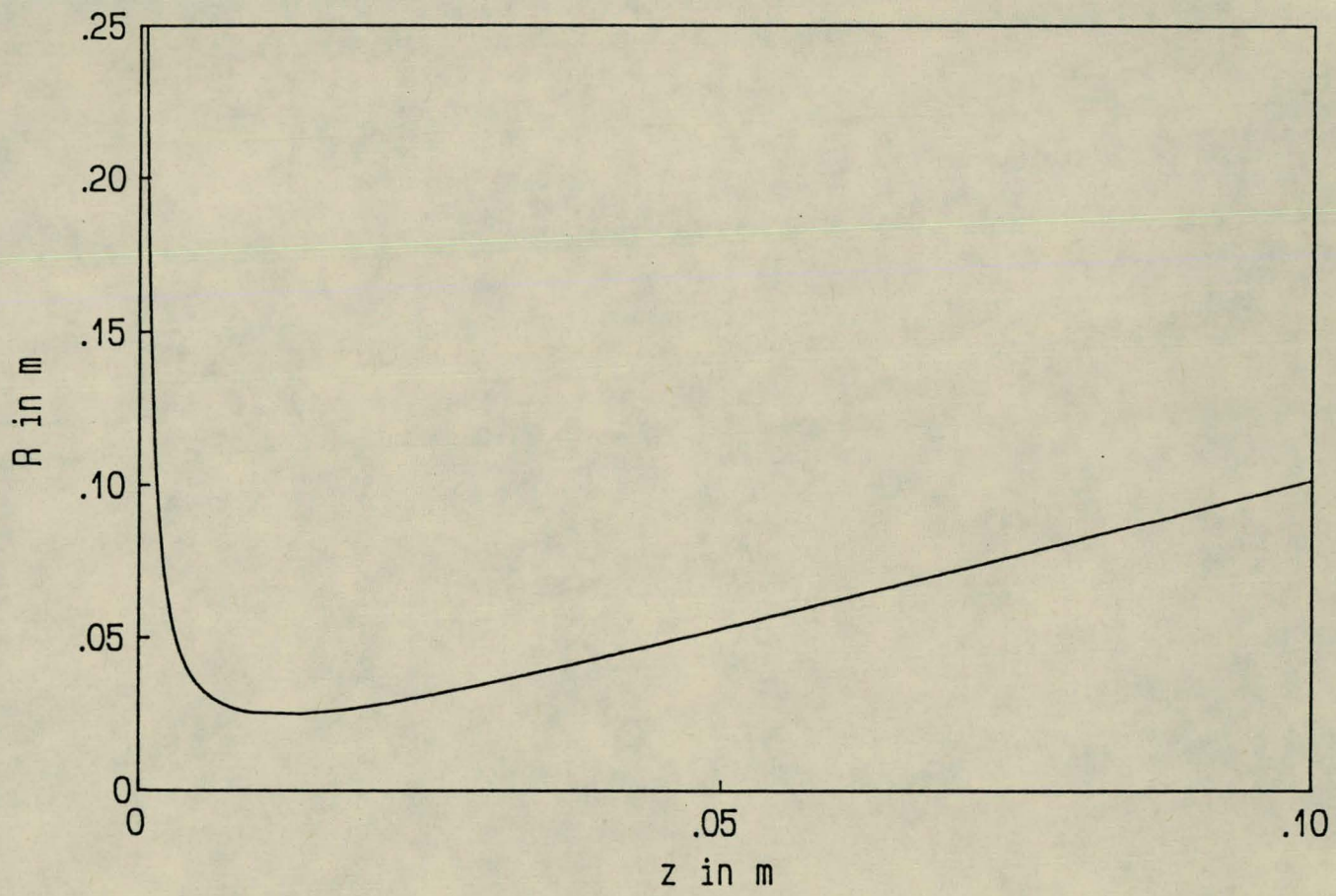

Figure 1.4 The Phase front radius R
$w_o = 0.5$ mm, $\lambda = 632.8$ nm

term becomes negligible. This turning point is at a z value called the Rayleigh range which is a useful quantity to define in optics. The Rayleigh range will be discussed further in section 1.5.

1.2.3 The far-field diffraction angle

An angle called the far-field diffraction angle may be defined and is given by

$$\theta = \frac{\lambda}{\pi w_o} \tag{1.23}$$

This determines a geometrical picture of the laser wave in the sense that this angle gives a limit on the angles a ray presentation of the Gaussian wave may have as shown in figure 1.5.

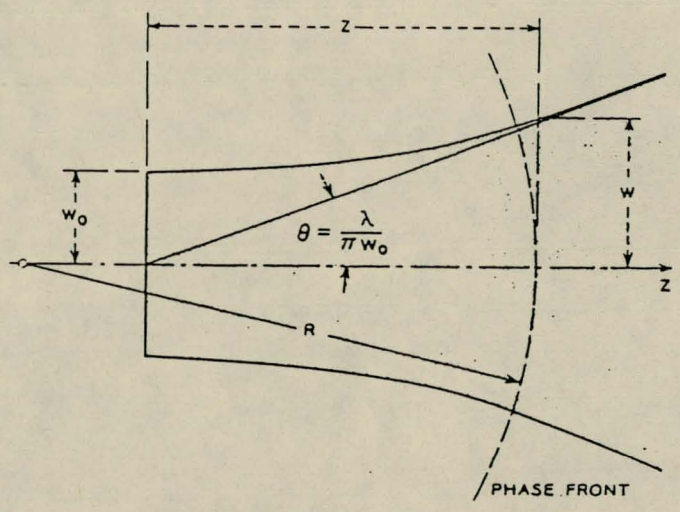

Figure 1.5 Gaussian Beam parameters

This is also the angle the asymptotes of the hyperbolic function $w(z)$ make with the z-axis.

From equation 1.14 follows that

$$w^2 = w_o^2 + (\frac{\lambda z}{\pi w_o})^2 \tag{1.24}$$

For large values of z the first term becomes negligible and one has

$$w = \frac{\lambda z}{\pi w_o} \tag{1.25}$$

This means that w as a function of z has a gradient given by $\frac{\lambda}{\pi w}$ which is equal to $\tan\theta$. Since θ is small one has that $\tan\theta = \theta$ which gives the result for the far field diffraction angle as found in equation 1.23.

1.2.4 The complex phase shift

To determine the complex phase shift a distance z away from the waist, one inserts equation 1.13 into equation 1.7 to obtain the following

$$P' = -\frac{j}{q} = -\frac{j}{z + j(\pi w_o^2/\lambda)} \tag{1.26}$$

If equation 1.26 is integrated one finds that [Ko 66]

$$\begin{aligned} jP(z) &= \ln[1 - j(\lambda z/\pi w_o^2)] \\ &= \ln\sqrt{1 + (\lambda z/\pi w_o^2)^2} - j\arctan(\lambda z/\pi w_0^2) \end{aligned} \tag{1.27}$$

As one may see P has a real and an imaginary part. The real part represents a phase shift difference Φ between a Gaussian beam and an ideal plane wave. Using this form of P to obtain the final result for the fundamental beam one has that the imaginary part produces a factor $\frac{w_o}{w}$ in the fundamental equation 1.28 which gives the peak intensity decrease along the z-axis due to the fact that w is a function of z and increases along the z-axis. Since the beam expands there must be a decrease in the peak intensity.

1.2.5 Final result for fundamental beam.

Combining all these results, the fundamental Gaussian beam function may be written down [Ko 66].

$$u(r,z) = \frac{w_o}{w}\exp\{-j(kz - \Phi) - \frac{r^2}{w^2} + \frac{jk}{2R}\} \tag{1.28}$$

The phase shift is given by

$$\Phi = \arctan\left(\lambda z/\pi w_o^2\right) \tag{1.29}$$

1.2.6 Sign convention

To define the sign of the phase front curvature one uses the convention that one always looks at the phase front from the position of the w_o value which determines the phase front. A convex phase front is then defined as such that the center of curvature lies in the direction of w_o and a concave radius if the center of curvature lies in the on the other side of the curvature than w_o.

The convention one uses when defining the sign of the radius is that if the curvature is convex when looking from w_o, then R is positive. If the curvature is convex, but one looks against the direction of propagation, then R is negative.

If the curvature is concave and one looks with the direction of propagation, then R is negative. If the curvature is concave, but one looks against the propagation direction, then R is positive.

Example 1:

Consider figure 1.6. Using the convention, R is positive, because the curvature is convex and one looks in the same direction as in which the beam propagates.

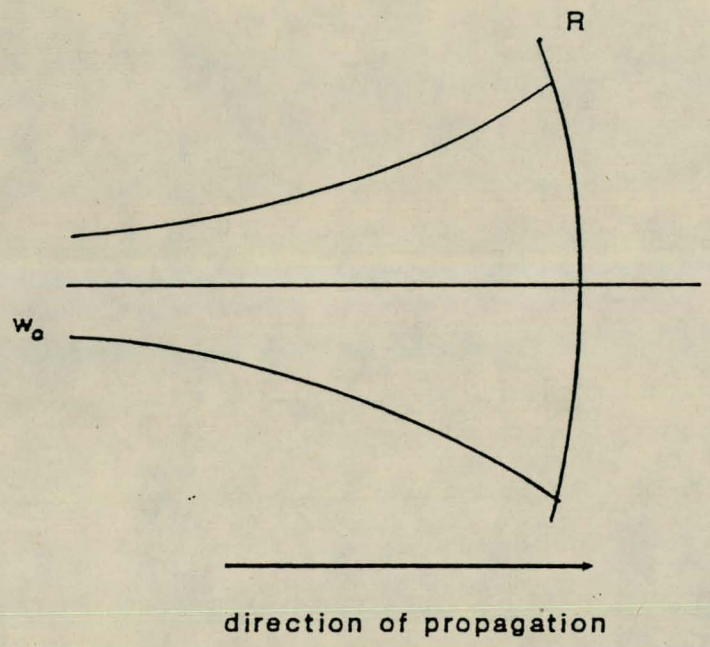

Figure 1.6 Sign Convention

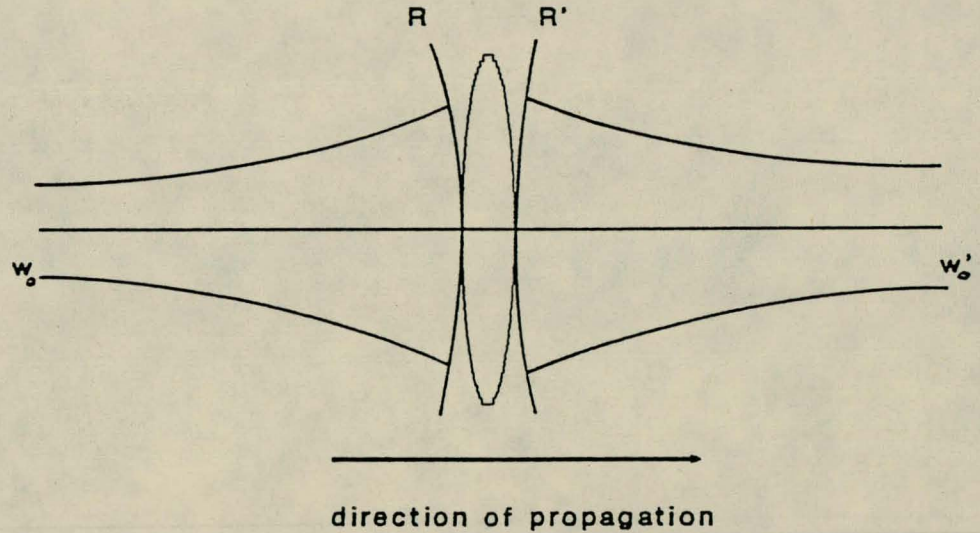

Figure 1.7 Sign Convention for focussed beam

Example 2:

In figure 1.7 the focussing of a Gaussian beam with radius R into a new radius R' is shown. Since R' is convex when looking from w_o', and one looks against the propagation direction, R'

is negative as it must be for a focussed beam.

1.3 Higher Order Modes

The Gaussian mode discussed in the previous section is only one solution of the wave equation 1.1. There are also other solutions of the wave equation which gives rise to other transverse modes. These modes form a complete and orthogonal set of functions and are called the modes of propagation. It is important to notice that every arbitrary distribution of monochromatic light can be expanded in terms of these modes because these modes form an orthogonal set of functions [Ko 66]. A Cartesian coordinate system is used to describe the transverse modes but another system may also be used.

1.3.1 Cartesian Coordinates

Consider a geometry with Cartesian coordinates and guess a solution for the wave equation of the following form:

$$\psi = g.h \exp\{-j[P + \frac{k}{2q}(x^2 + y^2)]\} \tag{1.30}$$

Since w is a function of z, g is a function of x and z and h is a function of y and z respectively. Substituting this trial solution into equation 1.4 gives the following differential equations for g and h [Ko 66].

$$\frac{w^2}{2}\frac{d^2 g_m}{dx^2} - x\frac{dg_m}{dx} + 2mg_m = 0 \tag{1.31}$$

A similar equation for h is obtained with m substituted by n.

Making a substitution that $x = \mathrm{c}\frac{w}{\sqrt{2}}$, the above equation reduces to the well known differential equation for the Hermite polynomial, say $H_m(c)$ of order m.

One then has that [Mi 88]

$$g.h = H_m(\sqrt{2}\frac{x}{w})H_n(\sqrt{2}\frac{y}{w}) \tag{1.32}$$

m and n are called the transverse mode numbers and an important result is that $w(z)$ is not a function of m or n so that $w(z)$ is the same for all the possible transverse modes. The parameter $R(z)$ is also the same for all modes implying that the the curvature of the phase front is also the same.

The phase shift Φ is not the same for every mode and is given by [Ko 66]

$$\Phi = (m + n + 1) \arctan (\lambda z / \pi w_o^2) \tag{1.33}$$

The expression obtained for the fundamental mode, equation 1.28 may also be used to describe higher order modes if one includes the factor $g.h$. This is because the solutions guessed for the higher order modes are the same as for the fundamental mode except for the factor $g.h$. Thus to obtain a mathematical description of certain higher order modes, one only has to calculate $g.h$ and multiply it with the solution obtained for the fundamental or Gaussian mode.

The transverse modes are generally written as TEM_{mn} modes where m corresponds to the x-coordinate and n to the y-coordinate. With this result the intensity distributions for various higher order modes in Cartesian coordinates may be determined.

The electric field distribution for the Gaussian mode is given by

$$E = E_o \exp [\frac{-r^2}{w^2}] \tag{1.34}$$

ignoring the phase depended parts.

Thus the intensity distribution is as follows

$$I = I_o \exp [\frac{-2r^2}{w^2}] \tag{1.35}$$

By using the following Hermite polynomials [Sp 68], one is able to obtain the following electric field distributions for certain higher order modes.

$$\begin{aligned} H_o(x) &= 1 \\ H_1(x) &= 2x \\ H_2(x) &= 4x^2 - 2 \\ H_3(x) &= 8x^3 - 12x \end{aligned} \tag{1.36}$$

The TEM_{10} mode, that is $m = 1$ and $n = 0$ have the following electric field distribution:

$$E = 2\sqrt{2}(\frac{x}{w}).E_o \exp[\frac{-r^2}{w^2}] \tag{1.37}$$

Thus the intensity distribution is given by :

$$I = 8(\frac{x^2}{w^2}).I_o \exp[\frac{-2r^2}{w^2}] \tag{1.38}$$

The TEM_{01} mode has the same intensity distribution as the TEM_{10} mode but with a changed axis.

By using the same approach, one may write the intensity distributions for some transverse modes of which some are listed below.

1.3.2 Intensity distributions for modes

$$\begin{aligned}
TEM_{00} &: I = I_o \exp(-2\frac{x^2+y^2}{w^2}) \\
TEM_{10} &: I = 8\frac{x^2}{w^2} I_o \exp(-2\frac{x^2+y^2}{w^2}) \\
TEM_{01} &: I = 8\frac{y^2}{w^2} I_o \exp(-2\frac{x^2+y^2}{w^2}) \\
TEM_{11} &: I = 64\frac{y^2x^2}{w^2} I_o \exp(-2\frac{x^2+y^2}{w^2}) \\
TEM_{20} &: I = (64\frac{x^4}{w^4} - 32\frac{x^2}{y^2} + 4) I_o \exp(-2\frac{x^2+y^2}{w^2}) \\
TEM_{21} &: I = \{(8\frac{x^2}{w^2} - 2)(2\sqrt{2}\frac{y}{w})\}^2 I_o \exp(-2\frac{x^2+y^2}{w^2}) \\
TEM_{22} &: I = \{(8\frac{x^2}{w^2} - 2)(8\frac{y^2}{w^2} - 2)\}^2 I_o \exp(-2\frac{x^2+y^2}{w^2})
\end{aligned}$$

Intensity profiles of some of the above modes is shown in figures 1.8 to 1.10. Note that the number of zeros in a mode pattern is equal to the corresponding mode number for a specific axis. This is a quick way to classify transverse modes.

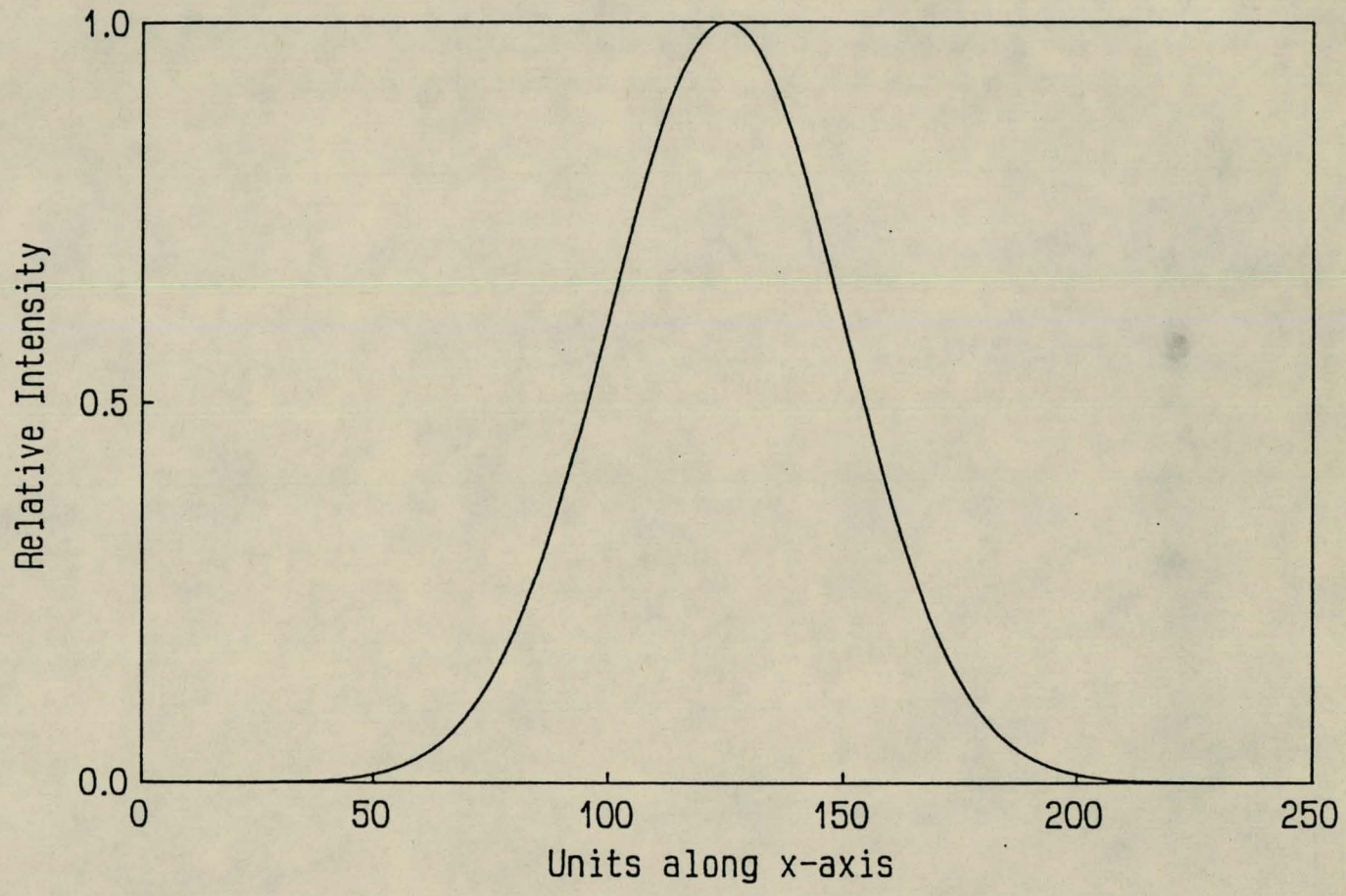

Figure 1.8 Intensity Profile of TEM_{00} mode

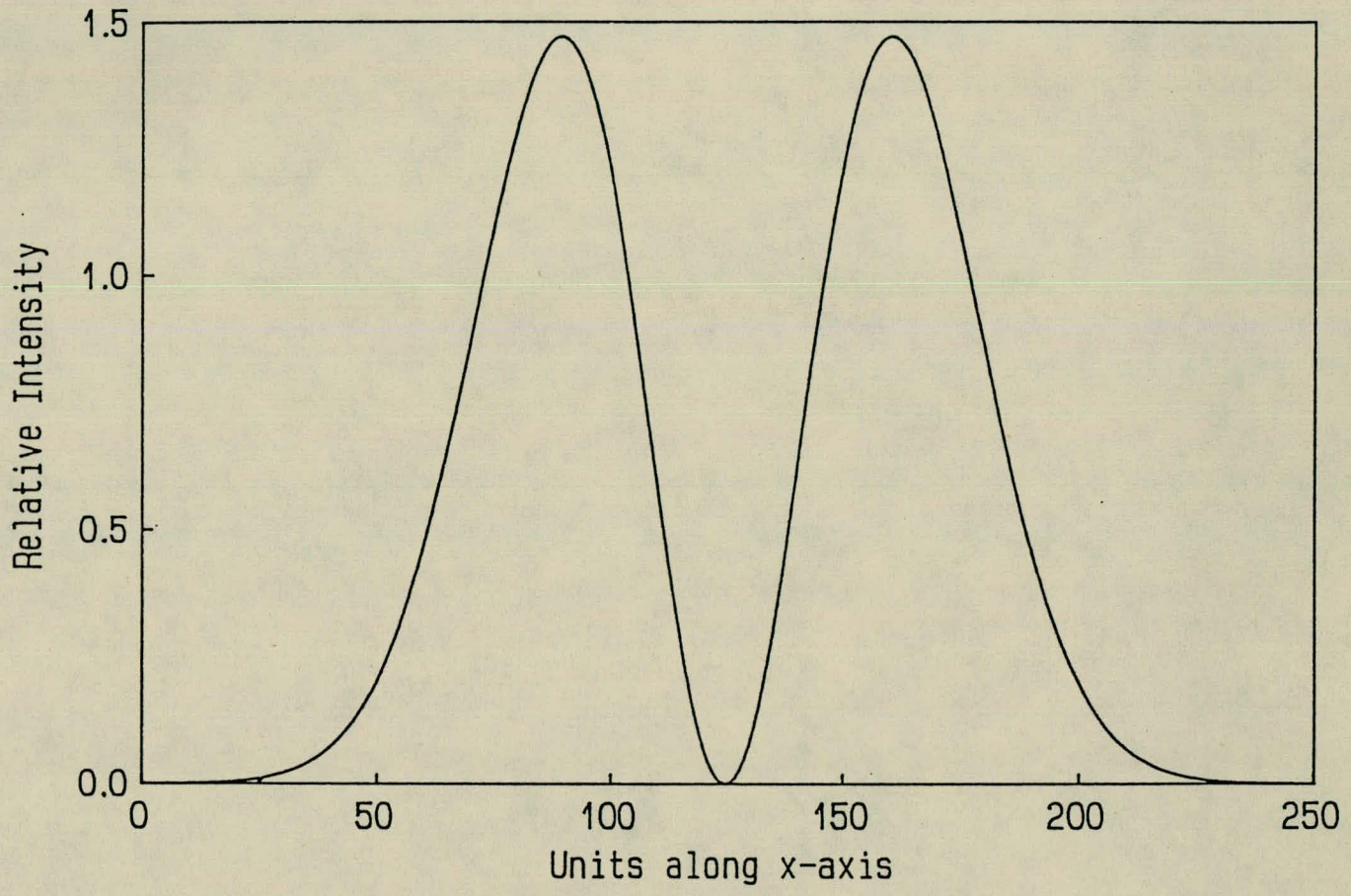

Figure 1.9 Intensity profile of TEM_{10} mode

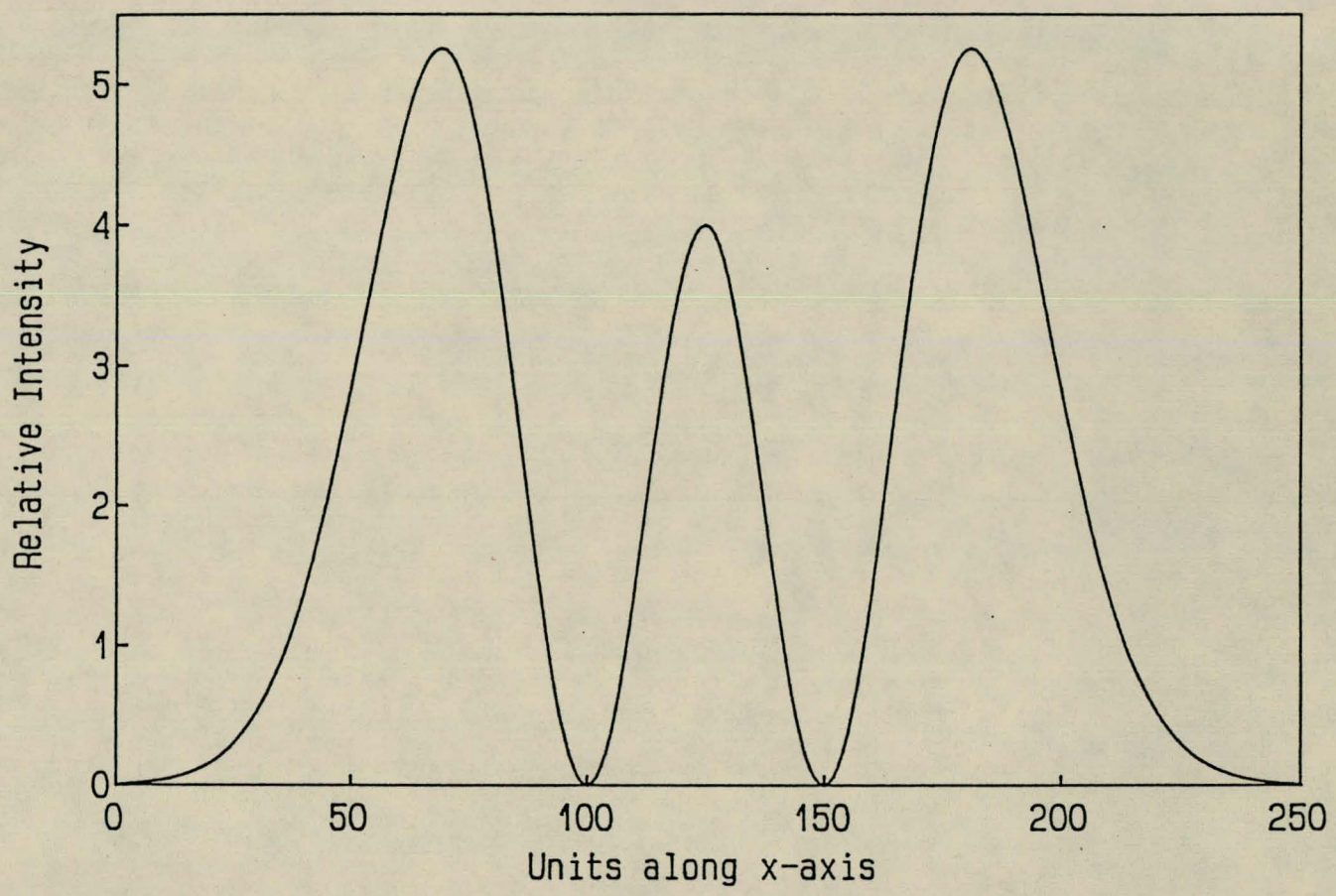

Figure 1.10 Intensity profile of TEM_{20} mode

1.4 The laser resonator

1.4.1 Introduction

The laser resonator has many functions in a laser of which the selection of a particular transverse mode of propagation is an important one. Other important functions are the feedback and long interaction length imposed by the resonator and also the reducing of the linewidth of the laser. This results in the longitudinal modes of the resonator which will be discussed later. These longitudinal modes are separated in frequency by $c/2L$ where L is the length of the resonator. In this treatment of the laser resonator it is assumed that the electromagnetic modes of the laser with the gain medium is the same as the modes of an *empty* resonator with no gain medium. The interest in laser resonators is that it is the tool with which the mode of propagation of laser radiation is produced. In this case the fundamental or TEM_{00} mode is of special interest. Resonator theory has been discussed in various articles and books [Ko 66, Mi 88].

1.4.2 The selection of transverse modes

First the characteristics of a resonator in which the Gaussian mode is allowed to propagate will be discussed and then will be shown how the resonator may be used to choose this Gaussian mode to propagate by suppressing of the higher order transverse modes.

Consider the simplest resonator which consists of two reflective mirrors separated by a distance L as shown in figure 1.11. Because of the properties of a resonator, the phase front of radiation in the resonator must equal the mirror curvature so that in a flat resonator only plane wave propagation is allowed. This is schematically shown in figure 1.11(a). A Gaussian mode or a higher order mode cannot propagate because the curvature of its phase front does not allow the resonator to function as a resonator. This is clearly shown in figure 1.11(b) where radiation is lost from the resonator after a few reflections. A a different type of resonator must thus be used to select transverse modes and in particular the Gaussian mode.

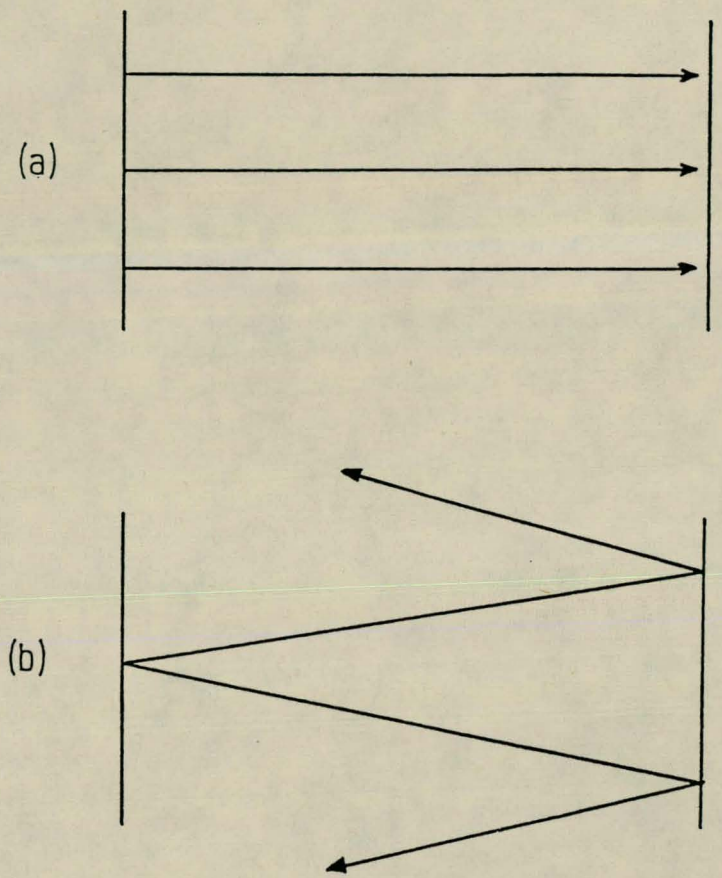

Figure 1.11 The Parallel Laser Resonator

Consider now a resonator with at least one mirror with a certain radius of curvature. In figure 1.12 such a resonator is shown in which one mirror is flat and the output coupler has a radius R. Because the Gaussian mode approximately has a phase front radius R, a Gaussian mode with the position of w_o at the flat mirror and with phase front equal to the radius R of the output coupler at the position of the output coupler may exist in the resonator. Any other higher order transverse mode may also exist if its phase front radius is the same.

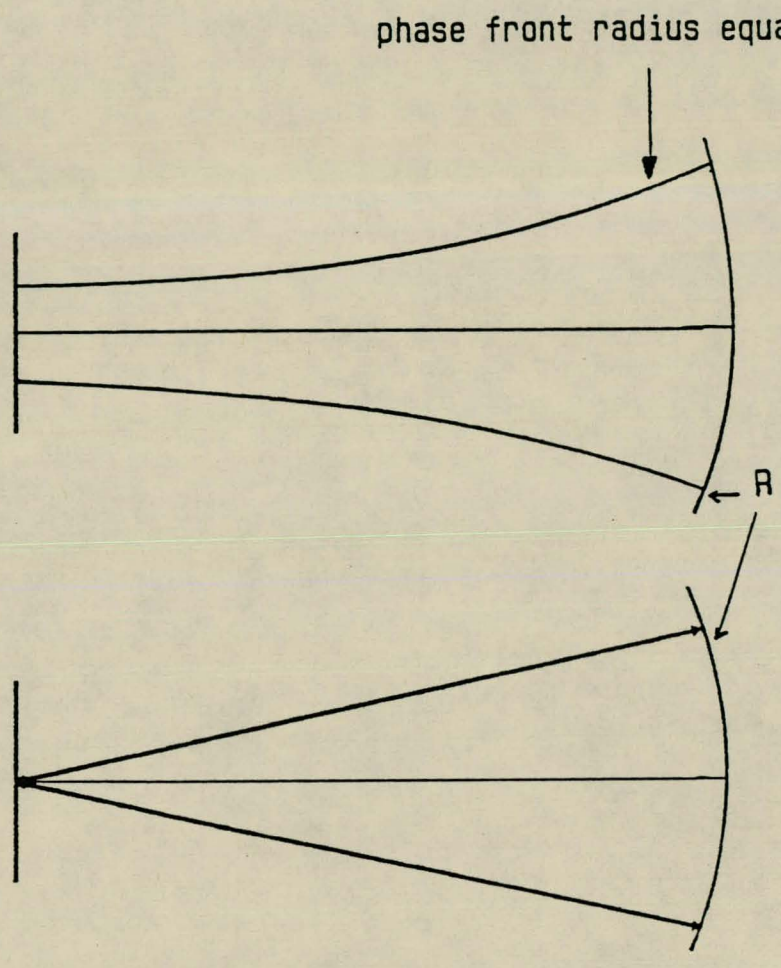

Figure 1.12 Laser Resonator with one curved mirror

Assume that only the Gaussian mode propagates in the resonator. The radius R of the output coupler now determines the form of the Gaussian mode allowed to propagate. For a resonator of given length L, every different value for R leads to a different Gaussian mode allowed to propagate. The difference lies in the relation between R and w_o as determined by the resonator configuration as shown in figure 1.13.

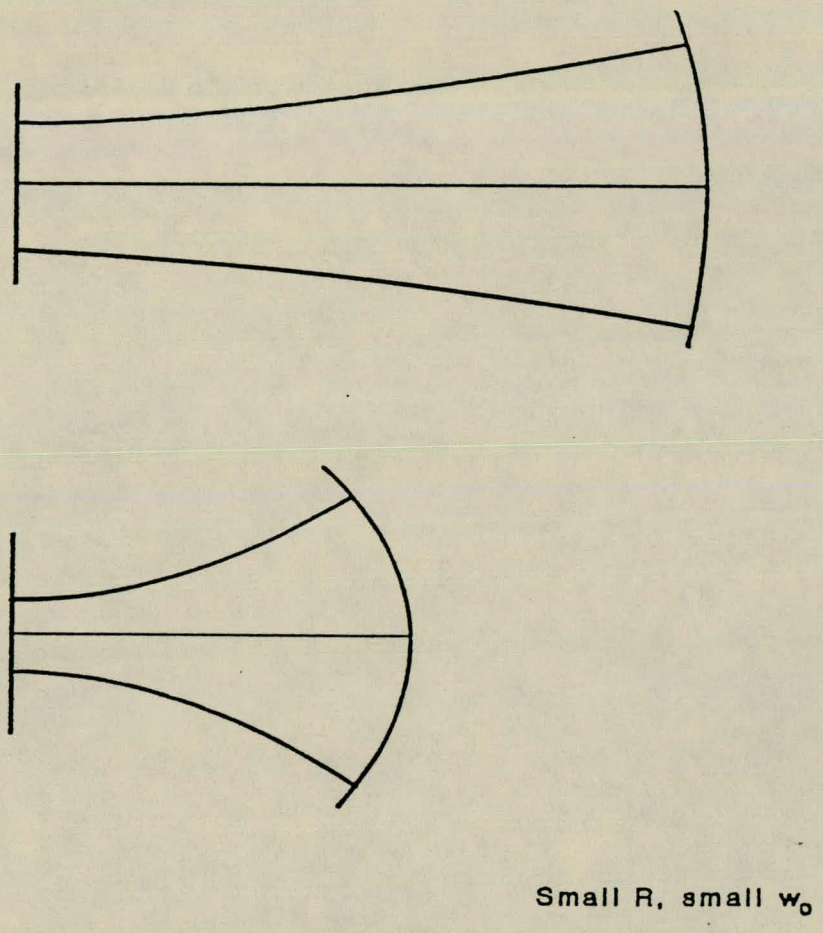

Figure 1.13 The relation between R and w_o

Larger values for R corresponds to larger values of the minimum beam waist w_o referring to the following relation between w_o and R as given by equation 1.15.

$$R(z) = z[1 + (\frac{\pi w_o^2}{\lambda z})^2]$$

The above reasoning is valid for the Gaussian mode as well as for higher order modes. In general one may also have a resonator with both mirrors curved and the position and size of w_o is then determined by R_1 and R_2 as well as the length of the resonator L. This will be shown in detail

in section 1.4.4.

For many applications a laser operating in the Gaussian or TEM_{00} mode is required. To obtain TEM_{00} operation, restrictions must be imposed on the other modes in order to prevent them from lasing. If one looks at the differences between the transverse modes one sees that the beam waist parameter w_o and phase front radius R are the same for every mode, but the higher order modes have larger transverse cross sections. An obvious way of preventing these modes from lasing would be to place a physical obstruction in the resonator.

This obstruction would partially block the higher order modes because of their larger transverse intensity distributions, and would allow more of the TEM_{00} mode to propagate. Because of the nature of the stimulated emission process, a mode which is given a lead with respect to the other modes, will grow more and more ahead of the other modes. This causes effectively only the Gaussian mode to propagate. This process of selection may also be obtained by choosing the tube which contains the lasing medium a certain size to allow only the TEM_{00} mode to propagate.

Although it is not obvious, the mirrors themselves also impose restrictions on the higher order modes. Because the mirrors have a finite size, the higher order modes have larger diffraction losses than the fundamental mode. If one takes an imaginary resonator with infinite sized mirrors, there is of course no diffraction and the output radiation will be an even distribution of all the possible transverse modes.

Note also that the Gaussian beam in practice is not a Gaussian beam by definition because from the definition of a Gaussian beam the intensity distribution extends to infinite in the transverse direction. This cannot be true for a practical resonator, because the mirrors have a certain size and thus a fraction of the radiation is lost due to diffraction.

1.4.3 Longitudinal modes of propagation

Any resonator whether flat or curved acts as a interferometer and has a set of longitudinal modes characterized by the length of the resonator. Consider the simplest resonator with both flat mirrors. This form of resonator is also known as a interferometer if the length L may be varied and an etalon if the length is fixed. A longitudinal mode can be represented by a plane wave propagating back and forth between the mirrors and as the beam that represents the mode travel in both directions between the mirrors it forms a standing wave pattern in the resonator.

A solution for a plane wave is $\sin(kz)$ and the condition for resonance may be written as

$$\sin kz = \sin k(z + 2L) \tag{1.39}$$

where L is the length of the resonator.

This yields the result that

$$k.2L = m.2\pi \tag{1.40}$$

where m is an integer and m = 1,2,3.....∞

Using

$$k = \frac{2\pi}{\lambda} \tag{1.41}$$

one may obtain

$$L = \frac{m\lambda}{2} \tag{1.42}$$

In terms of the frequency one has that

$$\nu = \frac{mc}{2L} \tag{1.43}$$

which means that the longitudinal modes in frequency differ by $c/2L$. One thus has a resonator in which different frequencies are allowed, each corresponding to a longitudinal mode. For each of these longitudinal modes, there is a infinite set of transverse modes. Because of these properties, etalons are often placed in other laser resonators in order to choose only one longitudinal mode of that resonator to oscillate. The number of longitudinal modes to oscillates in a resonator depends on the gain profile of the gain medium with respect to the frequency. A typical gain profile with longitudinal modes present is shown in figure 1.14. In the case of figure 1.14(a) there are a number of longitudinal modes which may propagate. By decreasing the length L of the resonator the situation shown as in figure 1.14(b) is obtained. Then there is only

one longitudinal mode which may propagate because the losses for the other modes are too large.

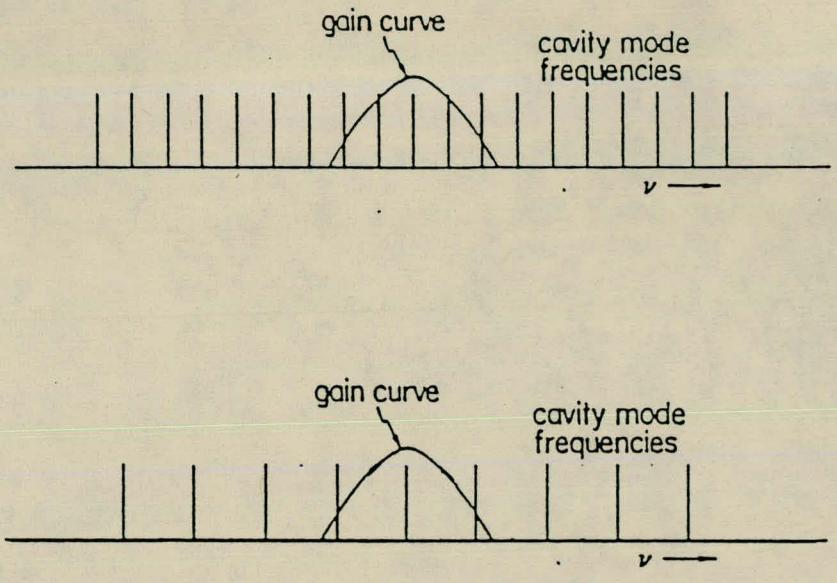

Figure 1.14 Longitudinal Mode Representation

Sometimes practical consideration restricts the decrease in the length of the resonator and then an etalon is used to select a longitudinal mode. The etalon imposes losses on all the longitudinal modes except one, so that in effect only one longitudinal mode is allowed to propagate.

The longitudinal frequencies given by the resonance condition do not have infinite widths, but are broadened. This is because wavelengths that do not exactly satisfy the resonance condition may also propagate, but with greater losses. This gives longitudinal mode patterns as shown in figure 1.15.

Due to this variation the resonator also reduces the linewidth of the laser as may be seen in figure 1.15. The losses ensure that only the frequency interval above the losses contributes to the laser action and without the resonator, the linewidth would be significant larger.

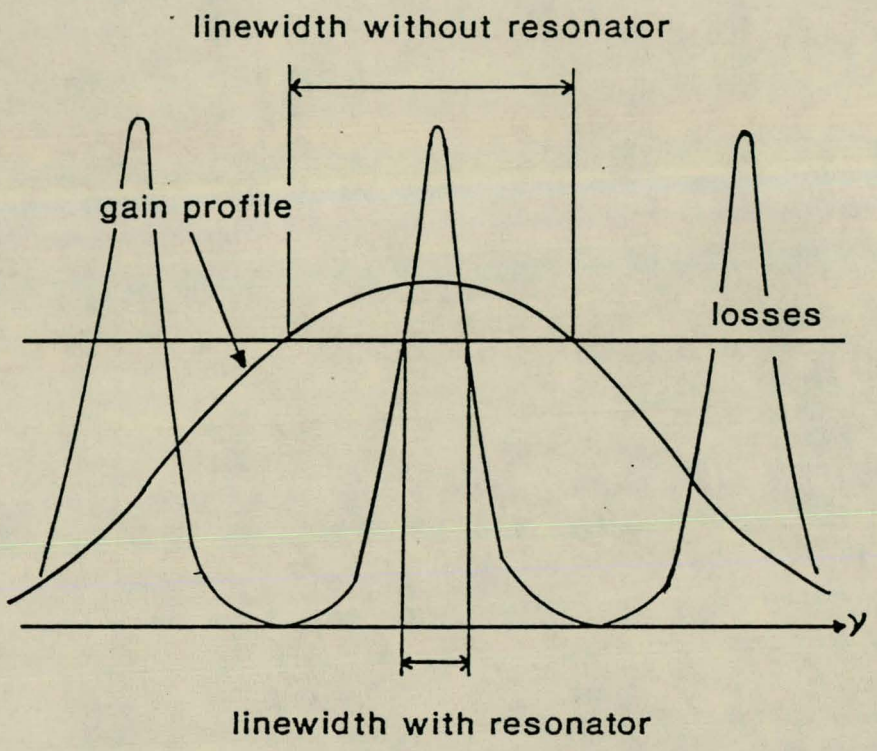

Figure 1.15 Linewidth of Laser

1.4.4 The determination of the position and size of w_o in a resonator

In this section the form of the laser mode to propagate in the resonator will be determined using the geometry of the resonator. Parameters which influences the form of the mode are the radii of the mirrors and the length of the resonator. This information may be used to calculate the position and size of w_o in the resonator. The form of the laser mode is then completely known.

Consider a resonator cavity as shown in figure 1.16.

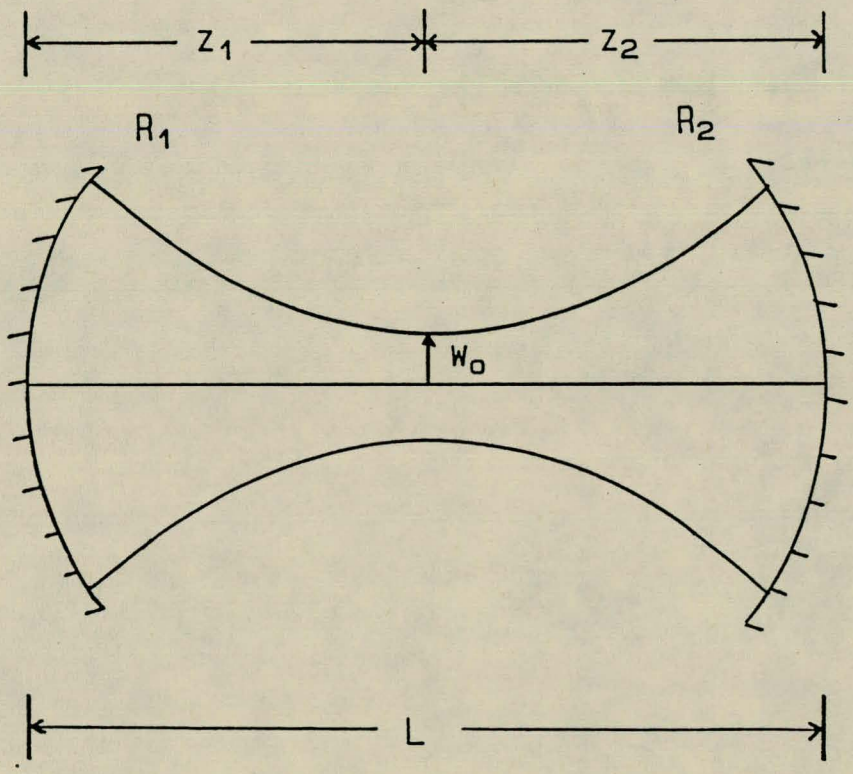

Figure 1.16 Resonator Cavity

The origin of the beam has been chosen at $z = 0$, that is at the position of w_o. From the geometry this means that $z_1 < 0$ and $z_2 > 0$. If L, R_1 and R_2 are known, z_1 and z_2 may be determined as well as the size and position of w_o. L is the length of the resonator and R_1 and R_2 are the radius of the mirrors respectively. The convention is used that both R_1 and R_2 are positive.

Consider the following equations [Mi 88].

$$R(z) = z + \frac{z_R^2}{z} \tag{1.44}$$

$$w(z) = w_o\sqrt{1 + (\frac{z}{z_R})^2} \tag{1.45}$$

The phase front radius R at both mirrors is now determined using equation 1.44 where z becomes z_1 and z_2 respectively.

$$-R_1 = z_1 + \frac{z_R^2}{z_1} \tag{1.46}$$

Because z_1 is negative, a negative sign in the above equation is used otherwise R_1 would be negative.

$$R_2 = z_2 + \frac{z_R^2}{z_2} \tag{1.47}$$

Because z_1 is negative and L is a positive length, L is given by the following equation.

$$L = z_2 - z_1 \tag{1.48}$$

The purpose now is to write z_1 in terms of L, R_1 and R_2. By repeating the same process with z_2 the position of w_o has thus been determined. These information may then be used to determine the size of w_o as will be seen later on.

Rearranging terms in equation 1.46 leads to

$$z_R^2 = z_1(-R_1 - z_1) \tag{1.49}$$

Substitution of this into equation 1.47 gives

$$R_2 = z_2 + \frac{z_1(-R_1 - z_1)}{z_2} \tag{1.50}$$

Substituting $z_2 = z_1 + L$ into above then leads to

$$R_2 = (L + z_1) + \frac{z_1(-R_1 - z_1)}{L + z_1} \tag{1.51}$$

This leads to

$$R_2 = \frac{L^2 + 2z_1L + z_1^2 - z_1R_1 - z_1^2}{L + z_1} \tag{1.52}$$

This may be written as

$$L^2 + 2z_1L - z_1R_1 = R_2L + R_2z_1 \tag{1.53}$$

or

$$z_1(R_2 - 2L + R_1) = L^2 - R_2L \tag{1.54}$$

This gives

$$z_1 = \frac{L^2 - R_2L}{R_2 - 2L + R_1} \tag{1.55}$$

Sometimes it is comfortable to write equations in terms of g parameters where

$$g = 1 - \frac{L}{R} \tag{1.56}$$

z_1 is now written in terms of these g parameters.

This gives [Tr 80]

$$z_1 = \frac{-Lg_2(1 - g_1)}{g_2 + g_1 - 2g_1g_2} \tag{1.57}$$

Using $z_2 = L + z_1$ the following may be obtained.

$$z_2 = \frac{g_1L(1 - g_2)}{g_1 + g_2 - 2g_1g_2} \tag{1.58}$$

The position of w_o has thus be determined and the next step is to determine the size of w_o. This is done by first calculating z_R, because it is connected to w_o as given by equation 1.59 and thus one will be able to calculate w_o from z_R.

$$z_R = \frac{\pi w_o^2}{\lambda} \tag{1.59}$$

One also has

$$R_2 = z_2 + \frac{z_R^2}{z_2} \tag{1.60}$$

Thus

$$\begin{aligned}
z_R^2 &= z_2(R_2 - z_2) \\
&= z_2\left(\frac{L}{1-g_2} - z_2\right) \\
&= \frac{Lz_2}{1-g_2} - z_2^2 \\
&= \frac{L}{1-g_2}\left(\frac{g_1(1-g_2)L}{g_1+g_2-2g_1g_2}\right) - \frac{g_1^2(1-g_2)^2L^2}{(g_1+g_2-2g_1g_2)^2} \\
&= \frac{\frac{L}{1-g_2}(g_1L(1-g_2)(g_1+g_2-2g_1g_2)) - g_1^2(1-g_2)^2L^2}{(g_1+g_2-2g_1g_2)^2} \\
&= \frac{L^2(g_1(g_1+g_2-2g_1g_2) - g_1^2(1-g_2)^2)}{(g_1+g_2-2g_1g_2)^2} \\
&= \frac{L^2(g_1^2+g_1g_2-2g_1^2g_2-g_1^2-g_1^2g_2^2+2g_1^2g_2)}{(g_1+g_2-2g_1g_2)^2}
\end{aligned} \tag{1.61}$$

Finally

$$z_R^2 = \frac{L^2g_1g_2(1-g_1g_2)}{(g_1+g_2-2g_1g_2)^2} \tag{1.62}$$

Using $w_o^2 = z_R\lambda/\pi$ one may obtain

$$w_o^2 = \frac{L\sqrt{g_1g_2(1-g_1g_2)}}{g_1+g_2-2g_1g_2}\frac{\lambda}{\pi} \tag{1.63}$$

The beam spot sizes at both mirrors, w_1 and w_2 may be calculated as follows.

$$w_1^2 = w_o^2[1 + (\frac{z_1}{z_R})^2] \tag{1.64}$$

By now substituting the equations for z_1 and z_R the following equation for w_1^2 may be obtained [Tr 80].

$$w_1^2 = \frac{L\lambda}{\pi}\sqrt{\frac{g_2}{g_1(1-g_1g_2)}} \tag{1.65}$$

To determine w_2, g_1 and g_2 must be interchanged which gives

$$w_2^2 = \frac{L\lambda}{\pi}\sqrt{\frac{g_1}{g_2(1-g_1g_2)}} \tag{1.66}$$

The above results may to used to determine whether a resonator is stable or not as will be shown in the next section. It is also very important that the sign of the mirror radii must be correct especially in complicated optical configurations where a number of mirrors are used to manipulate the beam. To determine the position of w_o and also the stability of a resonator, the mirror signs are of importance. Before looking at the resonator stability, a convention in which the mirror sign is determined will first be discussed. This convention relates closely to the phase front sign convention used in Gaussian beam propagation.

1.4.5 Mirror sign convention

The sign of the mirror R is determined by looking at the mirror in the same direction a wave is propagating having the same mirror radius. If this direction is in the same direction as the wave propagating onto the mirror, then the mirror radius has the same sign as the phase front radius of the imaginary wave. If the direction is reversed, the mirror sign is just the opposite. This is illustrated in the following examples.

When looking at figure 1.17, one says the mirror radius R is positive because the sign of the phase front radius is positive. In the same manner the radius of the mirror shown in figure 1.18 is also positive, because one is looking from w_o in the propagation direction and the phase front is convex and thus positive.

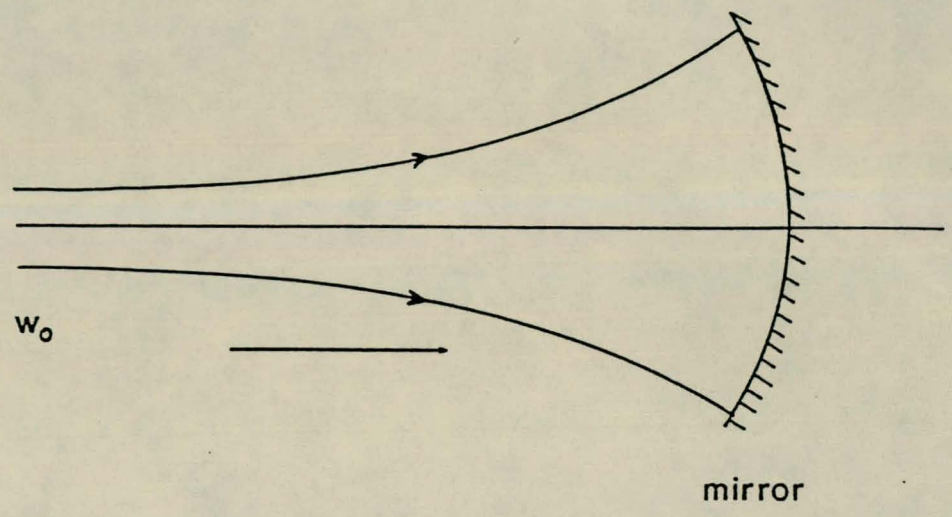

Figure 1.17 Resonator Sign convention

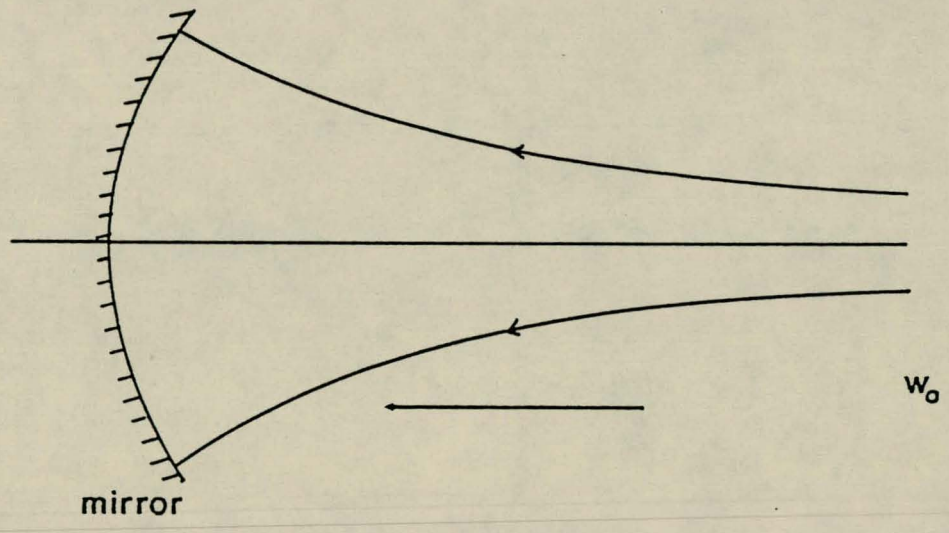

Figure 1.18 Resonator Sign Convention

In the example shown in figure 1.19, the mirror sign is negative because the wave propagating has a phase front similar to that of the mirror is shown by the dotted line with its w_o value to the right of the mirror. If one now looks from w_o to the mirror, one looks against the beam

coming from the left side to the mirror, so that the beam sees a mirror with negative radius sign.

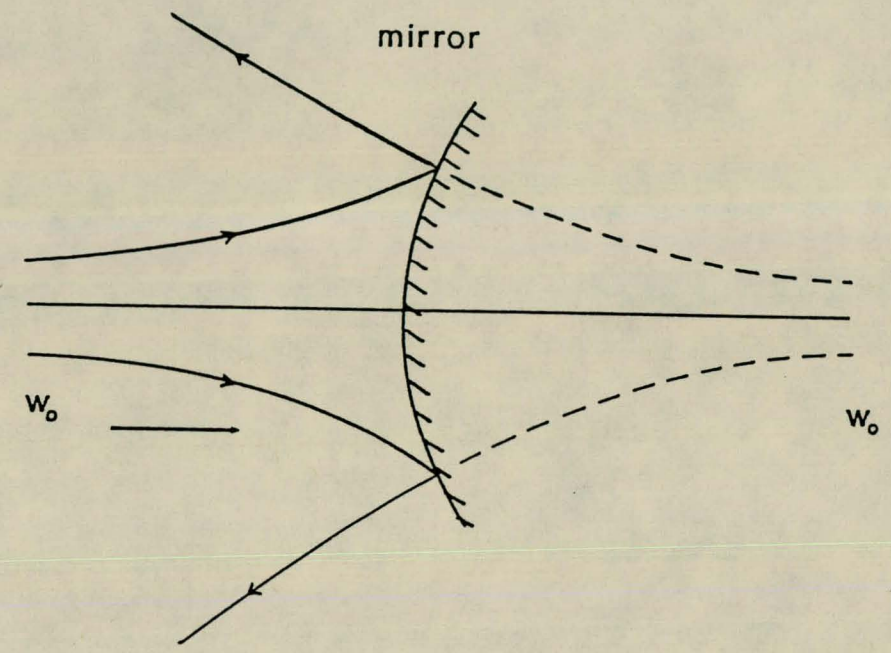

Figure 1.19 Resonator Sign Convention

For the specific case of resonators, the convention may also be written as follows.

The radius R of a mirror is positive when the center of curvature lies in the direction of the other mirror, and negative otherwise.

1.4.6 Resonator stability

Consider the stability of a resonator. There are different ways to calculate the stability requirements and in this case it will be derived from the relations for the spot sizes on the mirrors w_1 and w_2.

From equations 1.65 and 1.66, one is able to see that both spot sizes are not defined when

$$g_1 g_2 = 0 \tag{1.67}$$

or

$$g_1 g_2 = 1 \tag{1.68}$$

This now leads to the stability requirement that

$$0 \leq g_1 g_2 \leq 1 \tag{1.69}$$

In terms of the length and radii one has

$$0 \leq (1 - \frac{L}{R_1})(1 - \frac{L}{R_2}) \leq 1 \tag{1.70}$$

From this one notes the importance of the correct mirror sign to determine the resonator stability. Note also that the length L also plays an important role.

Following the convention, the mirror signs for the following resonator types are determined in order to determine the stability. Consider first a flat resonator. It is difficult to apply the convention in this case because the mirrors are not curved, but is not necessary because both g parameters are equal to 1. One then has that the stability requirement is just satisfied and as already been mentioned from a geometrical point of view, this resonator is critically stable and only a slight deviation of one of the mirrors causes the resonator to dysfunction as a resonator.

Consider a resonator with one flat mirror (hemispherical) as shown in figure 1.20. One has that R_2 is positive and $g_1 = 0$. For the resonator to be stable the fraction L/R_2 must be smaller than one. This means that for a given mirror, there is a maximum distance between the mirrors for which the resonator is stable. For larger values of L, the resonator becomes unstable.

Consider a resonator with two curved mirrors with positive sign. This type of resonator will be very stable because one may choose convenient combinations of L, R_1 and R_2. A resonator where both mirrors have negative sign is always unstable. In figure 1.20 the first five types of resonators are stable while the last four are types of unstable resonators.

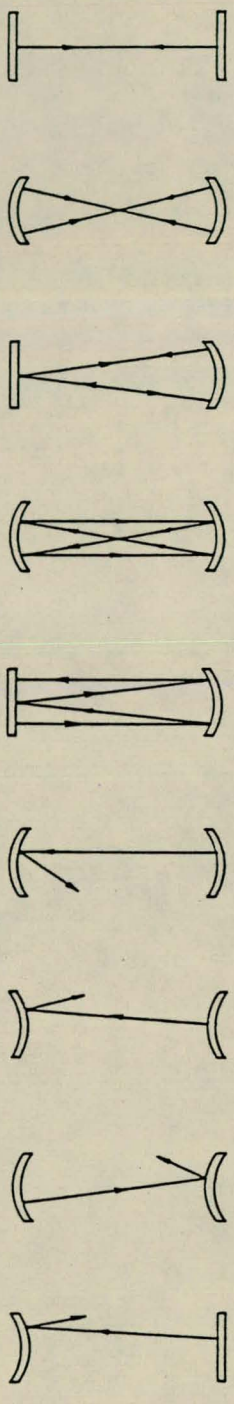

Figure 1.20 Types of Resonators

1.5 The Rayleigh Range

An useful quantity to define is called the Rayleigh range which is given by

$$z_R = \frac{\pi w_o^2}{\lambda} \tag{1.71}$$

Consider the phase front radius given by equation 1.44

$$R = z + \frac{z_R^2}{z}$$

Looking at figure 1.4 where R is plotted versus z, one sees that the graph has a turning point after which R is approximate linear with respect to z, that is that R is equal to z and the wave may be considered as a spherical wave. Thus rays may be considered as straight lines originating from a certain point.

The $z - value$ of the turning point may now be determined. By differentiating R with respect to z, and put the result equal to zero, one finds that the turning point is at the Rayleigh range. This means that for z values later than the Rayleigh value, the wave is approximate spherical and *geometrical optics* may be used to determine distances such as focal distances. At smaller z values, the laws for Gaussian propagation must be used to obtain distances, because geometrical optics becomes invalid. Remember that the size of w_o may only be determined by using Gaussian laws, because geometrical optics only gives information about distances and w_o is considered as infinitely small.

The above reasoning was tested by calculating of the focal distances for a lens with f = 15cm, at distances in and outside the Rayleigh range by using both geometrical and Gaussian laws of propagation.

The following typical values, $\lambda = 632.8$ nm and $w_o = 0.5$ mm are taken. The Rayleigh range is then given by $z_R = 1.241$ cm.

Distances 0.5, 1, 2 and 10 cm have been chosen which is the distances at which a lens is placed from the position of w_o (s), and the position at which the beam is focussed (s'), was calculated using both approaches.

Table 1.			
Distance(s)	Geometrical(s')	Gaussian(s')	Percentage error
0.5 cm	0.52 cm	1.38 cm	62.3
1.0 cm	1.07 cm	1.70 cm	37.1
2.0 cm	2.31 cm	2.70 cm	14.4
10.0 cm	30.0 cm	29.3 cm	2.33

As can be seen from Table 1, geometrical optics gives good results for z values larger than the Rayleigh value. For quick calculations the laws of geometrical optics may thus be used to determine certain distances for large enough z values.

The Rayleigh range is also important when designing a resonator using mirrors with certain curvature. The radius of such a mirror is spherical by design, but the phase front *is not* spherical, and is only approximately spherical for distances larger than the Rayleigh distance.

The conditions in a resonator is that the phase front radius must equal the radius of the mirror in order to reflect the phase front without distortion and this is only satisfied at z-values larger than z_R, because only then the phase front is equal to R to a good approximation.

It may then for example prove difficult to design a very short laser in the infrared regions because the Rayleigh distances is quite large. In the ultraviolet region there will be no such difficulties.

1.6 Transformation of Gaussian beam by a lens

A lens is often used to produce a beam with a certain diameter and phase front curvature. This is necessary when one wants to inject the laser beam into a optical structure such as a waveguide or a Raman cell.

If the lens is ideal, the transformation does not change the modal structure of the beam, that is a Gaussian mode stays the same mode and a higher order mode remains a higher order mode

with the same mode numbers [Ko 66]. The lens however does change $R(z)$ and $w(z)$.

Assume an incoming wave with phase front radius R_1. If an ideal thin lens is placed in the path of the phase front, in such a manner that the lens is immediately to the right of the phase front R_1, the lens changes the radius R_1 into a radius R_2 immediately to the right of the lens. This situation is shown in figure 1.21.

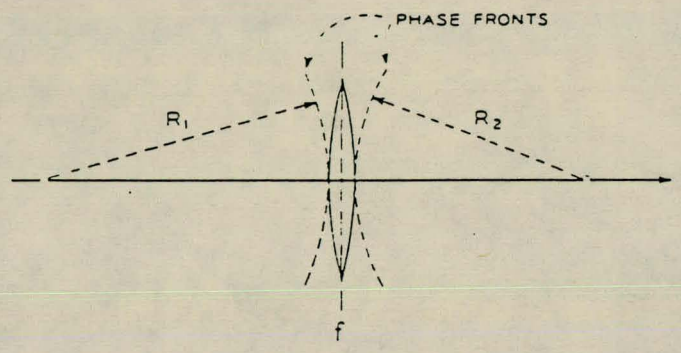

Figure 1.21 Focussing of Gaussian beam by lens

The following relation exist between R_1, R_2 and f [Ko 66].

$$\frac{1}{R_2} = \frac{1}{R_1} - \frac{1}{f} \tag{1.72}$$

In a practical situation a beam with waist w_o propagates in the positive z-direction. One now wants to determine the new waist, w_o' and the position of the waist z', the beam will be focussed to if a lens with focal length f, is placed at a distance z from w_o.

In this situation the following three aspects need to be considered.

1. The propagation of the beam towards the lens.
2. The change in phase front radius imposed by the lens.
3. The propagation of the beam after the lens.

From Appendix A, the value of the beam diameter w at the position of the lens is given by

$$w = w_o\sqrt{1 + (\frac{\lambda z}{\pi w_o^2})^2} \tag{1.73}$$

and the phase front radius at the lens is given by

$$R = z + \frac{1}{z}(\frac{\pi w_o^2}{\lambda})^2 \tag{1.74}$$

If an ideal thin lens is considered one may say that the beam radius after the lens w' is the same as the beam radius w before the lens.

It is shown in Appendix B that

$$w'_o = \frac{w'}{\sqrt{1 + (\frac{\pi w'^2}{\lambda R'})^2}} \tag{1.75}$$

$$z' = \frac{R'}{1 + (\frac{\lambda R'}{\pi w'^2})^2} \tag{1.76}$$

From the above two equations it is therefore possible to determine the size the beam is focussed to w'_o, and the distance from the lens at which the beam is focussed, z'.

2

WAVEGUIDE MODES

2.1 Introduction

Waveguides have played an increasingly important role in the industrial world if one thinks of applications of optical fibers in communications, medical industry and in military technology. Here the interest is in waveguides because it is a very suitable apparatus in which nonlinear processes may take place due to the high intensity that may be obtained in a waveguide. For nonlinear processes, such as the stimulated Raman effect, one requires as high an intensity region as possible ignoring saturation effects. This is necessary to obtain a high Raman gain factor.

In the Raman scattering process, the medium is pumped by a laser and therefore good coupling of the laser radiation with the waveguide is necessary to obtain a high transmission as possible through the waveguide. It is therefore important to consider the propagation of radiation in waveguides in terms of waveguide modes, and the coupling of the laser modes to these waveguide modes. This coupling of laser modes with waveguide modes will be considered in chapter 3.

There are different ways in which propagation of radiation in waveguides may be described [Sn 61]. The general one has to solve the wave equation obtained from Maxwell's equations by applying boundary conditions. This gives the different modes which may propagate in the waveguide. Another picture which is very useful may be applied when the dimensions of the guide is very much larger than the wavelength. Diffraction effects are then negligible and the radiation is considered as rays which corresponds to a geometrical approximation. This picture provides easy ways to determine the losses, transmission and other characteristics of the guide.

In this chapter two types of guides will be described, a dielectric medium bounded with a conductor and a dielectric bounded with another dielectric. The last case may be divided into two categories where the outer dielectric has a lower refractive index than the inner and where the inner dielectric has a lower refractive index than the outer. The well-known optical fiber

belongs to the former category and is normally made of glass or quartz bounded by air. In the optical fiber, propagation is by means of total internal reflection from the medium air boundary.

The case where one has air bounded with a medium like glass or quartz is related to the optical fiber category, but with the difference that total internal reflection will not take place as in the optical fiber. Propagation then relies on the good reflection of a wave from a dielectric medium at grazing angles. Fresnel equations may be used to determine the theoretical transmission of such a guide as will be shown in chapter 3. This transmission model is very important because such a guide has been used to investigate the Raman process. Optical fibers cannot be used because it is not possible to put the Raman medium in the fiber, and metallic guides have too large attenuation in the wavelength regions in which the experiment was to be conducted [Gl 70].

Before each one of these type of waveguides will be considered, the general modes that may propagate in a waveguide will be looked at. The modes are classified as TE, TM and hybrid modes. TE modes have no electric field component in the direction of propagation and the electric field lies entirely in the transverse direction. TM modes have no magnetic field in the propagation direction. Hybrid modes are combinations of TM and TE modes. Due to different boundary conditions, no hybrid modes are allowed to propagate in a metallic wall guide, but may propagate in a dielectric bounded guide [Sn 61].

One may also interpreted these modes as ray paths a shown in figure 2.1. Due to different grazing angles one would expect higher order modes, which have larger grazing angles than the lower order modes to have larger losses than the lower order modes [Ka 60]. This also follows when the wave equation is solved and the propagation characteristics of the various modes are determined. One then finds that higher order modes have larger losses than lower order modes [Ka 60].

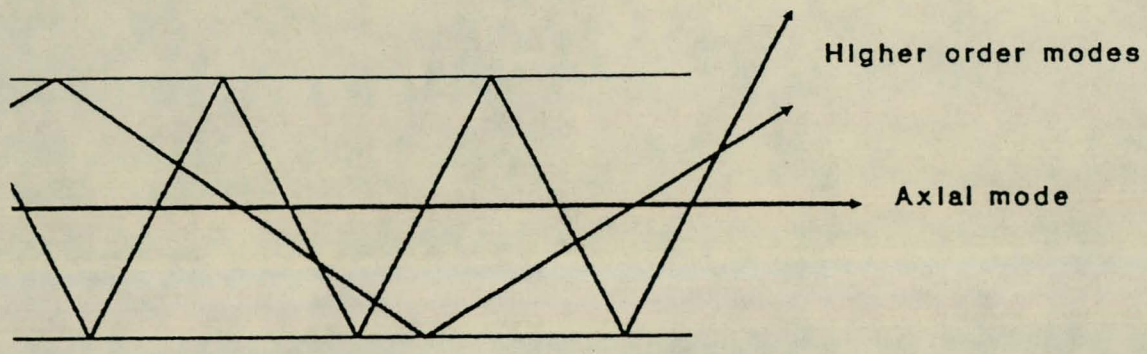

Figure 2.1 Mode Representation

2.2 The wave equation

Maxwell's equations are used to determine the wave equation which must fit the boundary conditions. For simplicity only straight and uniform waveguides are to be considered. A propagation factor given by $\exp(jwt - \gamma z)$ is assumed. The factor γ gives information about the degree of attenuation of the guide, and the phase velocity and group velocity of the waveguide modes.

Maxwell's equations in dielectric media are given by [Ra 65]:

$$\nabla.\mathbf{D} = \rho \tag{2.1}$$

$$\nabla.\mathbf{B} = 0 \tag{2.2}$$

$$\nabla \times \mathbf{E} = -\frac{\partial \mathbf{B}}{\partial t} \tag{2.3}$$

$$\nabla \times \mathbf{H} = \mathbf{J} + \frac{\partial \mathbf{D}}{\partial t} \tag{2.4}$$

where $\mathbf{D} = \epsilon\mathbf{E}$ and $\mathbf{B} = \mu\mathbf{H}$.

A medium where $\rho = 0$ and $J = 0$ is considered.

The Maxwell's equations now reduce to :

$$\nabla.\mathbf{D} = 0 \tag{2.5}$$

$$\nabla.\mathbf{B} = 0 \tag{2.6}$$

$$\nabla \times \mathbf{E} = -\frac{\partial \mathbf{B}}{\partial t} \tag{2.7}$$

$$\nabla \times \mathbf{H} = \epsilon \frac{\partial \mathbf{E}}{\partial t} \tag{2.8}$$

By differentiating the above equations one obtains

$$\nabla^2\mathbf{E} = \epsilon\mu \frac{\partial^2 \mathbf{E}}{\partial^2 t} \tag{2.9}$$

$$\nabla^2\mathbf{H} = \epsilon\mu \frac{\partial^2 \mathbf{H}}{\partial^2 t} \tag{2.10}$$

Assuming a time dependence of the electric and magnetic fields of the form $\exp(jwt)$ the above two equations are used to obtain

$$\frac{\partial^2 \mathbf{E}}{\partial^2 t} = -w^2\mathbf{E} \tag{2.11}$$

This results in

$$\nabla^2\mathbf{E} = -\epsilon\mu w^2\mathbf{E} \tag{2.12}$$

or

$$\nabla^2\mathbf{E} = -k^2\mathbf{E} \tag{2.13}$$

where $k = w/v = w\sqrt{\epsilon\mu}$

In the same manner

$$\nabla^2\mathbf{H} = -k^2\mathbf{H} \tag{2.14}$$

∇^2 is now divided in two parts to be able to write all the transverse field components in terms of the z component.

$$\nabla^2\mathbf{E} = \nabla_{xy}^2\mathbf{E} + \frac{\partial^2\mathbf{E}}{\partial z^2} \tag{2.15}$$

Combining

$$\frac{\partial^2\mathbf{E}}{\partial z^2} = \gamma^2\mathbf{E} \tag{2.16}$$

with equation 2.13 and equation 2.15, the following result may be obtained.

$$\nabla_{xy}^2\mathbf{E} = -(\gamma^2 + k^2)\mathbf{E} \tag{2.17}$$

$$\nabla_{xy}^2\mathbf{H} = -(\gamma^2 + k^2)\mathbf{H} \tag{2.18}$$

It is useful to write the Maxwell's equations in rectangular coordinates, thus dividing the electric field in E_x, E_y and E_z.

From Appendix C the electric field components may now be written as

$$\nabla \times \mathbf{E} = -jw\mu\mathbf{H} \tag{2.19}$$

$$\frac{\partial E_z}{\partial y} + \gamma E_y = -jw\mu H_x \tag{2.20}$$

$$-\gamma E_x - \frac{\partial E_z}{\partial x} = -jw\mu H_y \tag{2.21}$$

$$\frac{\partial E_y}{\partial x} - \frac{\partial E_x}{\partial y} = -jw\mu H_z \tag{2.22}$$

The magnetic field components are given by

$$\nabla \times \mathbf{H} = jw\epsilon\mathbf{E} \tag{2.23}$$

$$\frac{\partial H_z}{\partial y} + \gamma H_y = jw\epsilon E_x \tag{2.24}$$

$$-\gamma H_x - \frac{\partial H_z}{\partial x} = jw\epsilon E_y \tag{2.25}$$

$$\frac{\partial H_y}{\partial x} - \frac{\partial H_x}{\partial y} = jw\epsilon E_z \tag{2.26}$$

It is important to remember that E_x, H_x, and all the other are functions of x and y only. The z-dependence has already been taken care of in the assumed propagation factor $\exp(jwt - \gamma z)$.

If one consider the previous equations, one sees that it is possible to solve E_x, E_y, H_x or H_y in terms of E_z and H_z by elimination.

The components are derived in Appendix D and are given by

$$H_x = (\gamma^2 + k^2)^{-1}(jw\epsilon\frac{\partial E_z}{\partial y} - \gamma\frac{\partial H_z}{\partial x}) \tag{2.27}$$

$$H_y = -(\gamma^2 + k^2)^{-1}(jw\epsilon\frac{\partial E_x}{\partial x} + \gamma\frac{\partial H_z}{\partial y}) \tag{2.28}$$

$$E_x = -(\gamma^2 + k^2)^{-1}(\gamma\frac{\partial E_z}{\partial x} + jw\mu\frac{\partial H_z}{\partial y}) \tag{2.29}$$

$$E_y = (\gamma^2 + k^2)^{-1}(-\gamma\frac{\partial E_z}{\partial y} + jw\mu\frac{\partial H_z}{\partial x}) \tag{2.30}$$

2.3 GENERAL WAVE TYPES

General solutions are now derived for guides which will later be applied in specific cases. This solutions may then be applied to any type of guide using the appropriate boundary conditions.

2.3.1 Rectangular coordinates

In rectangular coordinates the wave equation is given by

$$\nabla_{xy}^2 E_z = -k_c^2 E_z \tag{2.31}$$

where $k_c = \sqrt{\gamma^2 + k^2}$. The assumption is now made that the z component of the field may be written as the product of two functions X and Y which are functions of x and y respectively [Ra 65].

$$TM\ modes : E_z = XY \tag{2.32}$$

$$TE\ modes : H_z = XY \tag{2.33}$$

where

$$X = A \cos k_x x + B \sin k_x x \tag{2.34}$$

$$Y = C \cos k_y y + D \sin k_y y \tag{2.35}$$

$$k_x^2 + k_y^2 = k_c^2 \tag{2.36}$$

2.3.2 Cylindrical coordinates

In cylindrical coordinates, the wave equation may be written as

$$\nabla_{xy}^2 E_z = \nabla_{r\phi}^2 E_z = \frac{\partial^2 E_z}{\partial r^2} + r^{-1}\frac{\partial E_z}{\partial r} + r^{-2}\frac{\partial^2 E_z}{\partial \phi^2} \tag{2.37}$$

This gives the following result

$$\frac{\partial^2 E_z}{\partial r^2} + r^{-1}\frac{\partial E_z}{\partial r} + r^{-2}\frac{\partial^2 E_z}{\partial \phi^2} = -k_c^2 E_z \tag{2.38}$$

By following the same steps as for the Cartesian coordinates case, a general result for E_z may be determined [Ra 65].

$$TM\ modes : E_z = RF_\phi \tag{2.39}$$

$$TE\ modes : H_z = RF_\phi \tag{2.40}$$

where

$$R = AJ_\nu(k_c r) + BN_\nu(k_c r) \tag{2.41}$$

$$F = C\cos(\nu\phi) + D\sin(\nu\phi) \tag{2.42}$$

J_ν is a Bessel function of the first kind and of order ν. N_ν is a Bessel function of the second kind and of order ν.

The other components E_ϕ, E_r, H_ϕ and H_r are given by [Ra 65]

$$E_r = -\frac{1}{k_c^2}[\gamma\frac{\partial E_z}{\partial r} + \frac{jw\mu}{r}\frac{\partial H_z}{\partial \phi}] \tag{2.43}$$

$$E_\phi = \frac{1}{k_c^2}[-\frac{\gamma}{r}\frac{\partial E_z}{\partial \phi} + jw\mu\frac{\partial H_z}{\partial r}] \tag{2.44}$$

$$H_r = \frac{1}{k_c^2}[\frac{jw\epsilon}{r}\frac{\partial E_z}{\partial \phi} - \gamma\frac{\partial H_z}{\partial r}] \tag{2.45}$$

$$H_\phi = -\frac{1}{k_c^2}[jw\epsilon\frac{\partial E_z}{\partial r} + \frac{\gamma}{r}\frac{\partial H_z}{\partial \phi}] \tag{2.46}$$

2.4 Metallic bounded rectangular waveguide

The general solution obtained will now be applied to determine the electric field configurations in a rectangular metallic guide. First the boundary conditions imposed by the conductor boundary are to be considered. At the surface of a perfect conductor the following boundary conditions exist [Ra 65].

$$E_t = 0 \tag{2.47}$$

$$B_n = 0 \tag{2.48}$$

The transverse component of the electric field and the normal component of the magnetic field must vanish at the boundary of a perfect conductor. In practice this assumption is valid in most cases. The geometry of the rectangular waveguide is shown in figure 2.2. Solutions for TE and TM modes are now obtained by applying different boundary conditions.

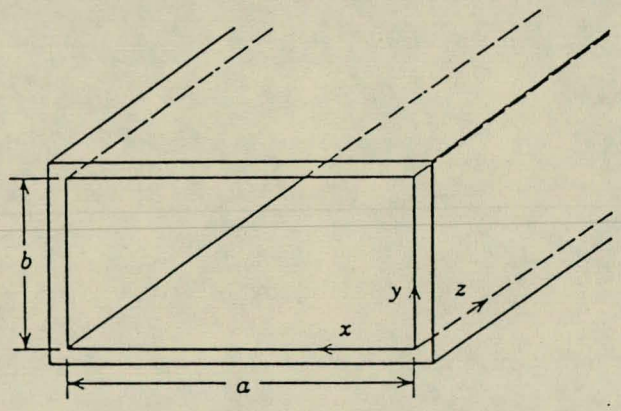

Figure 2.2 Rectangular waveguide

2.4.1 Transverse Magnetic Waves

For TM waves E_z are given by XY and the boundary conditions require that E_z must be zero at $x = 0$ and at $y = 0$. For this boundary condition to be valid, there may only be sine terms present in the solution given by equation 2.32. Other components are derived by using Appendix D.

E_z are thus given by

$$E_z = A \sin k_x x \sin k_y y \tag{2.49}$$

There is another set of boundary conditions which require that E_z must also be zero at $x = a$ and at $y = b$ where a and b are shown in figure 2.2.

This gives the following discrete values of k_x and k_y given by

$$k_x = \frac{m\pi}{a} \qquad k_y = \frac{n\pi}{b} \tag{2.50}$$

This discrete values of k_x define a set of TM modes where m and n are integral values assuming values from zero to infinite.

The following relation for k may be obtained [Ra 65].

$$(k_c)_{mn} = \sqrt{k_x^2 + k_y^2} = \sqrt{(m\pi/a)^2 + (n\pi/b)^2} \tag{2.51}$$

Solutions for the wave equation 2.32 are valid only for certain values of k_c and must also satisfy the boundary conditions. These values of k_c are called the *eigenvalues* of the problem and each of them determines a particular TM mode. Consider now the propagation constant

$$\gamma = \sqrt{k_c^2 - k^2} \tag{2.52}$$

The above form of γ determines frequencies at which the wave may not propagate. If $k < k_c$, γ is real for a perfect dielectric and for $k > k_c$, then γ is imaginary and γ is zero for $k = k_c$. If γ is real then a mode will not propagate and so $\gamma = 0$ determines a cutoff value for the mode which relates to the frequency.

At cutoff one has that

$$k = w\sqrt{\mu\epsilon} = 2\pi f_c\sqrt{\mu\epsilon} = 2\pi/\lambda_c = k_c \tag{2.53}$$

where f_c is called the cutoff frequency.

γ may now be written in terms of f and f_c [Ra 65].

$$\gamma = \alpha = k_c\sqrt{1-(f/f_c)^2}, \qquad f < f_c \tag{2.54}$$

$$\gamma = j\beta = jk\sqrt{1-(f_c/f)^2}, \qquad f > f_c \tag{2.55}$$

The phase velocity is given by [Ra 65]

$$v_p = w/\beta = v[1-(f_c/f)^2]^{-1/2} \tag{2.56}$$

The group velocity is given by [Ra 65]

$$v_g = \frac{dw}{d\beta} = v[1-(f_c/f)^2]^{1/2} \tag{2.57}$$

The relations obtained above are only valid for an ideal guide in which the conductor and dielectric are considered perfect. Only modes with frequencies larger than the cutoff frequency may propagate. The phase velocity is infinite and the group velocity is zero at cutoff. As the frequency increases far above the cutoff frequency, both the phase and group velocities approach the velocity of light in the dielectric. For the above calculations to be valid, k_c must be real [Ra 65]. If E_z is found by applying the boundary conditions, the transverse components of the electric as well as the magnetic field may be calculated from equations 2.27 to 2.30.

The following relations for the cutoff wavelength and frequency may now be obtained [Ra 65].

$$(\lambda_c)_{mn} = \frac{2\pi}{k_c} = \frac{2ab}{\sqrt{(mb)^2+(na)^2}} \tag{2.58}$$

$$(f_c)_{mn} = \frac{k_c}{2\pi\sqrt{\mu\epsilon}} = \frac{1}{2\sqrt{\mu\epsilon}}\sqrt{(m/a)^2+(n/b)^2} \tag{2.59}$$

2.4.2 Transverse Electric Modes

The general solution for H_z is given by XY, where X and Y are well-known. A different boundary condition now applies which state that $\partial H_z/\partial n$ must be zero where n is perpendicular on the boundary.

$$\frac{\partial H_z}{\partial x} = 0 \tag{2.60}$$

$$\frac{\partial H_z}{\partial y} = 0 \tag{2.61}$$

at the boundary where $x = 0$ and $y = 0$.

This means that in the derivative of H_z only sine terms may be present to fulfill the boundary requirement as stated above. The only cosine terms may be present in H_z which leads to

$$H_z = B \cos k_x x \cos k_y y \tag{2.62}$$

As in the TM case another boundary condition must be satisfied at $x = a$ and at $y = b$. This leads to the same k_x and k_y values for the TE waves as for the TM waves. The cutoff frequency and wavelength are thus the same for both waves.

From this a number of important results may be concluded. There are an infinite number of modes which may propagate which are denoted by the values of m and n. The lowest order TM mode which may propagate is the TM_{11} mode, because if m or n equals to zero, the mode do not exist and is thus not of interest. The lowest order TE mode which may propagate is the TE_{10} mode for which $n = 0$ and $m = 1$. One may argue that TE_{01} is also the lowest order TE mode, but this is only true when $a = b$ and then one has two lowest order modes. The lowest order mode is thus characterized by the lowest k_c value, and from the equation for k_c one sees that for $b < a$, the TE_{01} mode has a larger k_c value than TE_{10} and is classified as a higher order mode than the TE_{10} mode which is then the lowest order mode.

2.4.3 Mode Intensity Profiles

The intensity profiles of TE and TM modes are now considered.

The electric and magnetic field configurations for both cases are given by

$$TE\ modes : H_z = B \cos k_x x \cos k_y y \tag{2.63}$$

$$TM\ modes : E_z = A \sin k_x x \sin k_y y \tag{2.64}$$

E_x and E_y are given by equations 2.27 to 2.30 which gives

$$E_x = E_{xo} \cos k_x x \sin k_y y \tag{2.65}$$

$$E_y = E_{yo} \sin k_x x \cos k_y y \tag{2.66}$$

for TM as well as TE modes.

The resultant electric field E_{res} may now be written as a function of x and y in order to be able to draw intensity profiles of the modes with respect to these axis.

$$E_{res} = \sqrt{E_x^2 + E_y^2 + E_z^2} \tag{2.67}$$

For TM modes one has that

$$E_{res} = \sqrt{E_{xo}(\cos k_x x)^2(\sin k_y y)^2 + E_{yo}(\sin k_x x)^2(\cos k_y y)^2 + E_{zo}(\sin k_x x)^2(\sin k_y y)^2} \tag{2.68}$$

Assume that $E_{xo} = E_{yo} = E_{zo} = E_o$ for simplicity. E_{res} may then be simplified to

$$E_{res} = E_o\sqrt{(\sin k_y y)^2 + (\sin k_x x)^2(\cos k_y y)^2} \tag{2.69}$$

For TE modes one has that

$$E_{res} = E_o\sqrt{(\cos k_x x)^2(\sin k_y y)^2 + (\sin k_x x)^2(\cos k_y y)^2} \tag{2.70}$$

In the following figures the intensity profiles of a few of these modes are plotted as a function of the x coordinate.

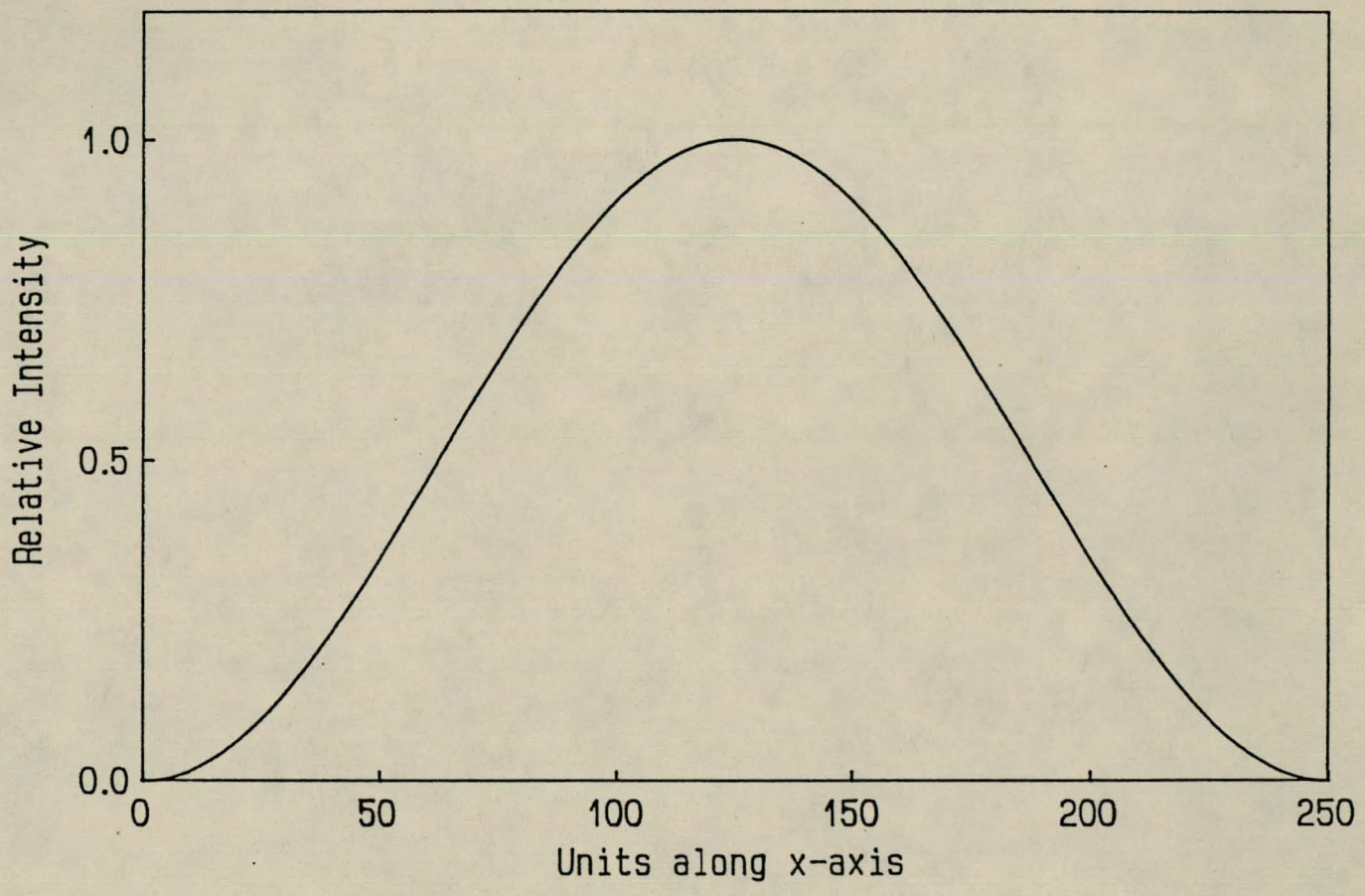

Figure 2.3 Intensity profile of TE_{10} mode

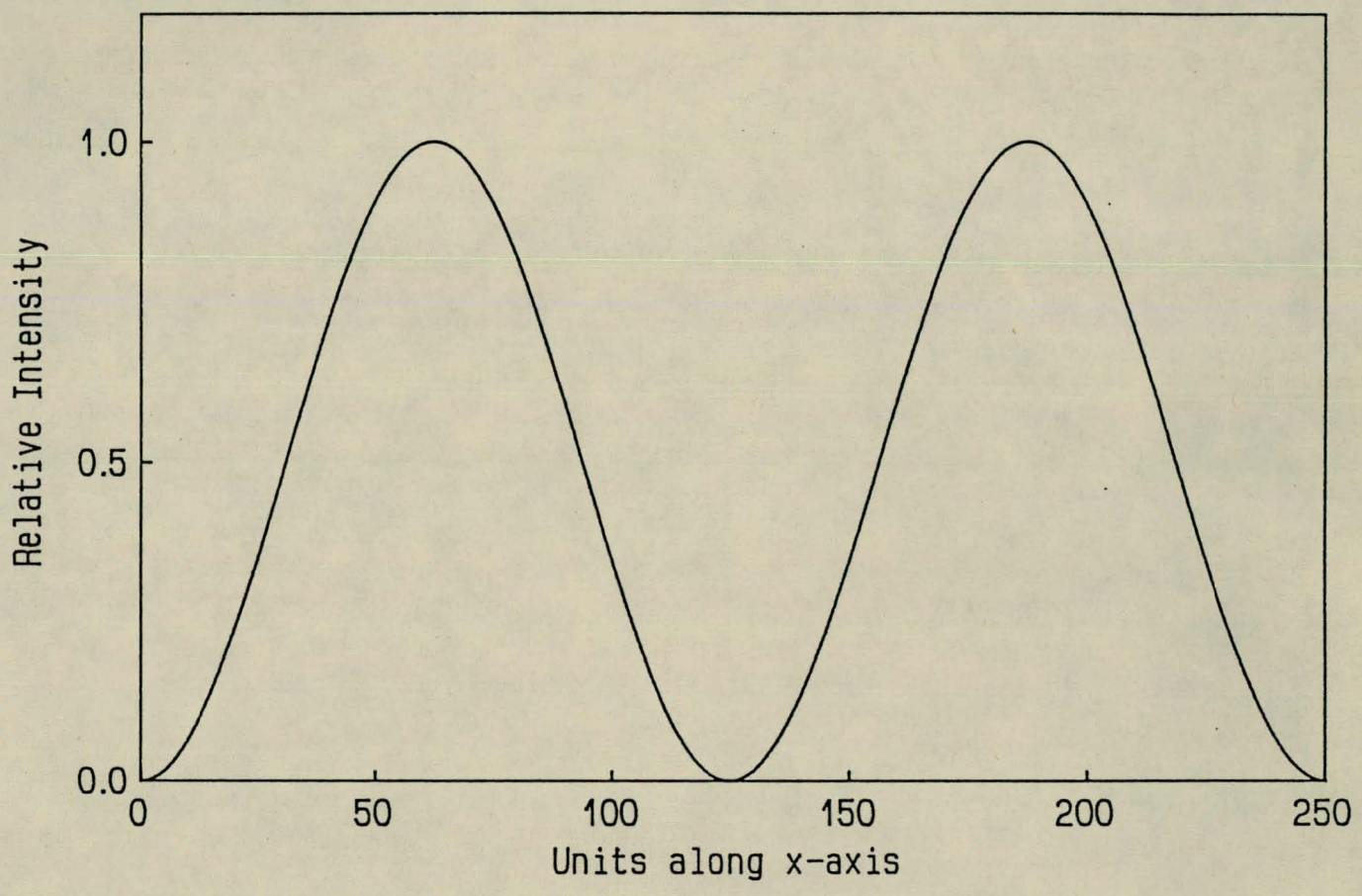

Figure 2.4 Intensity profile of TE_{20} mode

2.5 Fiber Waveguides

Fiber waveguides are made of dielectric material surrounded by material with a lower refractive index so that total internal reflection may take place. Total internal reflection is thus the propagation mechanism for fiber waveguides. Propagation in these guides also is by means of modes like in metal bounded guides, but there may also exist hybrid modes which are linear combinations of TE and TM modes [Sn 61]. These hybrid modes must be chosen to satisfy certain boundary conditions. Modes in fiber waveguides will not be discussed in detail like in the previous case of metal guides. Only practical aspects which have an influence on the transmission of radiation through the fiber will be looked at.

2.5.1 The numerical aperture

This quantity is a measure of the light gathering of the fiber and depends on the refractive index of the fiber and the cladding [He 88]. Most fibers are equipped with cladding to keep the surface of the fiber clean in order to minimize losses. Consider the optical fiber shown in figure 2.5.

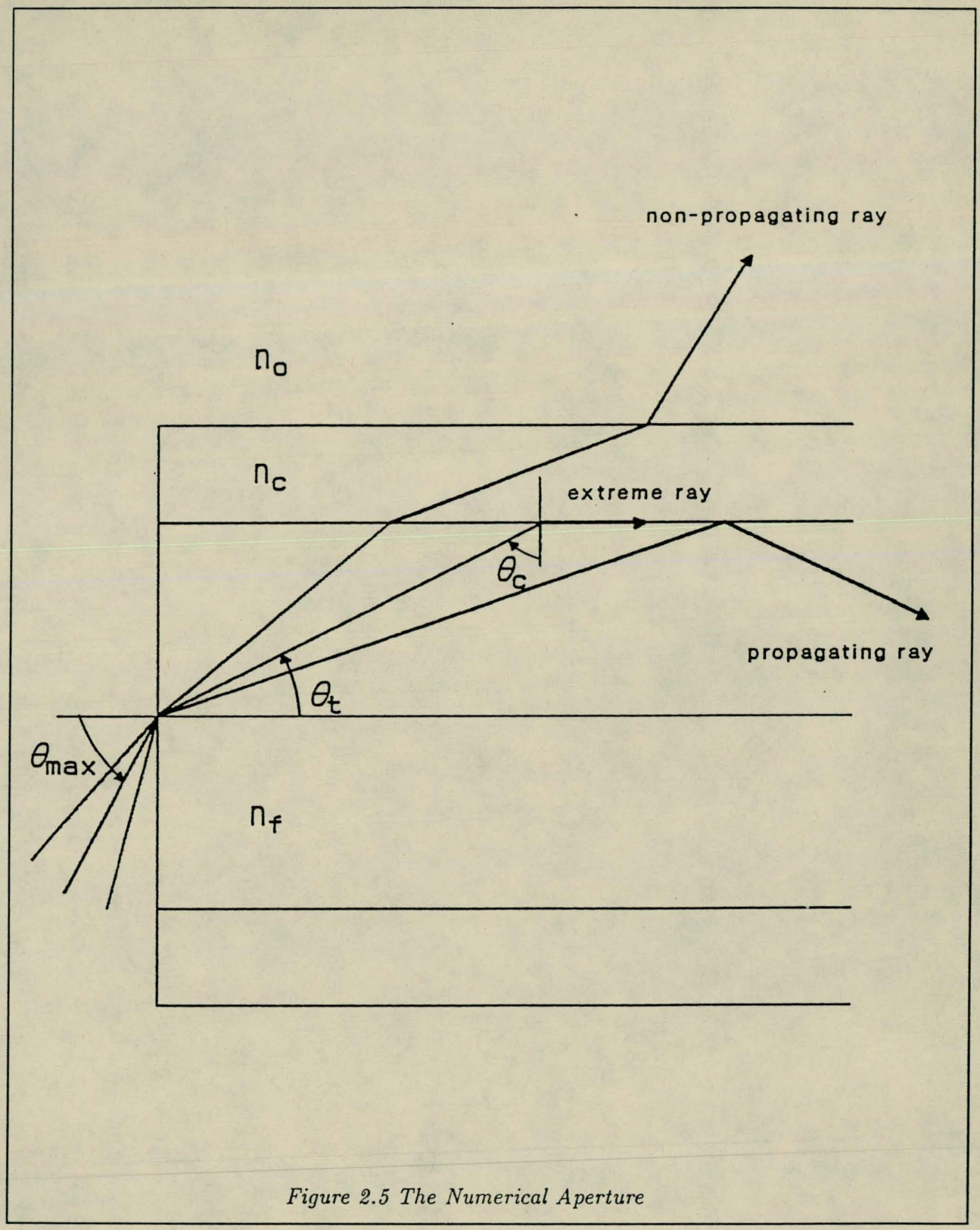

Figure 2.5 The Numerical Aperture

n_f, n_c and n_o are the refractive indices of the fiber, cladding and surrounding medium respectively. Consider a ray striking the fiber surface at a angle θ_i, and the fiber-cladding surface at angle θ.

When θ is equal to the critical angle θ_c one has that

$$\sin\theta_c = \frac{n_c}{n_f} = \sin(90 - \theta_t) \tag{2.71}$$

This means that

$$\frac{n_c}{n_f} = \cos\theta_t \tag{2.72}$$

or

$$\frac{n_c}{n_f} = (1 - \sin^2\theta_t)^{1/2} \tag{2.73}$$

Making use of Snell's law one may obtain the following result.

$$\sin\theta_{max} = \frac{1}{n_o}(n_f^2 - n_c^2)^{1/2} \tag{2.74}$$

From this it is obvious that the light gathering capabilities may be increased by choosing suitable fiber and cladding material. It is though not always preferable to have the light capabilities maximized, because of distortion effects like intermodal dispersion [Sn 83].

2.5.2 Transmission losses

There are various factors which produce transmission losses in a dielectric fiber of which some will be discussed briefly.

Rays that are incident on the face of the fiber with incident angles larger θ_{max} are lost because they are not internally reflected. A very directional source like a laser would thus in fact be better transmitted in the waveguide than for example a LED, because conditions in the waveguide is better for higher transmission.

Imperfections in the core-cladding surface may also prevent some rays to be totally internal reflected at that point and thus causes additional losses. The same rule applies when the fiber is bent very sharply.

There may also be absorption by the core material or impurities and scattering losses.

2.6 Hollow dielectric waveguides

This is an important type of guide for the process of Raman scattering to be investigated. Unlike the previous case, total internal reflection cannot take place and the propagation is by means of good reflection from a boundary. Propagation is also by means of hybrid, TE or TM modes and the highest order modes have the greatest losses [Ma 64]. In chapter 3 the propagation of radiation from a laser through a guide of this type will be discussed in detail and practical factors concerning the transmission will be looked at.

3

HOLLOW WAVEGUIDE TRANSMISSION

3.1 Mode Matching

Laser beams are often injected into certain optical instruments such as interferometers, crystals, waveguides etc. by making use of lenses with certain focal length. Coupling of a laser beam to a waveguide for example critically depends on the beam waist size of the laser at the waveguide entrance with respect to the diameter of the waveguide. The best coupling is obtained when the laser beam is focussed to a certain waist size w_o, at the waveguide entrance. Coupling of the laser modes to the waveguide modes depends on the size of w_o and the diameter of the waveguide. Coupling to the lowest order waveguide modes occurs for a optimum value of w_o/a where a is the diameter of the waveguide. One must thus be able to focus the laser beam to certain w_o values in order to be able to look at the influence of the size of w_o on the coupling of modes.

The theory of mode matching gives the distance at which a lens must be placed from the minimum beam waist of the laser (w_o) in order to focus the laser beam to a chosen w_o'. The sizes of the two waists must be known to determine the mentioned distance. This information together with f of the lens, then determines the positions of the two waists with respect to the lens. The focal length of the lens f must also be larger than a certain characteristic value f_o defined by the waists and the appropriate wavelength. Consider figure 3.1.

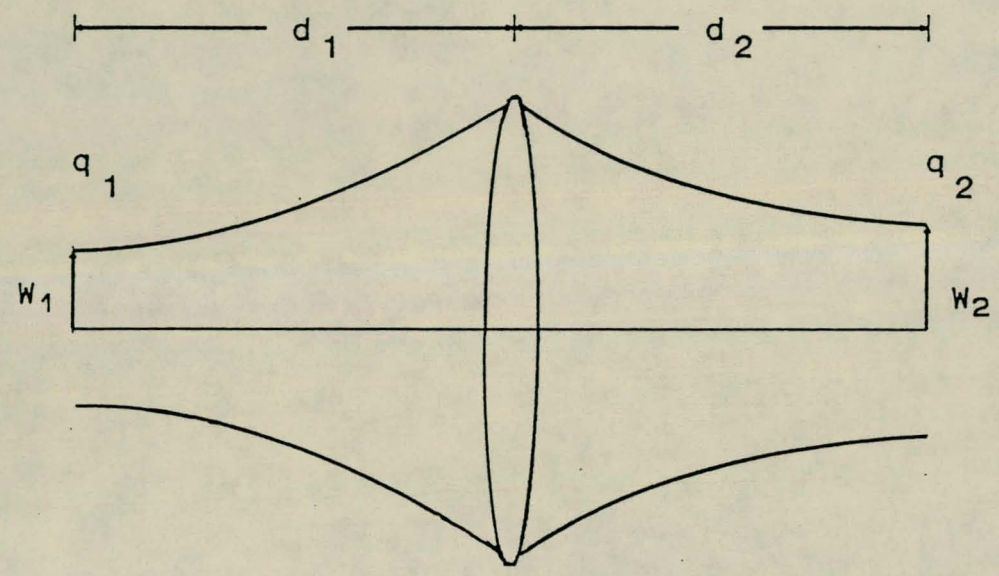

Figure 3.1 Mode Matching

At the waists the parameters q_1 and q_2 are completely imaginary and are given by

$$q_1 = \frac{j\pi w_1^2}{\lambda} \tag{3.1}$$

$$q_2 = \frac{j\pi w_2^2}{\lambda} \tag{3.2}$$

One also has that [Ko 66]

$$\frac{1}{q_2} = \frac{1}{q_1} - \frac{1}{f} \tag{3.3}$$

If q_1 and q_2 are now measured at distances d_1 and d_2 from the lens as shown in figure 3.1, one may obtain [Ko 66]

$$q_2 = \frac{(1 - d_2/f)q_1 + (d_1 + d_2 - d_1 d_2/f)}{-(q_1/f) + (1 - d_1/f)} \tag{3.4}$$

By substituting the given form of q_1 and q_2 into equation 3.4 and equating the imaginary parts the following may be obtained [Ko 66].

$$(d_1 - f)(d_2 - f) = f^2 - f_o^2 \tag{3.5}$$

where $f_o = \pi w_1 w_2 / \lambda$.

By equating the real parts [Ko 66], one obtain

$$\frac{d_1 - f}{d_2 - f} = \frac{w_1^2}{w_2^2} \tag{3.6}$$

By following the rule that $f > f_o$, one chooses a lens with certain f and then determine the distances by using the following two formulas. These last two formulas are determined by combining equations 3.5 and 3.6.

$$d_1 = f \pm \frac{w_1}{w_2}\sqrt{f^2 - f_o^2} \tag{3.7}$$

$$d_2 = f \pm \frac{w_2}{w_1}\sqrt{f^2 - f_o^2} \tag{3.8}$$

From the above result it is clear that f must be larger than f_o.

3.2 Transmission model of a hollow dielectric waveguide

In the previous chapter the propagation of radiation through different types of guides has been discussed. An important result was that lower order modes have the least attenuation in most cases. To obtain good transmission of a laserbeam through a waveguide, it is therefore essential that coupling of the laser mode, usually the TEM_{00} mode, must occur with the lowest order waveguide modes. In this section the parameters which influences this coupling efficiency will be investigated. As already been have mentioned in the section on mode matching, the beam size to which the laser beam is focussed, is an important parameter. Fresnel equations of wave reflection on a dielectric wall may be used to determine the power transmission through the guide.

One may also use a model in which the incident TEM_{00} mode is expanded into all the different waveguide modes and the expansion coefficients are determined [He 88]. These coefficients depend on the direction of the incoming field with respect to the waveguide opening, the geometry

of the waveguide opening and also on the form of the incident laser mode. This model involves complicated mathematics and will not be discussed here.

3.2.1 Model assumptions and approximations

The model to be derived is restricted to guides having diameters much larger than a wavelength and to low-order low-loss modes which propagation constants are nearly equal to the free-space propagation constant [Cr 82]. The wave theory of such guides was first derived by Marcatili and Schmeltzer [Ma 64]. Diffraction effects at the waveguide entrance are assumed to be ignorable.

The model also uses approximations of Gaussian beams as if the Gaussian beam consists of a bundle of rays. Gaussian parameters are given by

$$I(\rho, z) = I(o, z) \exp\left(-\frac{\rho^2}{r^2}\right) \tag{3.9}$$

$$r^2(z) = r_o^2[1 + (\frac{z}{kr_o})^2] \tag{3.10}$$

$$R(z) = z[1 + (\frac{kr_o^2}{z})^2] \tag{3.11}$$

As one may see, these equations are a bit different than the equations previously used. In this case the parameter ρ gives the variation in radial distance from the axis and r is the beam parameter defined as the radial distance from the axis at which the intensity has decreased from its maximum value to $1/e$ of the maximum value. In relation with previous work one has that $w = r\sqrt{2}$.

An asymptotic approximation is used in which every curved ray path and its asymptote is coincident as shown in figure 3.2.

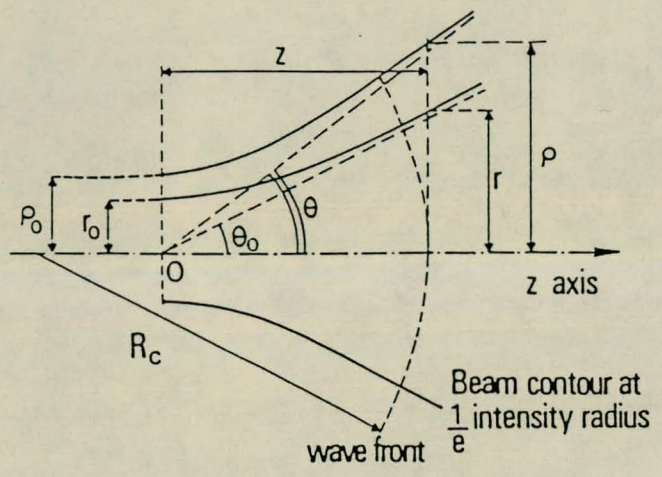

Figure 3.2 Asymptotic Approximation

$$r = \frac{z}{kr_o} \tag{3.12}$$

$$R = z \tag{3.13}$$

Secondly it is assumed that the beam divergence is very small so that

$$\tan(\theta) \simeq \theta \tag{3.14}$$

This is a paraxial approximation and it leads to

$$\theta_o = \frac{r}{z} = \frac{1}{kr_o} \tag{3.15}$$

One also has that

$$\frac{\theta}{\theta_o} = \frac{\rho}{r} \tag{3.16}$$

Using the following relation and the two previous equations the following result may be obtained.

$$\frac{\rho_o}{r_o} = \frac{\rho}{r} \tag{3.17}$$

$$\theta = \frac{\rho_o}{kr_o^2} \tag{3.18}$$

In the model the laser beam is focussed to a minimum beam waist r_o, at the entrance of the waveguide. One assumes that the Gaussian beam and the waveguide has the same propagation axis and that there are no losses due to absorption, scattering etc. The only losses are due to Fresnel losses.

Consider a hollow dielectric waveguide with inner radius R and length L. The refractive index of the wall dielectric material is denoted by ν. If P is the total power of the Gaussian beam and P_s is the power at the exit, the transmission fraction is defined as

$$T = \frac{P_s}{P} \tag{3.19}$$

The incident Gaussian beam is divided into different beams each with power dP. At the waist one has that

$$dP = I(\rho_o, o)\rho_o d\rho_o d\phi \tag{3.20}$$

$$dP = I_o \exp(-\frac{\rho_o^2}{r_o^2})\rho_o d\rho_o d\phi \tag{3.21}$$

If one integrates the previous equation one obtain [Cr 82]

$$\begin{aligned} P &= \int_0^{\infty}\int_0^{2\pi} I_o \exp(-\frac{\rho_o^2}{r_o^2})\rho_o d\rho_o d\phi \\ &= \pi I_o r_o^2 \end{aligned} \tag{3.22}$$

Because the Gaussian beam extends to infinite in the transverse direction, only a portion of the power P could be coupled into the waveguide. At the waist this is given by [Cr 82]

$$\begin{aligned} P_E &= \int_0^{R}\int_0^{2\pi} I_o \exp(-\frac{\rho_o^2}{r_o^2})\rho_o d\rho_o d\phi \\ &= \pi I_o r_o^2[1 - \exp(-\frac{R^2}{r_o^2})] \end{aligned} \tag{3.23}$$

Fresnel equations are now used to determine the reflection of these elementary beams of the dielectric wall surface.

Consider the propagation of a ray as shown in figure 3.3 with the 2 different electric field polarizations.

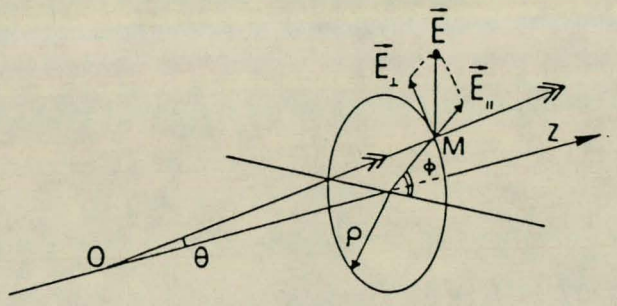

Figure 3.3 Electric field polarisation

The two reflection coefficients responds to the cases where the electric field is parallel and normal to the incident plane [He 87].

$$r_{\parallel} = -\frac{\tan(i_1 - i_2)}{\tan(i_1 + i_2)} \tag{3.24}$$

$$r_{\perp} = -\frac{\sin(i_1 - i_2)}{\sin(i_1 + i_2)} \tag{3.25}$$

In figure 3.4 the reflection and refraction of a plane wave is shown. $i_1 = (\pi/2) - \theta$ is the angle of incidence and i_2 is the angle of refraction.

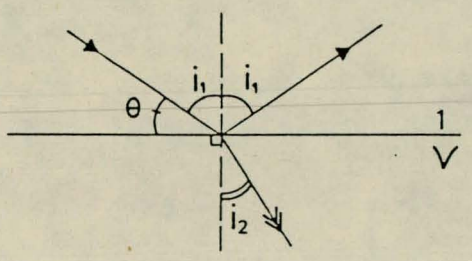

Figure 3.4 Reflection of Plane wave incident on boundry

Using Snell's law of refraction one obtains

$$\sin i_1 = \nu \sin i_2 \tag{3.26}$$

If the paraxial approximation is applied the following may be obtained [Cr 82].

$$\sin i_1 = \cos\theta \approx 1 \tag{3.27}$$

$$\sin i_2 \approx 1/\nu \tag{3.28}$$

$$\cos i_1 = \sin\theta \approx \theta \tag{3.29}$$

$$\cos i_2 \approx \sqrt{1 - (1/\nu^2)} \tag{3.30}$$

Making a first order development in θ one obtains [Cr 82]

$$r_{\|} = 1 - \frac{2\nu^2\theta}{\sqrt{\nu^2 - 1}} \tag{3.31}$$

$$r_{\perp} = -1 + \frac{2\theta}{\sqrt{\nu^2 - 1}} \tag{3.32}$$

The intensity of the incident ray is given by

$$I = E^2 = E_{\|}^2 + E_{\perp}^2 = E^2 \sin^2\phi + E^2 \cos^2\phi \tag{3.33}$$

The intensity of the reflected ray is given by

$$\begin{aligned} r^2(\theta,\phi)I &= r_{\|}^2 E_{\|}^2 + r_{\perp}^2 E_{\perp}^2 \\ &= (r_{\|}^2 \sin^2\phi + r_{\perp}^2 \cos^2\phi)I \end{aligned} \tag{3.34}$$

The reflected power for each corresponding beam having incident power dP is then given by

$$r^2(\theta,\phi)dP \tag{3.35}$$

Consider the Gaussian beam now as series of rings defined by ρ_o and $d\rho_o$. The power in one incident ring element is given by

$$dP(ring) = \int_0^{2\pi} I_o \exp(-\frac{\rho_o^2}{r_o^2})\rho_o d\rho_o d\phi \tag{3.36}$$

This may be written as

$$dP(ring) = 2\pi I_o \exp(-\frac{\rho_o^2}{r_o^2})\rho_o d\rho_o \tag{3.37}$$

The ring beam power after one reflection is thus given by

$$dP_r(ring) = I_o \exp(-\frac{\rho_o^2}{r_o^2})\rho_o d\rho_o \int_0^{2\pi} r^2 d\phi \tag{3.38}$$

The following integral must now be solved.

$$A = \int_0^{2\pi} r_{||}^2 \sin^2\phi d\phi + \int_0^{2\pi} r_{\perp}^2 \cos^2\phi d\phi \tag{3.39}$$

One has that [Sp 68]

$$\begin{aligned} A &= r_{||}^2\pi + r_{\perp}^2\pi \\ &= \pi(r_{||}^2 + r_{\perp}^2) \\ &= 2\pi(\frac{r_{||}^2 + r_{\perp}^2}{2}) \\ &= 2\pi t_1 \end{aligned} \tag{3.40}$$

where t_1 is called the reflection parameter. The reflected beam power thus becomes

$$dP_r(ring) = 2\pi t_1 I_o \exp(-\frac{\rho_o^2}{r_o^2})\rho_o d\rho_o \tag{3.41}$$

After n reflections of the dielectric wall, the transmitted power of the ring element is proportional to

$$t_n = (\frac{r_{\|}^2 + r_{\perp}^2}{2})^n \tag{3.42}$$

The total beam power P_s at the waveguide exit after n reflections is given by the integral

$$P_s = \int_0^R 2\pi I_o t_n(\rho_o) \exp(-\frac{\rho_o^2}{r_o^2}) \rho_o d\rho_o \tag{3.43}$$

Using equations 3.31 and 3.32 and neglect powers of θ larger than 1, one may obtain

$$t_1 = 1 - \frac{2(\nu^2 + 1)}{\sqrt{\nu^2 - 1}} \theta \tag{3.44}$$

Making use of equation 3.18 this may be written as

$$t_1 = 1 - G\rho_o \tag{3.45}$$

with

$$G = \frac{2(\nu^2 + 1)}{\sqrt{\nu^2 - 1}} \frac{1}{kr_o^2} \tag{3.46}$$

Parameter t_n may be written as

$$t_n = (1 - G\rho_o)^n \tag{3.47}$$

or

$$t_n = \exp[n \ln(1 - G\rho_o)] \tag{3.48}$$

Because only small angles of θ are considered one has that

$$G\rho_o \ll 1 \tag{3.49}$$

Because $0 < \rho_o < R$, one thus has that

$$GR \ll 1 \tag{3.50}$$

and

$$\ln(1 - G\rho_o) \approx -G\rho_o \tag{3.51}$$

and therefore equation 3.48 becomes

$$t_n = \exp(-nG\rho_o) \tag{3.52}$$

The problem now remains to solve n as a function of ρ_o and thus to calculate the power P_s. The number of reflections in a waveguide depends on the angle θ, the radius R and length L as shown in figure 3.5.

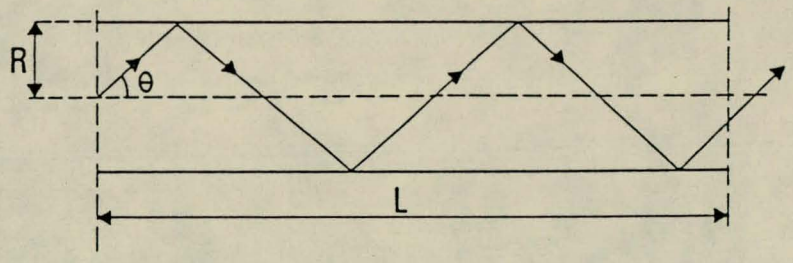

Figure 3.5 Number of reflections in waveguide

One calculates the distance between the reflections and divides the total length L by that distance. Combining this with equation 3.18 gives the following result

$$n = \text{Int}(\frac{L\theta}{2R} + \frac{1}{2}) = \text{Int}(\frac{L\rho_o}{2Rkr_o^2} + \frac{1}{2}) \tag{3.53}$$

The function n is a step function and is approximately a linear function given by

$$n = \frac{L\theta}{2R} = \frac{L\rho_o}{2Rkr_o^2} \tag{3.54}$$

Using this equation and equation 3.52 the following is obtained

$$t_n = \exp\left[-\frac{LG\rho_o^2}{2Rkr_o^2}\right] \tag{3.55}$$

One now has that

$$P_s = 2\pi I_o \int_0^R \exp\left[-\left(\frac{LG}{2Rk}+1\right)\frac{\rho_o^2}{r_o^2}\right]\rho_o d\rho_o \tag{3.56}$$

Calculating this integral the following result is obtained [Cr 82].

$$P_s = \frac{\pi I_o r_o^2}{F}\left[1-\exp\left(-F\frac{R^2}{r_o^2}\right)\right] \tag{3.57}$$

where

$$F = 1+\frac{LG}{2Rk} = 1+\frac{\nu^2+1}{\sqrt{\nu^2-1}}\frac{L}{R}\frac{1}{k^2r_o^2} \tag{3.58}$$

The beam power transmission as a fraction may now be obtained and is given by

$$T = \frac{1-\exp\left(-F\frac{R^2}{r_o^2}\right)}{F} \tag{3.59}$$

This theoretically derived formula for the transmission fraction will be tested in the practical part of the thesis when the transmission of a He-Ne laser through a hollow glass waveguide is investigated. Therefore this result will not be discussed further but will be applied later in a more appropriate situation.

4

RAMAN SCATTERING

4.1 Introduction

Nonlinear effects in materials have played an increasingly important role in spectroscopy in the last few years especially since the invention of the laser in the 1960's. The strength of the nonlinear effect depends on the strength of the applied field which may easily be provided by the output of a high power laser. This makes the laser an invaluable tool in the field of nonlinear optics. The stimulated Raman scattering process, which is one of many nonlinear processes is of special interest here. Good background articles and books are available on the subject of nonlinear optics [Bh 66, Bl 67, Gi 69, Ma 76, Mi 88, Mo 90, Sh 65].

4.2 What is nonlinear optics?

It is well-known that the intense light flux generated by lasers can produce nonlinear effects in various media. This nonlinear effects can be described by expressing the polarisation P induced in the medium as a series in ascending powers of the applied field E and in terms of the susceptibility χ [Ha 79].

$$P = \epsilon_0 \chi^{(1)} E + \epsilon_0 \chi^{(2)} E^2 + \epsilon_0 \chi^{(3)} E^3 + ... \tag{4.1}$$

The values of the susceptibilities become smaller for increasing order [Ha 79], so that the higher order effects would be produced only at very strong applied fields. The higher order terms in which the polarisation may be expressed, are responsible for producing various nonlinear processes. These terms create harmonics of a certain fundamental frequency (or frequencies), so that these new frequencies may be amplified and grow with the fundamental frequency (or frequencies). This is in fact one important use of the nonlinear effect; the conversion of a given frequency into new frequencies.

In linear optics the higher order terms in the polarisation expansion are ignored because the strength of the applied field is relatively small and only the first term contributes to the induced polarisation. The effect of the higher order terms are then assumed to be so small that it is negligible. When high intensity fields are applied, it is not possible to ignore the higher order terms which then also contributes to the induced polarisation P.

Since experiments first showed these nonlinear effects, there had been a rapid growth of interest in this field. Information about the microscopic properties of atoms or molecules may be found using the spontaneous Raman scattering process where information about the electronic, vibrational or rotational states of molecules or atoms may be obtained. This Raman scattering process can be a spontaneous or stimulated process and will be discussed later in more detail.

4.3 What medium is suited best for nonlinear optics?

It may be shown that $\chi^{(2)}$ is zero if the medium is *centrosymmetric* [Mi 88]. In *centrosymmetric* media one has that if the direction of the electric field is reversed, the direction of the induced second order polarisation terms is also reversed. In this case, one has that the induced polarisation is zero and no second order nonlinear effects may take place. Gases and vapors are examples of *centrosymmetric* media and nonlinear effects in them would thus depend on higher-order, and smaller susceptibility nonlinear terms.

Crystals therefore were first thought of as suitable nonlinear mediums due to the fact that the second order polarisation is not zero. Also may the birefringence of a crystalline medium be used to match the phase velocities of the fundamental and harmonic radiation, called phase matching which will be discussed later. However, infrared and ultraviolet absorption as well as other shortcomings in crystals shifted the interest to gases and vapors.

Advantages of gases and vapors:

1. Can be easily prepared.
2. No irreversible damages at very high intensities.
3. Good ultraviolet and infrared transparency.

Disadvantages:

1. Low densities compared with solid matter.
2. Because of inversion symmetry, most nonlinear effects are due to the $\chi^{(3)}$ term which is smaller than $\chi^{(2)}$ [Ha 79].

4.4 Nonlinear processes

Nonlinear processes are classified and described by the nature of the polarisation terms which exist in the induced polarisation P given by equation 4.1. Generally there are n-wave mixing processes in which a wave is generated by the mixing of n-1 waves. For example, for three wave mixing processes two waves are "mixed" to produce a third wave. The second order susceptibility describes three wave mixing processes which are thus called second order nonlinear processes. In the same manner the third order susceptibility describes four wave mixing processes. These are then third order processes.

Here some three wave mixing processes will be discussed shortly before considering four wave processes of which the spontaneous and stimulated Raman scattering process are important examples.

4.5 Three wave mixing processes

4.5.1 Second-harmonic generation

Second-harmonic generation is a three wave mixing process in which two waves of identical frequency w, are mixed to obtain a third wave with frequency $2w$. This is thus a specific case of the three wave mixing process in which generally two waves of different frequencies are mixed to obtain a wave with new frequency. This general case will be described later.

Suppose a lightwave of the form

$$E = E_0 \sin wt \tag{4.2}$$

incident on a medium.

The resulting polarisation in the medium is given by

$$P = \epsilon_0 \chi E_0 \sin wt + \epsilon_0 \chi_2 E_0^2 \sin^2 wt + \epsilon_0 \chi_3 E_0^3 \sin^3 wt + ... \tag{4.3}$$

This may be written as [He 87]

$$P = \epsilon_0 \chi E_0 \sin wt + \frac{\epsilon_0 \chi_2}{2} E_0^2 (1 - \cos 2wt) + \frac{\epsilon_0 \chi_3}{4} E_0^3 (3 \sin wt - \sin 3wt) + ... \tag{4.4}$$

The incident field thus creates a polarisation field in the medium which corresponds to a certain charge redistribution in the medium. From this equation it can be seen that other terms in the polarisation give rise to waves with different frequencies compared to the fundamental frequency.

The $\cos 2wt$ term means that there is a variation in the polarisation at twice the fundamental frequency and light that is radiated from the medium has a component with frequency $2w$. This process is called **second harmonic generation.**

In terms of a photon picture two photons of identical energy $\hbar w$ is converted into a single $\hbar 2w$ photon as shown in figure 4.1. This process of second harmonic generation is closely related to third harmonic generation (THG) which is a four wave mixing process. In THG three $\hbar w$ photons is converted into a single $\hbar 3w$ photon due to the presence of the $sin3wt$ term in equation 4.4.

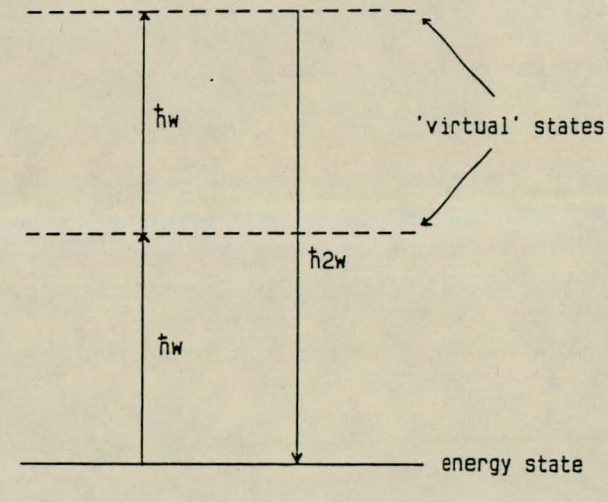

Figure 4.1 Second harmonic generation

4.5.2 General three wave mixing

One may also have two beams of different frequencies mixed in a medium. Consider a wave of the form

$$E = E_{01} \sin w_1 t + E_{02} \sin w_2 t \tag{4.5}$$

which is substituted into equation 4.1 given for the polarisation P. The second-order contribution is then given by [He 87]

$$\epsilon_0 \chi_2 \{E_{01}^2 \sin^2 w_1 t + E_{02}^2 \sin^2 w_2 t + 2E_{02}E_{02} \sin w_1 t \sin w_2 t\} \tag{4.6}$$

The first two terms in the above relation may be written in terms of $2w_1$ and $2w_2$ respectively and the last term gives rise to sum and difference terms $w_1 + w_2$ and $w_1 - w_2$ [He 87]. In the first case this corresponds to simply the transformation of two photons into a single photon of energy $w_1 + w_2$ which reduces to the case of second harmonic generation if w_1 is equal to w_2.

4.6 Phase matching

In any photon interaction process the laws of energy and momentum conservation must hold. Phase matching is the conservation of the momentum law in a nonlinear interaction between interacting photons.

Consider the case of second harmonic generation in which the energy of the two incident photons is unique and the dispersion of the medium is the same for all photons. The two incident photons with energy $\hbar w_1$, create a photon with double the energy given by $\hbar w_2$.

In a wave picture one has that the incident wave oscillating at frequency w_1, creates a polarisation wave at twice that frequency. A wave with frequency w_2, which is equal to the polarisation frequency, then experiences a gain and is allowed to grow. A wave with a different frequency than w_2 will not be enhanced.

The energy law for this process may be expressed as

$$w_1 + w_1 = w_2 \tag{4.7}$$

The phase matching criterion, which is the result of momentum conservation is given by

$$\vec{k_1} + \vec{k_1} = \vec{k_2} \tag{4.8}$$

Because energy states of different atoms or molecules do not have the same energy value, but there is a statistical energy distribution, there is a certain energy distribution of the incident photons $\hbar w_1$. In terms of the momentum one also has that the momentum of the incident photons have a certain distribution : $k_1 = k_1 \pm \Delta k$. Due to this, Δk is a measure of the phase mismatch that may be tolerated. The number of photons with energy $\hbar w_2$ and momentum $\vec{k_2}$ will decreases, because there are fewer photons which satisfy equation 4.7 and 4.8.

The definitions of the phase velocity and refractive index of a medium are given by

$$v = \frac{\omega}{k} \tag{4.9}$$

$$n = \frac{c}{v} \tag{4.10}$$

where v and n is the phase velocity and refractive index respectively.

If the dispersion of the medium is now taken into account, one has that photons with different energies, have momentum or k vectors lying in different directions. This causes an additional momentum mismatch between the waves which may only be corrected if the waves propagate at an angle with respect to one another.

For the process to be efficient for collinear beams , the difference in refractive indices must be corrected so that momentum is conserved. Various techniques are available which will not be discussed here.

It can be shown that in a medium with no dispersion phase matching may be obtained with all the momentum vectors lying in the same direction. In a medium with dispersion, phase matching usually is only possible when some of the momentum vectors lie at a angle with respect to one another.

The phase mismatch in the case of second-harmonic generation is described by [Mi 88]

$$\exp\left(2ik_w z - ik_w z\right) \tag{4.11}$$

The phase mismatch over a distance $z = L$ is given by ΔkL where $\Delta k = k_{2w} - 2k_w$. k_{2w} and k_w are the wavevectors of the second harmonic wave $2w$, and the fundamental waves w respectively. The phase mismatch increases for increasing interaction lengths. This leads to the definition of a *coherence length* which is a indication of the interaction length in which significant second harmonic generation takes place. For larger lengths, phase matching techniques must be apply to ensure further second harmonic generation.

In the case of the spontaneous and stimulated Raman scattering process the phase matching criterion will be looked at again in more detail.

4.7 Four wave mixing

In addition to three wave mixing process, four wave processes may occur in any medium. Third harmonic generation, in which three waves of identical frequency w, are mixed to produce a wave with frequency $3w$, and the Raman scattering process are well-known four wave mixing processes.

In four wave mixing theory, three electromagnetic waves are present with frequencies ω_1, ω_2 and ω_3, and wave vectors $\vec{k_1}$, $\vec{k_2}$ and $\vec{k_3}$ respectively. These three waves create a polarisation wave at frequency $\omega_p = \omega_1 + \omega_2 + \omega_3$ with a wave vector, $\vec{k_p} = \vec{k_1} + \vec{k_2} + \vec{k_3}$.

The polarisation wave will couple with a fourth vector k_4 if the phase mismatch, specified by $\Delta k = |\vec{k_4} - \vec{k_l}|$, is zero. This is true for a single interaction involving four waves because momentum must be conserved. In a statistical picture, where a ensemble of interactions is considered, one has that a phase mismatch, where Δk is not zero, may be tolerated. This was discussed in the previous section.

4.8 The Raman scattering process

The Raman scattering process may be spontaneous or stimulated. In the spontaneous Raman scattering process radiation is obtained in any direction and the intensity is rather weak. The stimulated process is very directional and is of much higher intensity. The two processes are closely related and to fully understand the Raman scattering process as a nonlinear effect requires expert knowledge of quantum mechanics and electromagnetic theory. Here only a short introduction to this effect is given and no attempt is made to give a fundamental description of the Raman effect.

4.8.1 The spontaneous Raman scattering process

The spontaneous Raman effect may be considered as an scattering process as shown in figure 4.2.

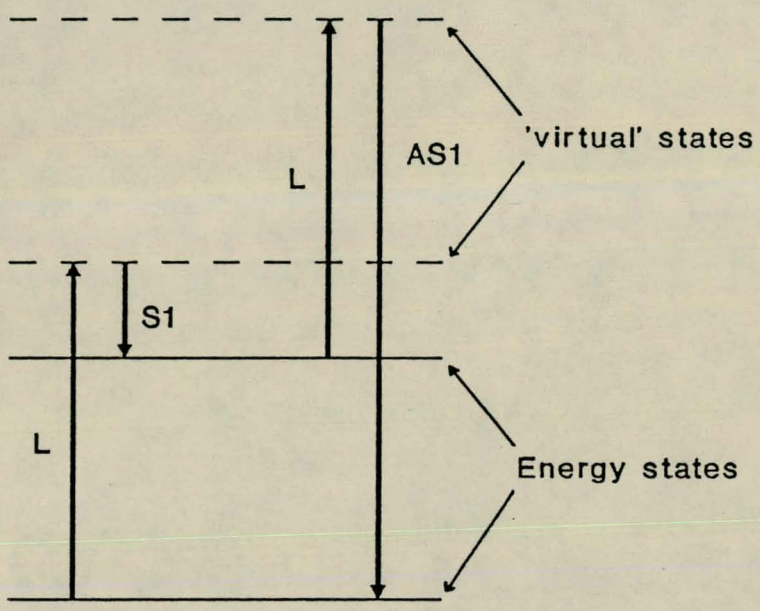

Figure 4.2 The Raman Process

For the spontaneous process an incident photon with energy $h\nu_L(L)$ is scattered by the medium or the scattering center. The scattered photon has energy $h\nu_s(S)$. The difference in energy which is given by $(h\nu_L - h\nu_s) = h\nu_{ab}$ is absorbed by the medium and may correspond to an electronic, vibrational or rotational energy difference. The frequency ν_s is called the Stokes frequency.

If the scattering medium had been in an excited state to begin with, it may be scattered to a lower energy state. The scattered light is then characterized by frequencies larger than the incident frequencies which are called Anti-Stokes frequencies.

It is important to realize that the Stokes process is in competition with the Anti-Stokes process. If the medium is unexcited the Stokes process will have greater intensity than that of the Anti-Stokes process. If the concentration of exited material centers increases, the Anti-Stokes process will also start to grow faster and can dominate the Stokes process.

4.8.2 Stimulated Raman scattering process (SRS)

The stimulated Raman scattering proses may take place via two four wave mixing processes. It may be considered as a process in which two laser and two Stokes waves are mixed which are described by the susceptibility [Mi 88]

$$\chi^{(3)} = \chi^{(3)}(-w_s, w_p, -w_p, w_s) \tag{4.12}$$

In this form, the stimulated process is called a *parametric* process which defines processes for which phase matching is automatically achieved. In a photon picture one has that a Stokes photon, which may be provided by background radiation, or a seed laser lasing at the Stokes frequency, stimulates other Stokes photons to be emitted via the process of stimulated emission of radiation.

To understand why phase matching is automatically achieved, the propagation of the four wave vectors as shown in figure 4.3 need to be considered.

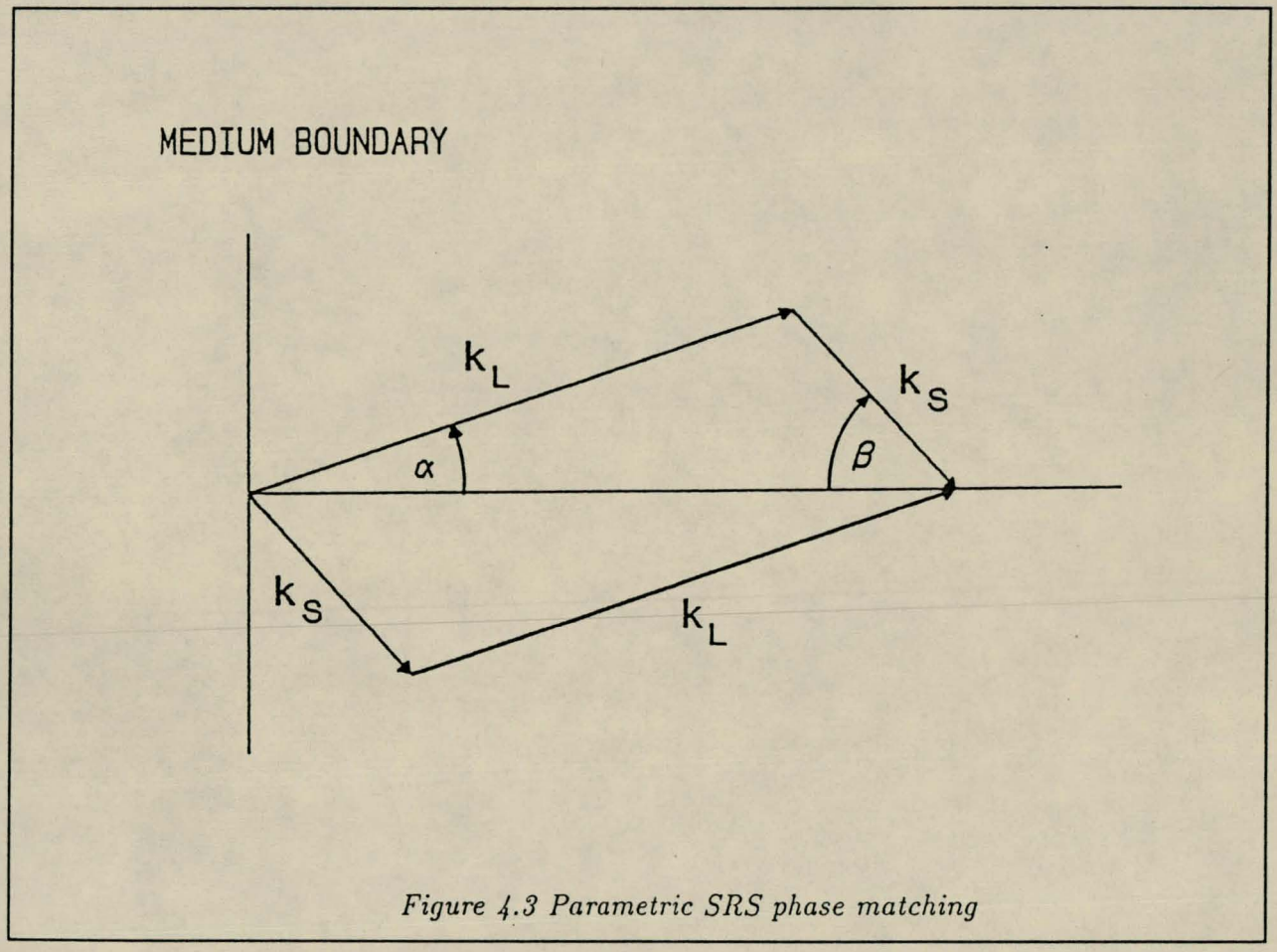

Figure 4.3 Parametric SRS phase matching

Clearly one has momentum and energy conservation for any angle α and β. As a result the *parametric* stimulated Raman scattering process requires no phase matching techniques and is therefore a very attractive process to investigate.

The form of the susceptibility may also be used to describe the spontaneous Raman scattering process for which phase matching is then also automatically achieved.

In the stimulated Raman process as described above it is assumed that no mixing with Anti-Stokes waves of frequency w_{as} takes place. If some scattering centers in the medium are in excited states, Anti-Stokes photons may be created and coupling may occur between the Stokes, Anti-Stokes and laser waves.

If coupling occurs between two laser and two Anti-Stokes waves, one has a process identically to the *parametric* SRS proses in which the Stokes waves are replaced by the Anti-Stokes waves. One would then have stimulated emission at the Anti-Stokes frequency and not the Stokes frequency. Also would phase matching automatically be achieved for this *parametric* Anti-Stokes stimulated Raman scattering proses (ASRS). The susceptibility takes on the following form for this process.

$$\chi^{(3)} = \chi^{(3)}(-w_{as}, w_p, -w_p, w_{as}) \tag{4.13}$$

Until now two *parametric* stimulated Raman processes had been described, the SRS and the ASRS processes. These two processes describe the coupling of the laser wave with either the Stokes or Anti-Stokes waves, but not the coupling of Stokes with Anti-Stokes waves.

This coupling gives the *nonparametric* SRS process because phase matching is not achieved automatically as will be seen later. Thus, rather than treating the Anti-Stokes process as a downward transition as for the spontaneous Raman scattering process, it is incorporated in the four wave mixing process in which the Stokes wave is mixed with two laser waves to produce one Anti-Stokes wave. The susceptibility then takes on the following form

$$\chi^{(3)} = \chi^{(3)}(-w_s, w_p, -w_p, w_{as}) \tag{4.14}$$

From the construction of the momentum or k-vectors it is easy to see the conditions for phase matching.

One may construct a diagram with k vectors which shows us the phase matching criteria for

the mixed Stokes and Anti-Stokes process as shown in figure 4.4.

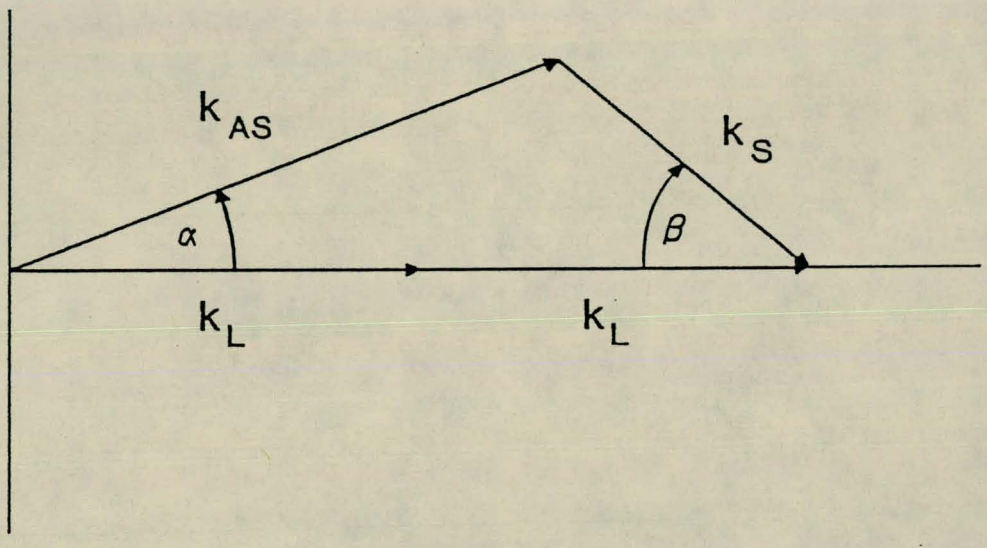

Figure 4.4 Nonparametric Raman Phase Matching

The two laser photons are chosen parallel to each other which is a valid assumption for laser beams. There are other configurations possible where the two laser photons lie with an angle with respect to each other, but for a process to be stimulated, it must grow in a certain fixed direction. The medium is usually enclosed in a cylinder so that its length is much longer than its width and the Stokes signal (or AS) grows in the length of the medium, that is where the two laser photons are parallel to each other.

From the laws of momentum conservation one has

$$X - direction : k_{as} \cos\alpha + k_s \cos\beta = 2k_L \tag{4.15}$$

$$Y - direction : k_{as} \sin\alpha = k_s \sin\beta \tag{4.16}$$

From the law of energy conservation one has that

$$2\omega_L = \omega_s + \omega_{as} \tag{4.17}$$

This may be written as

$$2v_L k_L = v_s k_s + v_{as} k_{as} \tag{4.18}$$

In general this can be written in the following way:

$$2k_L = \frac{v_s}{v_L} k_s + \frac{v_{as}}{v_L} \tag{4.19}$$

In a medium with finite dispersion $v_L \neq v_s \neq v_{as}$ Comparing equation 4.19 with equation 4.15 one sees that

$$\cos\alpha = \frac{v_s}{v_L} \tag{4.20}$$

and

$$\cos\beta = \frac{v_{as}}{v_L} \tag{4.21}$$

Because the medium has dispersion $\cos\alpha \neq 1$ and $\cos\beta \neq 1$.

This means that the k-vectors of the Stokes and Anti-Stokes waves must lie at an angle with respect to the two k-vectors of the laser photons for a medium with finite dispersion.

The Anti-Stokes radiation will thus be visible as a cone surrounding the Stokes radiation because of the momentum match requirement. One notes that only for a certain incident direction of the Stokes photon with respect to the laser photons, that momentum matching for the Anti-Stokes photon is satisfied. This will result in the forming of Anti-Stokes cones or rings.

Now if the medium does not have dispersion, one has that $v_L = v_s = v_{as}$ so that all three waves see the same refractive index. Then follows that

$$2k_L = k_s + k_{as} \tag{4.22}$$

If equation 4.15 is considered, one notes that $cos\alpha$ and $cos\beta$ must equal to unity so that $\alpha = \beta = 0$. It thus follows that for a medium with no dispersion momentum matching is obtained with all four waves co-linear.

As a final result one has that in the stimulated Raman process in which only the Stokes terms are present, phase matching is automatically satisfied. In the stimulated process where the Anti-Stokes and Stokes waves are 'mixed', phase matching techniques must be applied.

This first Anti-Stokes wave may also mix with the pump and the first Stokes wave to produce higher order Anti-Stokes waves. The first Stokes wave may also act as a pump to create higher order Stokes waves. These higher Stokes and Anti-Stokes orders are not found in the spontaneous Raman scattering process.

One thus has that in addition to the Stokes and Anti-Stokes frequencies, there may also be higher order Stokes and Anti-Stokes frequencies present as shown in figures 4.5 and 4.6 respectively.

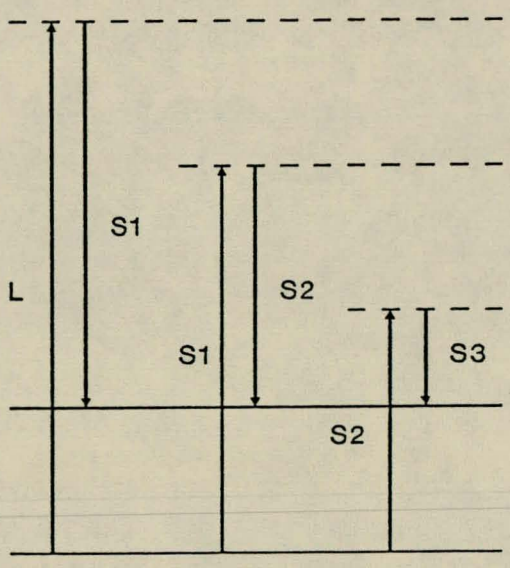

Figure 4.5 Higher order Stokes terms

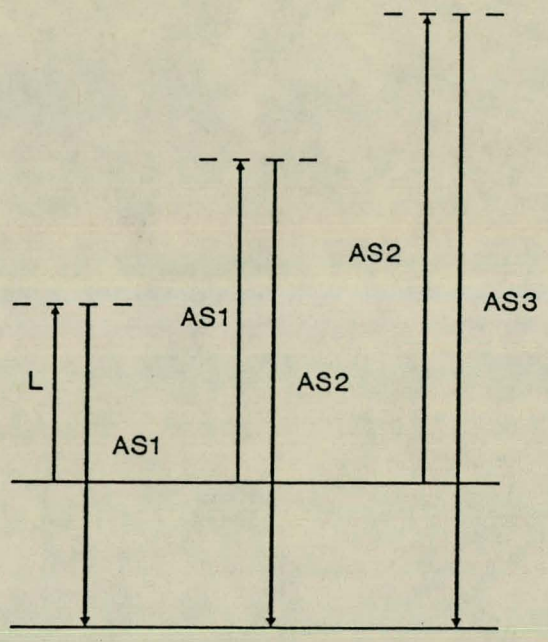

Figure 4.6 Higher order Anti-Stokes terms

The Stokes and Anti-Stokes frequencies are then given by

$$\hbar w_{Sn} = \hbar w_L - n\sigma \tag{4.23}$$

$$\hbar w_{ASn} = \hbar w_L + n\sigma \tag{4.24}$$

where σ is the energy difference between adjacent energy states as seen in figures 4.5 and 4.6..

The stimulated Raman process obeys the following relation

$$I_s = I_{bs} e^{gL} \tag{4.25}$$

where g is the gain coefficient and L is the interaction length. g depends on the intensity of the incident laser beam as will be seen when the Raman gain g, is calculated.

4.9 The Raman wave equation

The nonlinear polarisation may be coupled to Maxwell's equations to obtain the electromagnetic fields in the case of stimulated Raman scattering. Only plane waves will be considered, because a more realistic case which involves Gaussian beams are more complicated [Ha 79].

In a dielectric nonmagnetic medium, Maxwell's equations leads to the wave equation [Ha 79]

$$\nabla \times \nabla \times \mathbf{E} = -\mu_0 \frac{\partial^2 \mathbf{D}}{\partial t^2} \tag{4.26}$$

where the displacement vector $\mathbf{D}$ may be written as [Ha 79]

$$\mathbf{D} = \epsilon_0 \mathbf{E} + \mathbf{P}^L + \mathbf{P}^{NL} \tag{4.27}$$

Here $\mathbf{P}^L$ and $\mathbf{P}^{NL}$ are, respectively, the polarisations that are linear and nonlinear in $\mathbf{E}$.

By expanding the electric field $\mathbf{E}$ into the frequency domain with a Fourier transform, and substitute the result into the wave equation, the following equation may be obtained [Ha 79].

$$\frac{\partial E(z\omega)}{\partial z} = \frac{i\omega}{2\epsilon_0 c \eta_\omega} P^{NL}(z\omega) e^{-ik_\omega z} \tag{4.28}$$

This equation is the starting point for most plane-wave calculations of the growth of waves as they propagate through a nonlinear medium.

For stimulated Raman scattering this equation becomes [Ha 79]

$$\frac{\partial E_s(z)}{\partial z} = \frac{3i\omega_s}{4c\eta_s} \chi_R |E_p(z)|^2 E_s(z) \tag{4.29}$$

where χ_R is the third order Raman susceptibility and η_s is the refractive index of the medium at the Stokes frequency.

In the small signal region one may put $E_p(z) = E_p(0) = E_{po}$ in the previous equation which then gives us the Stokes field after a distance L,

$$E_s(L) = E_{so} \exp\left[\frac{3i\omega_s}{2\epsilon_0 c^2 \eta_s \eta_p} \chi_R I_{po} L\right] \tag{4.30}$$

If the electric field $E_s(L)$ has this form, the Stokes intensity which may be written as follows.

$$I_s = I_{so}e^{gL} = I_{so}e^{GI_{po}L} \tag{4.31}$$

where

$$g = \frac{-3w_s}{\epsilon_o c^2 \eta_s \eta_p}\chi'' I_{po} \tag{4.32}$$

g is defined as the stimulated Raman gain coefficient.

The Raman susceptibility may also be expressed in terms of the Raman cross section [Ha 79] which gives

$$g = \frac{8\pi^2 c^2}{\hbar \eta_s \eta_p w_s^2 w_p}\frac{N}{\Gamma}\frac{d\sigma}{d\Omega} \tag{4.33}$$

N is the molecular density, Γ is the Raman linewidth and $\frac{d\sigma}{d\Omega}$ is the Raman cross section. The Raman cross section is different for different materials and in table 4.1 a few of the cross sections of well-known materials are listed.

The Ratio of the Raman Cross Section per Molecule to That of N_2. The Value of N_2 is $(d\sigma/d\Omega)_{N_2} = (3.31 \pm 1.1) \times 10^{-30}$ cm^2/sr-molec. $\lambda_l = 4880$ Å (after Ref. 11)

Gas	Vibrational Frequency (cm^{-1})	$\frac{d\sigma}{d\Omega}$
N_2	2331	1.0
O_2	1556	1.3
H_2 (sum)	4161	2.4
H_2 (Q(1))	4161	1.6
CO	2145	1.0
NO	1877	0.27
$CO_2(v_1)$	1388	1.4
$CO_2(2v_2)$	1286	0.89
$N_2O(v_1)$	1285	2.2
$N_2O(v_3)$	2224	0.51
$SO_2(v_1)$	1151	5.2
$SO_2(v_2)$	519	0.12
$H_2S(v_1)$	2611	6.4
$NH_3(v_1)$	3334	5.0
$ND_3(v_1)$	2420	3.0
$CH_4(v_1)$	2914	6.0
$C_2H_6(v_3)$	992	1.6
$C_6H_6(v_1)$	3062	7.0
$C_6H_6(v_2)$	992	9.1

Table 4.1 Raman Cross sections

4.10 The Raman Threshold

Because of the nature of the stimulated Raman scattering process, a Raman laser has a gain threshold value. Only when the gain is larger than this threshold value, may there be net growth of the Raman signal. The gain is given by the parameter g and the losses are described by the parameter α. The losses may be due to scattering, absorption and diffraction. Consider a Raman cell with no mirrors of length l. For net Raman laser action the following condition must be satisfied.

$$e^{g_t l} = e^{\alpha l} \tag{4.34}$$

For gain values larger than g_t laser action would be obtained.

If the overall gain is not enough to provide enough laser action, mirrors may be used to provide a feedback mechanism to produce greater laser intensity levels.

Consider for the moment a Raman cell with mirrors of reflectivity R_1 and R_2 respectively and length L.

$$R_1 R_2 e^{2(g_t - \alpha)L} = 1 \tag{4.35}$$

This condition specifies a threshold value for the gain g. If the gain is smaller than this value, the above condition will not be satisfied and the gain will not be able to overcome the losses. This means that no laser action at the Raman frequency will exist. If the gain is initially larger than the threshold value, the gain g will adjust itself to the threshold value and to the steady-state regime.

For the stimulated Raman scattering process, the gain g depends on the intensity of the pump laser. By thus decreasing the pump intensity, the Raman intensity will decrease until no Raman laser radiation exist. In this way, the gain threshold value can be determined.

Ignoring losses, the following relation between the pump intensity I_p, and the Raman intensity I_R, exists

$$I_R = I_{RB} e^{gl} \tag{4.36}$$

where

$$g = G I_p \tag{4.37}$$

I_{RB} is the background Raman intensity and G is the plane wave gain coefficient respectively. One thus has exponential growth in Raman intensity with respect to the pump intensity. This gives the following relation between the Raman and pump intensities as shown in figure 4.7(a).

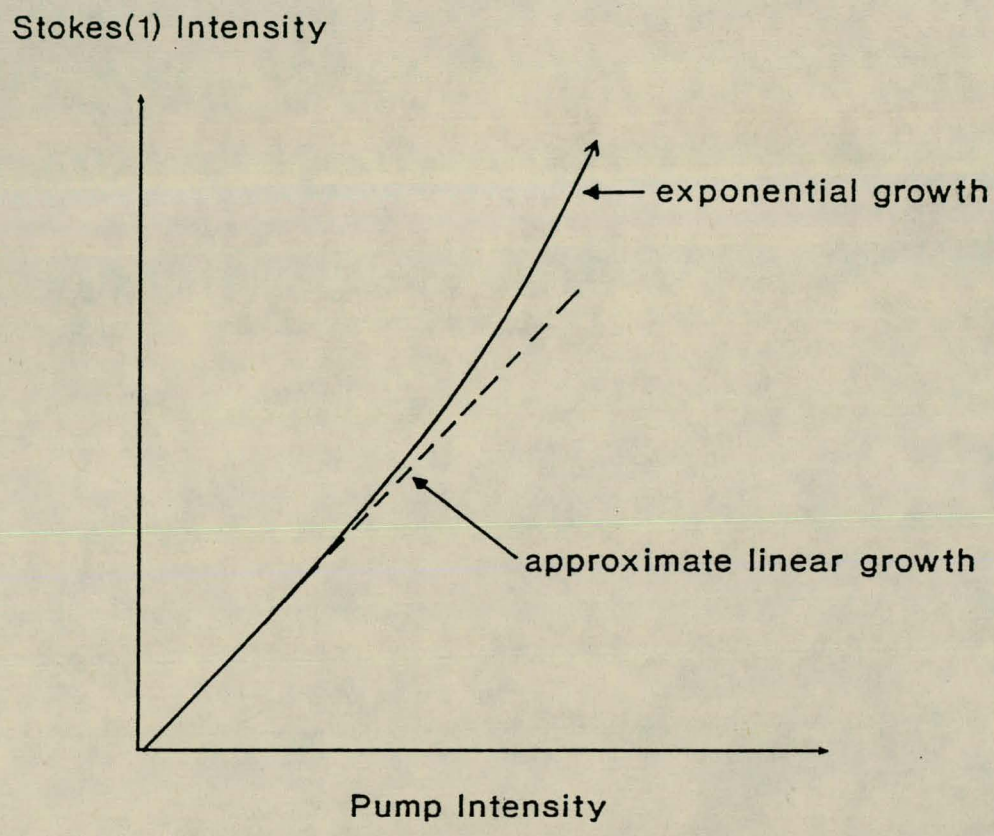

Figure 4.7(a) The Stokes Intensity with respect to the Pump Intensity

This relation is not exactly correct because other processes which also interacts with the first Stokes component such as the second Stokes component and gain saturation, have been ignored. Gain saturation occurs when the Stokes intensity becomes large and causes depletion of the pump intensity. The second Stokes component has the first Stokes component as pump beam and will start to grow exponentially when the intensity of the first Stokes wave (S1) reaches a high enough value so that the losses may be overcome and net stimulated emission takes place at the second Stokes (S2) frequency. This also means that the threshold value for this second order Stokes is higher than for the first Stokes and the same reasoning is valid for the third and second Stokes waves. This threshold is specified by the pump laser intensity.

Consider the S2 intensity dependence on the pump intensity. At the pump threshold value for

S1, the S1 intensity starts to grow exponentially. The S2 wave cannot start to grow because not enough S1 photons are present to be above the threshold value specified by the S1 intensity. At a certain pump intensity, larger than specified by the S1 threshold, the S2 wave will start to grow, because only then there are enough S1 photons present. The same reasoning holds for the higher order Stokes waves.

From above reasoning, a curve as given by figure 4.7(b) may be expected for the first order Stokes. At high pump intensities, the curve flattens out as the second Stokes process becomes significant and some of the first Stokes intensity is withdrawn. For small enough values for the pump intensity, a linear relation may be expected because an exponential function may be written as a linear function for small values of the argument. The experimental data will show whether this assumption is valid for the specific pump intensities used in the experiment.

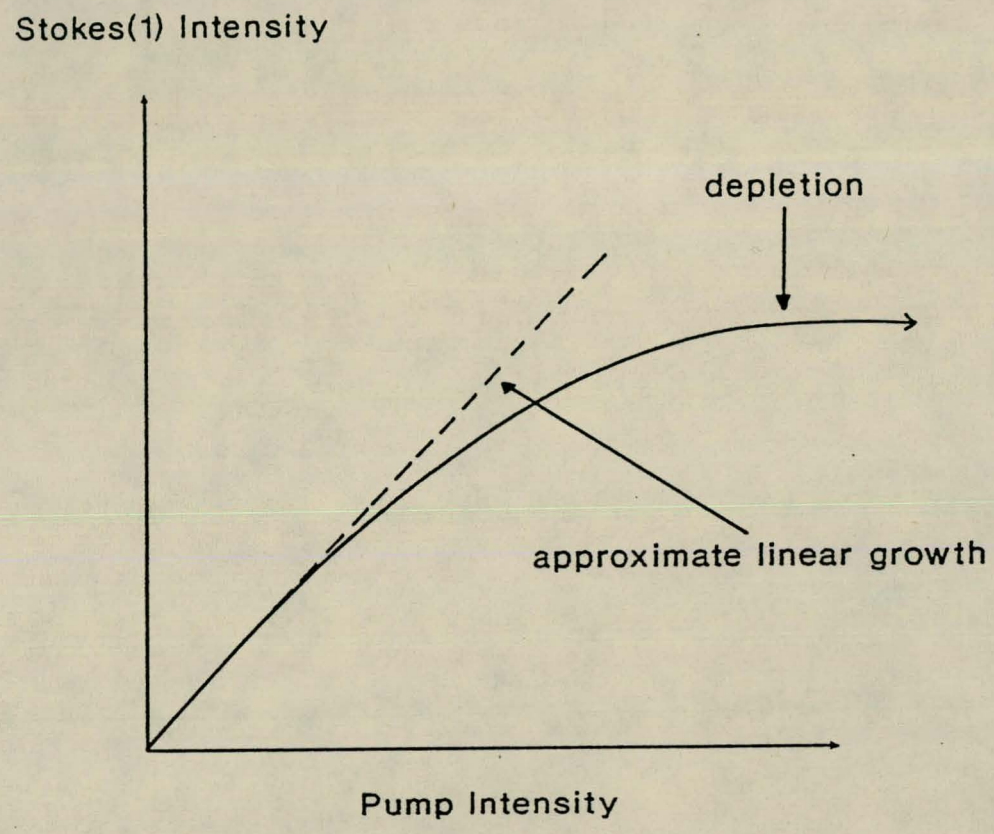

Figure 4.7(b) The Stokes Intensity with respect to the Pump Intensity

4.11 Parameters influencing the Raman gain

The Raman gain is given by equation 4.33 [Ha 79]. In this equation various factors are present such as the particle density, the molecular density, the pressure and the intensity of the incident laser beam. These are all factors that influence the gain and some will be discussed. The gain is of course dependent on the pump intensity and thus dependent on how the pump beam is focussed. The effect of focussing on the gain coefficient and on the Raman intensity as well as the influence of the pressure on the gain will be discussed.

4.11.1 The influence of the pressure

The linewidth term as well as the molecular density N in the gain causes the gain to vary with pressure. One thus have to look at the factor N/Γ where Γ is the linewidth of the transition. Assuming the ideal gas law one has that

$$N = aP \tag{4.38}$$

which means that the particle density is linear with respect to the pressure. a is given by $1/(RT)$ and is a constant for a given temperature T.

For relative high pressure values one also has that the linewidth is linear with respect to the pressure which gives [De 82]

$$\Gamma = bP \tag{4.39}$$

where b is a constant.

One may thus expect that the Raman gain will be constant with respect to the pressure at high pressure values. It is of course assumed that only the first Stokes process is present and the second Stokes process is ignorable.

At lower pressures the situation is different. As the pressure decreases the linewidth decreases until the natural linewidth is reached [De 82]. The situation is showed in figure 4.8.

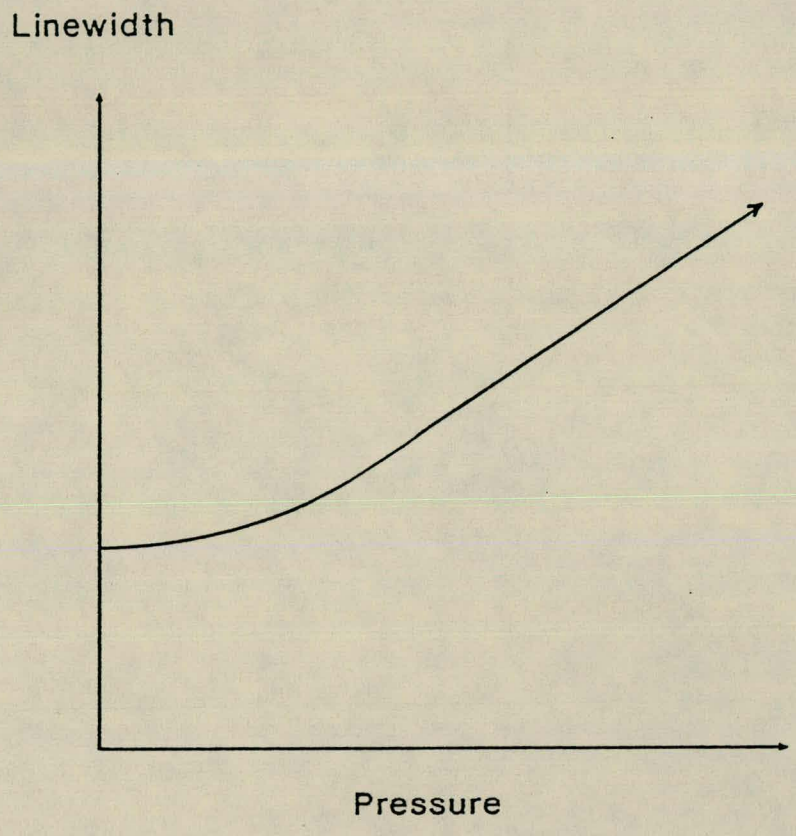

Figure 4.8 The Linewidth Γ versus the pressure P

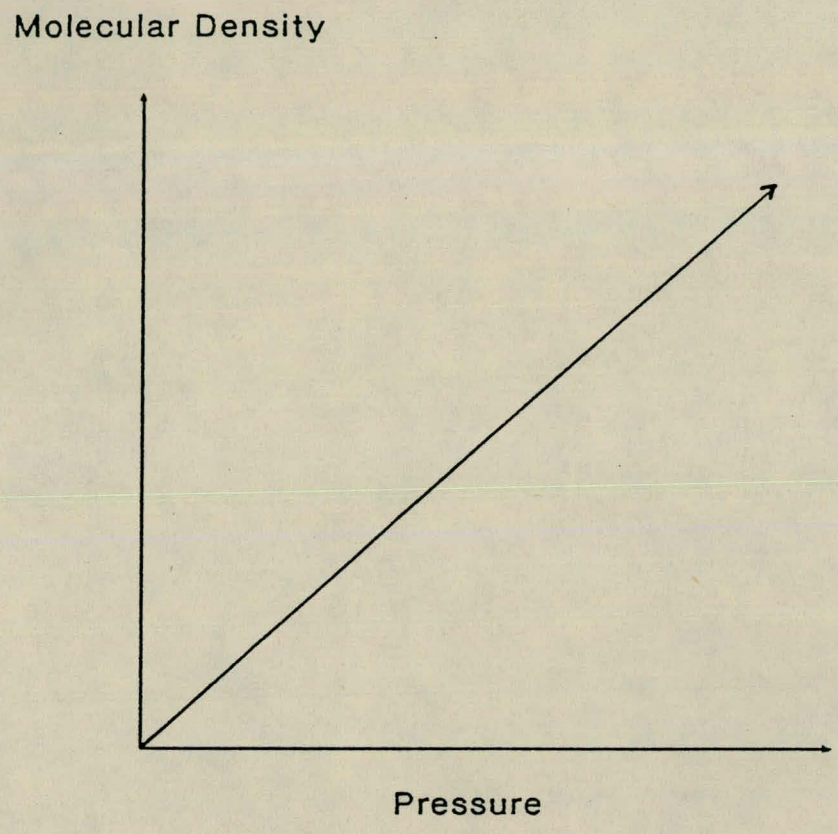

Figure 4.9 The Molecular Density N versus the pressure P

The relation between N and the pressure P, has a form as shown in figure 4.9. By now plotting the fraction N/Γ in the gain factor versus the pressure one obtains a relation as shown in figure 4.10.

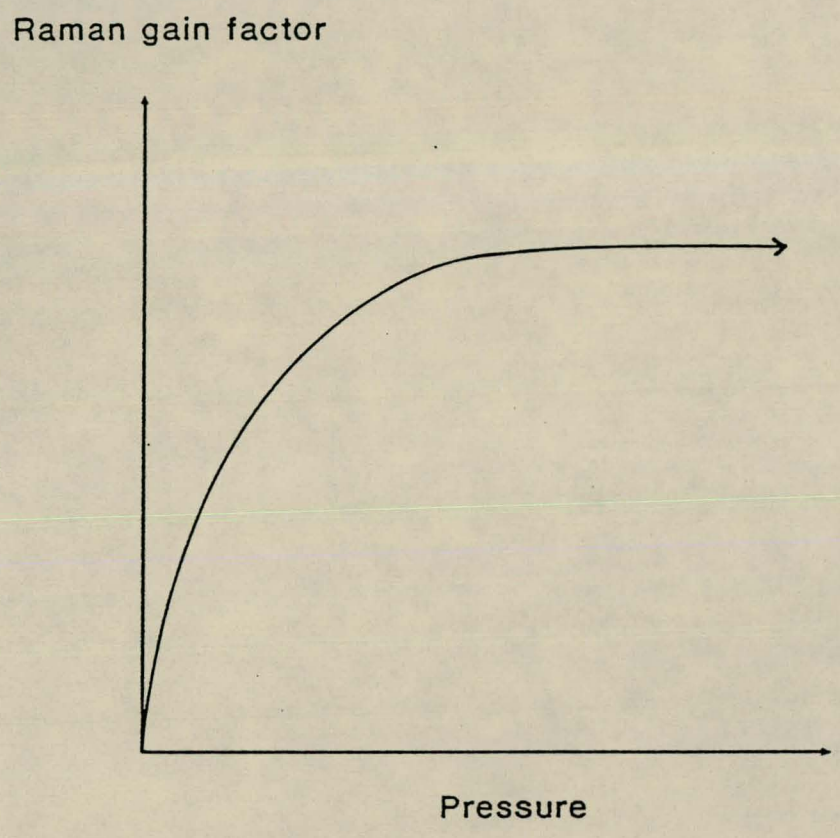

Figure 4.10 The influence of the pressure on the Raman gain

4.12 The influence of focussing on the Raman gain

4.12.1 The differential equation

The differential equation used to describe the propagation of Stokes radiation is given by [Tr 80]

$$\nabla_T^2 E_s + 2jk_s \frac{\partial E_s}{\partial z} - jk_s g E_s = 0 \tag{4.40}$$

This equation is used to calculate the form of the Stokes wave for a certain gain configuration.

Four different forms of the gain is assumed and the Raman intensity is calculated in each case. As the form for the gain becomes more complicated, the difficulties in calculating the Raman intensity wave will be noted and the reasons why some approximations must be used on the form of the gain will become clear.

Referring to equation 4.40, one notes that for a wave for which the second derivative with respect to the x and y coordinates vanishes, the first term vanishes and a reduced form of equation 4.40 is obtained which corresponds to the well-known gain equation.

$$\frac{\partial E_s}{\partial z} = \frac{1}{2} g E_s \tag{4.41}$$

In terms of the intensity this may also be written as

$$dI = gIdz \tag{4.42}$$

The derivation of equation 4.42 is shown in Appendix G.

In the above case equation 4.41 has been derived from the differential equation 4.40 but it may also be derived in the following manner

Consider an interaction region with thickness dz and assume the intensity I is uniform in the region. The increase in intensity, dI, is now proportional to the product of the intensity I in the interaction length and the length of the interaction region as given by equation 4.42. To derive equation 4.42 as above, a uniform intensity in the interaction region is assumed. This is consistent with the derivation of equation 4.42 from equation 4.40 where the non-uniform characteristics of the intensity, that is the x, y dependence of the intensity has also been ignored.

In integral form it looks as follows

$$\int_{I_{bs}}^{I_s} \frac{dI_s}{I_s} = \int_{z'}^{z} g_s dz \tag{4.43}$$

This may also be written as

$$I_s = I_{bs} e^{\int_{z'}^{z} g_s dz} \tag{4.44}$$

I_{bs} is the background intensity from which the Stokes wave grows and may be a function of x,y and z.

Normally one chooses $z' = 0$ and $z = l$ where l is the length of the Stokes medium. The wave form of the laser beam is important in this case only to determine what the gain g looks like. In all the cases the time dependence of the waves is ignored and the time independent part of the electromagnetic wave is used.

4.12.2 Gain configurations

Four specific cases which each corresponds to a certain form of the gain will now be considered.

1. Plane Stokes wave for constant gain
2. Gaussian Stokes wave for constant gain
3. Gaussian Stokes wave for z-depended gain
4. Gaussian Stokes wave for Gaussian gain

In the last three cases the Stokes wave does depend on the x, y coordinates and to be correct one must use the differential equation 4.40 and not equation 4.42 because $\nabla_T^2 E_S$ is not zero.

In all the calculations the approximation is made that $\nabla_T^2 E_S = 0$ for mathematical simplicity. In cases where the gradient of the electric field is relatively constant with respect to the x, y coordinates, it may be a good approximation to assume $\nabla_T^2 E_S = 0$.

Equation 4.42 is used in all four cases to determine the Raman intensity as it is valid for any gain and intensity variation.

4.12.3 Plane Stokes wave for constant gain

In this case the pump laser is considered as a plane wave with an uniform intensity distribution. As a result the Stokes gain is thus constant.

For a constant gain g_s, equation 4.42 may be written in an integral form because g is not a function of z and the Raman intensity I_s, may be calculated performing a simple integral. One thus has that

$$I_s = I_{bs} e^{gz} \tag{4.45}$$

I_{bs} is the background Stokes intensity and may be found from black body radiation. Because a plane Stokes wave is considered, the background Stokes wave from which the intensity grows by the process of stimulated emission is also a plane wave. Thus I_{bs} is not a function of x,y or z and so I_s is only a function of z.

The power P_s of the plane Stokes wave may also be calculated by integration of the intensity of the wave. The wave is considered as a block wave and one integrates from say $x = -a$ and $y = -b$ to $x = +a$ to $y = +b$. This gives

$$\int_{-a}^{+a} \int_{-b}^{+b} I_s dx dy = \int_{-a}^{+a} \int_{-b}^{+b} I_{bs} e^{gz} dx dy \tag{4.46}$$

This may be written as

$$\int_{-a}^{+a} \int_{-b}^{+b} I_s dx dy = e^{gz} \int_{-a}^{+a} \int_{-b}^{+b} I_{bs} dx dy \tag{4.47}$$

which gives

$$P_s = P_{bs} e^{gz} \tag{4.48}$$

where P_{bs} is the background Stokes power from which the Stokes process grows.

4.12.4 Gaussian Stokes wave constant gain

This case applies when the pump laser beam, which is a Gaussian beam, is focussed rather weakly. As an approximation one may say that the intensity distribution of the pump laser, which has a x and y dependence, remains constant over the interaction length and the gain g, may be considered independent of z.

One also considers the intensity distribution of the Gaussian laser beam near the peak intensity where the peak intensity varies little. As a result, the gain is considered also independent of x and y.

Equation 4.42 is again used to determine the Stokes intensity.

$$dI = gIdz$$

The integral may be solved as in the previous section. One is thus able to use equation 4.42 in a integral form which gives

$$I_s = I_{bs}e^{gz} \tag{4.49}$$

The Stokes background wave I_{bs} is considered as a Gaussian wave and is given by

$$I_{bs} = I_{bso}e^{-2(x^2 + y^2)/w_{so}^2} \tag{4.50}$$

I_{bso} is the peak intensity and w_{so} is the beam waist of the background Stokes wave at a certain position, normally $z = 0$ and is thus constant.

The peak intensity I_{bso} is related to the constant power P_{bs} of the background Stokes wave as shown in Appendix E.

$$I_{bso} = \frac{2P_{bs}}{\pi w_{so}^2} \tag{4.51}$$

Using equations 4.49 and 4.50, the following result may now be obtained.

$$I_s = I_{bs}e^{gz} = I_{bso}e^{-2(x^2+y^2)/w_{so}^2}e^{gz} \tag{4.52}$$

I_s may also be written as

$$I_s(x, y, z) = \frac{2P_{bs}}{\pi w_{so}^2}e^{gz}e^{-2(x^2+y^2)/w_{so}^2} = ABe^{-2(x^2+y^2)/w_{so}^2} \tag{4.53}$$

where

$$A = \frac{2P_{bs}}{\pi w_{so}^2} \tag{4.54}$$

$$B = e^{gz} \tag{4.55}$$

For a Gaussian beam one has that

$$I_s(x,y,z) = I_{so}e^{-2(x^2+y^2)/w_s^2} = \frac{2P_s}{\pi w_s^2}e^{-2(x^2+y^2)/w_s^2} \tag{4.56}$$

Comparing equations 4.53 and 4.56, and making the assumption that that $w_{so} = w_s$, the following may be obtained.

$$\frac{2P_{bs}}{\pi w_{so}^2}e^{gl} = \frac{2P_s}{\pi w_s^2} \tag{4.57}$$

and then

$$P_s = P_{bs}e^{gl} \tag{4.58}$$

As a result, the Stokes wave is a near Gaussian wave with only a different peak intensity I_{so} given by AB.

4.12.5 Gaussian Stokes wave for z-depended gain

Here the case where the laser beam is focussed sharply and the fact that the gain varies with z, is included. One again assumes that the gain is independent of x and y.

Equation 4.42 is again used in determining the Raman intensity.

$$dI = Igdz \tag{4.59}$$

This may be written as

$$I_s = I_{bs}e^{\int_o^z g(z)dz} \tag{4.60}$$

Substituting equation 4.51 for I_{bs}, I_s now becomes

$$I_s = I_{bso}e^{-2(x^2+y^2)/w_{so}^2}e^{C(z)} \tag{4.61}$$

where $C(z)$ is a function of z and may be calculated for a specific Stokes medium length.

$$C(z) = \int_o^z g(z)dz \tag{4.62}$$

The Stokes intensity may now be written as

$$I_s = I_{bso}e^{C(z)}e^{-2(x^2+y^2)/w_{so}^2} = I_{so}e^{-2(x^2+y^2)/w_s^2} \tag{4.63}$$

Again the approximation is made that $w_{so} = w_s$. The result is still a Gaussian beam with only a different peak intensity I_{so} determined by the product of the functions $e^{C(z)}$ and $I_{bso}(z)$. This function $C(z)$ is calculated by solving the integral equation 4.62. The form of the function g_s must first be known.

For the Raman scattering process, $g = GI_p$ where G is a constant and I_p is the intensity of the pump laser. In an practical system the laser intensity has a Gaussian distribution so that g also must have a Gaussian distribution with respect to the x and y coordinates. In the above case the x and y dependence of the gain g is ignored, and only the z dependence of the gain is considered. The gain is given by

$$g = GI_{po} = \frac{2GP_p}{\pi w_p^2} \tag{4.64}$$

where w_p is the pump beam radius, P_p is the power, and I_{po} is the peak intensity of the pump beam. Only the peak Raman intensity due to the gain corresponding to the peak intensity of the laser beam may thus be calculated. One notes that g is a function of z, because w is a function of z from the well-known propagation equations for a Gaussian beam.

That is,

$$w^2 = w_o^2[1 + (\frac{\lambda z}{\pi w_o^2})^2] \tag{4.65}$$

This may be reduced to

$$w^2 = w_o^2 + (\frac{\lambda z}{\pi w_o})^2 \tag{4.66}$$

g may now be written in terms of w_o and z.

$$g = \frac{2GP_p}{\pi} \frac{1}{w_o^2 + (\frac{\lambda z}{\pi w_o})^2} \tag{4.67}$$

This form of g may now be substituted into equation 4.62 and $C(z)$ may be determined.

$$C(z) = \int_{-L}^{+L} \frac{2GP_p}{\pi} \frac{1}{w_o^2 + (\frac{\lambda z}{\pi w_o})^2} dz \tag{4.68}$$

A practical configuration is considered where the beam is focussed by a lens and the intensity is calculated from $z = -L$ to $z = L$ so that the total interaction length is $2L$. The situation is shown in figure 4.11.

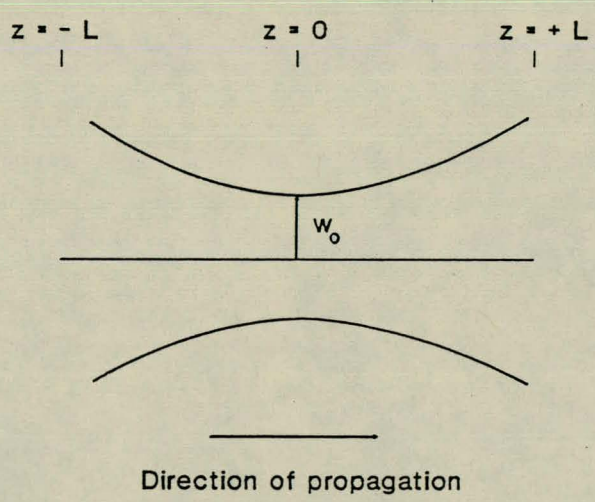

Figure 4.11 The Focussed Gaussian beam

The integral is solved in Appendix H. Making use of the integral solution the following equation for the Raman intensity from a initial value I_{bs} at $z = -L$ to the value I_s at $z = L$ may be obtained.

$$I_s = I_{bs} e^{\alpha} \tag{4.69}$$

where α is given by

$$\alpha = \frac{4GP_p}{\lambda_L} \arctan\left(\frac{\lambda_L}{\pi} \frac{L}{w_o^2}\right) \tag{4.70}$$

λ_L is the pump laser wavelength.

Conclusions

By plotting a graph of α versus the interaction length for different values of w_o the following conclusions may be made. For simplicity it is assumed that $G = 1$ and $P = 1$.

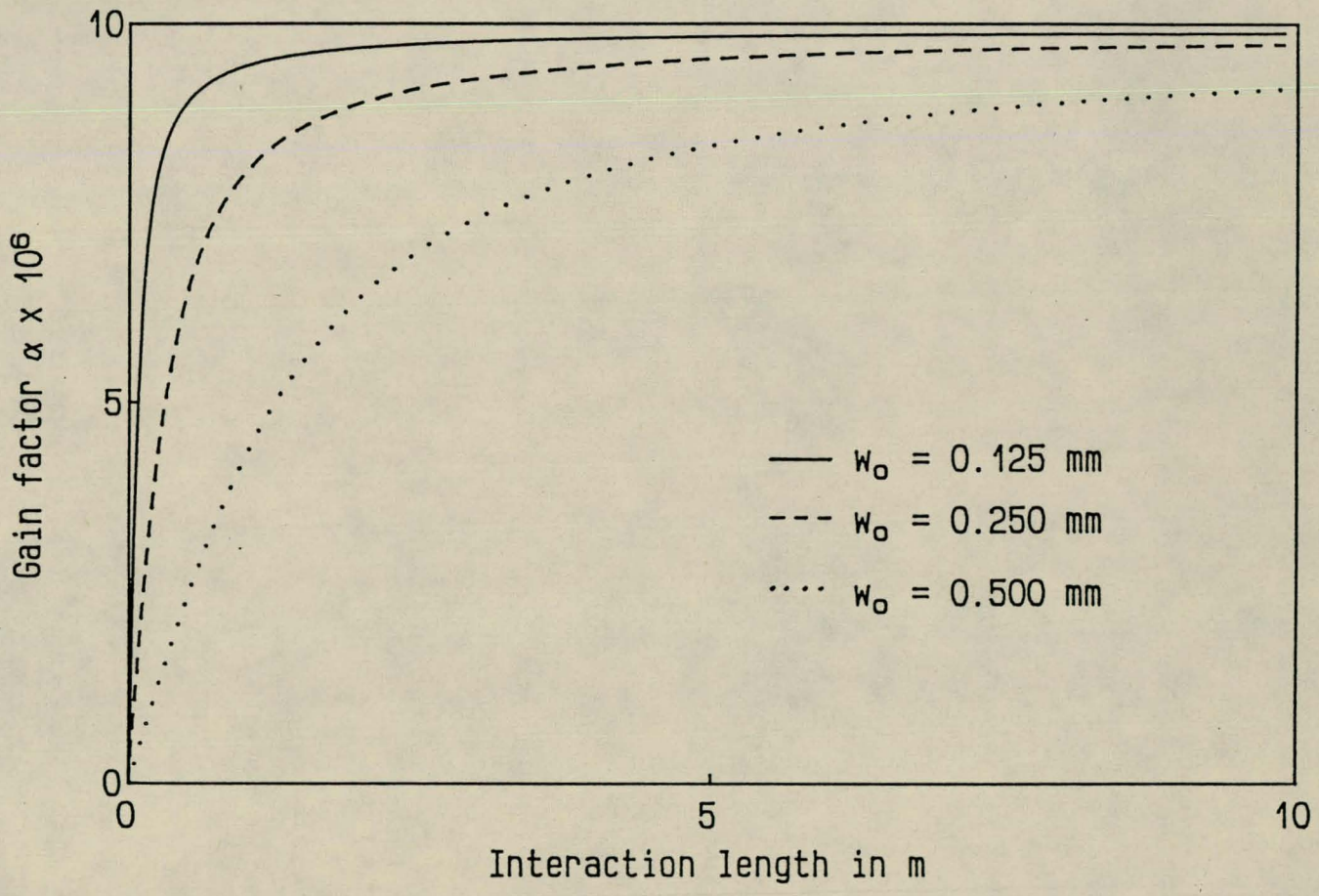

Figure 4.12 The gain factor α versus the interaction length L

One notes that α reaches a limit if the length is increased indefinitely. Thus in order to maximize α it is not enough to increase the interaction length. It is much more effective to reduces the spot size of the beam, that is to focus the beam to a smaller value of w_o. As shown in figure 4.12, the graph converges more quickly for smaller w_o values to the limit value for the same interaction length. In practise there is a limit on focussing because of 'gas breakdown'.

4.12.6 Gaussian Stokes wave for Gaussian gain

The fact that g is a function of x, y and z is now included in the analysis.

One thus has that

$$I_s = I_{bs} e^{\int_o^z g(x,y,z)dz} \tag{4.71}$$

As in the previous case, the Stokes background intensity I_{bs}, has a Gaussian profile given by

$$I_{bs} = I_{bso} e^{-2(x^2+y^2)/w_{so}^2} \tag{4.72}$$

The Stokes intensity I_s may thus be written as

$$I_s = I_{bso} e^{-2(x^2+y^2)/w_{so}^2} e^{\int_o^z g(x,y,z)dz} \tag{4.73}$$

This may also be written as

$$I_s(x,y,z) = I_{bso} e^{-2(x^2+y^2)/w_{so}^2} e^{D(x,y,z)} \tag{4.74}$$

$$D(x,y,z) = \int_o^z g(x,y,z)dz \tag{4.75}$$

The $x-y$ dependence of the term $D(x,y,z)$ changes the Gaussian character of the Stokes wave. If D only has a z dependence as in section 4.12.5, the Gaussian character would still be held. As a result the Raman profile is approximately a Gaussian profile, depending on the 'strength' of D with respect to x and y. To calculate I_s, g must be known to determine the value of D. The pump beam profile determines the character of the gain and in this case g is not constant,

but is a function of x, y and z. It decreases with increase in z and has the same form as the pump Gaussian beam.

The exact form of the gain : $g = GI_p$ where G is the plane wave gain coefficient is now included.

$$g_s = GI_{po}e^{-2(x^2+y^2)/w_p^2} \tag{4.76}$$

I_{po} may be written as

$$I_{po} = \frac{2P_p}{\pi w_p^2} \tag{4.77}$$

The gain g_s becomes

$$g = \frac{2GP_p}{\pi w_p^2}e^{-2(x^2+y^2)/w_p^2} \tag{4.78}$$

From this it is clear that the gain has a x, y and z dependence. The first factor, $2GP_p/\pi w_p^2$ causes the gain to decreases on the z-axis as z increases as seen in section 4.12.5. One now has an additional x and y dependence in the exponential factor which describes the fact that the gain is lesser on the flanks of the Gaussian beam and becomes less as z increases for specific $x-y$ coordinates because w_p increases as z increases. The problem remains to solve equation 4.75 which will not be attempted here.

The final result obtained after making approximations has the same character as in the previous case and will only be quoted here [Tr 80].

The power increase per transit is given by

$$P_s = P_{bs}e^{\alpha} \tag{4.79}$$

where α is given by

$$\alpha = \frac{4P_pG}{\lambda_p + \lambda_s}\arctan\left(\frac{L}{b}\right) \tag{4.80}$$

and b is given by

$$b = \frac{2\pi w_{po}^2}{\lambda_p} \tag{4.81}$$

From the last two discussions one has seen that the gain factor increases dramatically when the pump beam is focussed. Pump beams in the ultraviolet regions may be focussed easily and because the divergence of the beam is relatively small, a near high intensity region over the whole interaction region is obtained. In the infrared region, this behaviour changes dramatically and the beam divergence is much larger. A waveguide is then introduced to focus the beam repeatedly and to maintain a high intensity region over the whole interaction region. One also has that lasers in the infrared region normally have less output power than ultraviolet lasers, and a waveguide is used to enhance the Raman gain by focussing of the pump beam.

5

HE-NE TRANSMISSION EXPERIMENT

5.1 Why waveguide transmission?

The characteristics of a hollow glass waveguide were investigated in order to use a waveguide to produce high pump intensity levels through respective focussing of the pump laser through the waveguide [He 88]. This high intensity is important for the stimulated Raman scattering process because it enhances the Raman gain factor g. This has been discussed in detail in chapter 4.

Maximum transmission through the waveguide must thus be obtained to ensure that minimum losses for both pump and Stokes waves occur in the waveguide. In chapter 3 the theoretical transmission of a hollow glass waveguide with respect to the beam waist size of the laser at the entrance of the waveguide was investigated. The result obtained there will now be tested experimentally. By practical measurements other parameters which also influence the transmission were determined. A photo-diode detector was used as a power meter to determine the laser beam waist as well as the power transmission of the waveguide. This detector may be saturated at high intensities and therefore the properties of the detector were investigated.

5.2 Photodiode detector

The basic principles of operation of the detector and the saturation effect that occurs at high intensities was investigated. The detector measures *power* and not the *intensity* of the source, in this case the laser [Op 90].

5.2.1 Theory of operation

To understand the working mechanism of the detector semiconductor theory was looked at. Semiconductors are materials with a small energy gap between the conduction and the valence energy bands. For example, for silicon, this valence band is completely filled and the conduction

band is vacant at room temperature. For the semiconductor to be conductive, electrons must be excited from the valence to the conduction band. The excitation may take place thermally, by exposure to high energy particles, or by exposure to light. An incident photon with energy greater or equal to the bandgap of the semiconductor will excite an electron and will thus produce an electron-hole pair. By now using a P-N type junction, the intrinsic field of the junction prevents recombination of the pair and sweeps the electrons to the N type and the holes to the P type region. The anode becomes positive with the accumulation of holes and in the cathode becomes negative with electrons. The induced potential now causes current to flow in a external circuit which is known as the photovoltaic effect - the generation of a current from a P-N junction when exposed to light.

5.2.2 Relative Response

The relative response of a silicon photodiode is a measure of the sensitivity to light and is defined as the ratio of the photovoltage V, and the optical power P, of the incident light.

$$R_\lambda = \frac{1}{R_f}\frac{V}{P} \tag{5.1}$$

R_f is the resistance over which the photovoltage is measured.

The photovoltaic effect is a quantum effect: i.e. one incident photon produces one electron-hole pair or none at all. This means that the incoming light may be considered as a stream of photons which is converted to a stream of electrons with a certain efficiency. This efficiency is then a measure of the relative response. One may now expect that the efficiency is 100% or zero for a single photon interaction from above reasoning and that the relative response will be the same for photons with different energies but still larger than the energy gap. Because different energies correspond to different wavelengths, one expects the relative response to be independent of wavelength.

This is not the case. Because the light reflection and absorption coefficients of silicon changes with wavelength, the number of photons that may be converted to electron-holes, is different for different wavelengths. The relative response thus depends on the wavelength. In figure 5.1 a typical response curve with respect to wavelength is shown.

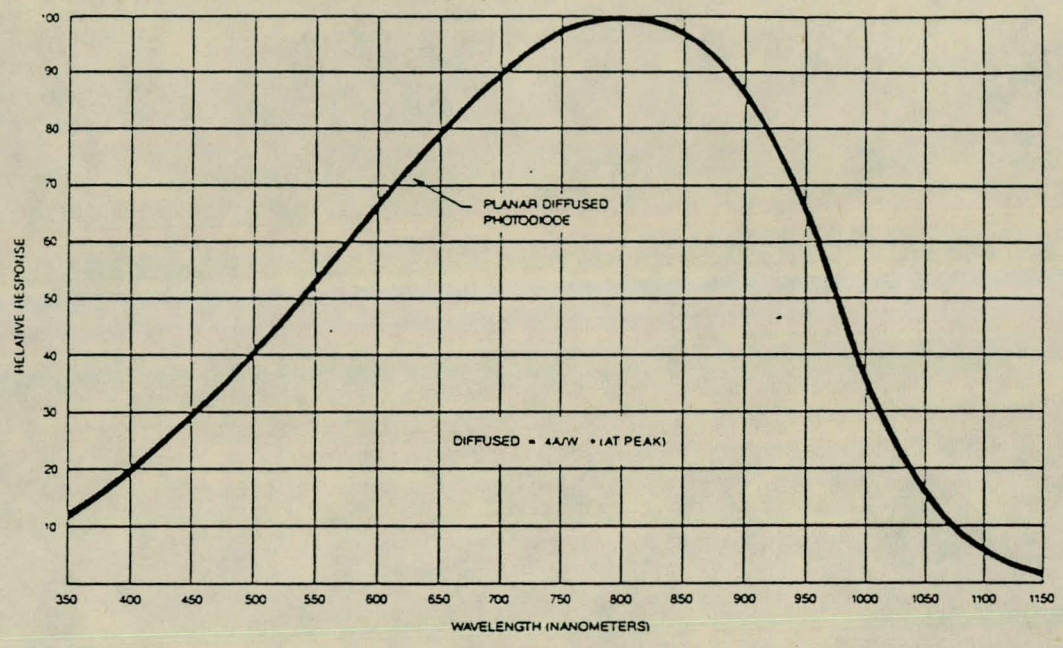

Figure 5.1 Relative Response of Detector

The applied voltage also effects the relative response because the voltage affects the collection of the electron-hole pairs. Temperature also effects the relative response, because optical properties of silicon such as reflection and absorption is temperature depended.

5.2.3 The output voltage

Considering the nature of the photovoltaic process one will expect that the output voltage signal which is generated by the incoming stream of photons, will be proportional to the number of photons incident in a period of time, or in other words, linear to the power of the incoming beam. This will be true only if the incoming intensity is such that no saturation of the detector occurs. This saturation effect will be explained in the next section. For the moment consider operation in the linear range.

The output voltage is given by the following expression.

$$\begin{aligned} V &= I_p R_f \\ &= (P_{in} \times R) R_f \end{aligned} \tag{5.2}$$

R is the relative response.

5.2.4 The relation between the optical power P and the peak intensity I_o of a Gaussian beam.

The relation between P and I_o is described by

$$I_o = \frac{P}{\pi b^2} \tag{5.3}$$

where $b = \sqrt{2}w$ and w is the Gaussian beam width. The derivation of the above equation is shown in Appendix E.

This relation shows that for a constant P, the peak intensity I_o decreases as the beam propagates because the beam width increases. If the beam is focussed, the peak intensity increases and reaches a maximum at the point of focussing and then decreases again.

5.2.5 Saturation effect

High intensity may cause the detector to saturate, this means that by increasing the intensity further, no higher output voltage signal will be obtained. This saturation effect is not desirable, because then the linear relation between the output voltage and the optical power does not hold.

As described by equation 5.3, the intensity depends on the beam size, as well as the optical power. Since saturation is caused by intensity, one may expect that by increasing the power of the laser at a certain beam size, saturation must occur at high enough power values.

In an experiment the detector was used to measure the optical power of the beam. The power of the laser was relatively measured say P_{rel} and filters with known attenuation were used to attenuate the beam power. The unattenuated power was called P_l, and P_{rel} may thus be written as fractions of P_l.

The experimental results are shown in figure 5.2 where the voltage reading is plotted against different relative input power values. Clearly saturation is present at relative power values above about $0.1P_l$. Considering figure 5.3, where P_{rel} values up to 0.04 are plotted, one sees that the graph is linear.

The equation which describes this relation is the following typical saturation curve

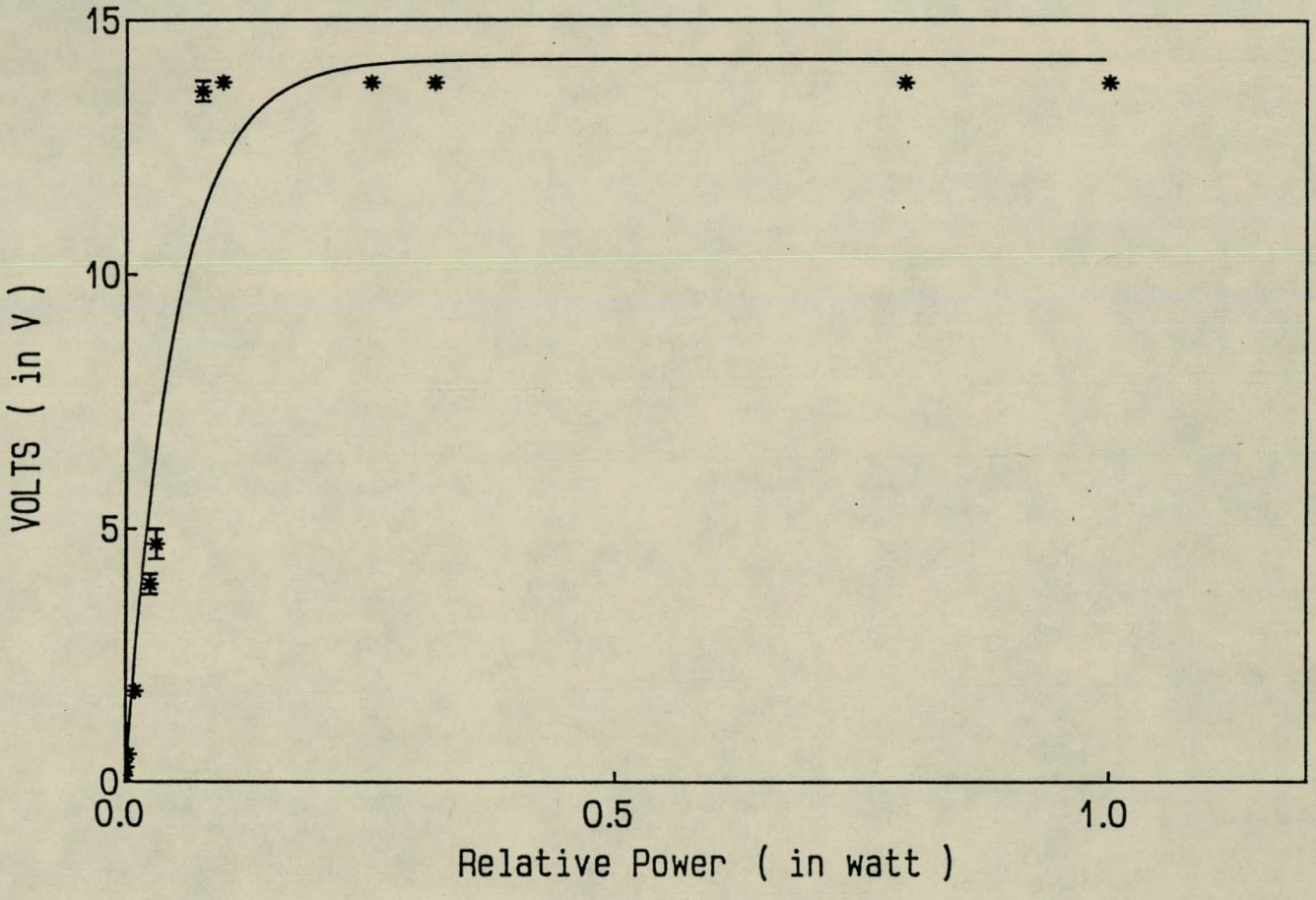

Figure 5.2 The Saturation curve

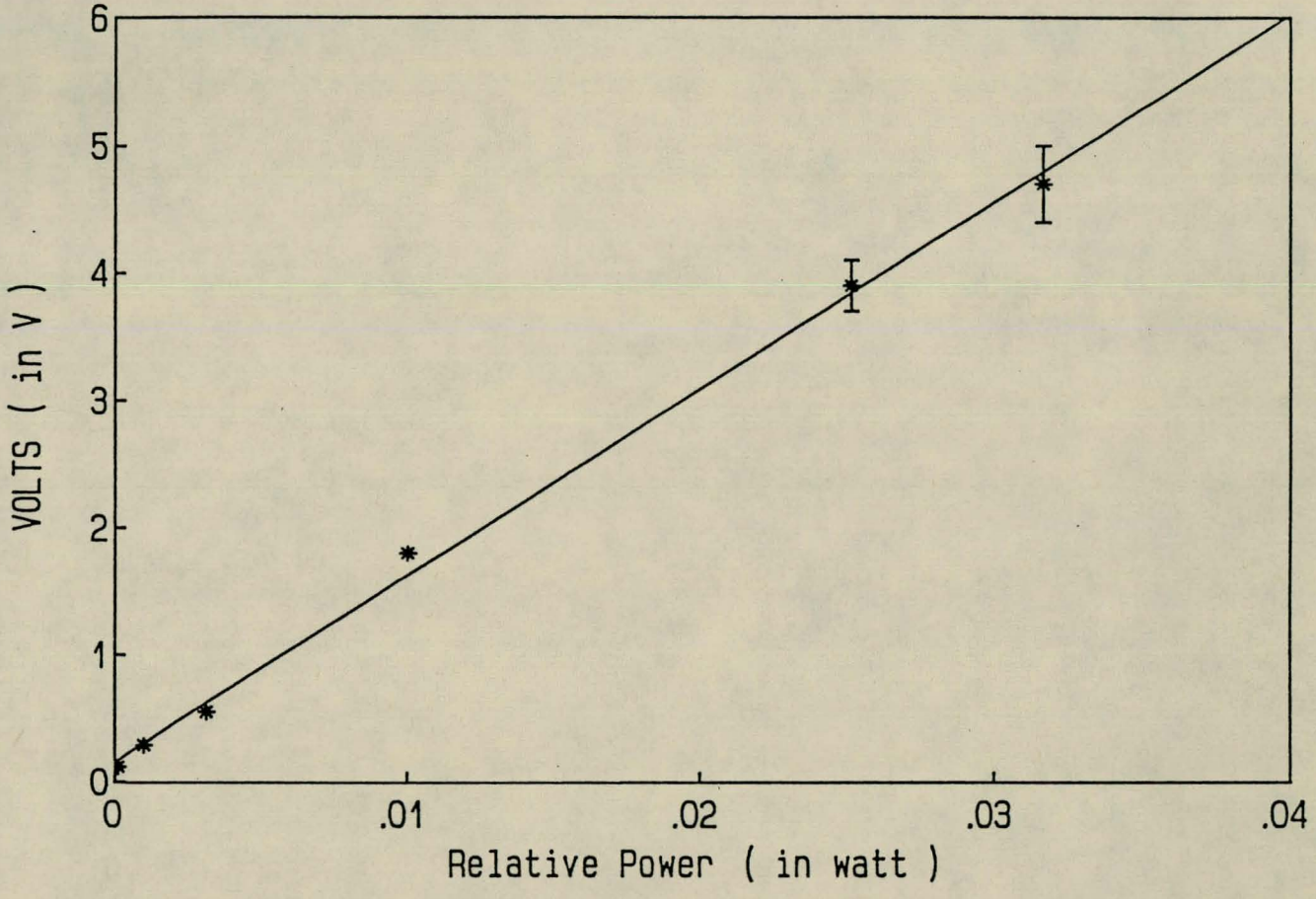

Figure 5.3 Linear range of detector

$$V = a(1 - e^{-bP_{rel}}) \tag{5.4}$$

where V and P_{rel} are the voltage and relative power respectively and a and b are constants which may be determined by fitting of the above function to experimental data. At low relative power the relation indeed becomes linear as the factor $-bP_{rel}$ becomes very small. This may be seen from the following expansion

$$e^{-bP_{rel}} = 1 + bP_{rel} - \frac{b^2 P_{rel}^2}{2} + \ldots \tag{5.5}$$

By assuming a function of the above form, a and b may be calculated from the experimental results using a least square fit. The following result is obtained.

$$V = 14.22(1 - e^{-19.44P_{rel}}) \tag{5.6}$$

These two values apply to the case where the power is measured relative. Because the intensity causes saturation, it is more useful to write equation 5.6 in terms of the real intensity, and not the relative power. The constant b which is valid for a function in which the real intensity appears will be determined later.

The relation between the peak intensity and the power of the Gaussian beam is very important because the saturation effect is caused by the intensity of the Gaussian beam and the high peak intensity will cause saturation while the average intensity may not be enough to cause significant saturation of the detector.

The detector is used to determine the optical power as well as the beam waist w_o to which the laser beam is focussed. This information is later used to determine the influence of the beam waist size on the transmission of a hollow waveguide. Accurate measurements with the detector is thus very important.

When measuring the beam power, one may put the detector in the beam path at any position if the peak intensity at that position is such that saturation is negligible. One would not try to measure the power at the position where the beam is focussed, because the peak intensity is then a maximum. The best position to measure the power is where the beam width is quite large so that the total sensitive area of the detector is illuminated. Care must be taken to ensure that all the incident radiation falls on the detector surface.

If at this specific beam width w, the power is measured with no saturation this means that the power may now be measured at any position where the beam width is the same or larger. The laser power stays the same and because the beam width w is larger than the specified width, the peak intensity must be smaller so that saturation is negligible. This simplifies measurements because one does not have to calculate the peak intensity each time a measurement is made to test for saturation.

From equation 5.3 the peak intensity at which saturation becomes too large to be ignored, may be determined if the beam width w discussed above has been determined experimentally. This saturation value is called I_{sat} and is given by

$$I_{sat} = \frac{P_{sat}}{2\pi w_{sat}^2} \tag{5.7}$$

P_{sat} is the power at which saturation occurs for a certain beam size w_{sat}. This value determined for the saturated peak intensity is now a specification for the specific detector used and may be used with lasers of different power. When using a laser with different optical power, one may again use equation 5.7 and determine for the new power P, the minimum beam width w at which the saturation effect may still be ignored.

Equation 5.7 may also be interpreted as follows. An upper limit for the power for a given beam width may be determined. Using higher output power lasers will result in saturation of the detector.

A practical method to prevent saturation is to use a filter with a known transmission, like neutral density filters. If the filter gives a voltage reading of the same fraction indicated by its transmission, then there clearly is no saturation. If the value is larger, then the detector is saturated. This method provides a quick check which is useful in a experimental setup.

5.2.6 Determination of I_{sat}

An intensity value was now determined at which one may safely assume that the effect of saturation is negligible. There is of course no value for the intensity above which saturation is present and which below no saturation occurs. The definition of the saturation peak intensity I_{sat} is thus defined as the intensity at which the effect of saturation is negligible, although present.

From figure 5.2 a value for the relative power is chosen at which the voltage reading has decreased with $1/e$ from the peak or saturated voltage reading. This gives

$$19.44P_{rel} = 1 \tag{5.8}$$

From this one may obtain that

$$P_{rel} = 0.05144\, P_l \tag{5.9}$$

The voltage reading at this intensity is

$$V = 14.22(1 - \frac{1}{e}) = 8.989 \text{ volt} \tag{5.10}$$

This value is now halved to make absolutely sure that the effect of saturation may be ignored. This gives a voltage reading of 4.50 volt. In figure 5.3, this value is in the linear range of the detector which support the above calculations.

The optical power is given by

$$P = 2.39 \times 10^{-5} \times 4.5 = 1.076 \times 10^{-4} \text{ watt} \tag{5.11}$$

The factor 2.39×10^{-5} was determined using equation 5.3 and the detector specifications.

From $b = 0.3089$ mm and using equation 5.3, one has that

$$I_{sat} = 3.589 \times 10^{-4} \text{ watt/mm}^2 \tag{5.12}$$

5.2.7 The saturation constant in terms of the real intensity

The following saturation curve where P_{rel} is the relative power of the laser was obtained and the constant b, which is equal to 19.44 is associated with the relative power.

$$V = 14.22(1 - e^{-19.44P_{rel}}) \tag{5.13}$$

An equation which connects the voltage reading with the real intensity and not the relative power is sought. The relation will have the same form as the above, but the constant 19.44 will have a different value. In the linear range of the detector one has that

$$P = 2.39 \times 10^{-5} \times V \text{ watt} \tag{5.14}$$

One also has that

$$P = 2\pi I_o w^2 \tag{5.15}$$

One may write down the following

$$V = 14.22(1 - e^{-cI}) \text{ volt} \tag{5.16}$$

where I is the real intensity.

This means that

$$-cI = -19.44 P_{rel} \tag{5.17}$$

If I may be calculated at a relative value of P_{rel}, c may be calculated. In the linear range a relative power value of 0.02 is chosen and the voltage reading is calculated by using the linear regression equation describing figure 5.3.

$$V = 146.6 P_{rel} + .1583 \tag{5.18}$$

Substituting $P_{rel} = 0.02$ in the above relation gives a voltage reading of 3.09 volt. The optical power P may be determined which is equal to 7.386×10^{-5} watt.

Using equation 5.15, the real peak intensity I_o may be calculated.

$$I_o = \frac{P}{\pi(w/\sqrt{2})^2} = \frac{7.386 \times 10^{-5}}{\pi(0.3089)^2} \tag{5.19}$$

This is equal to 2.4639×10^{-4} watt/mm^2.

Substitution of this into equation 5.17 yields the following result.

$$c = 19.44 \times \frac{P_{rel}}{I} \tag{5.20}$$

This gives $c = 1577.986$ mm^2/watt.

Equation 5.13 now becomes the following

$$V = 14.22(1 - e^{-1577.986I}) \text{ volt} \tag{5.21}$$

5.2.8 Practical determination of I_o using the detector

The determination of the peak intensity is of interest because comparison of it with the intensity saturation value will shown if the detector will saturate or not. Two practical ways to determine the peak intensity will be discussed here.

Method 1:

Combining equations 5.14 and 5.15 enables one to write the peak intensity in terms of the voltage reading obtained from the detector. This is only true if the detector is not saturated.

$$I_o = \frac{2.39 \times 10^{-5}}{2\pi w^2} V \tag{5.22}$$

By thus measuring the optical power P, which is given as a detector voltage reading and the beam width w, one is able to calculate I_o. Care must be taken to ensure that the detector is not saturated.

The peak intensity was experimentally calculated in a specific case. A voltage reading of 1.75 Volt measured at a beam width w of 0.413 mm gives an peak intensity value of 1.56 x 10^{-4} watt/mm^2.

Method 2:

One may also by scanning of the beam profile with a slit of known width, determine the peak intensity I_o. This is done by measuring the power radiating through the slit at each scanned position, and note the maximum voltage reading. In effect one has obtained a series of slices

of the Gaussian beam profile, each with its own Gaussian profile and peak intensity which is different at each scanned position. The slice with the highest peak intensity has a peak intensity equal to that of the whole Gaussian profile. This is the intensity value of interest here.

The area A, of this slice is given by

$$A = \int_{-\infty}^{+\infty} I_o e^{-2x^2/w^2} dx = 2wI_o\sqrt{\pi} \tag{5.23}$$

while scanning in the y-direction.

The power of the slice is then given by

$$P = A \times a \tag{5.24}$$

where a is the slit width.

The power P may also be written as

$$P = 2awI_o\sqrt{\pi} \tag{5.25}$$

The peak intensity is then given by

$$I_o = \frac{P}{2aw\sqrt{\pi}} \tag{5.26}$$

In the same practical setup as described in method 1, a maximum voltage reading of 0.183 V was obtained by scanning the beam profile using a slit of width 0.05 mm. Calculations gives P = 4.374 x 10^{-6} watt and a peak intensity value of 1.69 x 10^{-4} watt/mm^2 for the same beam width.

The percentage error is 7.69 % which shows that both methods give consistent results and any one may be used to calculate the peak intensity.

5.3 Experimental Transmission setup

Figure 5.4 shows a He-Ne laser on a stand and glass waveguide mounted on a straight piece of wood. A groove in the wood allows the glass waveguide to be mounted in such a way that

bending of the waveguide is minimized. The waveguide is mounted in a manner which allows complete aligning in all directions which is important for optimizing the transmission.

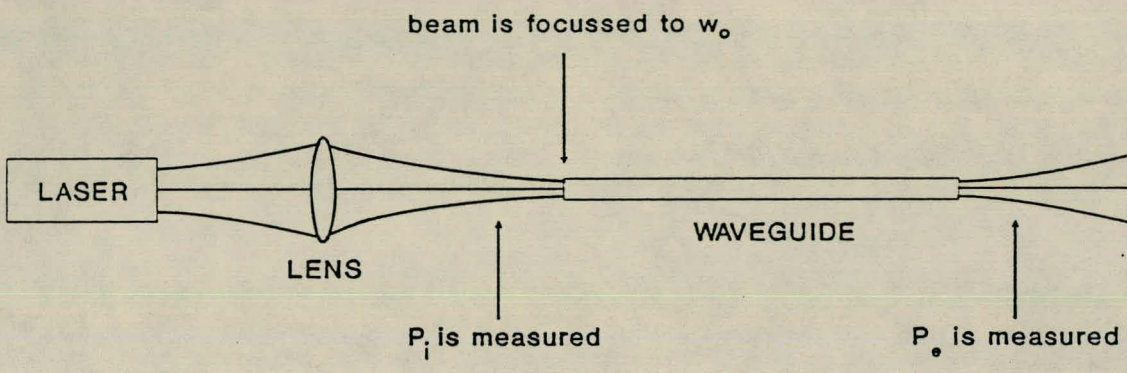

Figure 5.4 Transmission Setup

Neutral density filters with known transmission were used to lower the intensity of the laser beam to prevent saturation of the photo diode detector with which the power of the laser was measured. Glass waveguides with radii (R) 0.3 mm, 0.7 mm and length (L) 1110 mm respectively were used.

The transmission through the waveguide is defined as

$$T(\%) = \frac{P_e}{P_i} \times 100 \tag{5.27}$$

P_e and P_i is the exit and input power respectively.

The transmission of the waveguide was determined by measuring the input power of the laser before entering the waveguide P_i, and comparing it with the exit power measured P_e. In figure 5.4 it is shown where P_i and P_e is measured. Due to saturation of the detector, one cannot measure the power at any position.

The most important parameter which influences the transmission is the beam waist to which the

laser beam is focussed. This has been discussed in Chapter 3 where the transmission through a hollow waveguide discussed. The transmission was obtained for a number of waist sizes by focussing the laser with a lens to the required beam waist and optimizing of the transmission was obtained by aligning and adjusting of the waveguide. The transmission of waveguides with radii 0.3 and 0.7 mm were obtained as will be discussed later on.

The position at which the input power was to be measured was at a certain distance d away from the waveguide entrance, which had to be determined. At this position saturation of the detector must be negligible. If one assumes that the exit beam is still the same Gaussian beam as before entering the waveguide, one has that the beam size w, is the same for a distance d from the waveguide entrance, and exit respectively. The exit power P_e, was now measured at a distance larger or equal to d, because the exit power is of course less than the input power and the beam width is the same.

Following the above steps, the transmission may be determined accurately.

5.4 Parameters influencing the transmission

The transmission is determined by parameters of which some of the most important ones are listed below.

1. The laser wavelength
2. The w_o value of the laser beam.
3. The position of w_o with respect to the waveguide entrance.
4. The angle at which the radiation is injected.
5. The length of the glass waveguide.
6. The inside radius of the waveguide.

These parameters all have an influence on the transmission of the waveguide and therefore were investigated.

5.4.1 The influence of the minimum beam size

Convex lenses were used to focus the laser beam to chosen minimum beam widths w_o at the entrance of the waveguide. The theory of mode matching, which was discussed in chapter 3, was used to determine the position at which the lens and the waveguide entrance had to be

placed. For every chosen beam width, this position is different. Although the beam size w_o may be determined theoretically, it was also measured by means of a narrow slit which was moved across the beam while measuring the transmitted power. This method yields accurate results for the beam waist.

To determine the propagation of the laser beam one has to determine the position and size of w_o in the laser. If the beam size at a certain position z is determined experimentally, one would be able to calculate the size of w_o, if the position z of w_o is guessed. The physical length of the laser is about 40 cm, and it is guessed that the position of w_o is about in the middle of the laser. The error made may be minimized by measuring the beam size at a position z very large with respect to the length of the laser.

In Appendix B it is shown that if the beam waist w is known at a certain distance z, which is also known, it is possible to determine the magnitude of the beam waist w_o of the Gaussian beam by backtracking the beam. Consider figure 5.5.

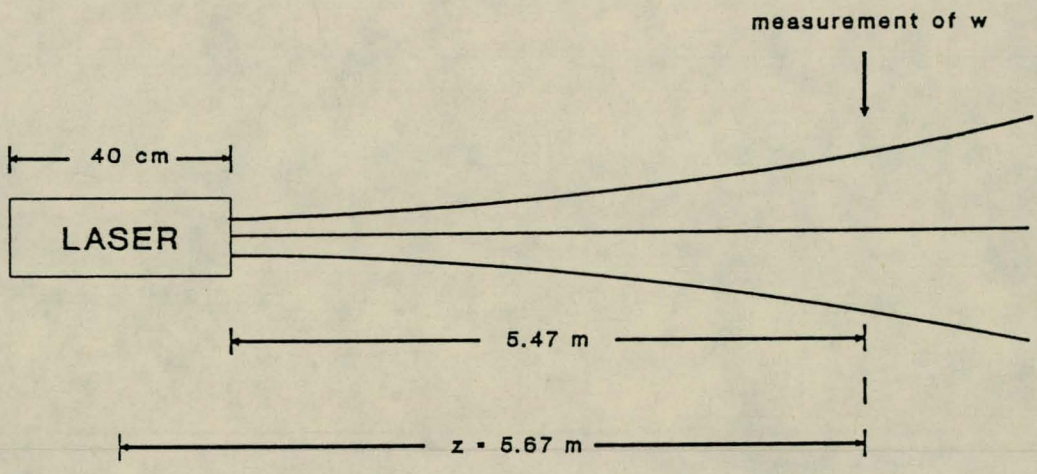

Figure 5.5 Measurement of w_o of laser

The waist has been measured at a distance 5.47 m from the laser which means that $z = 5.67$ m.

The beam waist was determined by scanning over the cross section of the beam with a narrow slit. Care was taken to ensure that the detector did not saturate. A Gaussian curve was then fitted to the experimental results. The experimental results with the Gaussian fit is shown in figure 5.6. From the fit the beam waist was determined as 2.644 mm.

A program was written which incorporates the results from Appendix B to determine w_o from a given w, distance z and wavelength which in this case is 632.8 nm. This gives $w_o = 0.5066$ mm.

Consider figure 5.7 which is the theoretical transmission for a waveguide of length $L = 1110$ mm and radius $R = 0.3$ mm. This is the transmission result obtained in chapter 3.

The dots are the experimental data points. The theoretical curve shows good correlation with the experimental data obtained. Note that the experimental data is always less than the theoretical data which is understandable, because the model does not include factors like diffraction losses and surface imperfections.

The data points show that there is a decrease in transmission for small as well as large w_o values. For large values of w_o there is a small decrease in the transmission due to the fact that the beam size becomes so large that less of the input beam rays enters the waveguide.

For small w_o values there is a sharp decrease in transmission which may be explained as follows. One has that the sharper a beam is focussed, the greater the beam divergence becomes so that there are more rays propagating at relative large angles with respect to the z-axis. This means that some of the rays are incident on the waveguide wall at large angles which means that the reflection losses are greater.

In figure 5.8 the transmission for a waveguide with radius 0.7 mm and the same length is shown. In this case the experimental and theoretical predictions also shows good agreement.

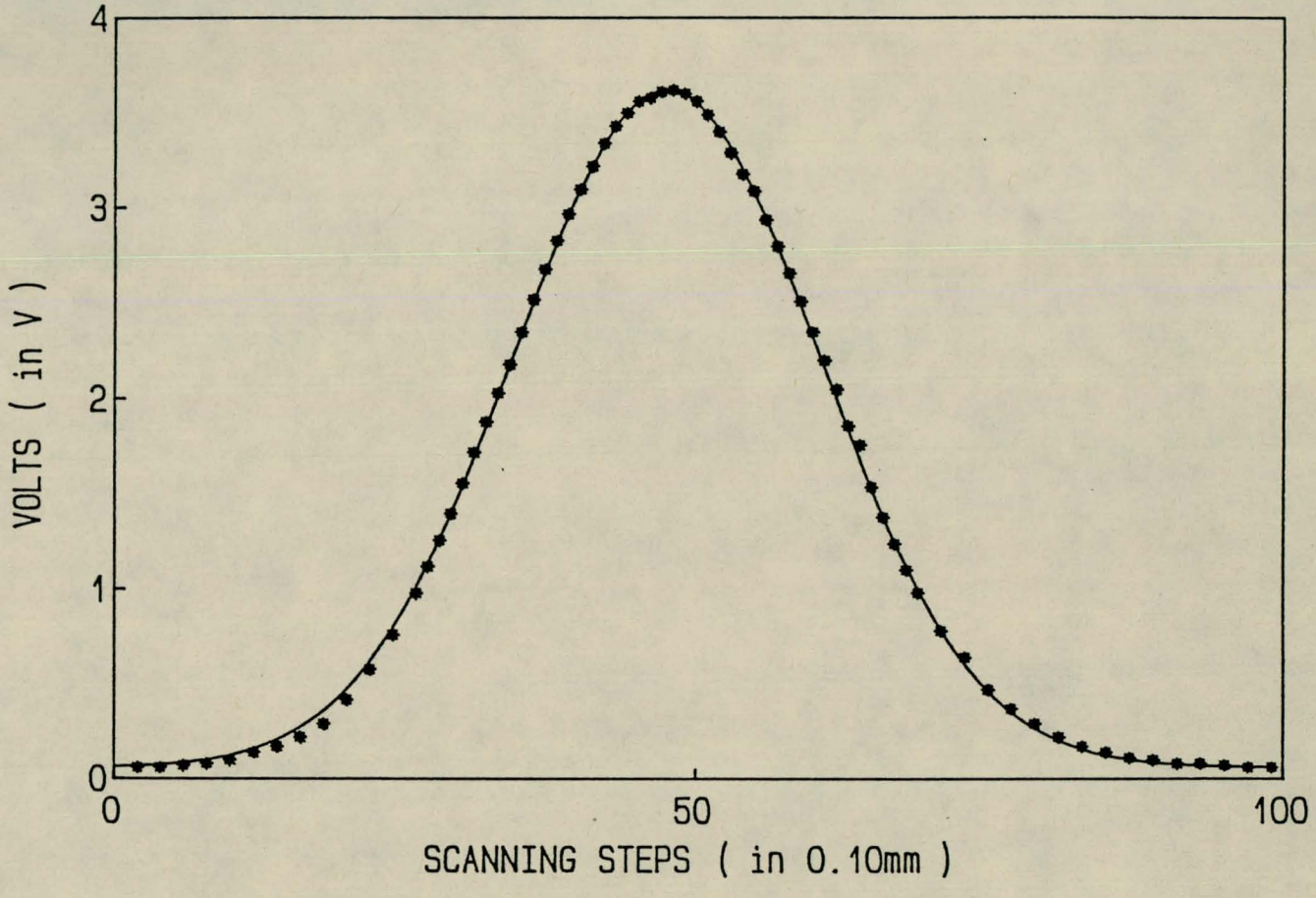

Figure 5.6 Gaussian beam width determination

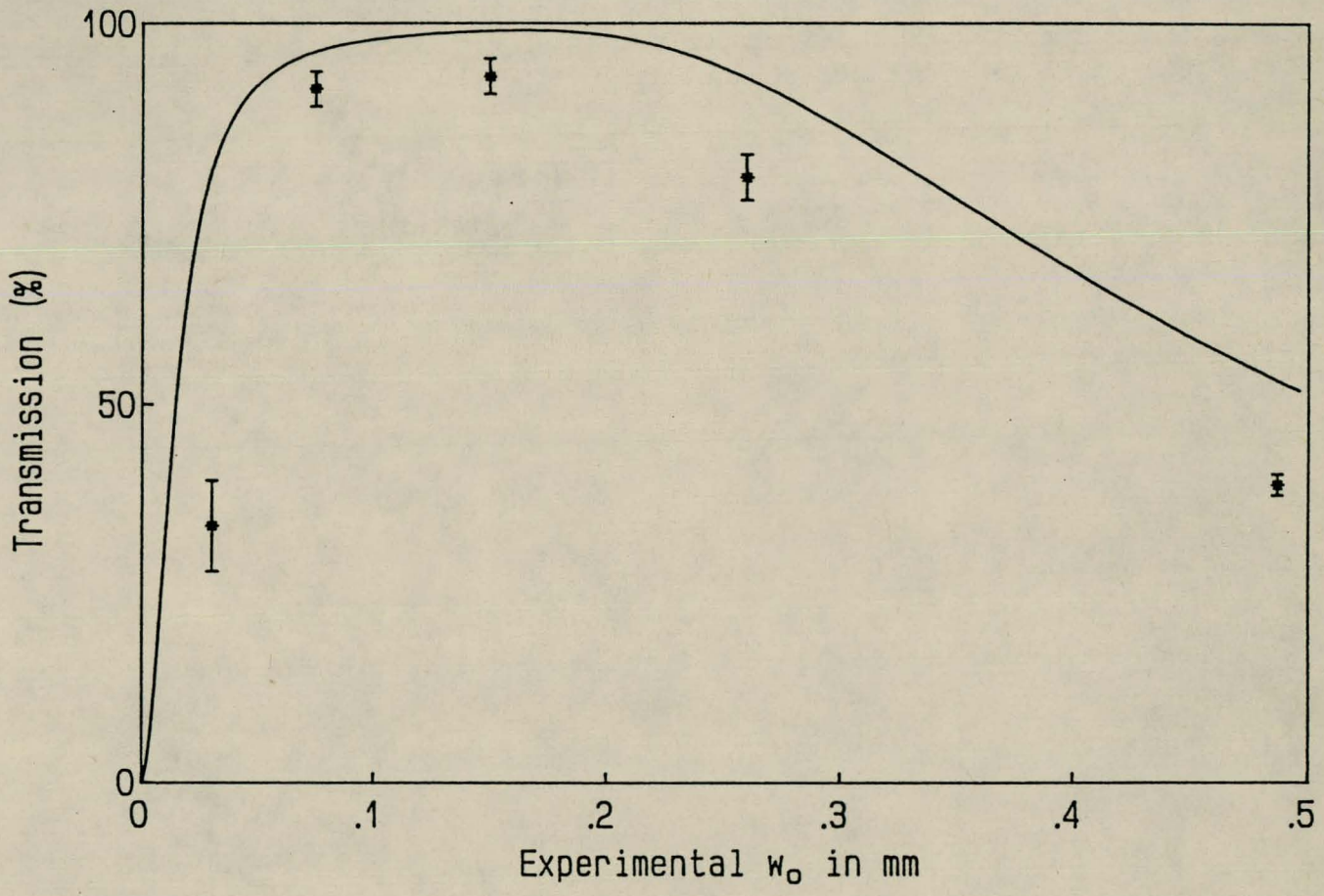

Figure 5.7 Waveguide Transmission for $R = 0.3$ mm

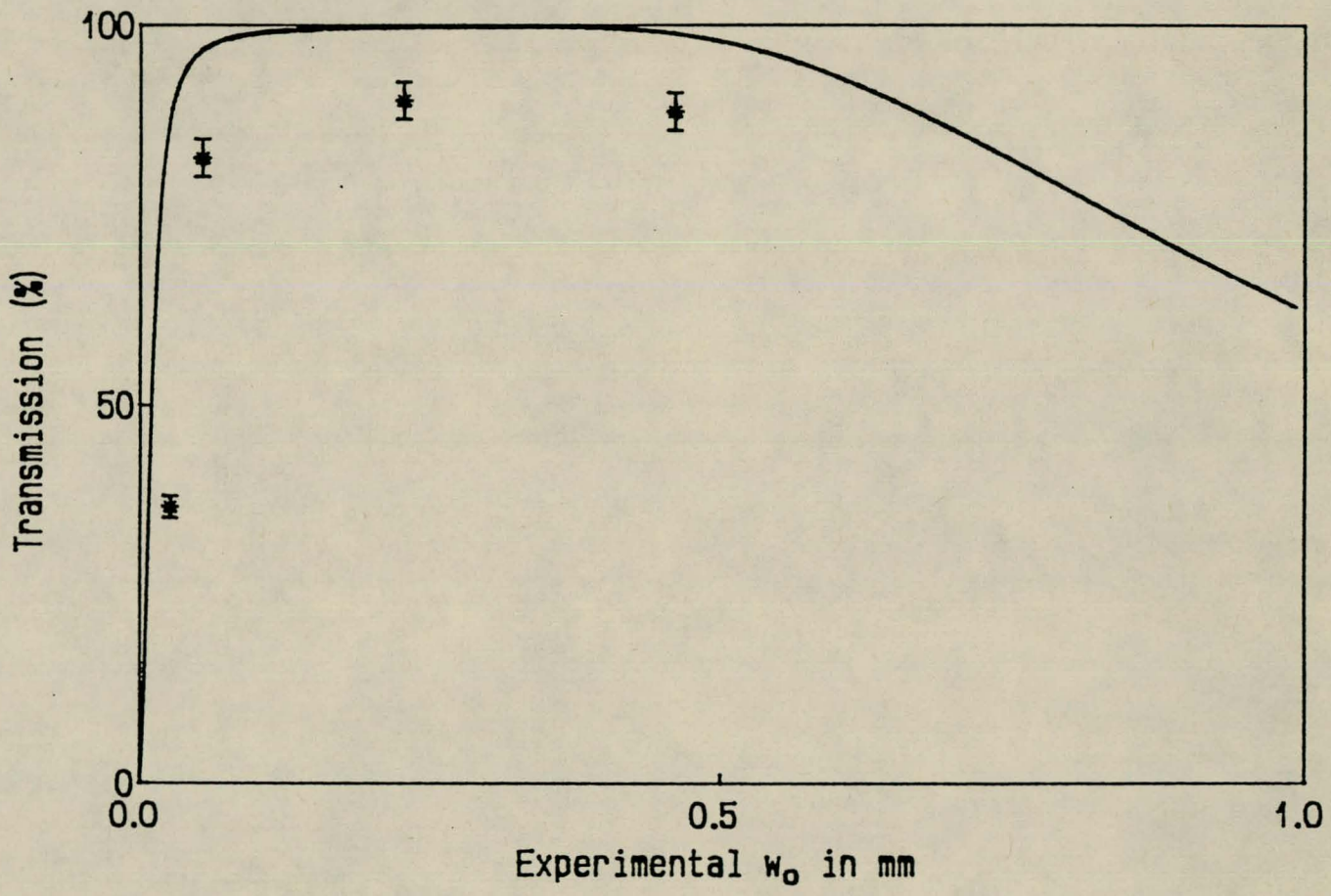

Figure 5.8 Waveguide Transmission for $R = 0.7$ mm

The maximum transmission was obtained at $w_o/R \approx 0.5$ as may be seen from the transmission curves in figures 5.7 and 5.8 [Cr 82]. In a experimental setup where optimum transmission is critical, the beam has to be focussed to the optimum w_o value. At the optimum w_o there is little variation in change in w_o so that a small error in the optimum beam waist should not have a large influence on the transmission.

5.4.2 The distance from w_o to the waveguide entrance

Because of practical error it is important to know how the transmission is influenced when the laser beam is not focussed exactly at the waveguide entrance as shown in figure 5.9. The waveguide was placed at distances smaller and larger than the optimum distance and the transmission was determined in each case.

In figures 5.10 and 5.11 in which the influence of the waveguide position on the transmission is showed, the transmission is plotted versus the distance between the waveguide and the lens. This distance is showed in figure 5.4. One feels that optimum transmission will be obtained when the waveguide is placed at the waist position. This was indeed the case as will be seen later from experimental results.

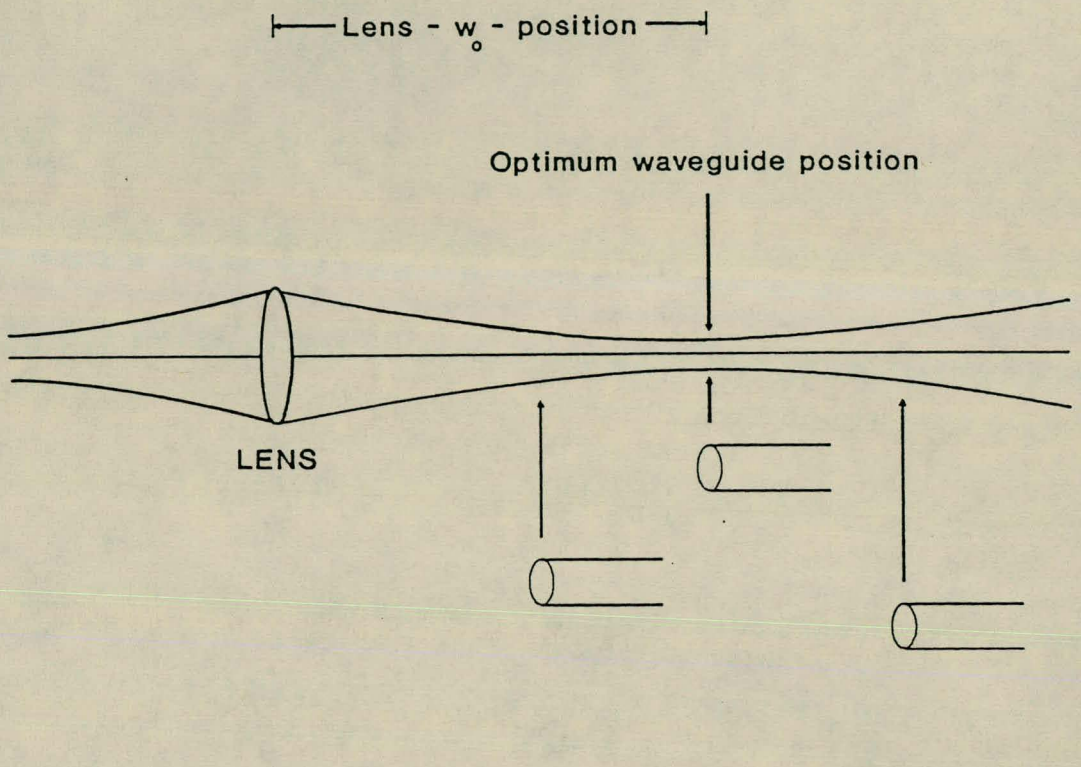

Figure 5.9 Waveguide Laser Position

Figure 5.10 is the result for a w_o value of 0.01 mm for which the distance between the lens and the waveguide is 4 cm. From the graph there is a small variation for a 3 cm variation in the optimum lens-w_o-distance. This certainly is not critical in a experimental setup because a 3 cm accuracy could be controlled easily in an experiment.

If one looks at the result for $w_o = 0.05$ mm as shown in figure 5.11, one notes that the influence of the lens-w_o-distance is less critical than in the previous case for $w_o = 0.01$ mm. One may assume that the effect would still be less for the larger w_o values. This may be attributed to the fact that the divergence of the beam is smaller for large w_o values. Over a certain distance one thus has a smaller change in the beam size and a variation in distance would have less effect than in the case of smaller w_o values. From both graphs one sees that optimum transmission was obtained when the waveguide was placed at the position of focussing as might have been anticipated.

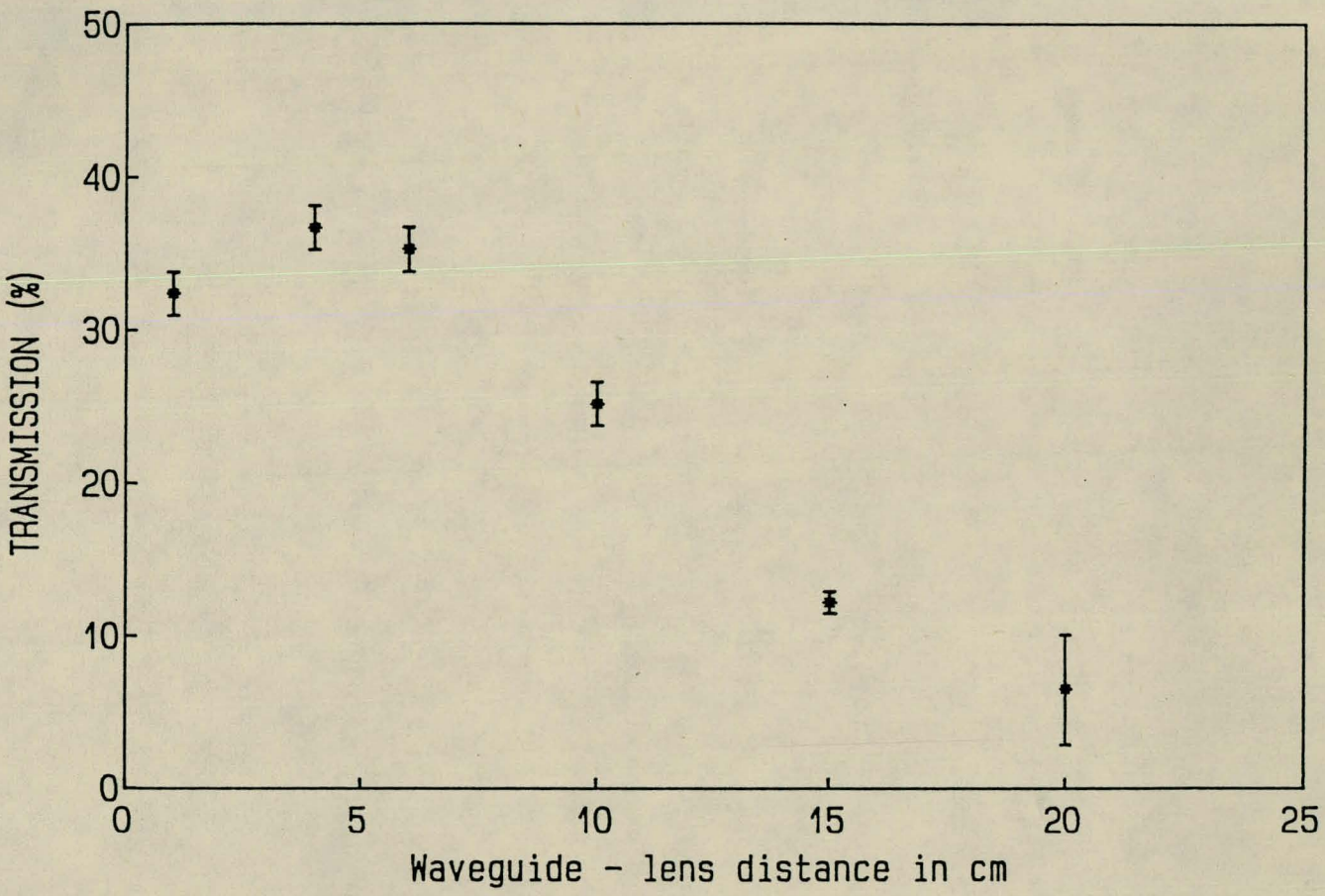

Figure 5.10 Influence of waveguide position

$w_o = 0.01$ mm

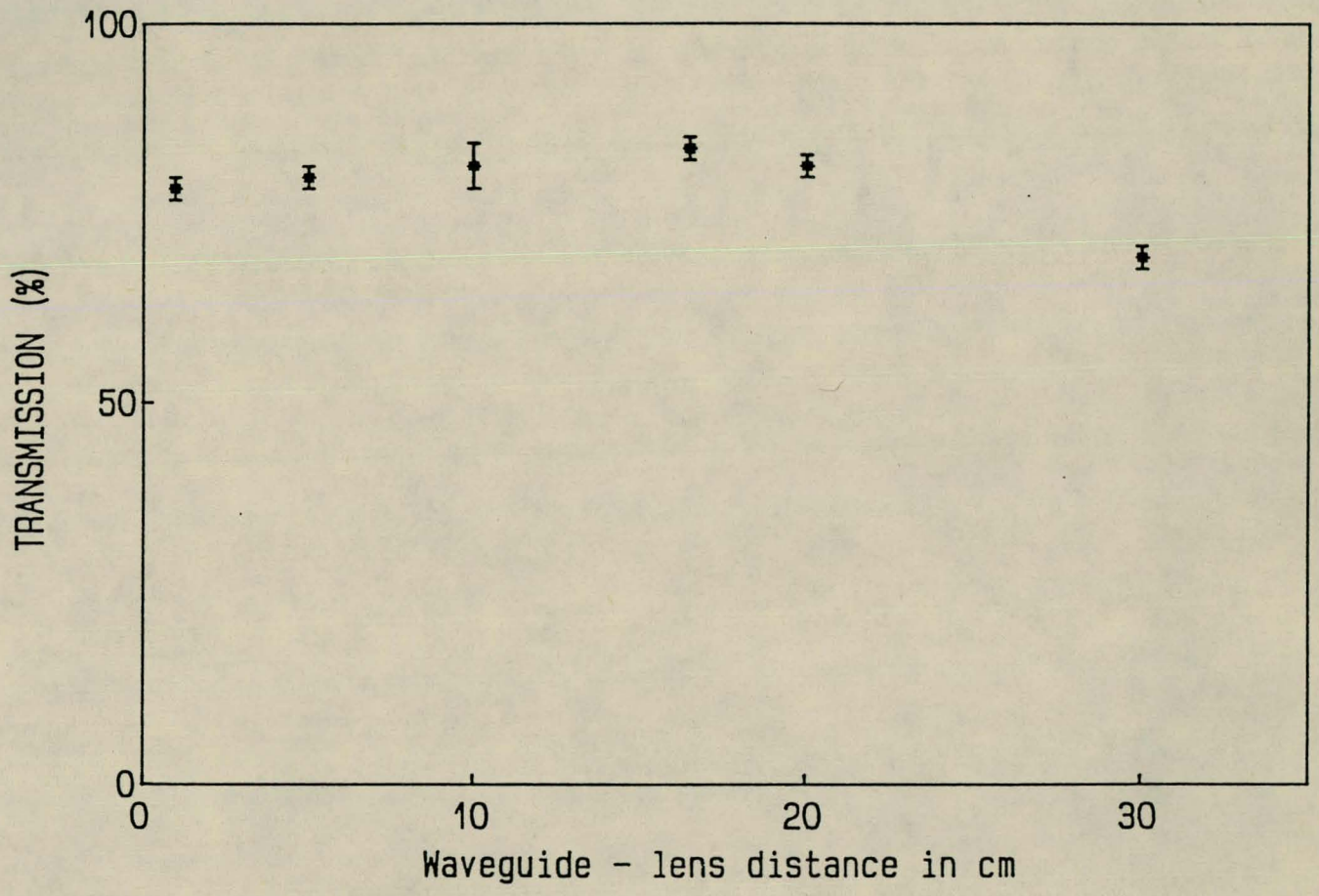

Figure 5.11 Influence of waveguide position

$w_o = 0.05$ mm

As a final result one thus has that an incorrect lens-w_o-distance does not have a critical influence on the transmission of the waveguide.

5.4.3 Non stable laser output

The He-Ne laser took about 2 hours to stabilize its output. This means that the experiment had to be completed in a short period, say about 15 minutes, to minimize the error. This was quite easily accomplished. Another and newer laser used later on was much better and had a more stable output. In effect this did not influence the transmission noticeably.

5.4.4 The angle of incidence

The angle θ, at which the laser beam is injected with respect to the waveguide axis as seen in figure 5.12, was very critical as shown in figure 5.13 for the case where $w_o = 0.05$ mm.

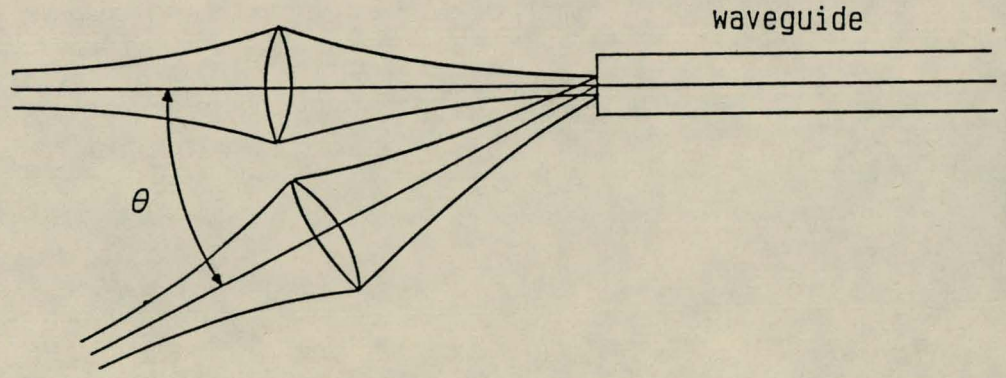

Figure 5.12 Angle of incidence

A small variation in the incident angle of less than a degree caused an enormous drop in transmission for all w_o values. The optimizing of the waveguide with respect to the laser beam is therefore of critical importance in the setup and the waveguide is mounted in such a manner which enables easy tuning of the waveguide.

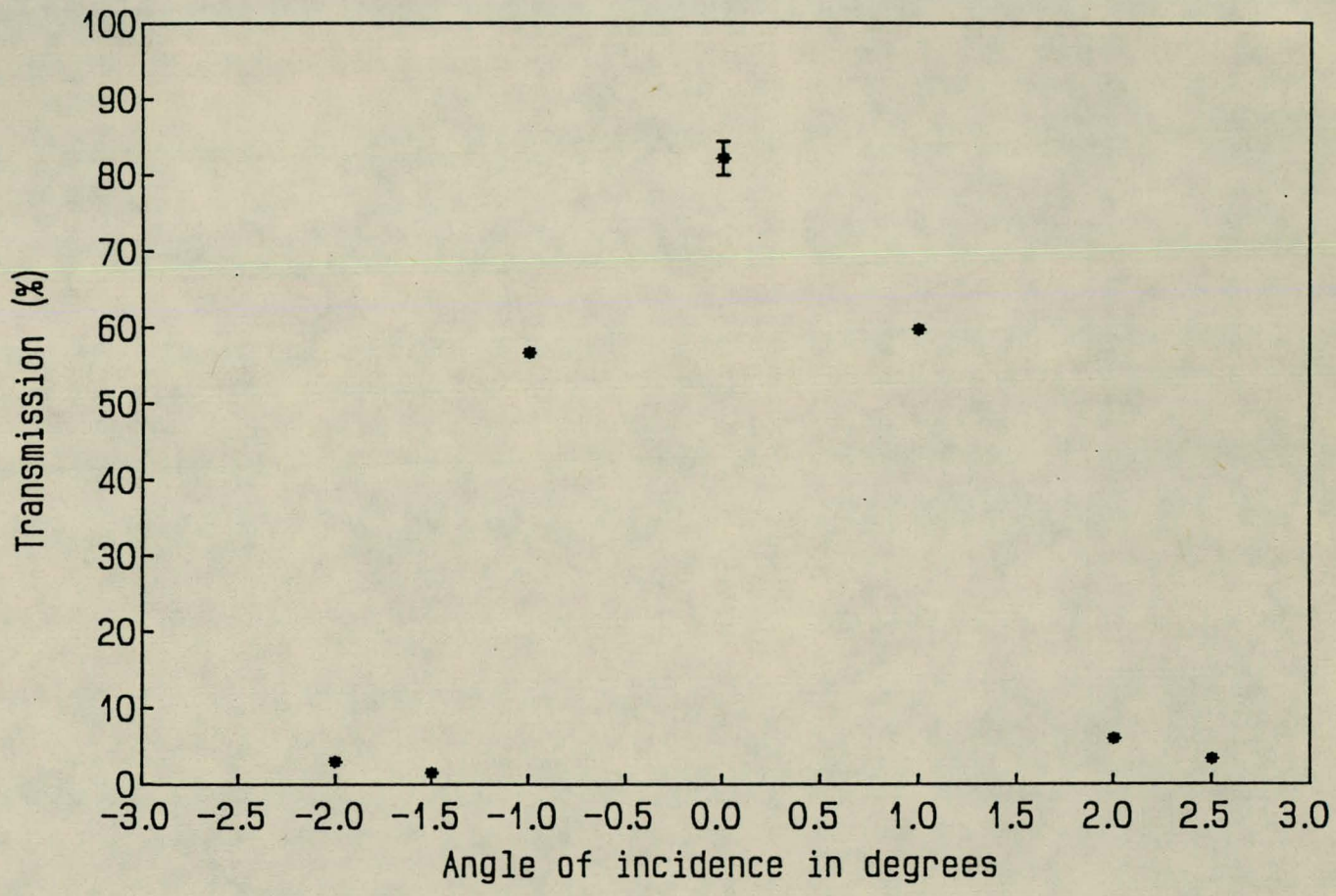

Figure 5.13 Influence of angle of incidence

$w_o = 0.05$ mm

5.4.5 Other parameters

The influence of other parameters like the length of the guide, is trivial to explain and was not determined experimentally. Larger lengths simply means that more reflections take place and one has more reflection losses. The radius R plays also a role because it determines the optimum w_o value. Larger radii corresponds to larger w_o values and thus smaller divergence of the beam. As already explained previously, this amounts to greater reflection in the waveguide and better transmission. Imperfections and impurities in the waveguide also causes losses because radiation is scattered or absorbed.

5.5 Recommendations

The experimental results showed that a very high transmission may be obtained experimentally, which shows that the current experimental setup is suitable in producing high transmission values.

The mounting of the waveguide may be improved in order to make the adjustments necessary to maximize the transmission, easier and more effective. Currently it is difficult to optimize the setup and practical experience is needed to perform the experiment successfully. A more fine tuning ability would thus improve the optimizing technique and would allow easier operation of the waveguide setup.

6

EXPERIMENTAL RAMAN INVESTIGATION

6.1 Introduction

In this final chapter the experimental investigation conducted concerning the Raman process will be discussed. Two mediums which are molecular hydrogen and nitrogen respectively were used. Four different pump lasers have been investigated as suitable pump sources namely a He-Ne laser, an argon ion laser, an excimer laser and finally a dye laser. A Raman shifter was used to contain the medium and could handle pressures up to 35 bar. A waveguide may also be fitted into the Raman shifter.

6.2 Parameters

In the next two tables the pump beam wavelength and the first three Stokes and first Anti-Stokes wavelengths for vibrational Raman scattering in hydrogen and nitrogen respectively are listed. The wavelengths are given in nm. σ is the vibrational energy difference in Kaysers.

Table 6.1

Pump (in nm)	Hydrogen : σ = 4155 cm^{-1}			
	S1	S2	S3	AS1
308	353	414	500	273
488	612	812	1246	406
500	696	980	1652	441
632.8	859	1335	2996	501

Table 6.2

Pump (in nm)	Nitrogen : σ = 2331 cm^{-1}			
	S1	S2	S3	AS1
308	332	360	393	287
488	551	632	741	438
500	618	722	868	480
632.8	742	898	1135	551

6.3 The Raman shifter

The Raman shifter has three different configurations for each spectral region namely, the vacuum ultraviolet (a), the ultraviolet (b) and the infrared configurations (c) as seen in figure 6.1 [La 85]. The first two configurations facilitate the use of an excimer laser as pump beam and lenses are used to focus the laser beam through the medium. For pump lasers in the infrared regions a waveguide is installed because of the low Raman gain in the infrared region. An external lens is then used to couple the laser beam which is a dye laser in this case, to a capillary tube of length 650 mm and radius 0.3 mm. This lens is AR coated for 500 - 700 nm and should not be used for shorter pump wavelengths.

The output side of the shifter is equipped with a Pelin-Broca prism which is used to select a particular wavelength by tuning the prism [Zo 66]. The Raman shifter may contain gases under pressure up to 35 bar after which a relieve valve is activated.

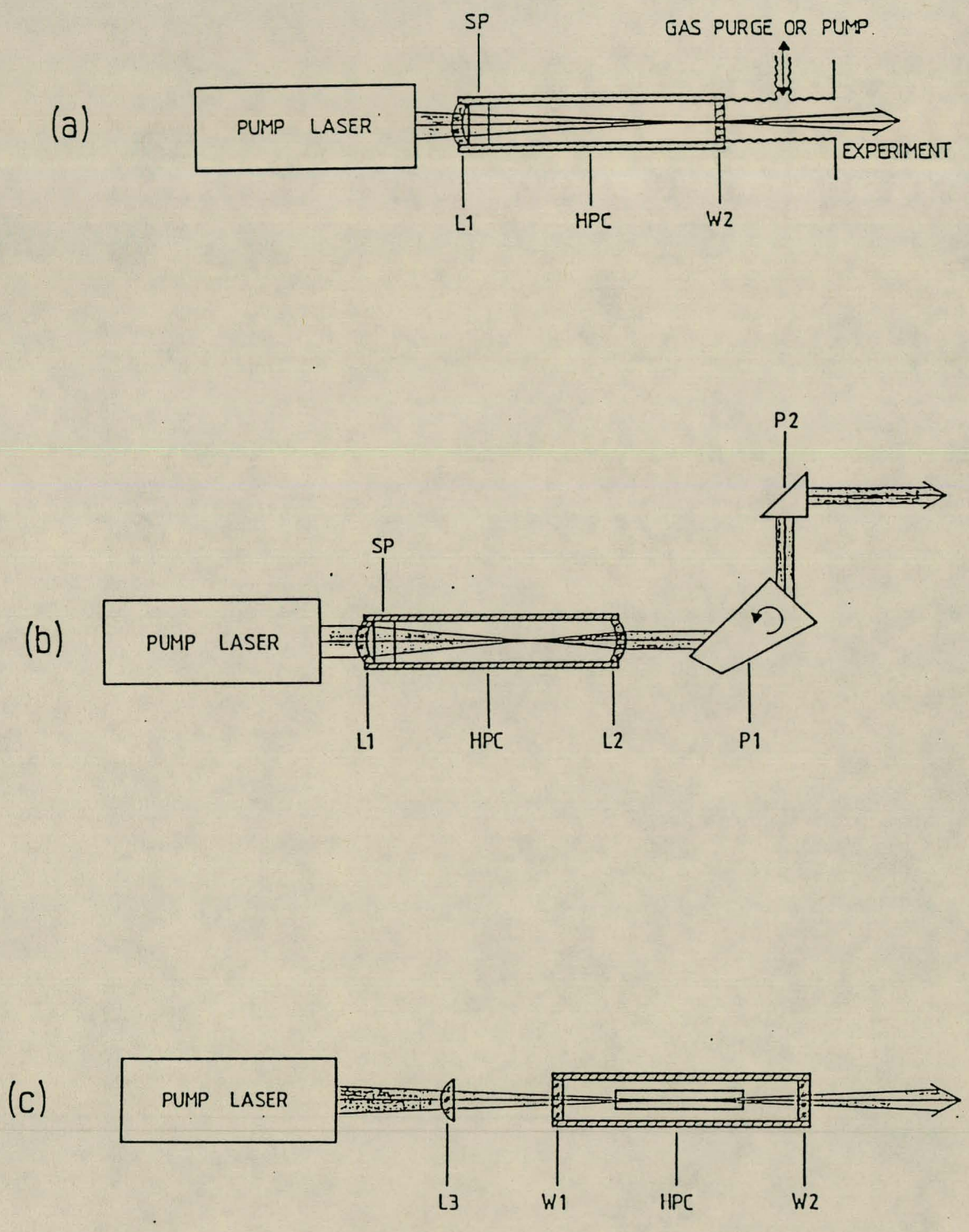

Figure 6.1 Raman Shifter Configurations

6.4 He-Ne laser as pump for Raman process

A He-Ne laser was chosen in a first attempt to obtain spontaneous Raman scattering because it is a continuous wave laser and simple to operate. Due to the relatively low laser intensity, it was expected that the losses would be too large for Raman laser action to be obtained, and that only the spontaneous Raman scattering process would be observed. The spontaneous process is always present in contrast with the Raman laser process which requires a threshold gain value before the losses can be overcome and the intensity starts to grow exponentially.

Since it is a cw laser, the Raman and pump spectral lines could be measured directly with a monochromator and a photomultiplier tube in contrast when a pulsed laser in conjuction with a Boxcar Integrator have too be used. The use of the Boxcar Integrator will be discussed in more detail when the excimer laser as a pump laser is described (section 6.6).

The output power of the He-Ne laser which was about 5 mW which is very small when compared with normally used powers of the Megawatt range. The capillary tube was thus used to enhance the Raman gain. For a pump wavelength of 632.8 nm, the first Stokes wavelength is at 742.3 nm for nitrogen as the Raman medium. The laser beam was focussed with the external lens to an optimum w_o value at the entrance of the waveguide and a transmission of 60% was obtained.

6.4.1 Line measurements

A wide input monochromator slit was used to increase the light acceptance of the monochromator. First some known helium and neon lines were investigated in order to calibrate the monochromator. The laser line 632.8 nm is a well-known line and at 730.6 nm there is also a relatively strong line. In figures 6.2 and 6.3 some profiles obtained from the monochromator are shown from which the wavelengths 632.9 $\pm$ 0.1 and 728.1 $\pm$ 0.1 nm were obtained. To obtain a better calibration the monochromator was scanned from 600 to 800 nm and a whole series of lines were measured which are plotted in figure 6.4.

From a linear fit of the data the monochromator reading at the first Stokes wavelength was 741.48 nm. The measured Stokes profile is shown in figure 6.5 with a nitrogen pressure of 20 bar. The wavelength measured was 743.0 nm. The question arose if this was the Stokes line or not. It could also have been a spontaneous helium or neon line at that particular wavelength. Because the Raman gain is pressure dependent a variation in pressure should cause a variation

in the signal intensity. No variation whatsoever could be measured after the pressure was varied from 35 bar down to 1 bar and a vacuum pump was used to obtain still lower pressures.

The above result could thus not verify if the line was indeed the first Stokes line or not. To obtain better results one should have a higher pump intensity or better measuring techniques. A cw argon ion laser with an specified output of nearly 3 Watt was then chosen because of its higher output intensity.

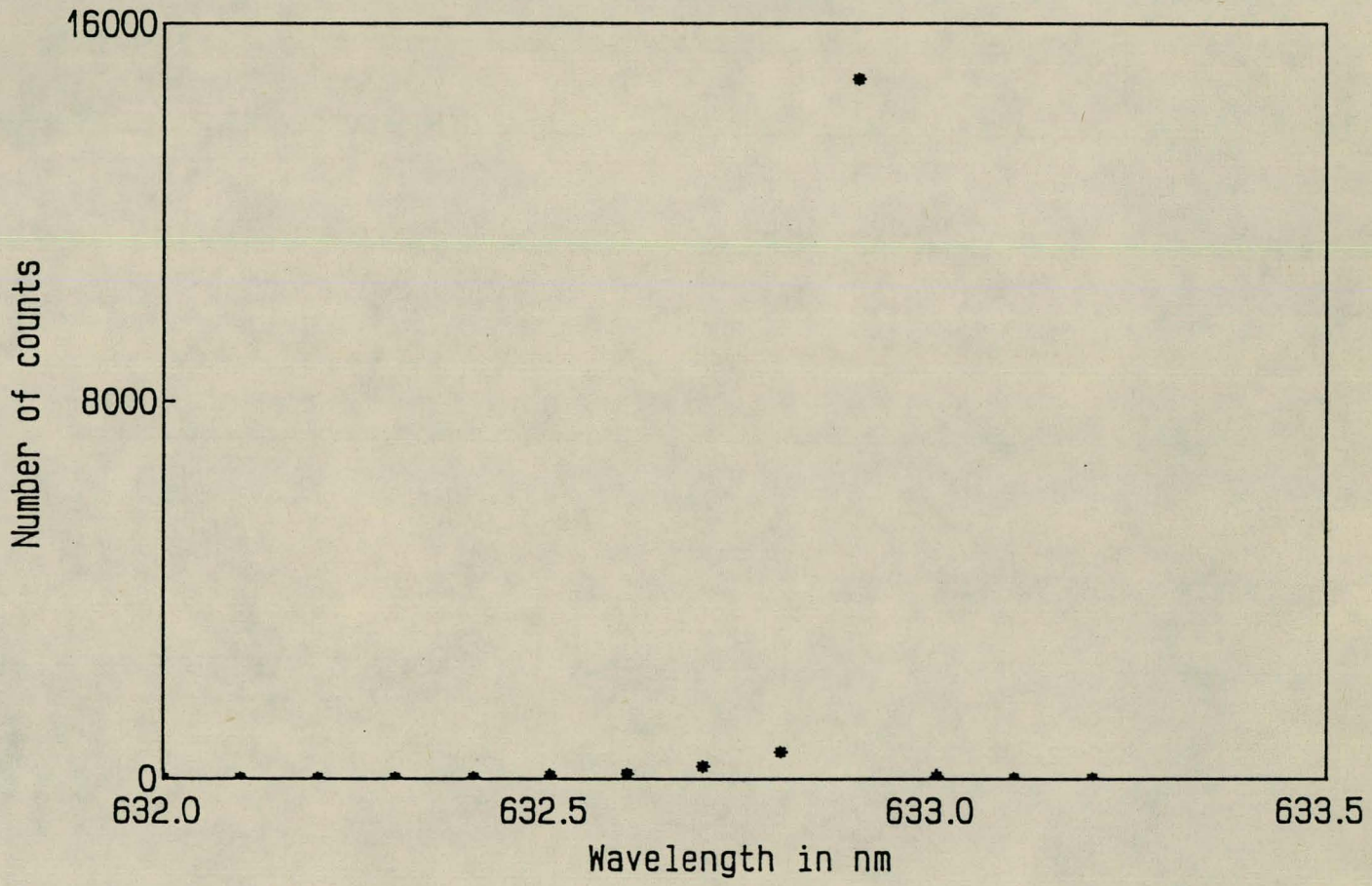

Figure 6.2 Measured Profile of Pump laser

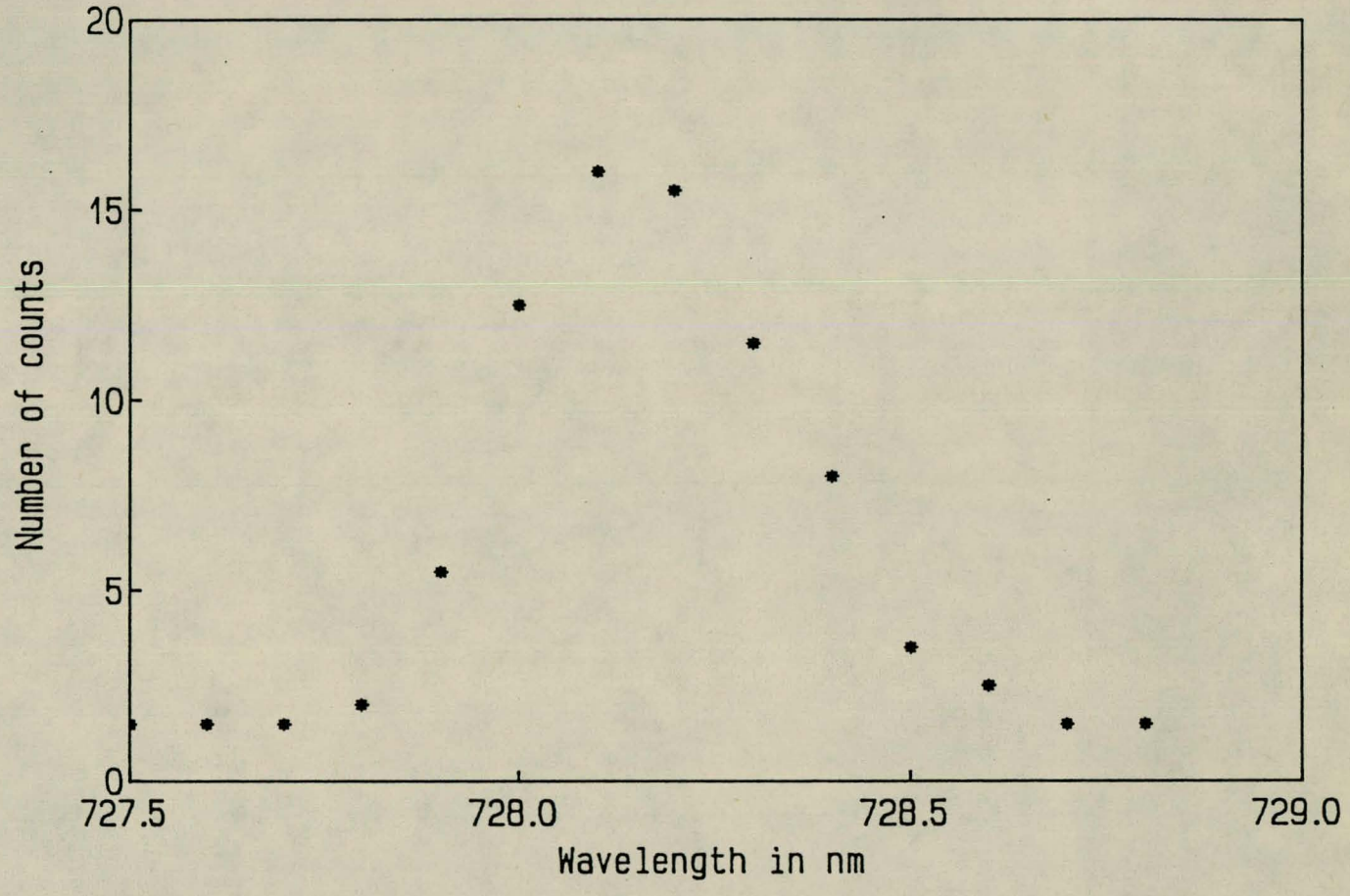

Figure 6.3 Measured Profile of 730.6 nm Neon Line

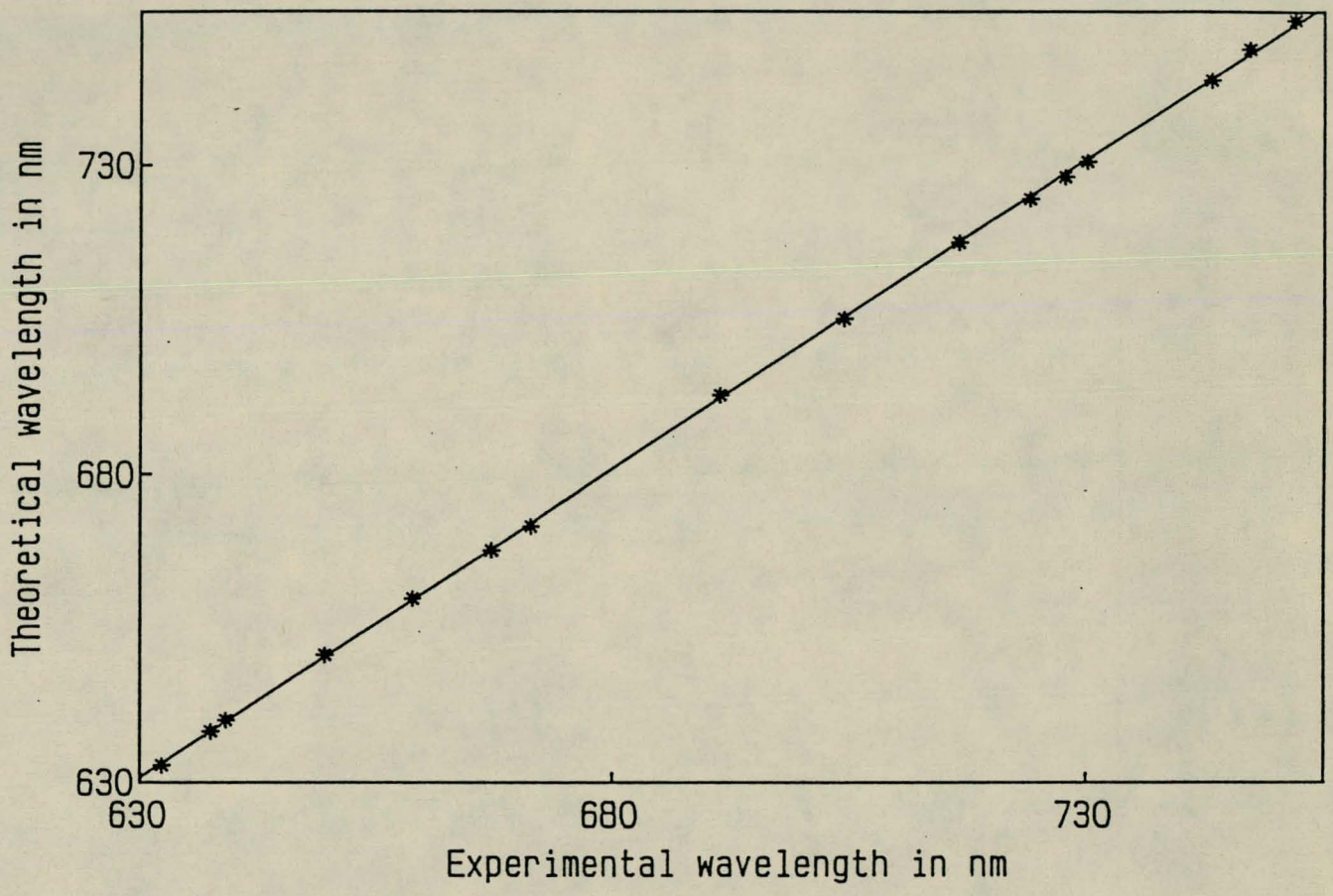

Figure 6.4 Calibration of Monochromator

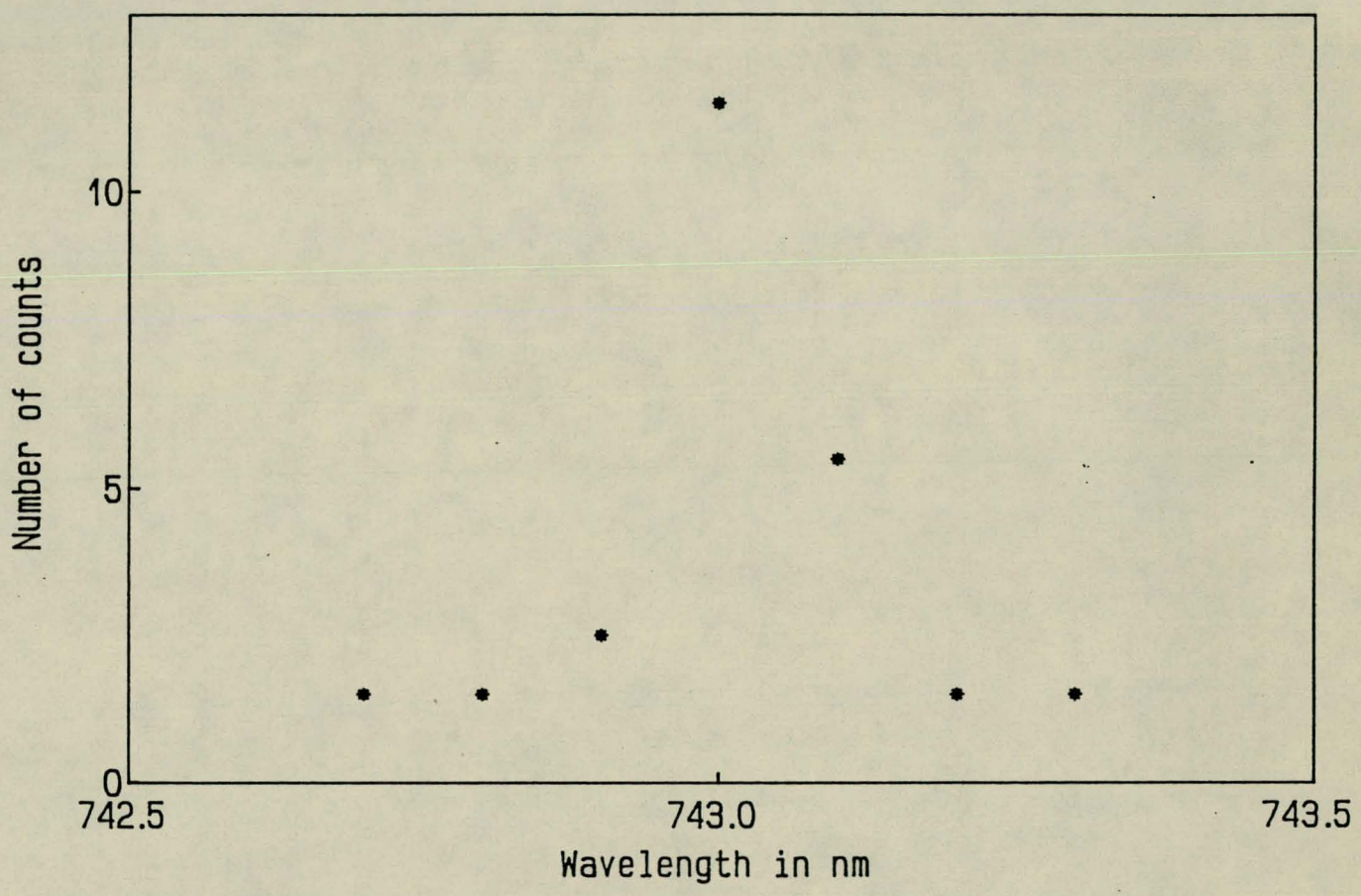

Figure 6.5 Measured Profile of possible First Stokes order

6.5 Argon ion laser as pump laser

The argon ion laser used lased at a wavelength of 488 nm and the propagation of the Gaussian mode first had to be determined because the waveguide was also used in this experiment to enhance the Raman gain. The laser radiation had to be coupled to the waveguide effectively to produce a high transmission and the laser mode parameters had to calculated. The position and size of w_o in the resonator was thus first determined.

6.5.1 The determination of the position and magnitude of w_o in the Argon Ion laser

The resonator consists of a flat high reflector, thus with an infinite radius and an output coupler with a radius of 10m. The cavity length L for single line operation is 1.016m. Figure 6.6 shows the resonator configuration.

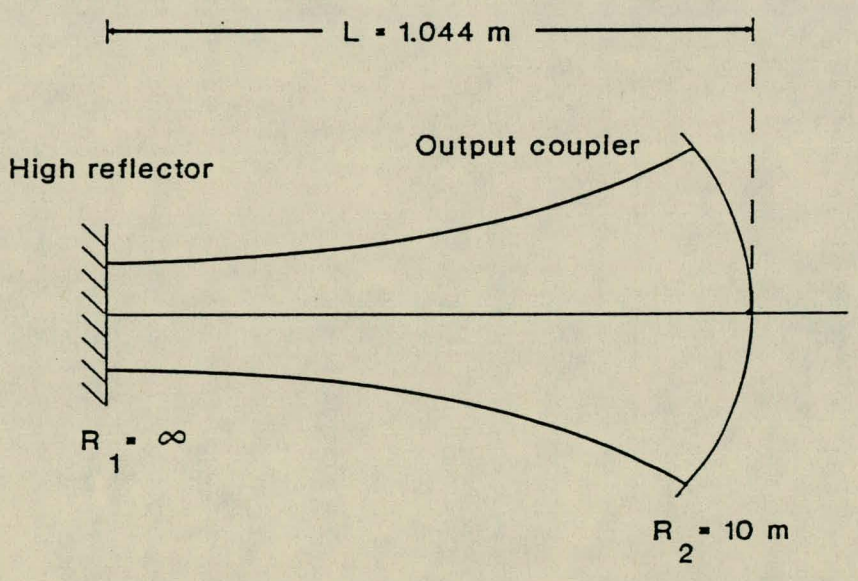

Figure 6.6 The Argon Ion Resonator

The g parameters are then given by

$$g_1 = 1 - \frac{L}{R_1} = 1 \qquad (6.1)$$

$$g_2 = 1 - \frac{L}{R_2} = 1 - \frac{1.044}{10.0} = 0.8956 \tag{6.2}$$

The position of w_o is simple to calculate because the high reflector is flat and this automatically means that w_o lies at the position of the high reflector. It could also be determined from the equation for z_1 which will yields $z_1 = 0$.

The equation which gives the magnitude of w_o is given in chapter 1 in the section on laser resonators.

$$w_o^2 = \frac{L\lambda}{\pi} \frac{\sqrt{g_1 g_2 (1 - g_1 g_2)}}{g_1 + g_2 - 2 g_1 g_2} \tag{6.3}$$

This depends on the wavelength and w_o is thus calculated for the two highest output power single line wavelengths, 488 and 514.5 nm.

The results obtained are the following.

$$\lambda = 488 \text{ nm} : w_o = 0.6892 \text{ mm}$$

$$\lambda = 514.5 \text{ nm} : w_o = 0.7077 \text{ mm}$$

6.5.2 Optical alignment of the argon ion laser

There are three basic alignment procedures which can be used in order to ensure that laser action takes place. The vertical search procedure is the one most often used. The coarse mirror alignment is only used if the vertical search procedure fails to produce laser action. The third procedure is used when the front mirror (output coupler) is not in perfect alignment with the tube in which the laser action takes place.

1. Vertical search procedure

When turned on the Argon laser did not lase and the following procedures given in the reference manual were followed to obtain laser radiation.

If the laser does not lase when turned on, this procedure is the first one to be followed in order to produce laser action. First it is assumed that the front mirror is aligned with the tube. The object of the procedure is to scan the rear mirror through a number of possible positions to

find the position at which the two mirrors are aligned. If this procedure fails to produce laser radiation, one then follows the second procedure.

The back mirror is equipped with a lever and knob which make search in the vertical direction possible as well as a knob for the horizontal direction. First the mirror is tipped forward by the vertical knob as far as possible. Then the lever is used to move the mirror back and forward while turning the horizontal knob in one direction. If no radiation appears the same steps are followed while the horizontal knob is turned in the other direction. This ensures that the mirror is scanned through all possible positions. When a flash of radiation appears the vertical knob is turned slowly until the laser action is continuous.

2. Coarse mirror alignment

This procedure is used when the front mirror is misaligned with respect to the back mirror and the tube. This procedure basically corrects the mirror so that the first procedure will initiate laser radiation.

In order to align the mirror, the laser must be on and the interlocks must be defeated. A small white card with a hole of approximate 1 mm in diameter is put between the laser discharge and the output coupler so that the hole is situated in the middle of the discharge on the resonator axis.

The discharge which goes through the hole will then be reflected by the output coupler and would be visible as a small spot on the card. By now adjusting the position of the output coupler so that the spot goes exactly through the hole in the card, the output coupler may be aligned with respect to the front mirror and the tube.

Following the first procedure again will now result in some laser action. If the laser output is less that specified, the next procedure must be followed.

3. Optimizing the mirror alignment

Although laser action takes place and the mirrors are parallel with respect to each other, it may be that the mirrors are not aimed straight down the bore which means that not all of the lasing medium is used to create laser radiation. This is shown in the following exaggerated figure 6.7. By following a 'walk in' procedure the mirrors may be aligned.

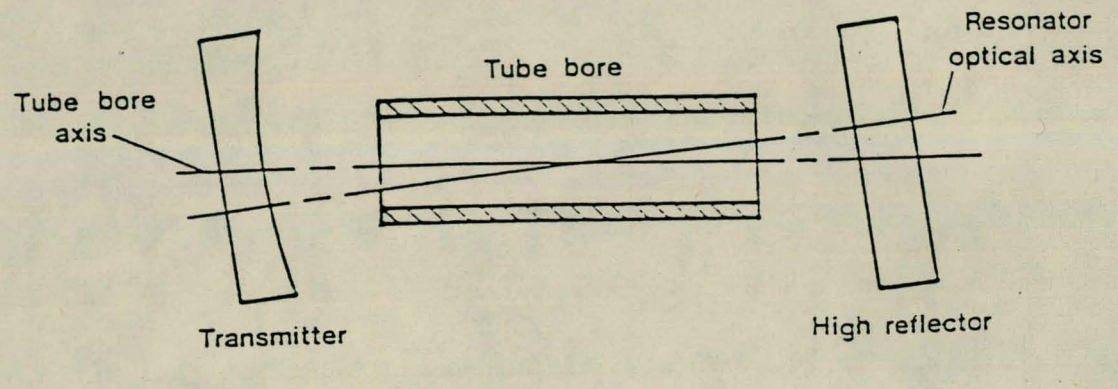

Figure 6.7 Mirror Alignment

First the power is peaked by adjustment of the vertical and horizontal adjustments of the front mirror and this peak power is noted. Now either the horizontal or vertical nuts of the rear mirror is turned in a certain direction until the power drops to half the peak power value. Now again the power is optimized as previously described. If the output power is higher than before, then further corrections are made in the same direction. If the power has decreased then corrections are made in the opposite direction. The same steps are used until the power reaches a maximum.

6.5.3 Power measurements of Argon Ion laser

In order to measure the output power of the laser a power meter was used. This meter gave an optimum output power of 450 milliwatt at multiline operation which is about 15% of the specified value of 3 Watt. Further attempts to maximize the output power by following the 'walk in' procedure was not successful in increasing the power. Because the power meter originally was calibrated for CO_2 radiation at a wavelength of 10.6 microns it could mean that the meter was not calibrated for wavelengths like 488 nm. A chopper with a power meter (RjP-735), used to measure very fast pulses, was then used to measure the output power. The mentioned power probe measured the energy of the laser pulse and by measuring the pulse time on a oscilloscope, the power could be calculated. It was found that this method gave a power reading of about

900 milliwatt which was double previously found. This was still less than specified but further attempts could not improve the output power of the laser.

6.5.4 Matching of the Argon laser to the waveguide in the Raman shifter

For optimum transmission through the waveguide the condition as discussed in chapter 5, section 5.4.1 must be satisfied.

$$\frac{w_o'}{R} \approx 0.5 \tag{6.4}$$

w_o' is the beam waist to which the laser beam was focussed and R is the radius of the capillary tube or the waveguide. For $R = 0.30$ mm this corresponds to a w_o' value of 0.15 mm. The laser beam had to be focussed to a minimum radius of 0.15 mm at the entrance of the waveguide. A lens was used to focus the laser beam and the distances at which a lens with focal length f must be placed were determined using mode matching theory discussed in chapter 3. Using a lens with a focal length of 1 m the following values for distances z_1 and z_2 were obtained.

$z_1 = 4.31$ m and $z_2 = 1.16$ m.

z_1 and z_2 are the distance from w_o to the lens and the distance from the lens to w_o' respectively. This values were quite large and made the experimental setup difficult.

A solution to this problem is to use two lenses. By using a intermediate w_o value which is quite small, one may obtain smaller overall distances than in the case with only one lens. First the w_o value of 0.15 mm at the waveguide entrance was matched to a chosen w_o' value of 0.03 mm using a lens with focal length of 50.2 mm. The distances obtained were $z_1 = 5.82$ cm and $z_2 = 25.72$ cm. This intermediate w_o value of 0.03 mm was then matched to the w_o value of the argon laser which gave $z_1 = 1.739$ and $z_2 = 15.30$ cm. This gave an overall distance of 96.84 cm from the laser end to the waveguide which made the experimental setup much more simpler.

In obtaining the above result, a couple of lens combinations were tested to give practical distances. One could of course with more effort find a combination with still smaller distances. A practical limit on the value of z_1 was that is had to be larger than 1.2 m which is the physical length of the laser.

The first try gave a transmission of 30% which was less than expected. The minimum beam waist w_o was measured experimentally to test the accuracy of the theoretical transmission

predications. The results were

Experimental measurement : $w_o = 0.218$ mm

Theoretical prediction : $w_o = 0.15$ mm

The percentage error was 31.2% which was large but reasonable. From the transmission curve shown in figure 5.7, a variation of say 0.05 mm in the optimum w_o value will result in a nonsignificant drop in transmission percentage. This incorrect w_o value then did not give a reason for the low transmission. After checking and aligning of the waveguide a transmission of 50% was obtained. This was less than predicted due to losses at the lenses and could not be improved on.

6.5.5 Experimental results

A photomultiplier tube was used to measure the spontaneous Raman scattered radiation. The main laser beam may not enter the photomultiplier tube because the high intensity will damage it. A filter had to be used to filter the Raman scattered light from the laser beam and a prism spectrograph was used to perform this function. It was found that this prism spectrograph was not able to filter all the laser light from the Raman scattered light so that the laser light, although very little was so intense that the Raman scattered light could not be measured. It was then decided to use the excimer laser and hydrogen as a medium. Hydrogen has a larger cross section than nitrogen and would have a larger Raman gain for the same pump beam and experimental conditions.

6.6 Excimer laser as pump source

Due to the fact that the spontaneous Raman scattering process could not be observed in the previous cases, is was decided to use an excimer laser (EMG 101 MSC) with wavelength 308 nm, which has a much higher output power. In experiments conducted by other researchers, the output power was sufficient to obtain stimulated Raman scattering [Br 82].

6.6.1 Experimental setup

In figure 6.8 the experimental setup is shown. The distance between the laser and the Raman shifter was about 1.4 meters. The Raman shifter was equipped with spacers and an input

and output lens which were responsible for focussing of the pump beam through the hydrogen medium.

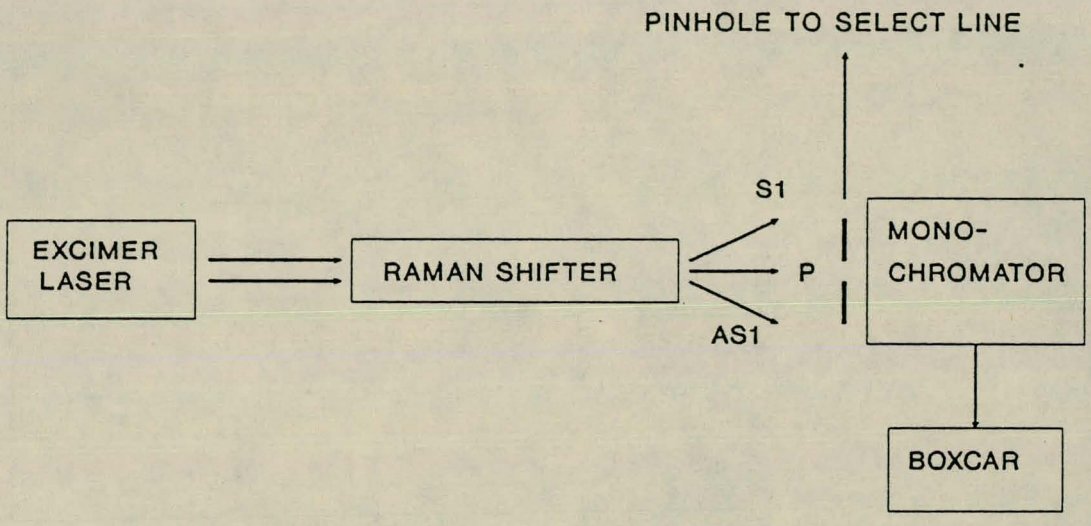

Figure 6.8 Experimental setup

6.6.2 Pump energy measurement

The pump energy was measured in order to be able to determine the conversion efficiency of the pump laser to the Stokes orders. Every individual pulse was measured with a joule meter which gave an 1.8 Volt signal for every 1 Joule pulse measured. Several pulses were stored on a oscilloscope and an average energy of 110 mJ was obtained. As the length of the laser pulse in time was roughly between 5 and 10 ns, the output power was 10 to 20 MW.

6.6.3 Visual results obtained

A visual pattern consisting of various dots of different colors could be seen when placing a white card at the output of the Raman shifter. This was thought to be fluorescence belonging to

the pump laser (blue color), the first Stokes order (green color) and the second Stokes order (yellow color). The visual patterns obtained were highly directional and together with the high intensities it provided evidence that this indeed was stimulated Raman scattering that was seen. Only the first Raman order was intense enough to be measured with an energy meter (RjP-735) of which the experimental results obtained would be shown later.

6.6.4 Measurement of Stokes Profiles

Since the excimer laser pulse has a short time duration, an ordinary oscilloscope was not able to measure the pulse. A Boxcar Integrator (Gated Integrator & Boxcar Averager) was then used because it was able to measure such short pulses. It was used in conjunction with a monochromator (Schoeffel). The Boxcar instrument may be triggered in step with the excimer laser and only took a measurement when the pulse from the pump laser was detected by the Boxcar. The Boxcar has a gate of which the width is adjustable and may be placed at a suitable position on the pulse to be measured. The pulse is measured with respect to time and the gate is normally placed at the peak position of the pulse.

Hydrogen pressure was set at 20 bar and the input and output slits of the monochromator were set at 1 mm. The wavelengths of the first three orders are respectively 354, 414 and 500 nm.

Each profile was obtained by scanning of the monochromator over a wavelength region and determining the voltage reading given by the Boxcar at each wavelength position. This voltage reading was obtained from an amplified signal produced by the photomultiplier tube. A pinhole was used to select each Raman order which was not really necessary because the monochromator is able to filter unwanted scattered light.

In figures 6.9 to 6.12 the profiles of the pump and each Stokes line are showed. Using the monochromator wavelengths for each line, a calibration curve as in figure 6.13 was obtained.

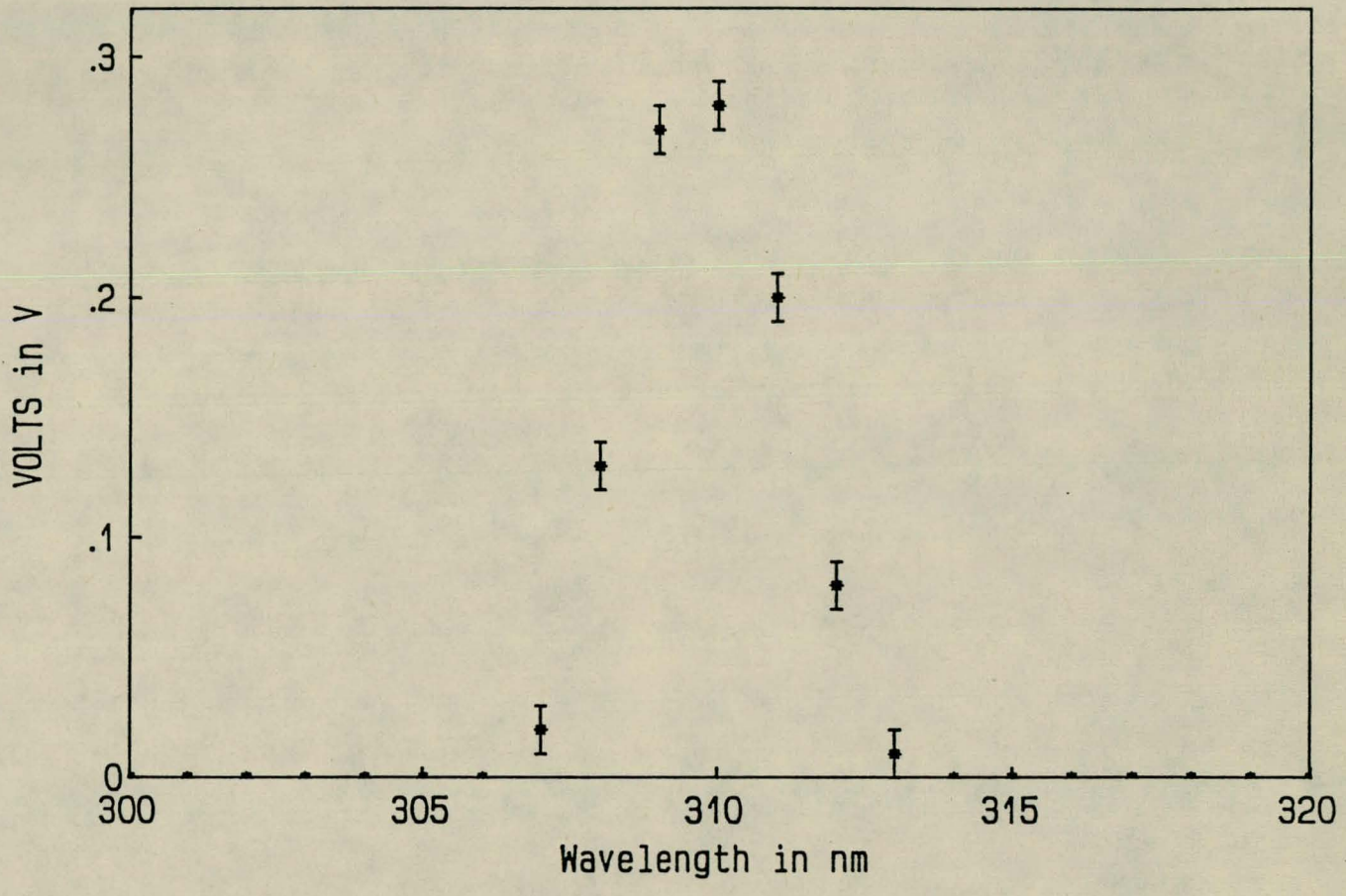

Figure 6.9 Measured Profile of Excimer Laser

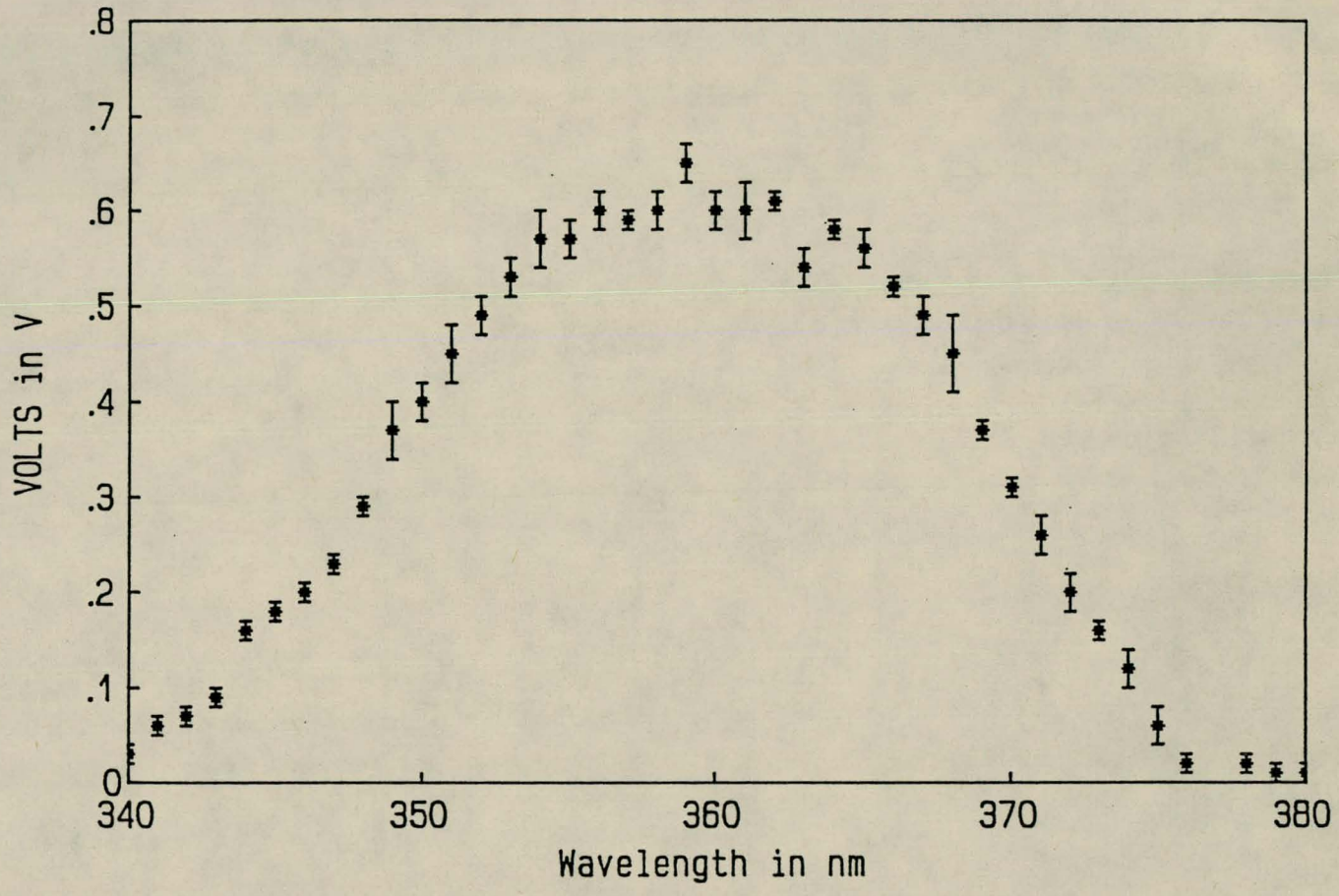

Figure 6.10 Measured Profile of First Stokes Order

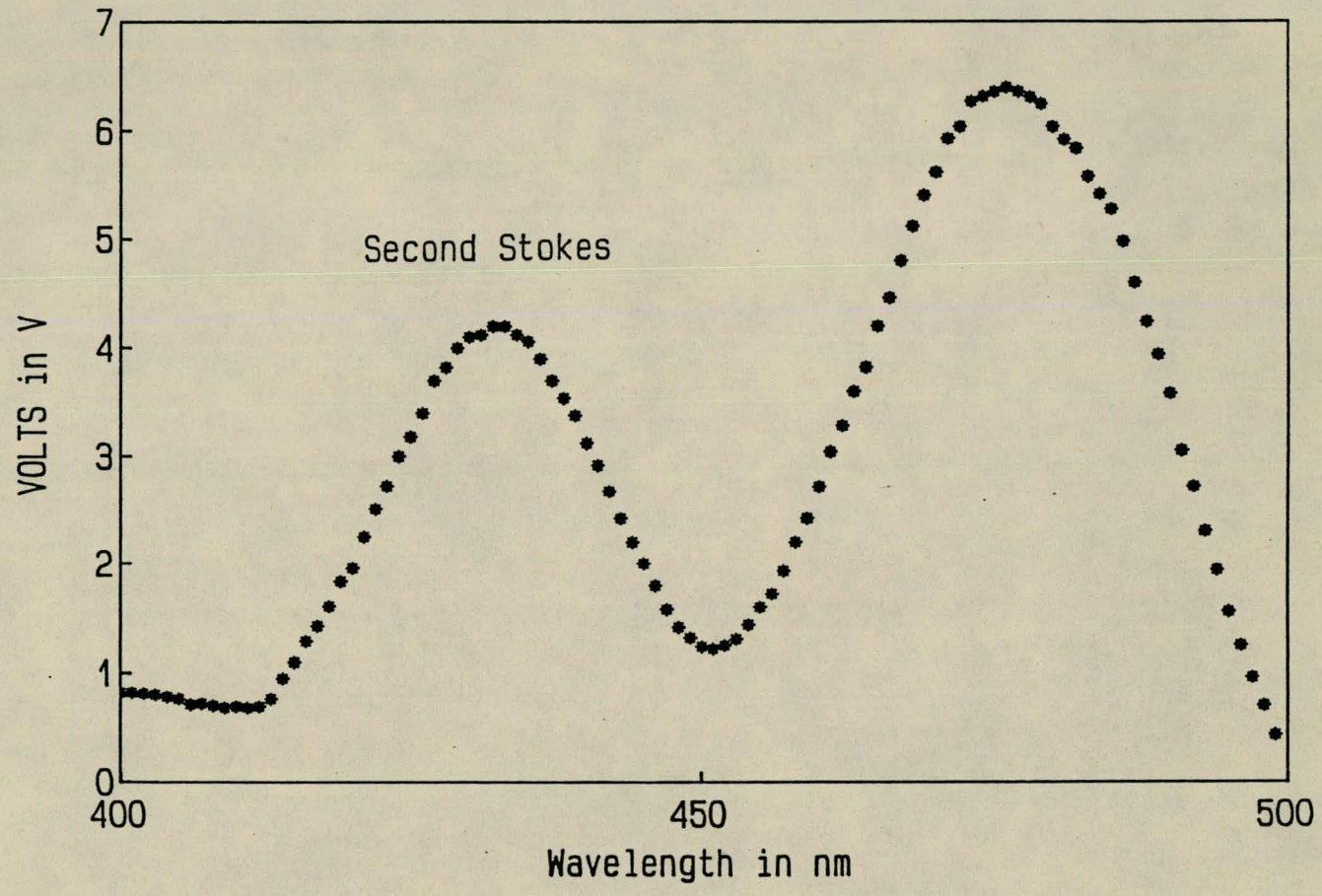

Figure 6.11 Measured Profile of Second Stokes Order

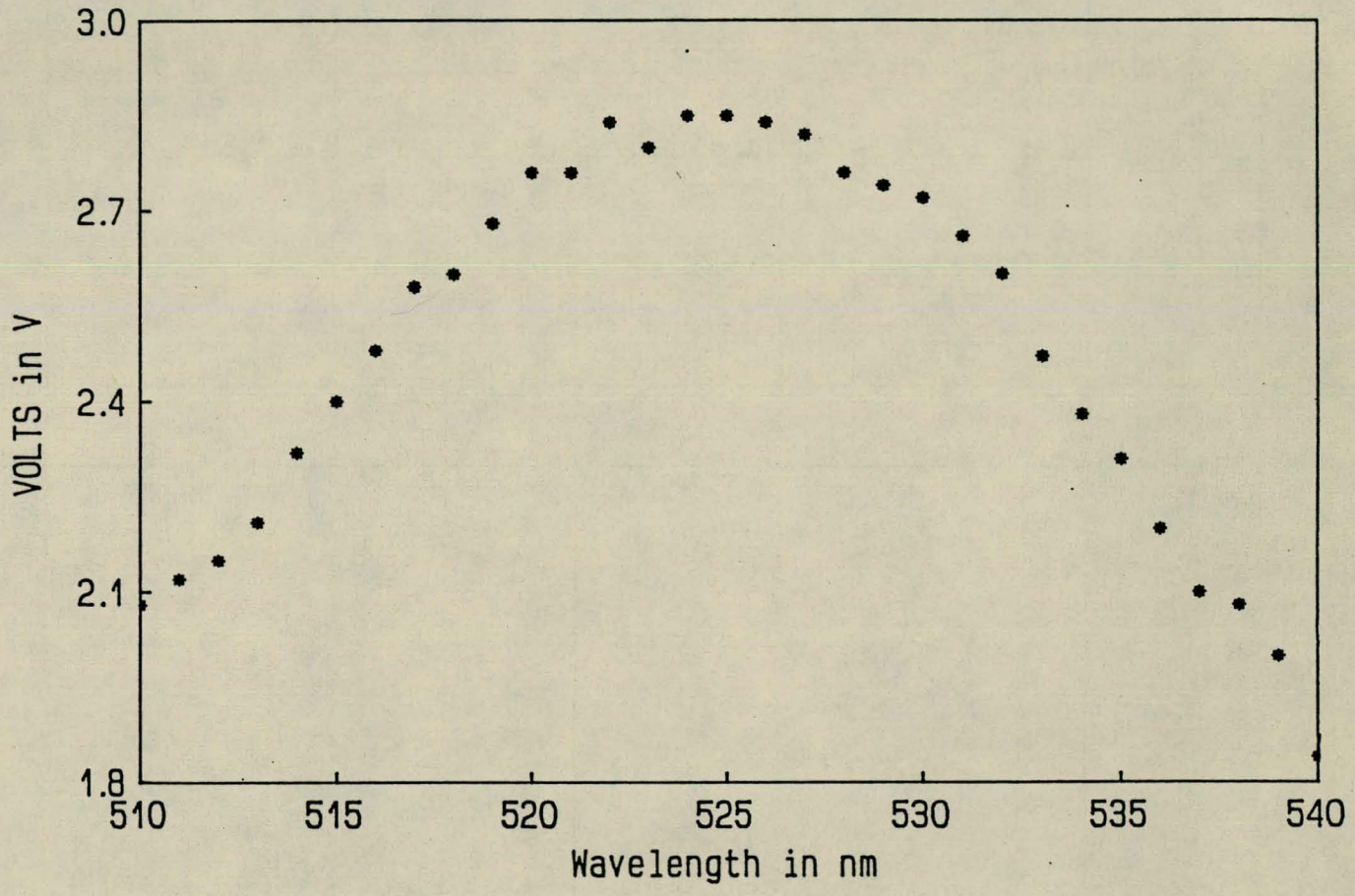

Figure 6.12 Measured Profile of Third Stokes Order

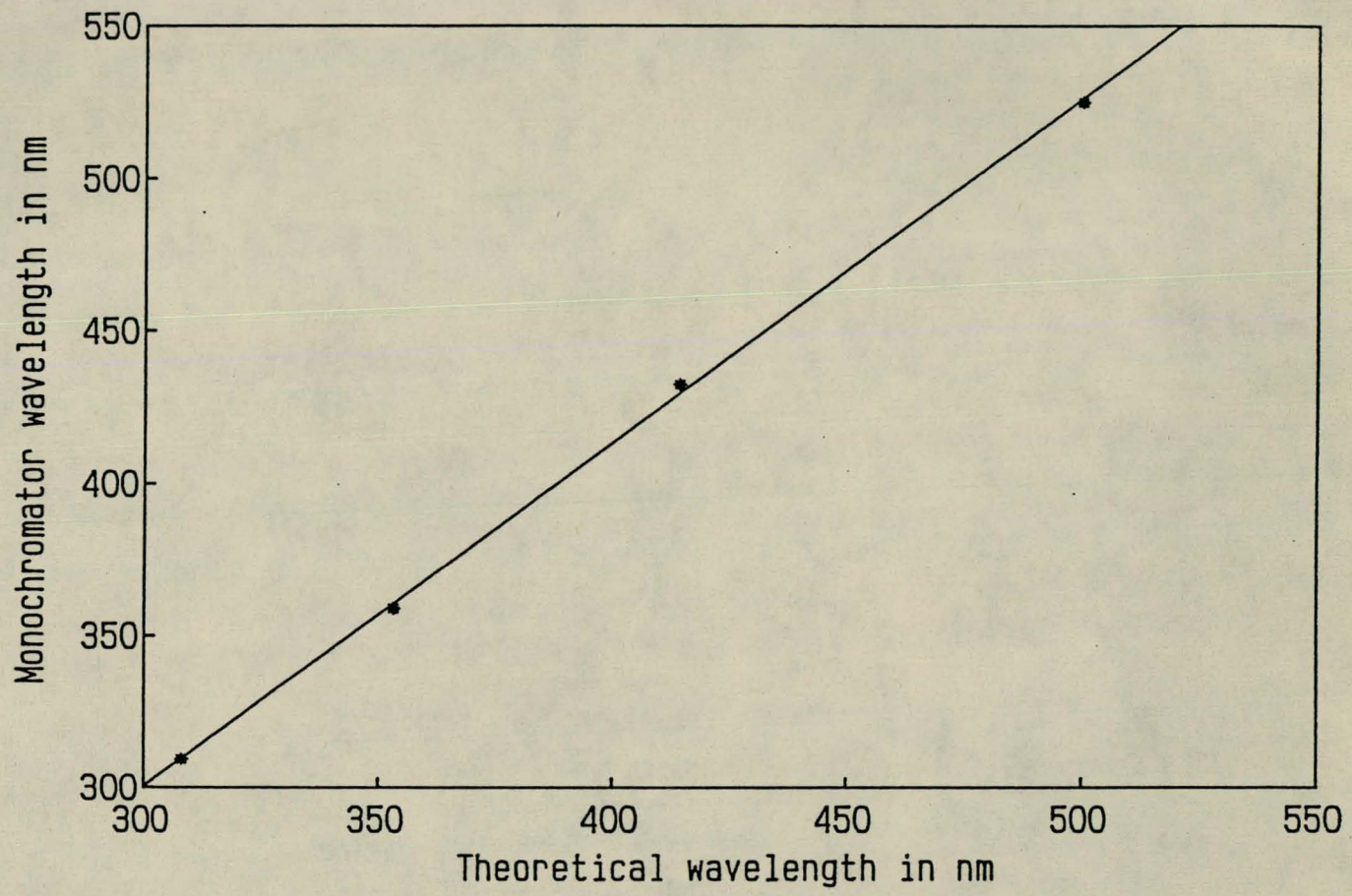

Figure 6.13 Calibration of Monochromator

As one may see from figure 6.11, there is also a unknown peak at about 476 nm. Not belonging to the hydrogen Stokes orders, it was thought to be either a fluorescence peak or a Stokes or Anti-Stokes order belonging to some other element that may be present in the hydrogen mixture. If it was a fluorescence peak it should be radiated evenly in every direction. Slight tuning of the Pelin-Broca prism caused the signal to decrease quickly which leads to the conclusion that it could not be a fluorescence peak. Elements such as nitrogen and oxygen may be possible elements causing the peak, but no first or second order wavelengths even come near the wavelength of 476 nm. The peak thus remained unidentified.

Only the first order Stokes energy could be measured directly with an energy meter because the energy of the other orders was insufficient to be measured with the energy meter used. A energy of about 16 μJ was obtained at an optimum pressure of 35 bar. This output energy was only a fraction of output energies given by specification [La 85]. The conversion efficiency determined was 0.0145 %.

There are two factors which may be the cause of the low output energy. The hydrogen used was not as pure as specified and could cause additional absorption and losses. The way the laser beam is focussed through the medium is critical and improvement of the beam focussing could lead to a larger gain and higher Raman energy. Later the experimental results obtained after trying to improve the way the beam is focussed, will be shown.

6.6.5 Influence of the pressure on the Stokes energy

In figure 6.14 the first Stokes energy versus the hydrogen pressure has been plotted. At pressures below 25 bar no energy at all could be measured. At high pressures of about 35 bar there was a very large variation in energy which was not present at the lower pressures. This variation is discussed in the next section.

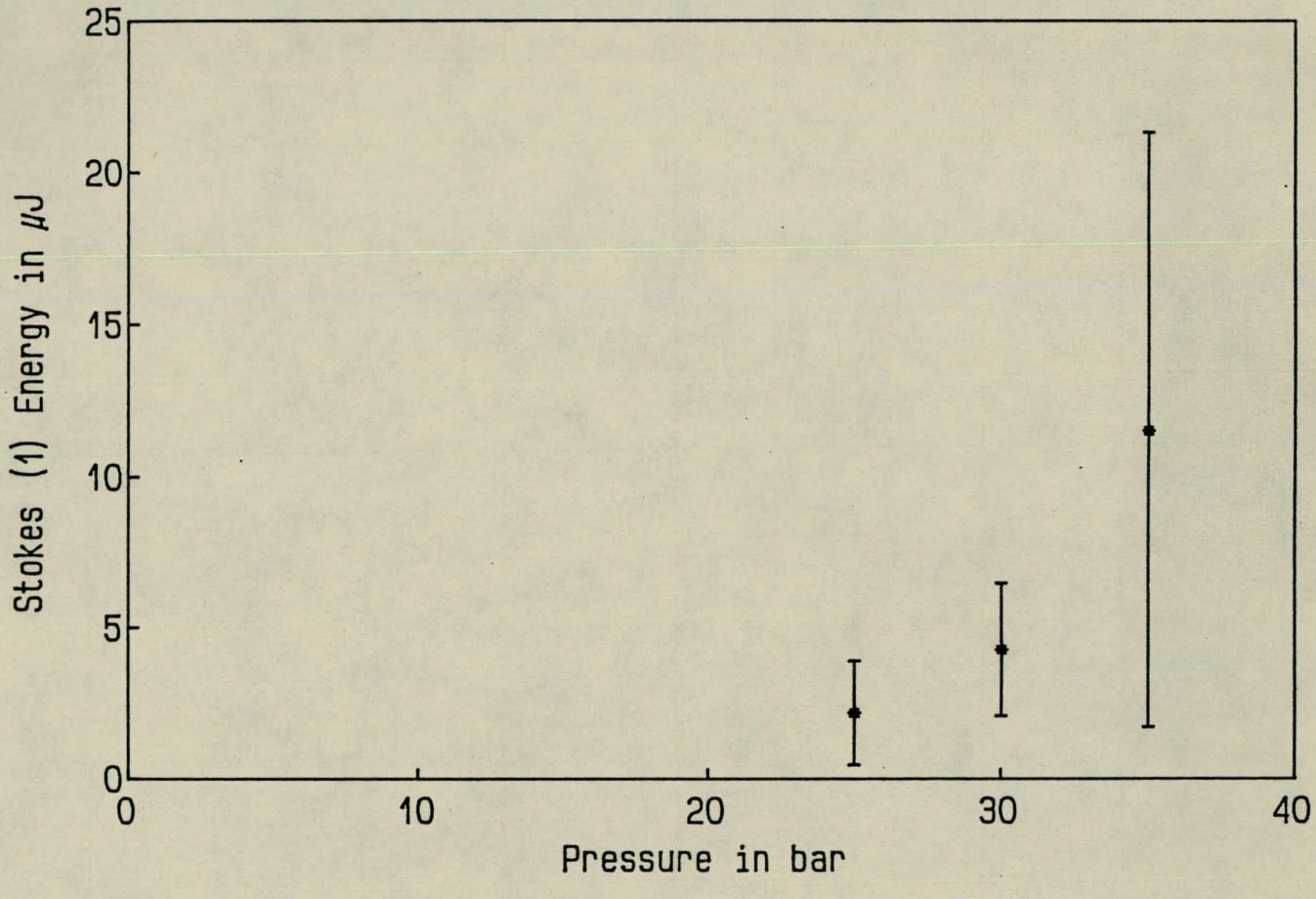

Figure 6.14 Influence of the pressure on the first Stokes intensity

6.6.6 Variation in the Stokes energy

A large variation in the Stokes energy was observed at high pressures. It was first thought to be due to a large variation in the pump energy, but this was not the case. In this section some factors which may be responsible for this variation, will be discussed.

1. The 'origin' of the background photon

The stimulated Raman process will start to grow exponentially only if there is already a Stokes photon present or if one is emitted. This background Stokes photon normally is present due to spontaneous emission or blackbody radiation.

In figure 6.15 the interaction region is shown. There is two regions of interest, A and B because the beam is focussed and the gain is thus a function of length.

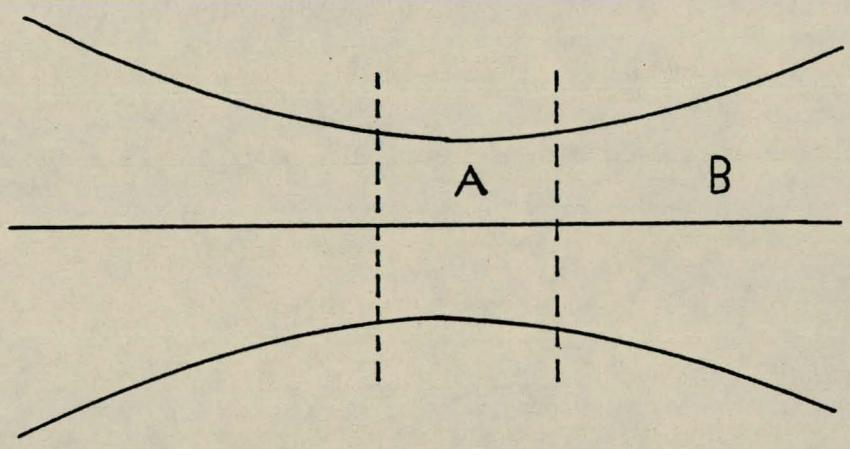

Figure 6.15 Interaction Region

It is assumed that the background photon is emitted in region A. Because of the high gain in this region there is exponential growth of the first Stokes wave described by

$$I_r = I_b e^{gl} \tag{6.5}$$

g is the Raman gain coefficient and l is the interaction length.

If the background photon is emitted in region B, the final I_r would be smaller than in the first case, because the interaction length is smaller and the gain is smaller. One would thus expect

variations in the Stokes intensity because there is no fixed position at which the background Stokes photon may be emitted and for each different position the final Stokes intensity would be different. To calculate the practical variation one may expect in an experiment, the gain constant g must be known.

2. The variation in the pump energy

The pump laser does not have a constant energy output, but it varies from pulse to pulse. The energy is of course related to the intensity which appears in the gain factor. Larger pump intensities would result in larger Raman intensities. This clearly also contributes to the variation in the Stokes intensity. Because of the exponential growth of the Stokes energy, a variation of say 10% in the pump intensity will cause a variation of more than 10% in the Stokes intensity.

The Stokes intensity is given by

$$I_s = I_{bs} e^{GI_pL} \tag{6.6}$$

where G is the plane wave gain coefficient, I_p is the average pump intensity, I_{bs} is the background Stokes intensity and L is the interaction length. For a given experimental setup the pump intensity is proportional to the pump energy. It is assumed that there is a variation in the pump energy described by

$$E_p = E_{avr} \pm cE_{avr} \tag{6.7}$$

where E_{avr} is the average pump energy and c is the fraction variation in the pump energy. For example a c value of 0.1 corresponds to a 10% variation in the pump energy.

One now has that

$$I_p = I_{avr} \pm cI_{avr} \tag{6.8}$$

because of the linearity between the pump intensity and energy.

The factor GI_pL now becomes

$$GI_pL = GL(I_{avr} \pm cI_{avr}) \tag{6.9}$$

or

$$GI_pL = GLI_{avr} \pm cI_{avr}GL \tag{6.10}$$

The Stokes intensity may now be written as

$$I_s = I_{bs}e^{gL}.e^{cgL} \tag{6.11}$$

where $g = GI_p$.

The variation in the Stokes intensity ΔI_s, is now given by

$$\Delta I_s = I_{bs}e^{gL}.e^{cgL} - I_{bs}e^{gL} \tag{6.12}$$

This gives

$$\Delta I_s = I_{bs}e^{gL}(e^{cgL} - 1) \tag{6.13}$$

The percentage variation is then

$$\Delta I_s = \frac{I_{bs}e^{gL}(e^{cgL} - 1)}{I_{bs}e^{gL}} \times 100 \tag{6.14}$$

Division with $I_{bs}e^{gL}$ gives

$$\Delta I_s(\%) = (e^{cgL} - 1) \times 100 \tag{6.15}$$

From this it is clear that the percentage variation in the Stokes intensity will depend on the coefficient c, g and the interaction length L. Practical values for gL ranges between 5 and 40 [Be 85].

For $c = 0.1$ and $gL = 5$, that is a 10% variation in the pump energy energy, one has that

$$\Delta I_s(\%) = 64.9\% \tag{6.16}$$

which is much larger than the 10% variation in the pump energy. Because of this large variation one believes that the variation in the first Stokes energy is mainly because of the variation in the pump energy.

3. The threshold value for the Raman laser process

Because of certain losses, one has a threshold value for the gain g which is called g_t. For gain values smaller than this gain g_t, no net stimulated emission is obtained and for larger values, one has exponential growth of the Stokes intensity. Certain parameters which have an influence on the gain such as the pump intensity and the pressure, will cause the gain to fluctuate if that parameter also fluctuates during the experiment. The pump intensity is such a factor as already have been mentioned in the previous section. Because of the fluctuations in the gain, it may happen that the gain may be less than the threshold value for relative low pump intensity values and larger than the threshold value for larger pump intensities. This lower and larger values occurs because of fluctuations in the pump intensity. This will have the effect that sometimes there will be a Raman pulse and sometimes no pulse will be present.

In a practical setup where the beam is focussed this is not so simple because the gain also depends on the interaction length. This means that at certain distances net stimulated emission is obtained and for other distances net losses. For high enough pump intensities one has net stimulated emission throughout the whole interaction region and for very low pump intensities no stimulated emission. This means that while there are fluctuations in the pump intensity, there rarely is cases where no net stimulated emission at all takes place. Only in certain regions there will occur losses and in effect will the losses reduce the final output intensity. In effect will the fluctuations in the pump intensity cause fluctuations in the Raman intensity if the pump intensity is such that one is near the threshold region.

4. The influence of the second Stokes wave

The intensity of the second Stokes wave depends on the intensity of the first Stokes wave and the intensity of the first order determines the gain for the second Stokes wave. Fluctuations in the first Stokes may cause that conditions for the second Stokes are such that for some pulses one is and sometimes above the threshold value for the second Stokes. If above the threshold value, the second Stokes will grow exponentially and will withdrew some of the first order intensity. This will cause an additional fluctuation in the first Stokes energy.

For above reasoning to be valid, there must also be fluctuations in the second Stokes energy if

this effect do causes fluctuations in the first Stokes energy.

How large must these fluctuations be to be responsible for fluctuations in the first Stokes energy? Due to the difference in the photon energy of the first and second Stokes, a variation of say 50% in the first Stokes energy will not cause a fluctuation of 50% in the second Stokes energy.

This is due to two factors. One is the quantum efficiency of the process, that is the percentage of S1 photons that will produce a S2 photon. Not all the S1 photons will produce S2 photons because of absorption, scattering and other processes.

In addition to the quantum efficiency losses, the following effect is also present. It is assumed that the quantum efficiency is 100%. A variation of 50% in the first Stokes intensity thus corresponds to a energy variation given by ΔE_{S1}.

The number of photons associated with this energy is

$$n_{S1} = \frac{\Delta E_{S1}}{h\nu_{S1}} \tag{6.17}$$

Because of 100% quantum effectivity each of these first Stokes photons result in a second Stokes photon. Now the variation in the second Stokes energy is given by

$$\Delta E_{S2} = \frac{\Delta E_{S1}}{h\nu_{S1}} . h\nu_{S2} \tag{6.18}$$

This may be written as

$$\Delta E_{S2} = E_{S1} \frac{\lambda_{S1}}{\lambda_{S2}} \tag{6.19}$$

Consider the following values:

$\lambda_{S1} = 353.2$ nm

$\lambda_{S2} = 414.3$ nm

This gives

$$\Delta E_{S2} = 0.8525 \Delta E_{S1} \tag{6.20}$$

This means that a variation of 50% in the first Stokes energy will cause a 42.63% variation in the second Stokes energy and in practise less because the quantum effectivity is less than 100%.

6.6.7 Focussing improvement

The distance between the pump laser and the Raman shifter was varied to increase the Raman gain by better focussing of the excimer laser through the hydrogen medium.

Figure 6.16 shows the measurement of the first Stokes energy under the same experimental conditions as before with the distance between the excimer laser and the Raman shifter changed. The pressure was varied from zero to 35 bar.

With a excimer Raman shifter distance of 1.7 m, a Stokes energy of 15 μJ had previously been obtained at a optimum H_2 pressure of 35 bar. According to the specifications this is about a factor 1000 less of what it should be. Explanations may be the purity of the hydrogen and also the way the pump beam is focussed through the Raman shifter. Because of the dramatic effect of focussing on the Raman gain, one could expect that a different distance between the excimer laser and the Raman cell could have a drastic effect on the Raman energy.

Changing this distance to 1.2 m gave an optimum Raman energy of about 600 μJ (refer to figure 6.16), which is 40 times larger than in the previous case. This illustrates the enormous effect focussing have on the Raman gain. Due to experimental limits the distance could not be decreased further in order to have a still better focussing and larger gain. Decreasing the distance too much would also result in poor focussing and a small overall gain. Experimentally one would be able to find the distance at which optimum Raman energy is observed. Note that in the last case the pump energy was only 72 mJ in contrast with the previous 110 mJ, which mean that the factor 40 is in fact larger because of the lower pump energy in this case.

In both cases the trend of figures 6.14 and 6.16 are the same which also concludes that the only parameter which had changed was the focussing of the laser beam. In figure 6.16 energies are observed at lower pressures as in figure 6.14 which also shows the gain improvement.

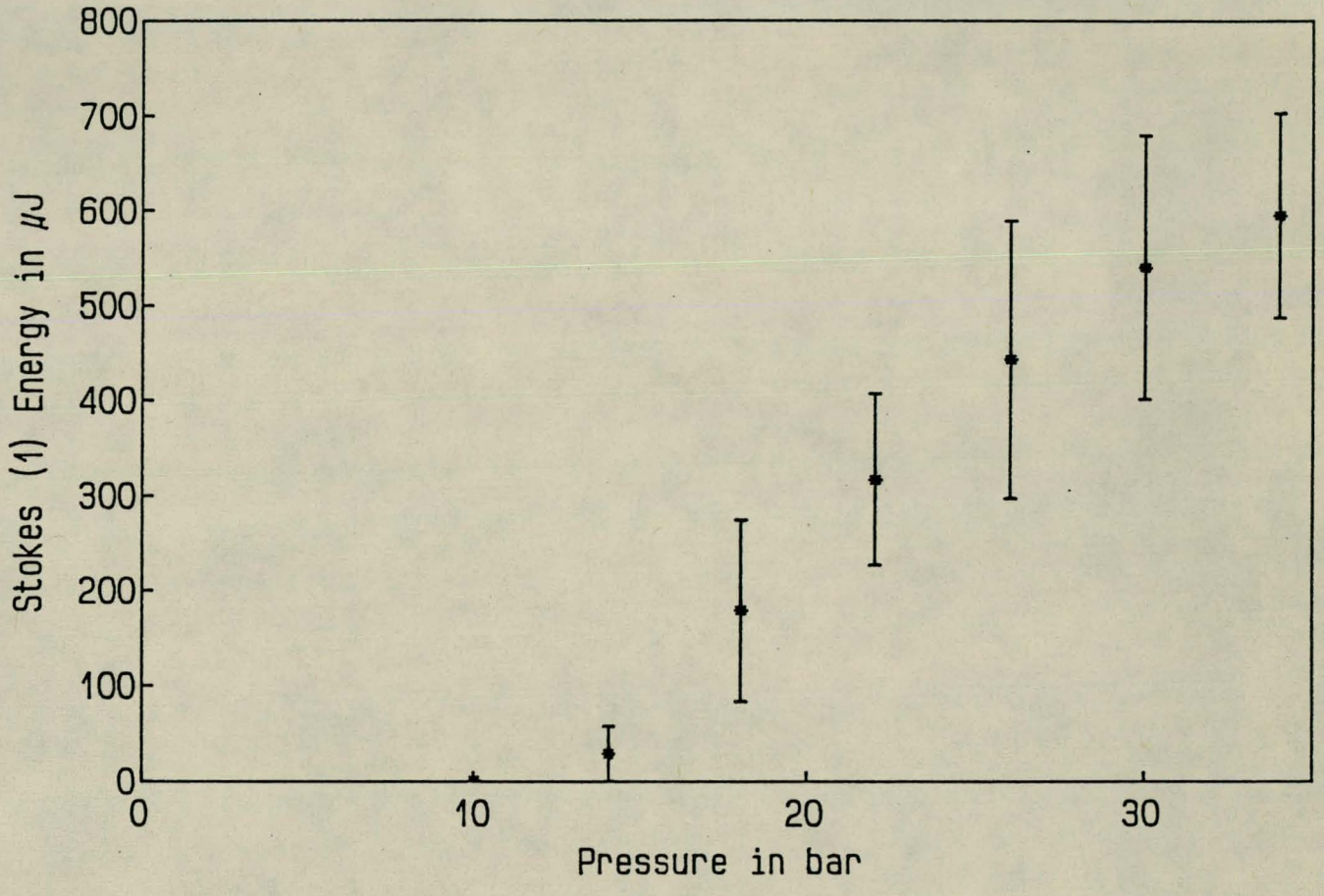

Figure 6.16 Influence of Pressure on the First Stokes Energy

6.6.8 The Raman threshold

As already have been explained in chapter 4, the Raman process has a gain threshold value under which no Raman laser action could take place. As the gain depends on the pump intensity, the threshold value could be determined by decreasing the pump intensity until no Raman signal could be measured.

In an experiment the influence of the pump intensity on the intensity of the first three orders was investigated. The pump energy was measured, but because there exists a linear relation between the energy and the intensity if the experimental conditions stay the same, the pump energy is related to the pump intensity.

The Raman signal was measured as a voltage signal using a monochromator with a photomultiplier and a Boxcar integrator. There also exists a linear relationship between the voltage reading and the intensity if the experimental setup remains the same and if the photomultiplier tube is not saturated.

A photomultiplier has no space resolution and measures the rate at which photons are absorbed or the number of photons per second. This may also be written as the power per energy, where the energy is the energy of an individual photon.

One has that

$$P = \frac{E}{\Delta t} \tag{6.21}$$

$$\frac{1}{\Delta t} = \frac{P}{E} \tag{6.22}$$

where P is the power and Δt is the time interval measured.

Also

$$I = \frac{P}{A} \tag{6.23}$$

$$P = I.A \tag{6.24}$$

where A is the area of the beam and I is the intensity of the beam. Thus

$$\frac{1}{\Delta t} = \frac{I.A}{E} \tag{6.25}$$

As A and E is constant for a specific experiment, one may safely say that the voltage signal given by the Boxcar is linear with respect to the intensity. Therefore one is able to use an graph where the voltage is plotted against pump energy as a indication of the relationship between the relative Raman intensity and the pump intensity. The experimental results that were obtained is shown in figures 6.17 to 6.19.

Although there is a good linear relationship between the Raman signal and the pump energy as expected, the threshold values obtained cannot be considered accurately measured. A linear fit has in all three cases showed a threshold value just above zero pump energy, but it could also have been that the linear fit could not have crossed the horizontal axis at all. It looks as if the loss coefficient is very small because one definitely has Stokes laser action at very low pump energies.

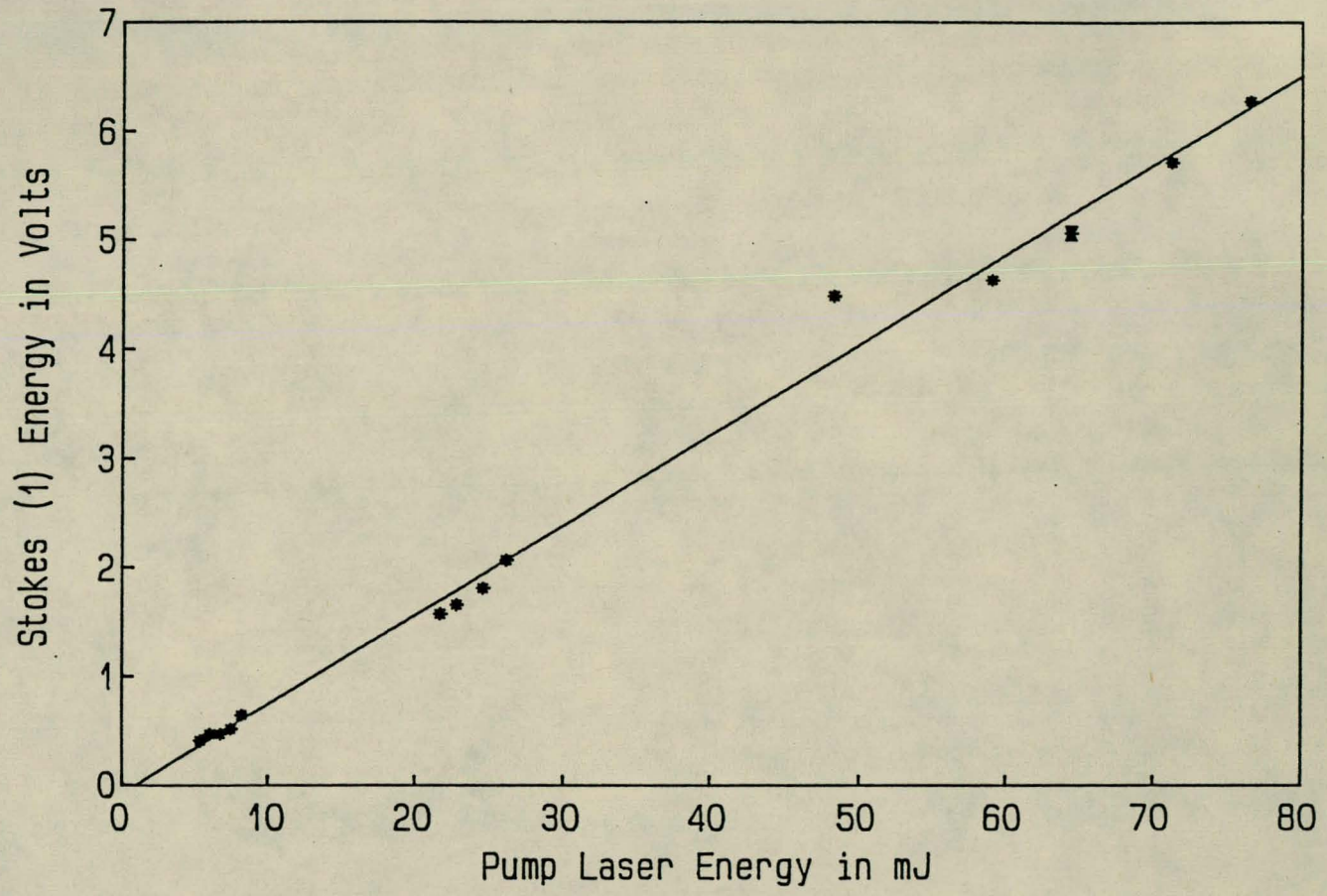

Figure 6.17 Relative intensity (S1) versus pump energy

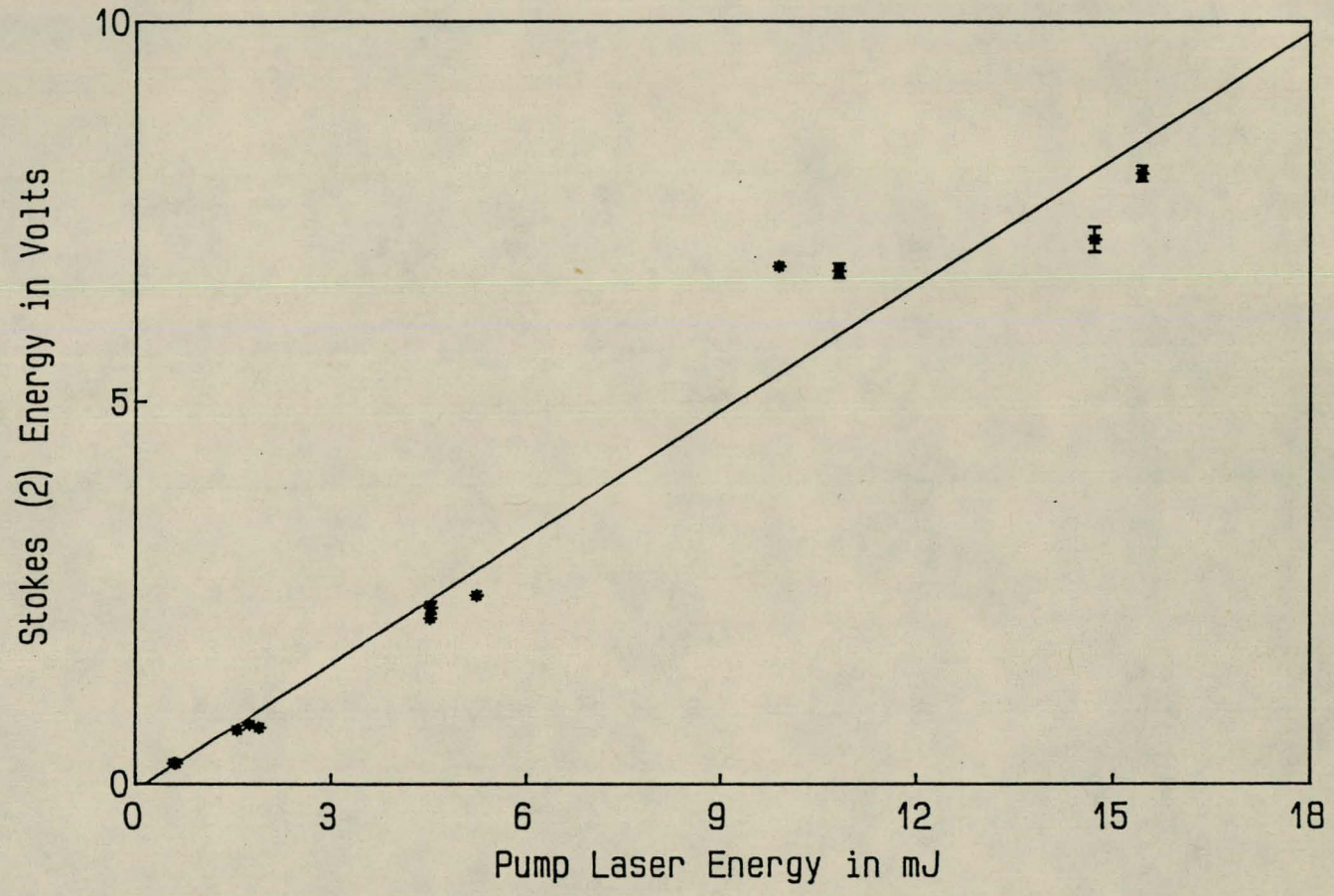

Figure 6.18 Relative intensity (S2) versus pump energy

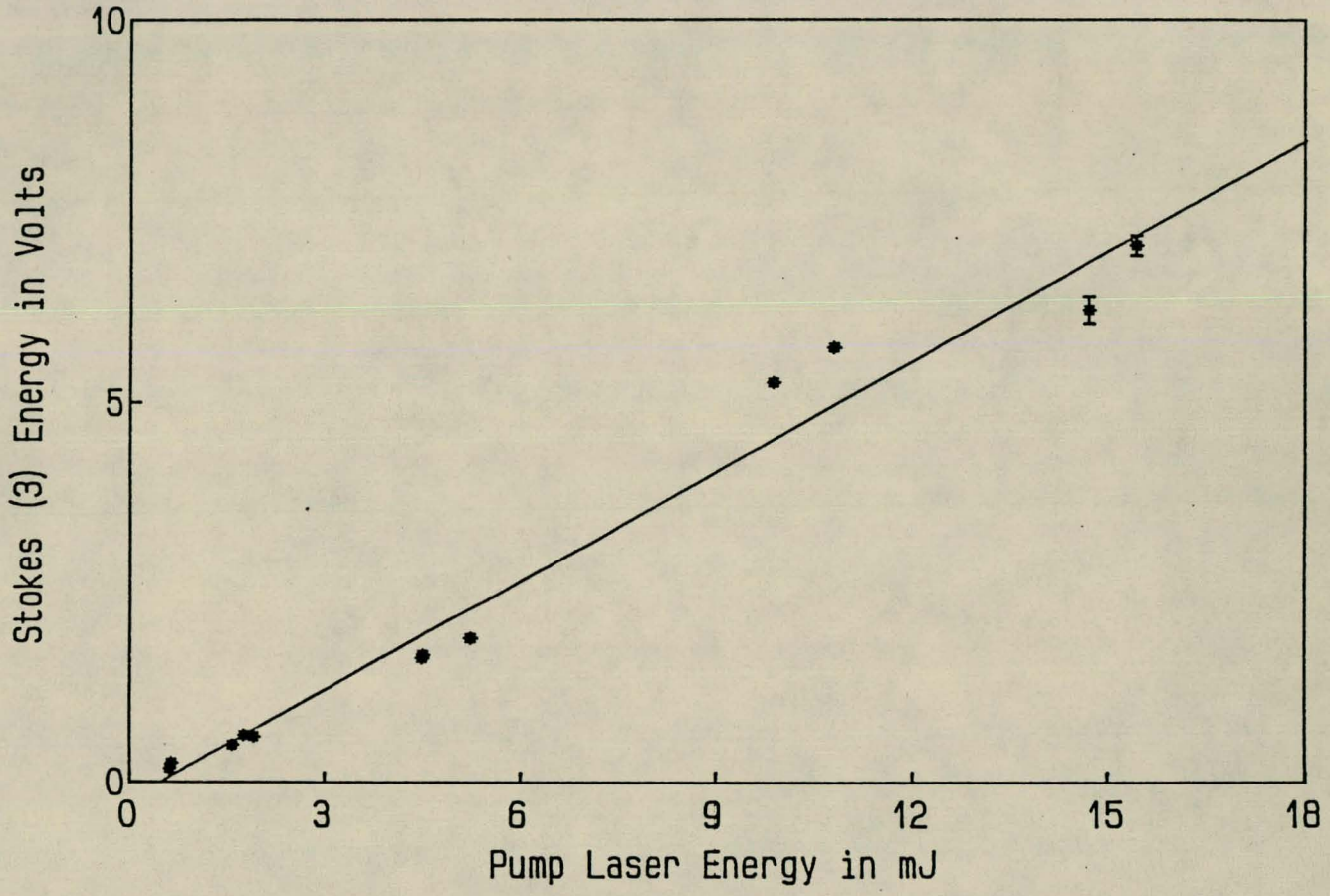

Figure 6.19 Relative intensity (S3) versus pump energy

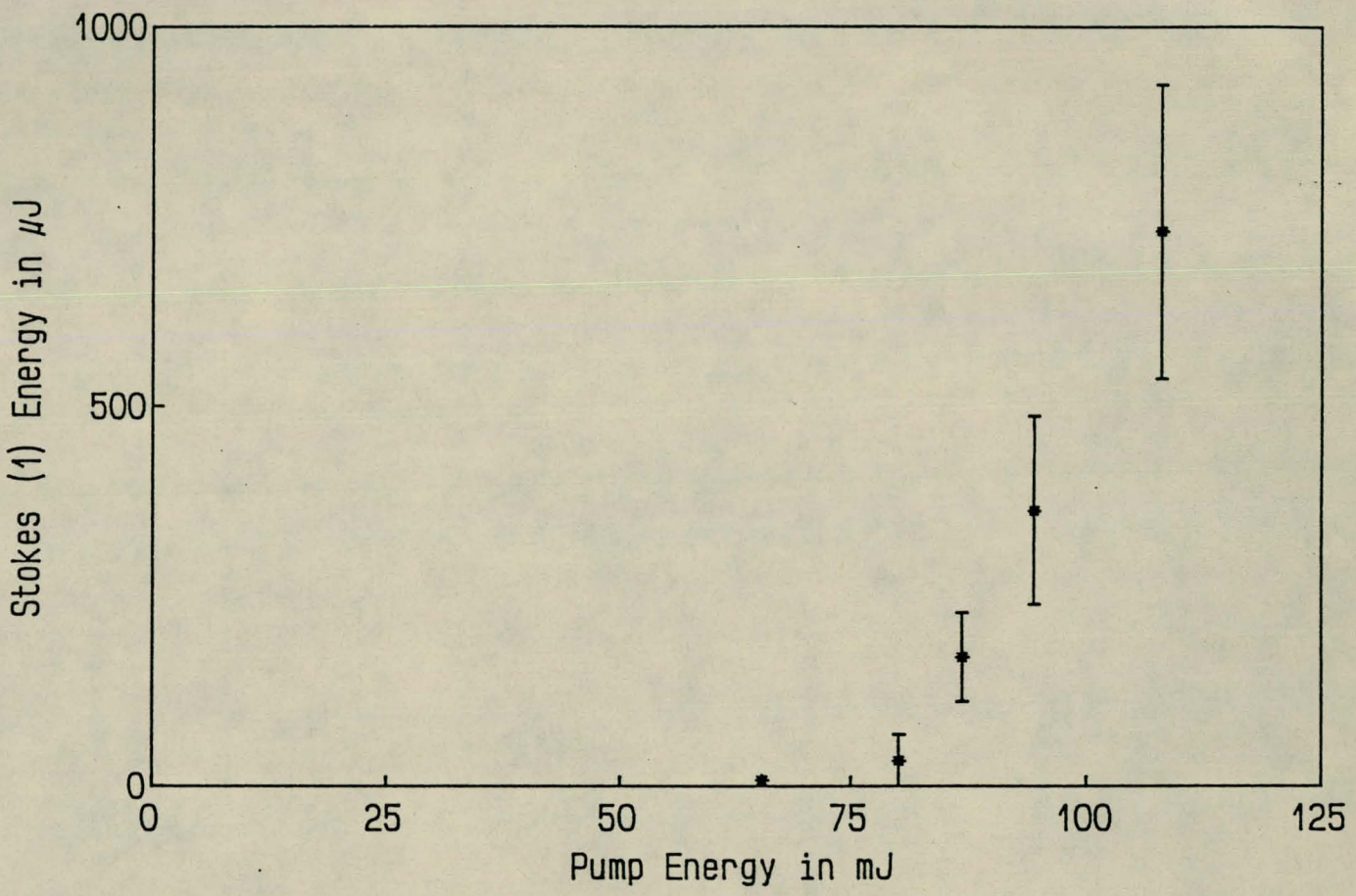

Figure 6.20 First Stokes Energy versus Pump Energy

In figure 6.20 the first Stokes energy is plotted versus pump energy and it predicts a threshold value for the pump energy of about 75 mJ. In figure 6.17 where the relative Stokes energy as a voltage difference is plotted against the pump energy, the threshold value is just larger than zero. This apparently is a contradiction between the results, but the following explanation may provide a solution.

The following difference in experimental observation exits. The energy ratiometer is able to measure minimum energies of about 20 μJ [Rj 87], where the photomultiplier actually is able to count individual photons.

A approximation was made that the intensity is uniform and linear with respect to the energy, which is not true, because the intensity profile of the pump and thus the Raman beam consists of various transverse modes. There are thus peaks in the intensity profile, but only the energy was measured and connected to a average intensity. This meant that the gain could have been high enough in some places to ensure net stimulated emission, while the average energy was still not enough to be measured with the energy meter. The photomultiplier tube was able to measure the Raman intensity which means that with the energy meter a cutoff value was found while with the photomultiplier tube no cutoff value was found. This is exactly what was found experimentally.

The above reasoning, together with the sensitivity factor may provide a solution to the apparent contradiction between the experimental results obtained. Although figure 6.20 could thus not be used to determine the threshold value, it may well be used to determine the pump energy needed to obtain a significant amount of net stimulated emission.

6.6.9 Number of shots

The influence of the number of excimer pulses on the Raman energy was also investigated. Since the Raman energy depends on the pump energy, the Stokes energy divided by the pump energy versus the number of pulses was plotted. As one may see in figure 6.21 there was no significant variation in the Stokes energy for up to 10000 pulses fired.

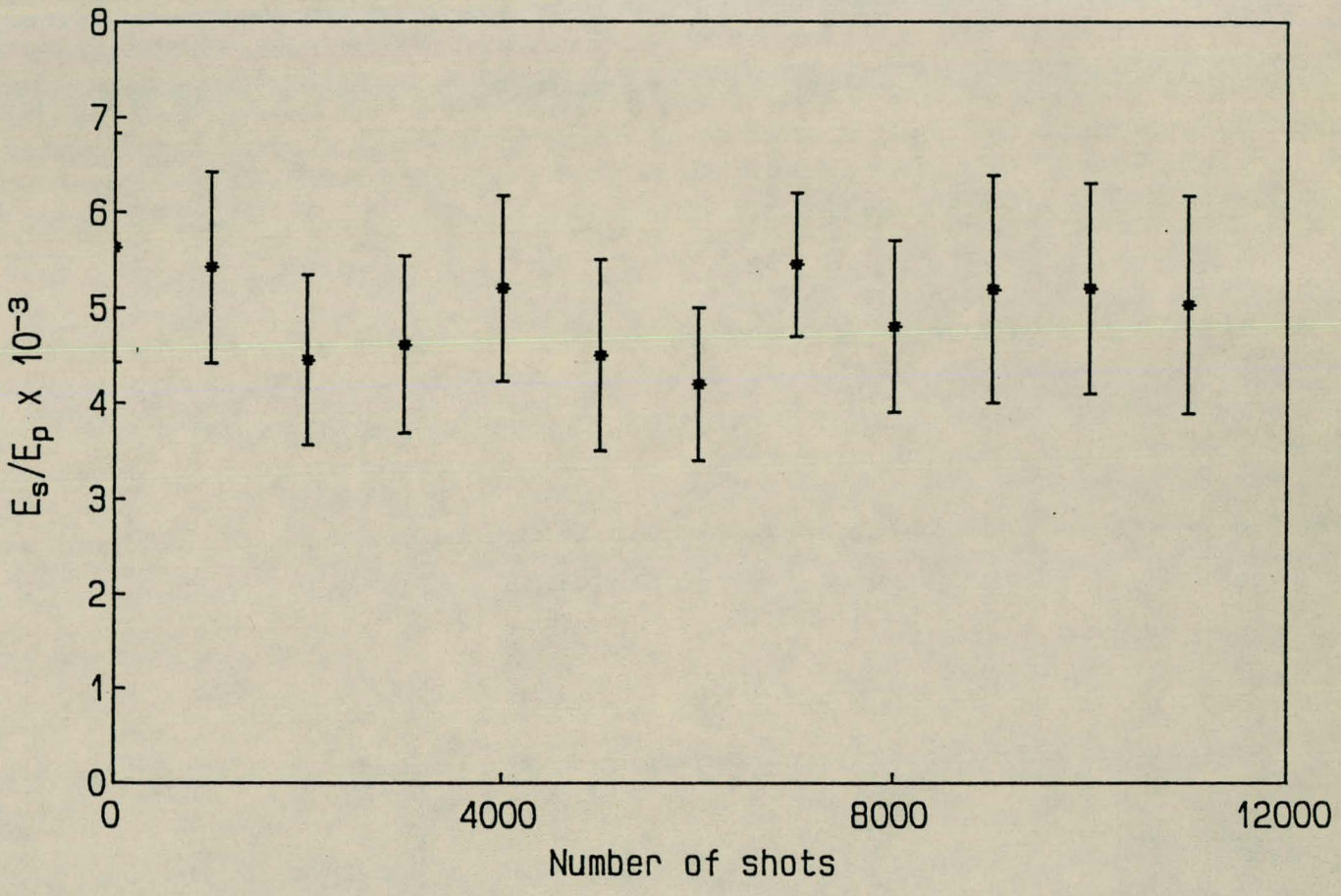

Figure 6.21 Influence of the Number of Shots on the Stokes Energy

6.7 Dye laser used as pump source

In this last section the use of a dye laser in producing the stimulated Raman effect will be described. The experiment was conducted for each of the following cases:

1. Pump beam focussed through waveguide
2. Pump beam focussed once
3. No focussing of the pump beam.

In this way the practical results for different ways in which the pump laser is focussed through the Raman medium is obtained. In chapter 4 the effect of focussing on the Raman gain was discussed. The experimental results obtained here will show the comparison with the predictions made.

6.7.1 Optimizing of the laser output energy

In a previous experiment a beam splitter was used to split the excimer output to pump two separate dye lasers. By removing this beam splitter to pump only one laser at full excimer power, the beam was shifted by a small amount which caused the dye laser to operate inefficient. At a wavelength of 540 nm, the output energy was about 2 mJ for a pump of 100 mJ which corresponds to an efficiency of 2%. This is less than the specified 15.1% efficiency. By following steps given in the reference manual the output energy could be improved to 5.78 $\pm$ 0.12 mJ which is still less than specified, but it could not be improved on. The variation in the energy was nearly 2%.

6.7.2 Waveguide setup

The laser radiation was focussed into the waveguide using a lens with a focal length of 300 mm. This lens was connected to the front of the Raman shifter a distance 295 mm from the waveguide entrance and could be tuned horizontally and vertically. The Raman shifter was positioned so that the distance between the dye laser and the lens was 1.04 m. In contrast with previous transmission experiments where the optimum position for the Raman shifter was calculated, the Raman shifter in this case was placed at a random position and the transmission was optimized. A output energy of 3.68 mJ was obtained which corresponds to a transmission of 63.7 %.

After filling the Raman shifter with 35 bar, a visual pattern consisting of three colors could be seen. Above the green circular pattern which is the incident laser beam of 540 nm, a red circular pattern could be seen which corresponds to the first Stokes beam. Underneath the green pattern, a blue pattern could be seen which corresponds to the first Anti-Stokes beam.

The deviation between the different colors was very little, and it was very difficult to separate the different beams even when focussing the beams. By using a red filter with transmission of 87% at the first Stokes wavelength of 696.6 nm, the green and blue laser light could be filtered out and the energy of the first Stokes beam could be measured.

6.7.3 Pressure influence on first Stokes energy

In figure 6.22, the energy of the first Stokes is plotted versus the hydrogen pressure after correcting for the filter transmission. There is a sharp increase in the energy after 5 bar and it reaches a maximum at about 10 bar. Increasing the pressure further did not increase the Stokes energy, in fact it decreases slightly at very high pressures. This decrease in the energy may be attributed to the second Stokes wave which starts to grow at high pressures and also the depletion of the gain at high pressures.

It was not possible to obtain a filter which could filter the green and red from the blue to be able to measure the first Anti-Stokes energy.

6.7.4 Line measurements

Only the first order Stokes line could be measured because the higher order wavelengths are too large to be measured with the photomultiplier tube. The first Anti-Stokes line was also measured. In figures 6.23 to 6.25 the measured profiles are shown. The profiles had been obtained in the same manner as in the case where the excimer laser was used as a pump beam.

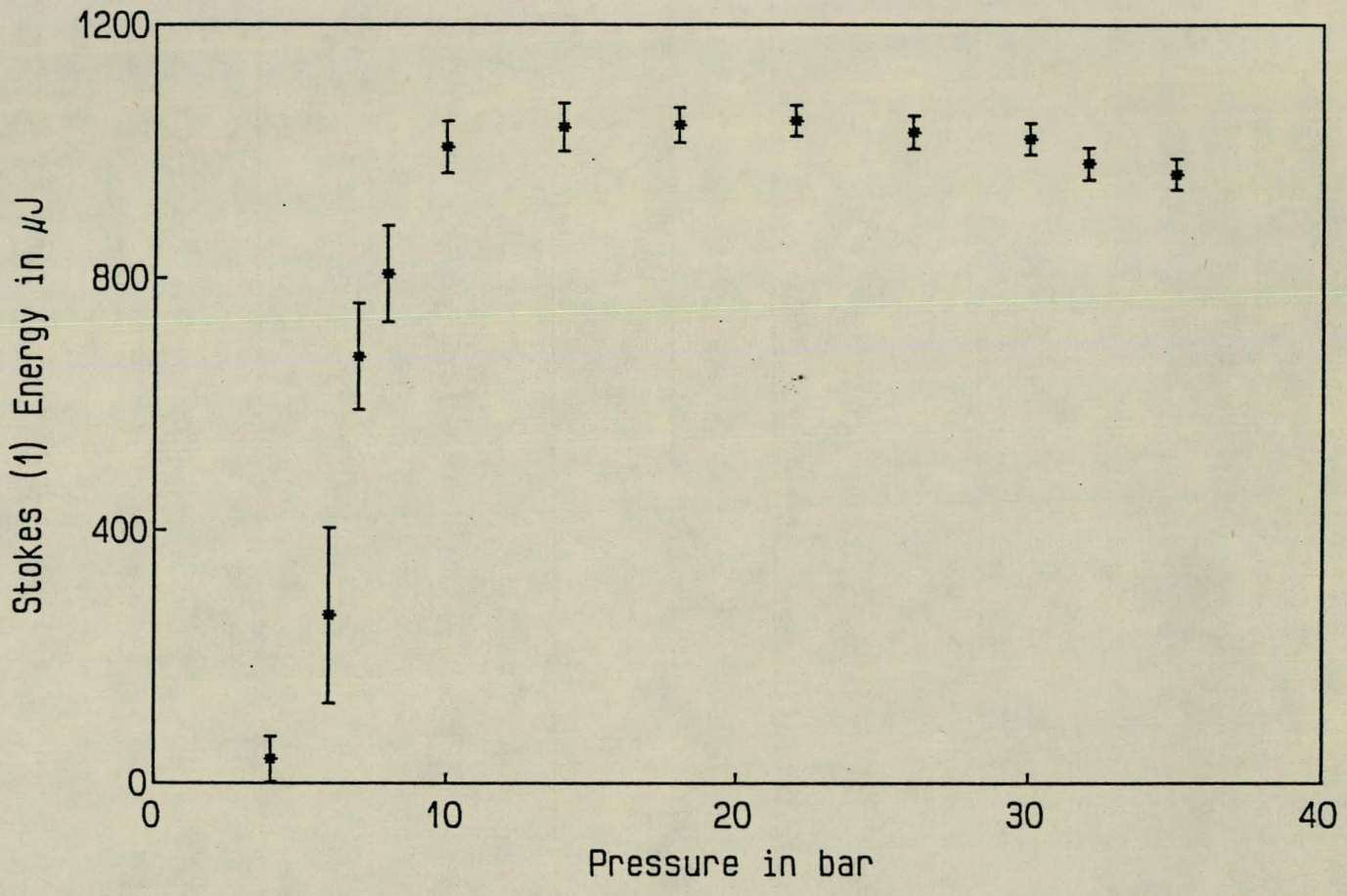

Figure 6.22 First Stokes Energy versus the Pressure

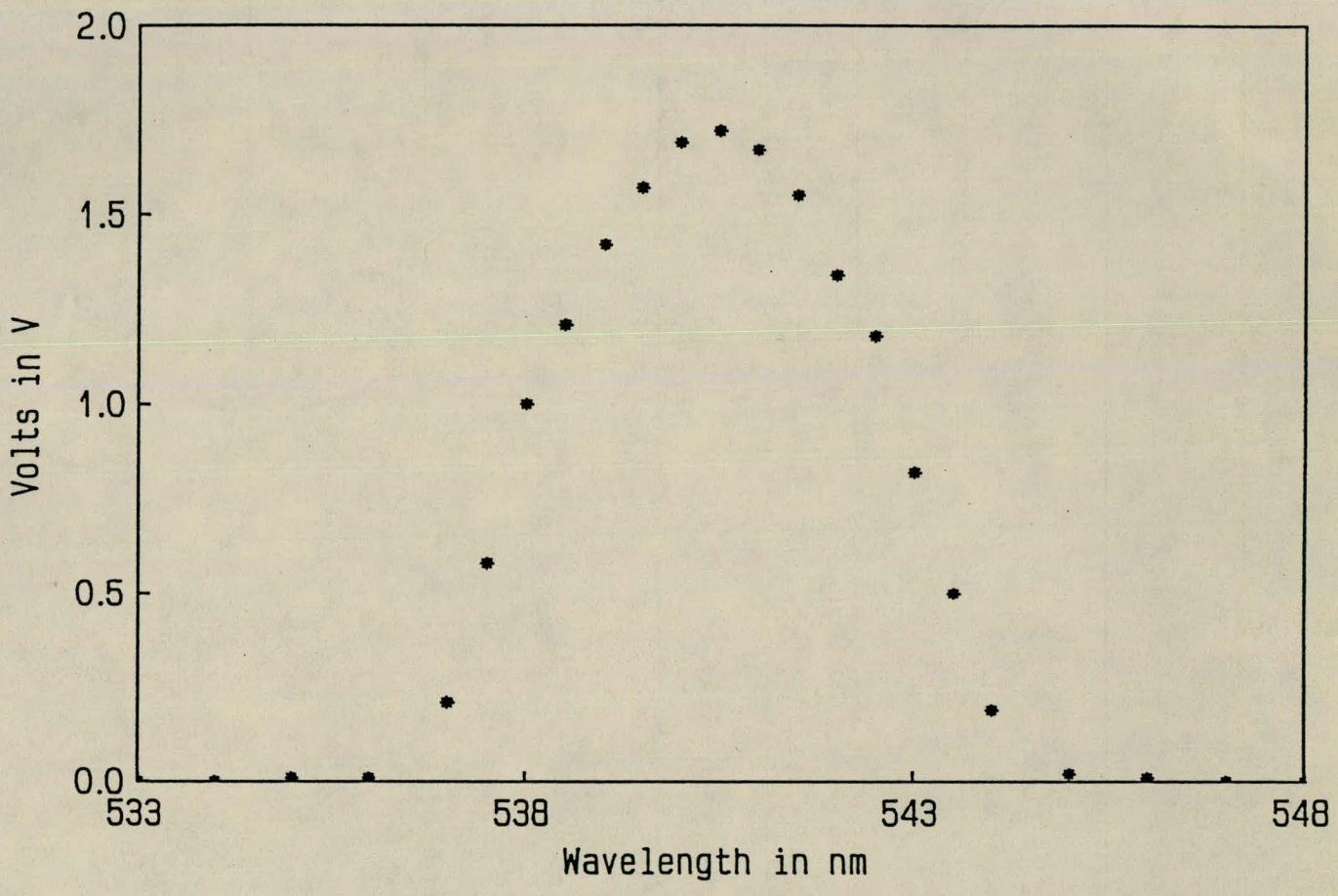

Figure 6.23 Measured Profile of Dye Laser

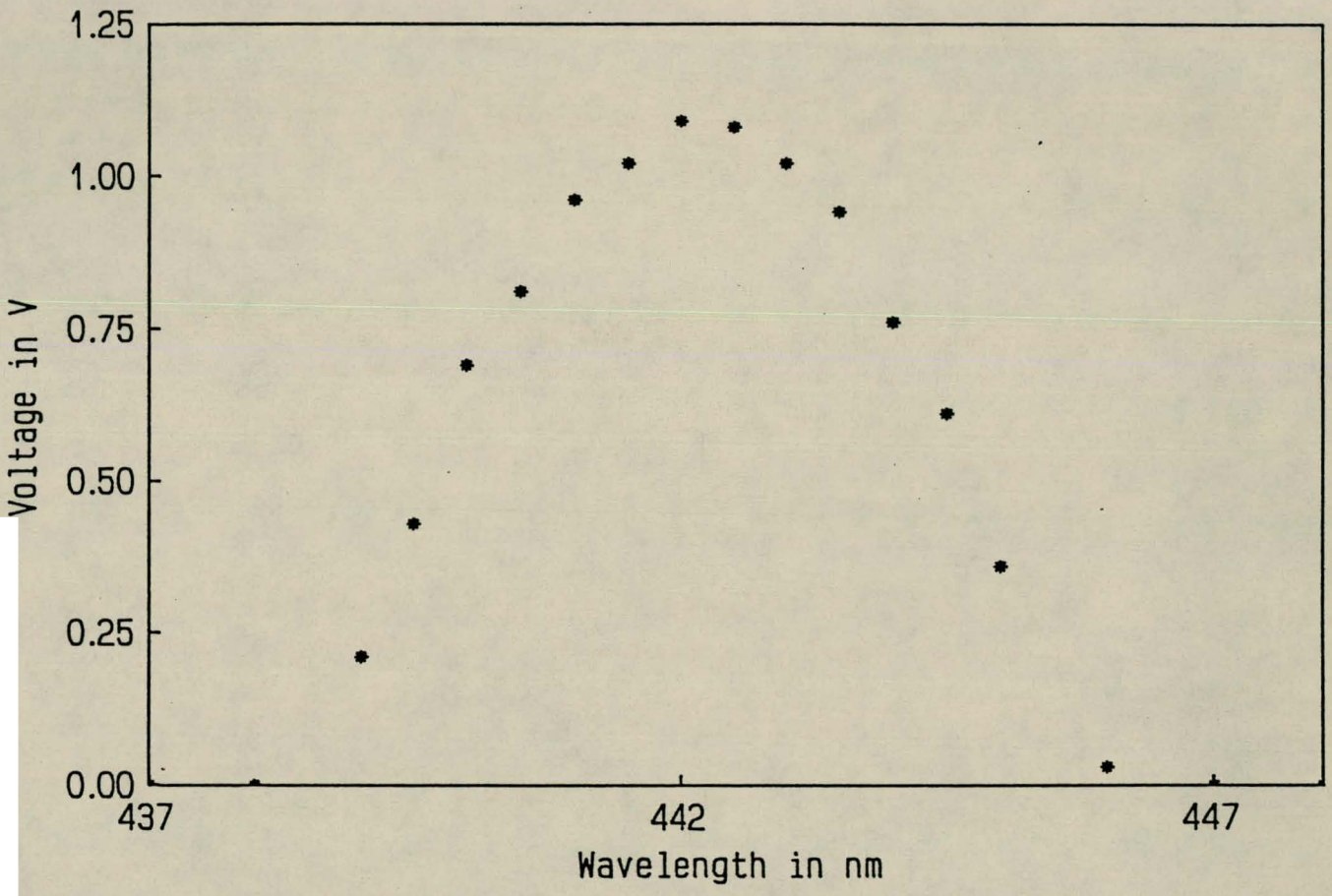

Figure 6.25 Measured Profile of First Anti-Stokes Line

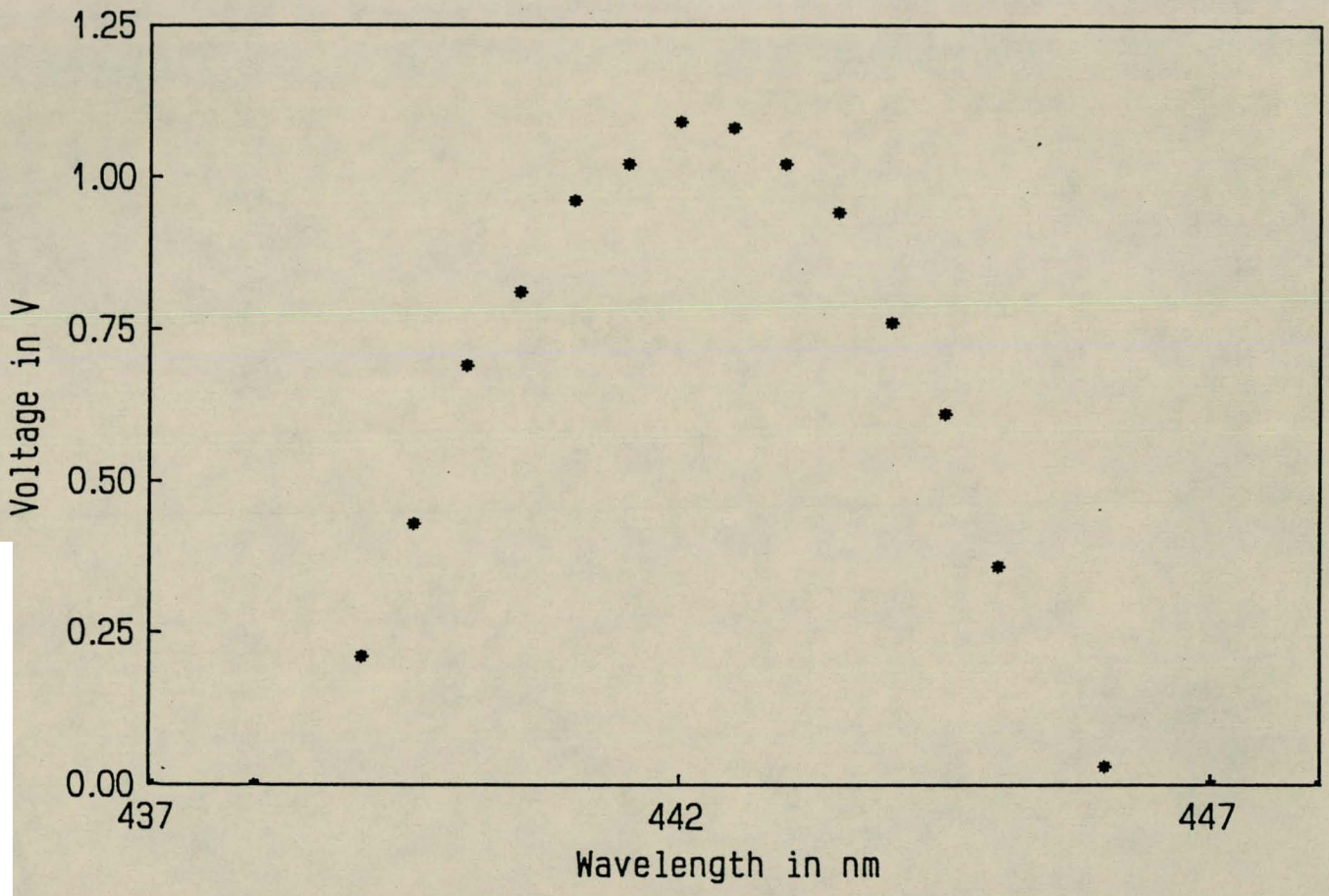

Figure 6.25 Measured Profile of First Anti-Stokes Line

6.7.5 Influence of the pump wavelength on Stokes energy

The Raman gain also depends on the pump wavelength and thus in theory one would be able to measure the variation in Stokes energy when tuning over the pump wavelength region. It could prove to be difficult when the pump wavelength is far from a resonance and tuning does not really have such a great effect that it could be measured. One also has that the pump energy itself varies as the laser is scanned through the wavelength region which complicates the situation further. This variation is plotted in figure 6.26. It shows the same from as the dye effectivity as expected.

There is also the effect that the Stokes energy varies with variation in the pump energy which also must be included in the calculations. Making approximations the Stokes energy divided by the pump energy is plotted as a function of the pump wavelength in figure 6.27. No certain from could be seen and one would thus need more sophisticated apparatus to be able to measure the variation.

6.7.6 Influence of the pump energy

Using attenuators the Stokes energy versus the pump energy could be plotted as in figure 6.28. It shows a linear relation as expected.

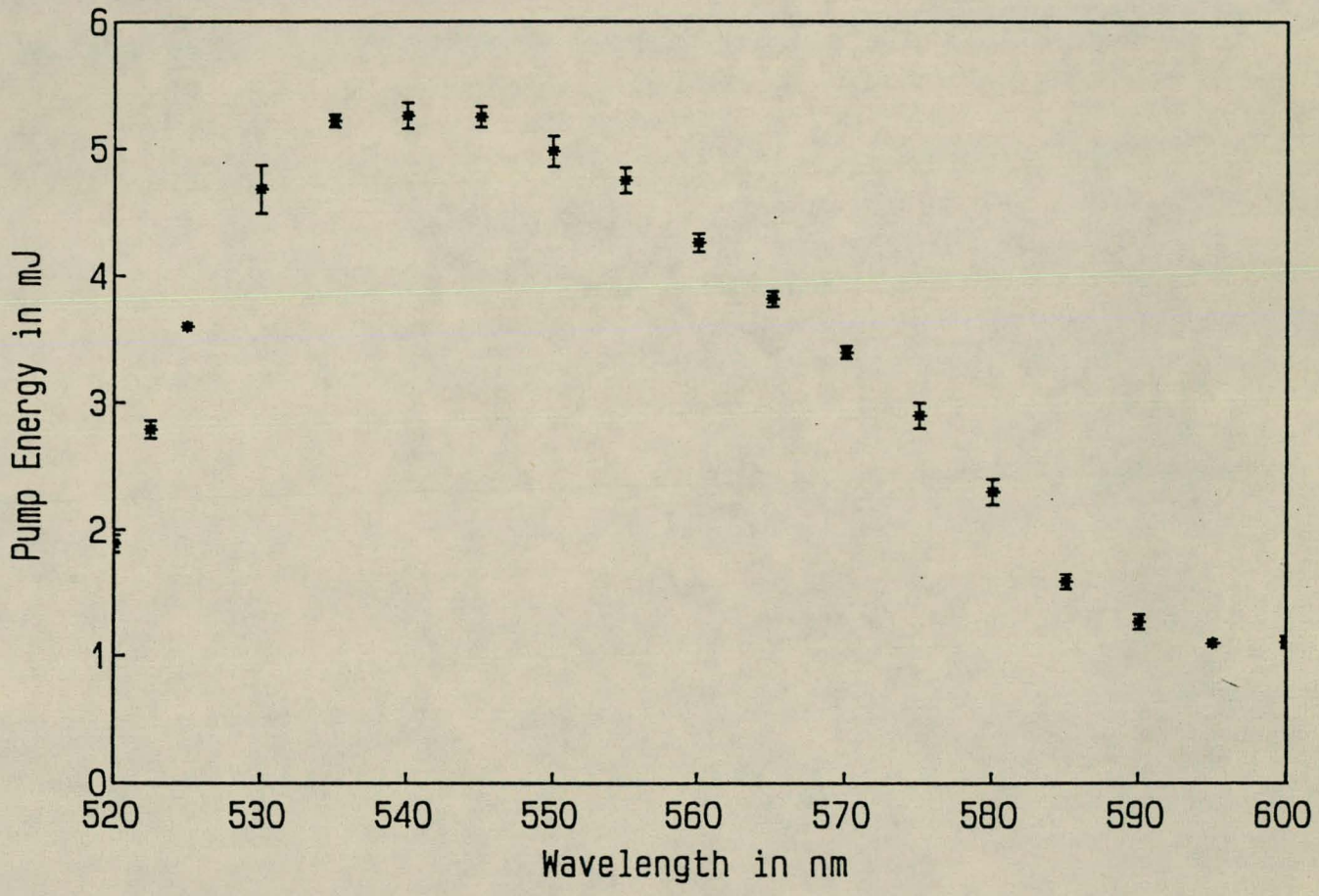

Figure 6.26 Dye efficiency versus wavelength

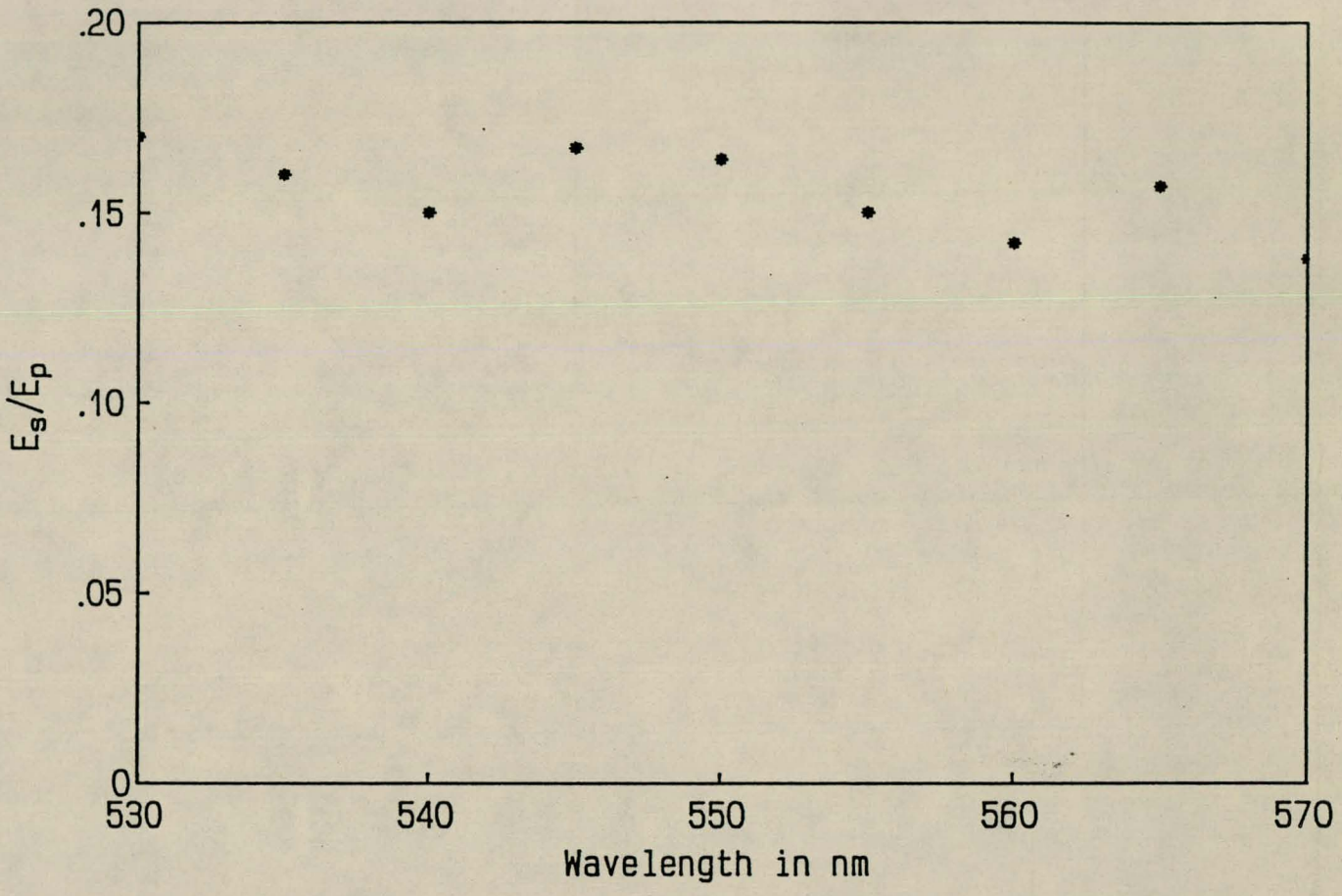

Figure 6.27 Relative Stokes energy versus pump wavelength

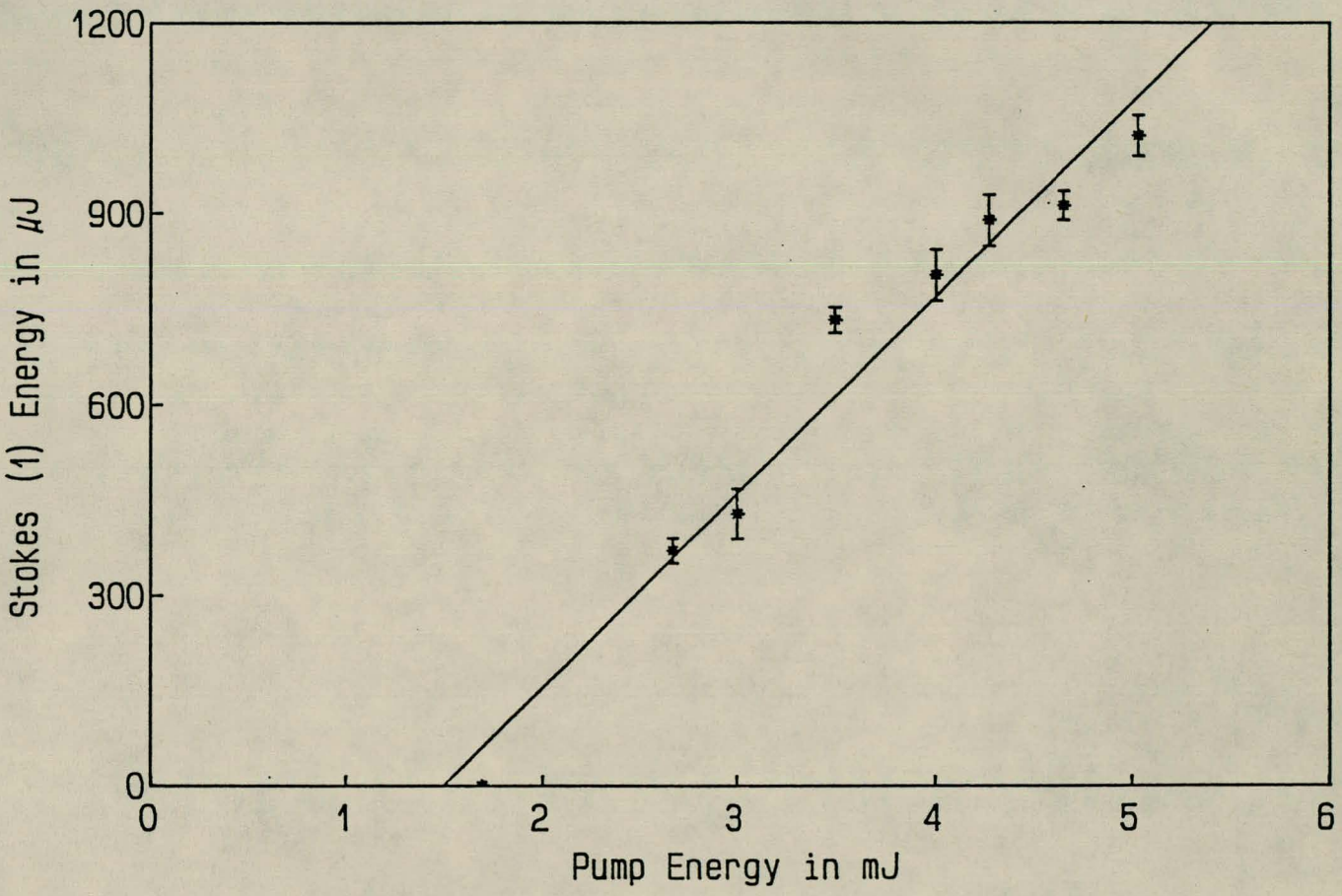

Figure 6.28 First Stokes energy versus pump energy

6.8 Pump beam focussed once

The pump laser was also focussed once through the Raman medium without the waveguide. The experimental setup stayed the same. In figure 6.29 the Stokes energy versus the hydrogen pressure is shown. Comparison of this graph may be made with figure 6.22. In the case where the waveguide was used, the maximum energy was obtained at a pressure of about 10 bar, where in the present case no Stokes energy could be measured at 10 bar. The pressure had to be increased to 35 bar to obtain nearly the same Stokes energy as in the waveguide case. This showed that the waveguide certainly enhances the Raman gain effectively.

When the lens was removed, no Stokes energy could be measured at all at any pressure, nor was any radiation expect that of the pump laser visible. This whole experiment has demonstrated the effect of focussing on the Raman gain as discussed in chapter 4. Indeed focussing has an dramatic effect on the Raman gain and therefore waveguides are often used in the infrared regions to increase the gain factor.

No Raman radiation could be obtained when using nitrogen as a medium probably due to its smaller cross section as discussed in chapter 4.

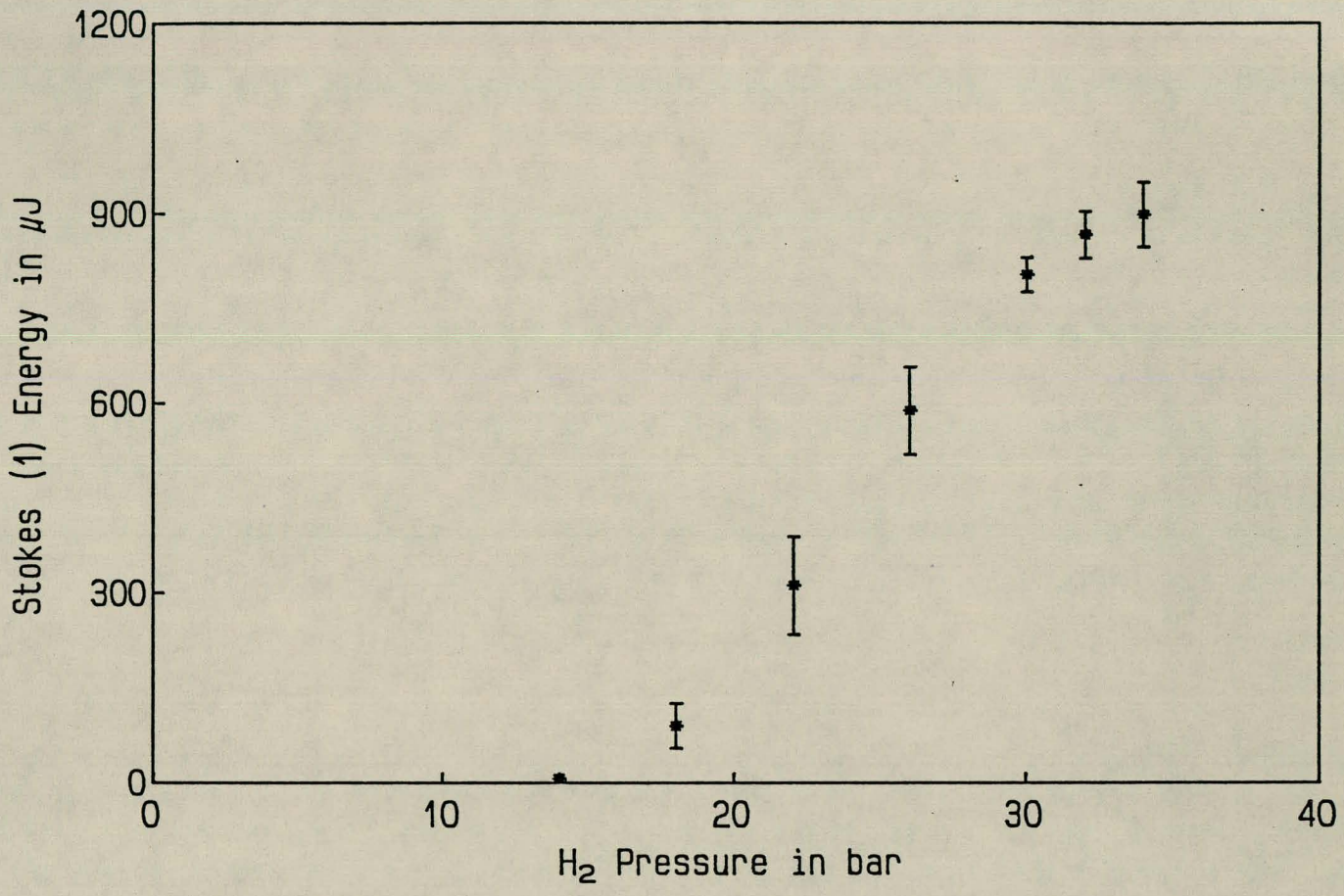

Figure 6.29 First Stokes energy versus pressure

7

CONCLUSIONS AND RECOMMENDATIONS

The purpose of this thesis was to investigate the nonlinear stimulated Raman scattering process. Several other aspects were investigated, such as the propagation of laser radiation and the propagation of radiation in a waveguide, as well as the coupling between a laser beam and a waveguide. Various studies of the stimulated Raman process were undertaken such as the determination of the threshold value and the influence of a waveguide on the Raman gain. Valuable results and information were obtained which may provide background material for further studies.

A high output laser was used to obtain stimulated Raman scattering in a medium and therefore the propagation of laser radiation was studied in detail. Experimental and theoretical information about laser propagation using a He-Ne laser were obtained. Also the propagation of radiation in a waveguide was studied in detail, since the Raman medium was contained in a waveguide. Special attention was paid to the coupling of laser radiation to the waveguide in order to maximize the transmission, and the parameters which influence the transmission of the waveguide were identified. A model was derived to determine the theoretical transmission of a hollow waveguide and was tested successfully in experiments. Recommendations were made concerning experimental difficulties in the transmission setup.

The Raman process was investigated first by using low power cw He-Ne and Argon Ion lasers. Due to the relatively low intensity of these lasers, only the spontaneous Raman effect was detected. It was not possible to measure the Raman effect mainly because of the low intensity obtained due to too much losses and small gain factor. The practical difficulties experienced in measuring the intensity also made the measurements very difficult. The high intensity of the pump laser caused large amounts of scattered light in the monochromator which caused saturation of the Raman signal. The experimental setup was also very sensitive and small changes in the alignment caused unwanted scattered light. Although the experiment was thus not success-

ful in the sense that the spontaneous Raman scattering process could not be measured, valuable information concerning alignment and measuring techniques was obtained.

An excimer and dye laser were then used because of their high output power. Both provide sufficient pump intensity to generate stimulated Raman scattering and important experimental results were obtained. These experimental results obtained agreed well with theoretical predictions. Because these two lasers are pulsed lasers, other experimental techniques involving the use of a Boxcar Integrator had to be applied to measure the various spectral profiles. As may be seen from these measured profiles, the profiles are much broadened and in effect only the instrument profile of the monochromator was measured. To be able to measure the various line profiles an interferometer must be used because of its high resolving power.

In conclusion some of the important parameters which have a influence on the Raman process have been identified and various techniques were applied to obtain experimental results. The basic theory and practical aspects underlining the process were looked at and important aspects of the process were discussed.

Future studies would involve the measuring of the spectral profiles with an interferometer and the identification of parameters which influence the line profile shape. Techniques involving the classification of materials using spontaneous Raman scattering may also be applied and investigated. One may also look at other nonlinear effects like second and third harmonic generation and the application of various phase matching techniques.

Appendix A

Gaussian Beam Parameters

The parameters R,w and q are connected in the following manner.

$$\frac{1}{q} = \frac{1}{R} - j\frac{\lambda}{\pi w^2} \tag{A.1}$$

q_o is given by

$$q_o = j\frac{\pi w_o^2}{\lambda} \tag{A.2}$$

At a distance z, q is given by

$$q = q_o + z = j\frac{\pi w_o^2}{\lambda} + z \tag{A.3}$$

Combining equations A.1 and A.3 leads to the following

$$[\frac{1}{R} - j\frac{\lambda}{\pi w^2}]^{-1} = j\frac{\pi w_o^2}{\lambda} + z \tag{A.4}$$

$$[\frac{\pi w^2 - j\lambda R}{R\pi w^2}]^{-1} = j\frac{\pi w_o^2}{\lambda} + z \tag{A.5}$$

$$\frac{R\pi w^2}{\pi w^2 - j\lambda R} = j\frac{\pi w_o^2}{\lambda} + z \tag{A.6}$$

One may now obtain

$$\begin{aligned} R\pi w^2 &= (\pi w^2 - j\lambda R)(z + j\frac{\pi w_o^2}{\lambda}) \\ &= \pi w^2 z + j\frac{\pi^2 w^2 w_o^2}{\lambda} - j\lambda R z + \pi w_o^2 R \end{aligned} \tag{A.7}$$

(A.8)

By combining the real and imaginary parts one obtain

$$R\pi w^2 - \pi w^2 z - \pi w_o^2 R = j(\frac{\pi^2 w^2 w_o^2}{\lambda} - \lambda R z) \tag{A.9}$$

For the above condition to be satisfied both sides must equal to zero.

This then gives

$$R\pi w^2 - \pi w^2 z - \pi w_o^2 R = 0 \tag{A.10}$$

which may be written as

$$Rw^2 - w^2 z - w_o^2 R = 0 \tag{A.11}$$

Division by R leads to

$$w^2 - \frac{w^2 z}{R} - w_o^2 = 0 \tag{A.12}$$

Equating the imaginary parts to zero leads to

$$j(\frac{\pi^2 w^2 w_o^2}{\lambda} - \lambda R z) = 0 \tag{A.13}$$

This gives

$$R = \frac{1}{z}\frac{\pi^2 w^2 w_o^2}{\lambda^2} \tag{A.14}$$

Substituting this into equation A.12 gives

$$w^2(1 - z^2\frac{\lambda^2}{\pi^2 w^2 w_o^2}) = w_o^2 \tag{A.15}$$

That is

$$w^2 - \frac{z^2\lambda^2}{\pi^2 w_o^2} = w_o^2 \tag{A.16}$$

Thus

$$w^2 = w_o^2 + \frac{z^2\lambda^2}{\pi^2 w_o^2} \tag{A.17}$$

This leads to the well known equation

$$w^2 = w_o^2[1 + (\frac{z\lambda}{\pi w_o^2})^2] \tag{A.18}$$

The same procedure may be done to obtain an similar equation which describes R.

From equation A.12 one has that

$$\frac{w^2 z}{R} = w^2 - w_o^2 \tag{A.19}$$

Division with w^2 leads to

$$\frac{z}{R} = 1 - \frac{w_o^2}{w^2} \tag{A.20}$$

From equation A.14 may be written that

$$w^2 = \frac{zR\lambda^2}{\pi^2 w_o^2} \tag{A.21}$$

Substituting this into equation A.12 leads to

$$\frac{z}{R} = 1 - w_o^2[\frac{zR\lambda^2}{\pi^2 w_o^2}]^{-1} \tag{A.22}$$

$$\frac{z}{R} = 1 - w_o^2[\frac{\pi^2 w_o^2}{zR\lambda^2}] \tag{A.23}$$

Multiplication with R leads to

$$z = R - w_o^2 \frac{\pi^2 w_o^2}{z\lambda^2} \tag{A.24}$$

From this R may be written as

$$R = z + \frac{\pi^2 w_o^4}{z\lambda^2} \tag{A.25}$$

$$R = z + \frac{1}{z}\left(\frac{\pi w_o^2}{\lambda}\right)^2 \tag{A.26}$$

This leads to the final equation for R.

$$R = z\left[1 + \left(\frac{\pi w_o^2}{\lambda z}\right)^2\right] \tag{A.27}$$

Appendix B

Backtracking of Gaussian beam

If the parameters R and w are known at a certain unknown distance z, it is possible to determine the value and position z of w_o by tracking back the beam. Consider figure B.1.

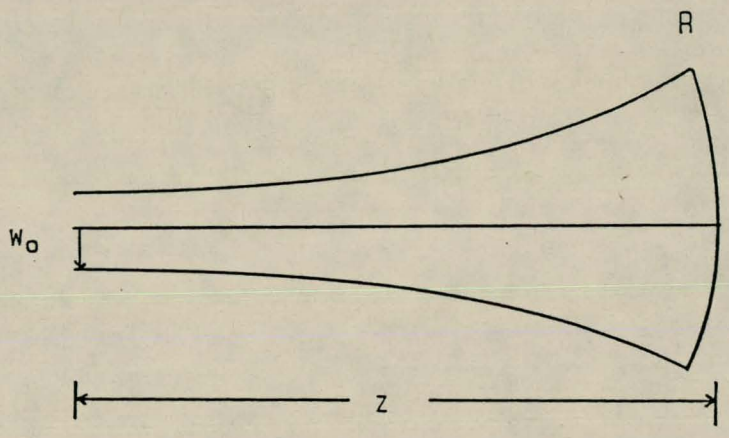

Figure B.1 Backtracking of Gaussian beam

From Appendix A one has that

$$w^2 - \frac{w^2 z}{R} - w_o^2 = 0 \tag{B.1}$$

$$R = \frac{1}{z}\frac{\pi^2 w^2 w_o^2}{\lambda^2} \tag{B.2}$$

Using the above equation one may obatain

$$\frac{1}{z} = \frac{R\lambda^2}{\pi^2 w^2 w_o^2} \tag{B.3}$$

This leads to

$$z = \frac{\pi^2 w^2 w_o^2}{R\lambda^2} \tag{B.4}$$

Substituting this into equation B.1 gives the following:

$$w^2 - \frac{w^2}{R}\frac{\pi^2 w^2 w_o^2}{R\lambda^2} - w_o^2 = 0 \tag{B.5}$$

This may be written as

$$w_o^2 + \frac{1}{R}\frac{\pi^2 w^4 w_o^2}{R\lambda^2} = w^2 \tag{B.6}$$

Then

$$w_o^2\left(\frac{\pi^2 w^4}{R^2\lambda^2} + 1\right) = w^2 \tag{B.7}$$

From this one may obtain that

$$w_o^2 = \frac{w^2}{1 + \left(\frac{\pi^2 w^4}{\lambda^2 R^2}\right)} \tag{B.8}$$

Then

$$w_o = \frac{w}{\sqrt{1 + \left(\frac{\pi w^2}{\lambda R}\right)^2}} \tag{B.9}$$

The size of the Gaussian waist w_o, has thus been determined. An equation for z, the position of w_o may also be derived.

From equation B.2 one has that

$$w_o^2 = \frac{zR\lambda^2}{\pi^2 w^2} \tag{B.10}$$

By substituting this into equation B.1 one may obtain

$$w^2 - \frac{w^2 z}{R} - \frac{zR\lambda^2}{\pi^2 w^2} \tag{B.11}$$

Division by w^2 gives

$$1 - \frac{z}{R} - \frac{zR\lambda^2}{\pi^2 w^4} \tag{B.12}$$

or

$$z(\frac{1}{R} + \frac{R\lambda^2}{\pi^2 w^4}) = 1 \tag{B.13}$$

Then

$$z = \frac{1}{\frac{1}{R} + \frac{R\lambda^2}{\pi^2 w^4}} \tag{B.14}$$

which gives the final result written as

$$z = \frac{R}{1 + (\frac{R\lambda}{\pi w^2})^2} \tag{B.15}$$

Appendix C

Maxwell's equations in Cartesian coordinates

From Maxwell's equations one has that

$$\nabla \times \mathbf{E} = -\frac{\partial B}{\partial t} = -\mu \frac{\partial \mathbf{H}}{\partial t} \tag{C.1}$$

$$\nabla \times \mathbf{H} = +\frac{\partial D}{\partial t} = \epsilon \frac{\partial \mathbf{E}}{\partial t} \tag{C.2}$$

Let

$$\mathbf{H} = \mathbf{H_o} \exp(jwt - \gamma z) \tag{C.3}$$

and

$$\mathbf{E} = \mathbf{E_o} \exp(jwt - \gamma z) \tag{C.4}$$

Then

$$\frac{\partial \mathbf{H}}{\partial t} = \mathbf{H_o} jw \exp(jwt - \gamma z) = jw\mathbf{H} \tag{C.5}$$

In the same manner

$$\frac{\partial \mathbf{E}}{\partial t} = jw\mathbf{E} \tag{C.6}$$

By substituting these into equations C.1 and C.2 one may obtain

$$\nabla \times \mathbf{E} = -jw\mu\mathbf{H} \tag{C.7}$$

$$\nabla \times \mathbf{H} = +jw\epsilon\mathbf{E} \tag{C.8}$$

All the quantities are now written in terms of Cartesian coordinates.

$$\nabla = \hat{i}\frac{\partial}{\partial x} + \hat{j}\frac{\partial}{\partial y} + \hat{k}\frac{\partial}{\partial z} \tag{C.9}$$

where $\hat{i}$, $\hat{j}$ and $\hat{k}$ are unit vectors in the x, y and z directions respectively.

One also has that

$$\mathbf{E} = \hat{i}E_x + \hat{j}E_y + \hat{k}E_z \tag{C.10}$$

$$\mathbf{H} = \hat{i}H_x + \hat{j}H_y + \hat{k}H_z \tag{C.11}$$

Let the operator *div* or ∇ operates on the electric field **E**.

This may be written as

$$\nabla \times \mathbf{E} = (\hat{i}\frac{\partial}{\partial x} + \hat{j}\frac{\partial}{\partial y} + \hat{k}\frac{\partial}{\partial z}) \times (\hat{i}E_x + \hat{j}E_y + \hat{k}E_z) \tag{C.12}$$

This is equal to

$$\hat{i}(\frac{\partial E_z}{\partial y} - \frac{\partial E_y}{\partial z}) + \hat{j}(\frac{\partial E_x}{\partial z} - \frac{\partial E_z}{\partial x}) + \hat{k}(\frac{\partial E_y}{\partial x} - \frac{\partial E_x}{\partial y}) \tag{C.13}$$

From equation C.7, this must be equal to

$$-jw\mu(\hat{i}H_x + \hat{j}H_y + \hat{k}H_z) \tag{C.14}$$

Then

$$\frac{\partial E_z}{\partial y} - \frac{\partial E_y}{\partial z} = -jw\mu H_x \tag{C.15}$$

$$\frac{\partial E_x}{\partial z} - \frac{\partial E_z}{\partial x} = -jw\mu H_y \tag{C.16}$$

$$\frac{\partial E_y}{\partial x} - \frac{\partial E_x}{\partial y} = -jw\mu H_z \tag{C.17}$$

One also has

$$\frac{\partial E_{x,y,z}}{\partial z} = -\gamma E_{x,y,z} \tag{C.18}$$

The above equations then reduce to

$$\frac{\partial E_z}{\partial y} + \gamma E_y = -jw\mu H_x \tag{C.19}$$

$$-\gamma E_x - \frac{\partial E_z}{\partial x} = -jw\mu H_y \tag{C.20}$$

$$\frac{\partial E_y}{\partial x} - \frac{\partial E_x}{\partial y} = -jw\mu H_z \tag{C.21}$$

The same may be done to for $\nabla \times \mathbf{H} = +jw\epsilon\mathbf{E}$ to obtain a similar set of equations [Ra 65].

$$\frac{\partial H_z}{\partial y} + \gamma H_y = -jw\epsilon E_x \tag{C.22}$$

$$-\gamma H_x - \frac{\partial H_z}{\partial x} = +jw\epsilon E_y \tag{C.23}$$

$$\frac{\partial H_y}{\partial x} - \frac{\partial H_x}{\partial y} = +jw\epsilon E_z \tag{C.24}$$

Appendix D

Transverse Electric and Magnetic components

Equations C.19 to C.24 may be used to write the transverse components E_x, E_y, H_x and H_y in terms of the axial components E_z and H_z. Only one example in which H_x is calculated will be considered. The other transverse components may be derived in the same manner.

From equation C.23 one has that

$$E_y = (iw\epsilon)^{-1}(-\gamma H_x - \frac{\partial H_z}{\partial x}) \tag{D.1}$$

Substituting of this into equation C.19 and the elimination of E_y leads to the following result.

$$\frac{\partial E_z}{\partial y} + \gamma(iw\epsilon)^{-1}(-\gamma H_x - \frac{\partial H_z}{\partial x}) = -jw\mu H_x \tag{D.2}$$

That is

$$\frac{\partial E_z}{\partial y} - \gamma^2(iw\epsilon)^{-1}H_x - \gamma(iw\epsilon)^{-1}\frac{\partial H_z}{\partial x} = -jw\mu H_x \tag{D.3}$$

Multiplying with $(iw\epsilon)$ leads to

$$(iw\epsilon)\frac{\partial E_z}{\partial y} - \gamma^2 H_x - \gamma\frac{\partial H_z}{\partial x} = w^2\mu\epsilon H_x \tag{D.4}$$

Rearranging terms gives

$$w^2\mu\epsilon H_x + \gamma^2 H_x = (iw\epsilon)\frac{\partial E_z}{\partial y} - \gamma\frac{\partial H_z}{\partial x} \tag{D.5}$$

Then

$$H_x = (k^2 + \gamma^2)^{-1}(iw\epsilon\frac{\partial E_z}{\partial y} - \gamma\frac{\partial H_z}{\partial x}) \tag{D.6}$$

where $k^2 = w^2\mu\epsilon$.

The other components may be derived in the same manner.

Al four transverse components are then given by [Ra 65]

$$H_x = (k^2 + \gamma^2)^{-1}(iw\epsilon\frac{\partial E_z}{\partial y} - \gamma\frac{\partial H_z}{\partial x}) \tag{D.7}$$

$$H_y = -(k^2 + \gamma^2)^{-1}(iw\epsilon\frac{\partial E_z}{\partial x} + \gamma\frac{\partial H_z}{\partial y}) \tag{D.8}$$

$$E_x = -(k^2 + \gamma^2)^{-1}(\gamma\frac{\partial E_z}{\partial x} + jw\mu\frac{\partial H_z}{\partial y}) \tag{D.9}$$

$$E_y = (k^2 + \gamma^2)^{-1}(-\gamma\frac{\partial E_z}{\partial y} + jw\mu\frac{\partial H_z}{\partial x}) \tag{D.10}$$

Appendix E

The relation between the peak intensity and the power of a Gaussian laser beam

When using a detector to scan over the laser profile in the x-direction, one obtains voltage readings that obeys the following form

$$V = V_{max} e^{\frac{-x^2}{r^2}} \tag{E.1}$$

This gives values for V_{max} and r, but no information on the peak intensity of the beam.

The optical power P, of the beam may be written in terms of the intensity in two dimensions.

$$P = \int_{-\infty}^{+\infty} I_o e^{\frac{-(x^2)}{r^2}} dx \tag{E.2}$$

Note that $w = \sqrt{2}r$ where w is the beam diameter defined by the amplitude and r is the beam diameter defined by using the intensity. This means that the intensity distribution has the form of a cone and that the total volume under this cone is equal to the optical power of the beam. For a certain waist r, the peak intensity is thus determined by the power.

In three dimensions one has that

$$V = \int_{-\infty}^{+\infty} \int_{-\infty}^{+\infty} I_o e^{\frac{-x^2}{r^2}} e^{\frac{-y^2}{r^2}} dxdy \tag{E.3}$$

This may be written as

$$V = \int_{-\infty}^{+\infty} \int_{0}^{+\infty} 2I_o e^{\frac{-x^2}{r^2}} e^{\frac{-y^2}{r^2}} dxdy \tag{E.4}$$

because e^{-x^2/r^2} and e^{-y^2/r^2} are both even functions.

Now [Sp 68]

$$\int_0^\infty e^{-ax^2}dx = \frac{1}{2}(\frac{\pi}{a})^{\frac{1}{2}} \tag{E.5}$$

Thus

$$V = 2I_o \int_{-\infty}^{+\infty} e^{-y^2/r^2}(\frac{1}{2}r\sqrt{\pi}) \tag{E.6}$$

By treating the y integral in the same manner the following result may be obtained.

$$V = 4I_o\frac{1}{2}r\sqrt{\pi}\frac{1}{2}r\sqrt{\pi} \tag{E.7}$$

which gives

$$V = I_o r^2\pi \tag{E.8}$$

From this one has that

$$I_o = \frac{V}{r^2\pi} \tag{E.9}$$

and in terms of w

$$I_o = \frac{2V}{w^2\pi} \tag{E.10}$$

or

$$I_o = \frac{2P}{w^2\pi} \tag{E.11}$$

Because w is a function of z and the beam size increases as the beam propagates, the above relation clearly shows that the peak intensity I_o must decrease with increasing z, because the power P of the beam remains constant.

Appendix F

Kayser Units

Most of the vibrational and rotational energies in books are given in the Kayser units or cm^{-1}. The simbol mostly used are σ. In this appendix a relation will be determined which enables quick determination of the various Stokes or Anti-Stokes wavelengths for a energy difference given in Kaysers.

The relation between the energy difference and σ is given by

$$\Delta E = \sigma(cm^{-1}) \times 100hc \tag{F.1}$$

The wavelength are related in the following manner.

$$\frac{1}{\lambda(m)} = 100 \times \sigma(cm^{-1}) \tag{F.2}$$

Consider the first Stokes line. The energy associated with the transition is given by

$$\Delta E_{R1} = \Delta E_L - \Delta E_V \tag{F.3}$$

where ΔE_L and ΔE_V are the laser and the vibrational energies respectively.

If one now substitutes $E = hc/\lambda$ and equation F.1 into equation F.3, one obtains equation F.4.

$$\frac{hc}{\lambda_{S1}} = \frac{hc}{\lambda_L} - \sigma.100hc \tag{F.4}$$

Division by hc leads to

$$\frac{1}{\lambda_{S1}} = 1/\lambda_L - 100.\sigma \tag{F.5}$$

This may be written as

$$\lambda_{S1} = [1/\lambda_L - 100.\sigma]^{-1} \tag{F.6}$$

With this result it is easy to calculate the wavelength for the first Stokes order. To determine the second, third and higher order wavelengths a more general equation must be used.

$$\lambda_{S1} = [1/\lambda_L - n.100.\sigma]^{-1} \tag{F.7}$$

Here n = 1 corresponds to the first Stokes line, n = 2 to the second etc. With this relation one may thus calculate for any given laser and vibrational frequency (or energy) in Kaysers, the wavelength of any Stokes line. The Anti-Stokes wavelengths may be calculated by using the following equation.

$$\lambda_{S1} = [1/\lambda_L + n.100.\sigma]^{-1} \tag{F.8}$$

Appendix G

Stimulated Emission equation

In this appendix the derivation of the stimulated emission equation from is shown.

From chapter 4 one has that

$$\frac{dE}{dz} = \frac{1}{2}gE \tag{G.1}$$

The intensity is proportional to the square of the electric field amplitude so that

$$I = aE^2 \tag{G.2}$$

where a is a constant.

If one differentiates the above equation with respect to z, one obtains

$$\frac{dI}{dz} = 2aE\frac{dE}{dz} \tag{G.3}$$

Substitution of equation G.1 into the above equation leads to

$$\frac{dI}{dz} = 2aE(\frac{1}{2}gE) \tag{G.4}$$

This may finally be written as

$$\frac{dI}{dz} = gI \tag{G.5}$$

which is the well-known gain equation.

Appendix H

Solving of integral equation $C(z)$

The following equation from chapter 4 is solved here.

$$C(z) = \int_{-L}^{+L} \frac{2GP_p}{\pi} \frac{1}{w_o^2 + (\frac{\lambda z}{\pi w_o})^2} dz \tag{H.1}$$

This may be written as

$$C(z) = \frac{2GP_p}{\pi} \int_{-L}^{+L} \frac{1}{w_o^2 + (\frac{\lambda z}{\pi w_o})^2} dz \tag{H.2}$$

The following integral thus remains to be solved

$$\int \frac{1}{w_o^2 + (\frac{\lambda z}{\pi w_o})^2} dz \tag{H.3}$$

The following solution is used for an integral of the following type [Sp 68].

$$\int \frac{dx}{ax^2 + bx + c} = \frac{2}{\sqrt{4ac - b^2}} \arctan\left(\frac{2ax + b}{\sqrt{4ac - b^2}}\right) \tag{H.4}$$

Comparison with equation H.3 leads to the following connections.

$$a = (\frac{\lambda}{\pi w_o})^2, b = 0, c = w_o^2 \tag{H.5}$$

One then has that

$$\int \frac{1}{w_o^2 + (\frac{\lambda z}{\pi w_o})^2} dz = \frac{2}{\sqrt{4(\frac{\lambda}{\pi w_o})^2 (w_o)^2}} \arctan\left(\frac{2(\frac{\lambda}{\pi w_o})^2 z}{\sqrt{4(\frac{\lambda}{\pi w_o})^2 (w_o)^2}}\right) \tag{H.6}$$

This is equal to

$$\frac{\pi}{\lambda} \arctan\left[\frac{\pi}{\lambda}(\frac{\lambda}{\pi w_o})^2 z\right] \tag{H.7}$$

and this may be written as

$$\frac{\pi}{\lambda}\arctan\left(\frac{\lambda}{\pi}\frac{z}{w_o^2}\right) \tag{H.8}$$

Substituting equation H.8 into equation H.1 leads to

$$C(z) = \frac{2GP_p}{\lambda}\arctan\left(\frac{\lambda}{\pi}\frac{z}{w_o^2}\right)\Big|_{z=-L}^{x=+L} \tag{H.9}$$

One also has that

$$\arctan(-z) = -\arctan(z) \tag{H.10}$$

so that equation H.1 becomes

$$C(z) = \frac{4GP_p}{\lambda}\arctan\left(\frac{\lambda}{\pi}\frac{L}{w_o^2}\right) \tag{H.11}$$

REFERENCES

[Be 85] E. Berik, B. Davidenko et al., "Stimulated Raman Scattering of Dye Laser Radiation in Hydrogen. Improvement of the Spectral Purity," *Optics Communications*, Vol. 56, p. 283-287, December 1985.

[Bh 66] M. L. Bhaumik, "Physics of Raman Lasers," 1966.

[Bl 67] N. Bloembergen, "The Stimulated Raman Effect," *Americal Journal of Physics*, Vol. 35, p. 989-1022, November 1967.

[Bo 69] G. D. Boyd, W. D. Johnston and I. P. Kaminov, "Optimizing of the Stimulated Raman Scattering Threshold," *IEEE Journal of Quantum Electronics*, Vol. 5, p. 203-206, April 1969.

[Br 82] D. J. Brink et al, "A simple efficient way to VUV and IR generation," *Laser und Optoelectronik*, Nr. 3, p. 41-48, 1982.

[Co 75] D. Cotter, D. C. Hanna and R. Wyatt, "Infrared Stimulated Raman Generation : Effects of Gain Focussing on Threshold and Tuning Behaviour," *Applied Physics*, Vol. 8, p. 333-340, 1975.

[Cr 82] J.P. Crenn, "Optical theory of Gaussian beam transmission through a hollow circular dielectric waveguide, " *Applied Optics*, Vol. 21, p. 4533-4541, December 1982.

[De 82] W. Demtröder, *Laser Spectroscopy*, New York, 1982.

[Fe 73] W. R. Fenner, H. A. Hyatt et al., "Raman cross section of some simple gases," *J. Opt. Soc. Am.*, Vol. 63, p. 73-77, January 1973.

[Fu 84] S. F. Fulgam, D. W. Trainor et al., "Stimulated Raman Scattering of XeF Laser Radiation in H_2 - Part 11", *IEEE Journal of Quantum Electronics*, Vol. 20, p. 218-222, March 1984.

[Gi 69] J. A. Giordmaine, "Nonlinear Optics," *Physics Today*, p. 39-44, January 1969.

[Gl 70] Detlef Gloge, "Optical Waveguide Transmission," *Proceedings of the IEEE*, Vol. 58, p. 1513-1522, October 1970.

[Ha 79] D. C. Hanna et al, *Nonlinear Optics of free Atoms and Molecules*, Springer Verlag, 1979.

[He 87] E. Hecht, *Optics*, Second Edition, 1987.

[He 88] Wilhelm Heuer and Helmut Zacharias, "Stimulated Raman Effect and Four-Wave Mixing in a Hollow Waveguide," *IEEE Journal of Quantum Electronics*, Vol. 24, p. 2087-2100, October 1988.

[Ka 60] N. S. Kapany, *Fiber Optics*, New York : Academic Press, Inc., 1967.

[Ko 66] H. Kogelnik and T. Li, "Laser Beams and Resonators," *Applied Optics*, Vol. 5, p. 1550-1567, October 1966.

[La 85] Lambda Physik : Raman Shifter RS 75 Operational Manual.

[Ma 76] M. Maier, "Applications of Stimulated Raman Scattering," *Applied Physics*, Vol. 11, p. 209-231, 1976.

[Ma 64] E. A. J. Marcatilli and R. A. Schmeltzer, "Hollow Metallic and Dielectric Waveguides for Long Distance Optical Transmission and Lasers," *The Bell System Technical Journal*, Vol. 43, p. 1783-1809, July 1964.

[Mc 84] R. L. McCally, "Measurement of Gaussian beam parameters," *Applied Optics*, Vol. 23, p. 2227, July 1984.

[Mi 88] P. W. Milloni and J. H. Eberly, *Lasers*, John Wiley and Sons, 1988.

[Mo 90] J. V. Moloney and A. C. Newell, "Nonlinear Optics," *Physica D*, Vol. 44, p. 1-37, 1990.

[Ne 86] S. Nemato, "Determination of waist parameters of a Gaussian beam," *Applied Optics*, Vol. 25, p. 3859-3863, November 1986.

[Op 90] Udt Sensors Inc., Optoelectronic Components Catalog., 1990.

[Ra 65] S. Ramo *et al*, *Fields and Waves in Communication Electronics*, John Wiley and Sons, 1965.

[Re 89] C. Reiser and T. D. Raymond, "Efficient anti-Stokes Raman conversion in collimated beams," *J. Opt. Soc. Am. B*, Vol. 6, p. 1859-1869, October 1989.

[Rj 87] RjP 735, Operational Manual.

[Sh 65] Y. R. Shen and N. Bloembergen, "Theory of Stimulated Brillouin and Raman Scattering," *Physical Review*, Vol. 137, No. 6A, p. 1787-1805, March 1965.

[Sn 61] E. Snitzer, "Cylindrical Dielectric Waveguide Modes," *J. Opt. Soc. Am.*, Vol. 51, p. 491-498, May 1961.

[Sn 83] A. W. Snyder and J. D. Lowe, *Optical Waveguide Theory*, Chapman and Hall Ltd., 1983.

[Sp 68] M. R. Spiegel, *Mathematical handbook of Formulas and Tables*, 1968.

[Ta 65] C. L. Tang and T. F. Deutsch, "Generation of Anti-Stokes Radiation in the Higher Order Coherent Raman Processes," *The Physical Review*, Vol. 138, No. 1A, p. 1-8, April 1965.

[Tr 80] W. R. Trutna and R. L. Byer, "Multiple-pass Raman gain cell," *Applied Optics*, Vol. 19, p. 301-312, January 1980.

[Zo 66] R. M. Zoot, "A Laser End Reflector with Spectral Tuning Capability, " *Applied Optics*, Vol. 5, p. 349-350, February 1966.